

The ESAB logo is located in the top right corner, consisting of the word "ESAB" in a bold, sans-serif font, with a stylized graphic element to its right.

THE RULES, DEMOLISHED.



ESAB's breakthrough 2017 product releases are here and redefining what's possible in welding and cutting. Consider yourself warned, and head to esab.com/impact now.

SEE THEM ALL >

WELDING *Journal*

FEBRUARY 2017



- Welding Aluminum
- Certification Program Update
- Solder Joint Reliability
- The American Welder:
Pulsed GMAW

PUBLISHED BY THE AMERICAN WELDING SOCIETY TO ADVANCE THE SCIENCE, TECHNOLOGY, AND APPLICATION OF WELDING AND ALLIED JOINING AND CUTTING PROCESSES WORLDWIDE, INCLUDING BRAZING, SOLDERING, AND THERMAL SPRAYING

Select 70C-6 SR

Low Temperature Toughness



Select-Arc has introduced a gas-shielded, composite metal cored electrode designed to produce excellent mechanical properties in the as-welded and stress-relieved conditions. Select 70C-6 SR is an E70C-6MJ-H4 wire, delivering optimal results in root/hot pass welding applications requiring low temperature toughness properties down to -60°F. Through unique alloying techniques, Select 70C-6 SR exhibits superior mechanical properties and generates fewer silicate islands which results in exceptional weld quality.

Select 70C-6 SR provides:

- Robust notch toughness at -60°F before and after post-weld heat treatment.
- Superb mechanical properties after extended stress relief (up to 6 hours)
- Very low diffusible hydrogen levels (less than 4.0mL/100g).
- True spray transfer with virtually no spatter.
- Increased productivity for low temperature root/hot pass welding.

Select 70C-6 SR, available in .045", .052" and 1/16" diameters, is ideally suited for welding pressure vessels, piping /repair applications, flanges, valves and high quality structural steel fabrication.

For more information on Select 70C-6 SR, call us at **1-800-341-5215** or visit our website at www.select-arc.com.

Select 70C-6 SR (E70C-6MJ-H4) Mechanical Properties*

	As-Welded	SR 6 hr. @ @ 1150°F
Ultimate Tensile Strength (ksi)	86.1	85.0
Yield Strength (ksi)	73.2	70.6
Elongation (%)	28.0	28.0
CVNs @ -40°F (Ft-Lbs)	63.0	30.0
CVNs @ -60°F (Ft-Lbs)	49.0	27

*Shielding Gas = 90% Ar/10% CO₂



For Info, go to aws.org/ad-index



PERFECT WELDERS.
**THE BEST
FOR THE BEST.**
PERFECT WELDS.

Wherever and whatever you have to weld, Böhler Welding has the best stick electrode for the job. We supply any type you may need and our electrodes are always easy to handle, with fine arc ignition and stability.

voestalpine Böhler Welding

www.voestalpine.com/welding

For Info, go to aws.org/ad-index

voestalpine

ONE STEP AHEAD.

WHY WE DO IT

CLEAN AIR MATTERS

We believe breathing clean air is a human right that employees, friends and family members in the workplace all deserve.

Contact Camfil APC to learn more.

camfilapc.com/cleanairmatters



Farr Gold Series®
Dust Collector
camfilapc.com/videos/fgs

Farr Gold Series®
Packaged Collector
camfilapc.com/videos/gsp

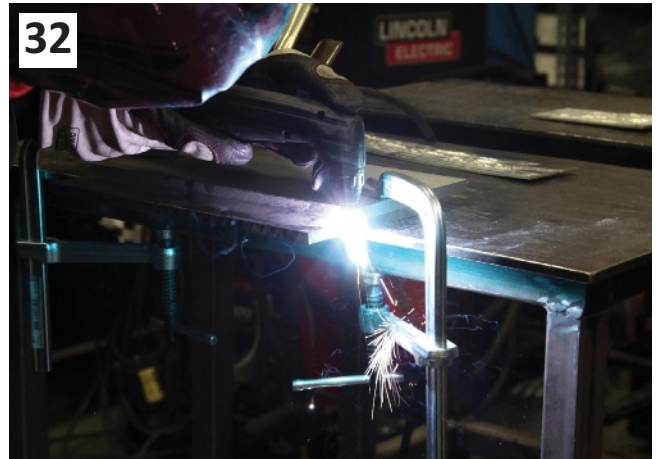
Looks Like a Safe Because It's
**BUILT LIKE
A SAFE™**



Dust, Mist and Fume Collectors

FEATURES

- 32** **Preparing Aluminum before Welding**
The various process options available to get aluminum alloys prepped for welding are discussed — **M. D. Carriere**
- 36** **AWS Certification Program Update**
Important changes to the AWS inspection-related certifications are detailed — **M. Lucia**
- 40** **European Law Requires Assessment of Workers' Exposure to Electromagnetic Fields**
Specialized software was developed to gauge workers' exposure to electromagnetic fields in answer to a new law in Europe — **E. Assunção and G. Melton**



THE AMERICAN WELDER

- 76** **An Introduction to Pulsed GMAW**
Here's a basic guide to this process — **E. Brown**
- 79** **Measuring the Effective Throat of Groove Welds**
This method allows you to determine the minimum effective throat of a combined flare-bevel-groove weld with a reinforcing fillet weld — **G. R. Frazee**



WELDING RESEARCH SUPPLEMENT

- 39-s** **Understanding the Reliability of Solder Joints Used in Advanced Structural and Electronics Applications: Part 1 — Filler Metal Properties and the Soldering Process**
Part 1 of the 2016 Adams Lecture examines the effects of filler metal properties and the soldering process on joint reliability — **P. T. Vianco**
- 53-s** **Influence of Welding Pressure on Diffusion Welded Joints using Interlayer**
Welding pressure created a significant influence on the tensile properties of diffusion welded joints — **G. Thirunavukarasu et al.**
- 63-s** **Microstructure and Mechanical Property of Aluminum/Copper Dissimilar Friction Welded Joints**
Sound aluminum/copper joints were produced using continuous-drive friction welding followed by postweld heat treatment — **S. Chen et al.**
- 71-s** **Weld Formation Characteristics in Resistance Spot Welding of Ultra-Thin Steel**
High welding current along with a short welding time proved a good combination for RSW of ultra-thin steels — **Y. Y. Zhao et al.**

DEPARTMENTS

- 6 Editorial
- 8 Press Time News
- 10 International Update
- 12 Washington Watchword
- 14 News of the Industry
- 20 Business Briefs
- 22 Aluminum Q&A
- 26 Brazing Q&A
- 28 Product & Print Spotlight
- 42 Technology
- 46 Coming Events

- 48 Certification Schedule
- 49 Society News
- 57 Tech Topics
- 61 Section News
- 73 Guide to AWS Services
- 74 Personnel
- The American Welder**
- 83 Learning Track
- 90 Fact Sheet
- 91 Classifieds
- 92 Advertiser Index



On the cover: Pulsed GMAW provides advantages such as improved control over arc starts and stops. (Photo courtesy of Miller Electric Mfg. Co., Appleton, Wis.)



OFFICERS

President John R. Bray
Affiliated Machinery, Inc.

Vice President Dale Flood
TRI TOOL, Inc.

Vice President Thomas J. Lienert
Los Alamos National Laboratory

Vice President Robert Roth
RoMan Manufacturing, Inc.

Treasurer Carey Chen
Cincinnati Incorporated

Executive Director Ray W. Shook
American Welding Society

DIRECTORS

T. Anderson (At Large), ITW Welding North America
U. Aschemeier (Dist. 7), Subsea Global Solutions
T. Brosio (Dist. 14), Major Tool & Machine
J. Burgess (Dist. 8), General Electric
D. A. Desrochers (Dist. 1), Old Colony RVTHS
D. L. Doench (At Large), Hobart Bros. Co.
D. K. Eck (At Large), Praxair Distribution, Inc.
K. Fogleman (Dist. 16), Consultant
P. H. Gorman (Dist. 20), Sandia National Laboratories
S. A. Harris (Dist. 4), Altec Industries
R. L. Holdren (At Large), ARC Specialties
J. Jones (Dist. 17), Harris Products Group
M. Krupnicki (Dist. 6), Mahany Welding Supply Co., Inc.
D. J. Landon (Past President), Vermeer Corp.
S. Lindsey (Dist. 21), City of San Diego
D. E. Lynnes (Dist. 15), Lynnes Welding Training, Inc.
J. T. Mahoney (Dist. 5), American Arc, Inc.
S. M. McDaniel (Dist. 19), Big Bend Community College
D. L. McQuaid (Past President), D. L. McQuaid and Associates, Inc.
D. K. Miller (At Large), Lincoln Electric
D. J. Roland (Dist. 12), Airgas USA, LLC
M. Seberandio (Dist. 3), CNH Industrial America, LLC

K. E. Shatell (Dist. 22), Pacific Gas & Electric Co.
M. Sherman (Dist. 10), SW&E, LLC
M. Skiles (Dist. 9), Airgas, Inc.
W. J. Sperko (At Large), Sperko Engineering Services
J. Stoll (Dist. 18), Voestalpine Bohler Welding Group
K. Temme (Dist. 12), Matrix NAC
P. I. Temple (Dist. 11), Energy Wise Consulting, LLC
J. A. Willard (Dist. 13), Kankakee Community College

WELDING JOURNAL

Publisher/Editor Mary Ruth Johnsen

Editorial

Sr. Editor Cindy Weihl
Features Editor Kristin Campbell
Associate Editor Katie Pacheco
Peer Review Coord. Sonia Aleman
Publisher Emeritus Jeff Weber

Design and Production

Production Manager Zaida Chavez
Assistant Production Manager Brenda Flores
Manager of International Periodicals and Electronic Media Carlos Guzman

Advertising

Sr. Advertising Sales Exec. Sandra Jorgensen
Sr. Advertising Sales Exec. Annette Delagrange
Manager of Sales Operations Lea Owen
Sr. Advertising Production Manager Frank Wilson

Subscriptions

Subscriptions Representative Evelyn Andino
eandino@aws.org

MARKETING ADVISORY COUNCIL (MAC)

D. L. Doench, Chair, Hobart Brothers Co.
S. Bartholomew, Vice Chair, ESAB Welding & Cutting Prod.
Lorena Cora, Secretary, American Welding Society
D. Brown, Weiler Brush
C. Coffey, Lincoln Electric
D. DeCorte, RoMan Manufacturing
S. Fyffe, Astaras, Inc.
D. Levin, Airgas
R. Madden, Hypertherm

D. Marquard, IBEDA Superflash
J. F. Saenger Jr., Consultant
S. Smith, Weld-Aid Products
D. Wilson, Wilson and Associates
J. N. DuPont, Ex Off., Lehigh University
L. G. Kvidahl, Ex Off., Northrop Grumman Ship Systems
D. J. Landon, Ex Off., Vermeer Mfg.
S. P. Moran, Ex Off., American Hydro Corp.
E. Norman, Ex Off., Southwest Area Career Center
R. G. Pali, Ex Off., J. P. Nissen Co.
N. Scotchmer, Ex Off., Huys Industries
R. W. Shook, Ex Off., American Welding Society

American Welding Society

8669 NW 36 St., # 130, Miami, FL 33166-6672
(305) 443-9353 or (800) 443-9353

Welding Journal (ISSN 0043-2296) is published monthly by the American Welding Society for \$120.00 per year in the United States and possessions, \$160 per year in foreign countries: \$7.50 per single issue for domestic AWS members and \$10.00 per single issue for nonmembers and \$14.00 single issue for international. Not available for resale in either print or electronic form. American Welding Society is located at 8669 NW 36th St., # 130, Miami, FL 33166-6672; telephone (305) 443-9353. Periodicals postage paid in Miami, Fla., and additional mailing offices. **POSTMASTER:** Send address changes to *Welding Journal*, 8669 NW 36th St., # 130, Miami, FL 33166-6672. **Canada Post:** Publications Mail Agreement #40612608 Canada Returns to be sent to Bleuchip International, P.O. Box 25542, London, ON N6C 6B2, Canada.

Readers of *Welding Journal* may make copies of articles for personal, archival, educational or research purposes, and which are not for sale or resale. Permission is granted to quote from articles, provided customary acknowledgment of authors and sources is made. Starred (*) items excluded from copyright.

Copyright © 2017 by American Welding Society in both printed and electronic formats. The Society is not responsible for any statement made or opinion expressed herein. Data and information developed by the authors of specific articles are for informational purposes only and are not intended for use without independent, substantiating investigation on the part of potential users.



Certified Chain of Custody
Promoting Sustainable
Forest Management
www.sfi-program.org



HODGSON

CUSTOM ROLLING INC

North America's largest Brake Forming, Plate Rolling and Structural Rolling facility delivers cost effective solutions.

We serve a wide range of industries including energy, transportation, architectural, construction, mining, metals, and agricultural as well as OEMs across North America.



2" TH x 70" ID
x 7" ID x 50" OAH

For all your rolling, forming and bending needs, please email info@hcrsteel.com or visit www.hcrsteel.com

Fax 1-905-356-6025
Call toll free **1-800-263-2547**



ASSOCIATE

ASME-S

ASME-U

CONTROLLED GOODS & ITR COMPLIANT

CERTIFIED

SUSTAINING COMPANY MEMBER

ISO 9001:2008

For Info, go to aws.org/ad-index

Make a Plan and Set Your Welding Goals High



Dale Flood
AWS Vice President

“There are plenty of opportunities out there that can take you to places you may never have imagined...believe in big, bold, and amazing things for yourself and the welding industry.”

Author and motivational speaker Jack Canfield once stated, “Successful people maintain a positive focus in life no matter what is going on around them. They stay focused on their past successes rather than their past failures, and on the next action steps they need to take to get them closer to the fulfillment of their goals rather than all the other distractions that life presents to them.”

This philosophy carried Canfield to the peaks of fulfillment in business and his personal life. You can do the same with your welding career. Maybe you have decided you would like to start pursuing welding as a profession and think that means, for the rest of your life, you will be watching metal fuse. Before you end at that point, I would like to challenge you to set your goal wickedly high and don’t stop until you get there.

When I started my career in this industry, I had no interests other than fitting pipes together and installing hangers, supports, and whip restraints to hold the pipes in place so I could get lost in the many hours that would pass while welding these large pipes. In some ways, it would excite me each time a pipe weld was finished because I knew it would be x-rayed or ultrasound tested, and each time one passed, it was another proverbial feather in my hat. Do you think as I watched the tungsten tip sway back and forth, the 7018 flow, or the chains on chainfalls move that I was thinking someday I’d be in line to be president of the American Welding Society (AWS)? Surely not.

AWS is the most prestigious welding organization in the world. How do you go from being a welder to then serving as AWS president? The answer is by setting your goals insanely high and going after them.

Two very good friends of mine both attended community colleges in northern California, graduated, and became instructors at their college for a few years. While teaching, they started studying to be certified as welding inspectors, succeeded, and became AWS Certified Welding Inspectors (CWIs). The young man decided to start his own weld inspection business and did quite well. One of the biggest electric and gas utility companies

in the country noticed him, and now he has a prestigious position as a corporate quality assurance inspector. The young lady decided to move to Texas where, at the time, the oil and gas industry was booming. She worked there for a while as a college instructor and started her own inspection business. She is also considering starting her own welding school to train and mentor new students.

There is another young man I met at an AWS Section meeting while we were taking a tour of a huge train car manufacturing company in northern California. Unbeknownst to me, he thought someday he would like to work there. He finished college and shortly after I was pleased to learn he was, in fact, working as a welder for the train manufacturer. He also started studying, became a CWI, and decided to try his sales skills for a major weld equipment manufacturer. He did quite well and within a reasonably short period of time was offered a management position at the train car facility, where he is again positioned today.

These are all good positions, but what about compensation? There are all sorts of studies out there comparing welders’ wages to any other occupation you can imagine. Once in a while, you see these quoted in a periodical discussing the welding industry’s need for more welders.

I am usually disheartened when hearing discussions about welding jobs offering an hourly range of \$15–\$18. Most of the good welders I know can earn three to four times those wages, and when they move on to inspection, management, or company ownership, most are making well into the six figure range. Don’t allow yourself to settle for mediocrity. In 1984, I knew welders who were making more than \$100,000 per year, and today some of them make twice that.

There are plenty of opportunities out there that can take you to places you may never have imagined. Study, work hard, apply yourself, keep yourself to the proverbial “grindstone,” and when you think no one notices keep trying. Believe in big, bold, and amazing things for yourself and the welding industry. Someday, you might be the next AWS president. [WJ](#)



Joining with light: Flawless fusion by design

It's easy to see why thousands of manufacturers have made the switch to laser joining. Benefits include minimal heat input and distortion, improved stiffness and strength, high productivity, elimination of secondary processes, and reduction of cost per part. And when parts are designed specifically for laser welding, manufacturers get the best of these benefits. In the pursuit of making products lighter, stronger, safer, or more affordable, TRUMPF's broad laser portfolio and applications expertise provide the perfect solution.

www.us.trumpf.com

For Info, go to aws.org/ad-index

Linde and Praxair Merger to Produce Revenues in Excess of \$65 Billion

Linde AG, Munich, Germany, and Praxair, Inc., Danbury, Conn., plan to combine in an equal merger under a new holding company through an all-stock transaction. They recently signed a nonbinding term sheet and expect to execute a definitive business combination agreement.

“The strategic combination between Linde and Praxair would leverage the complementary strengths of each across a larger global footprint and create a more resilient portfolio with increased exposure to long-term macro growth trends,” said Steve Angel, Praxair’s chairman and CEO.

Based on 2015 reported results, the combination would create a company with pro forma revenues of approximately \$30 billion, prior to any divestitures, and a current market value in excess of \$65 billion. The proposed merger would also enable positions in key geographies, create a more diverse global portfolio, and deliver advanced products.

“Under the Linde brand, we want to combine our companies’ business and technology capabilities and form a global industrial gas leader...[the] value-creating combination would achieve a robust balance sheet and cash flow, and generate financial flexibility to invest in our future,” said Professor Aldo Belloni, Linde’s CEO.

AWS Hires New Chief Operating Officer



Matt Miller

The American Welding Society (AWS), Miami, Fla., has hired Matt Miller as its new chief operating officer (COO).

Before joining AWS, Miller worked at the National Association of Corrosion Engineers (NACE International). He served as its COO from 2014 to his hiring at AWS. Prior to working at NACE, Miller was with the Society of Automotive Engineers for 12 years, where he served as director of the SAE

Foundation and SAE’s Pre-Professional Program.

Miller earned a master’s degree in nonprofit management from Robert Morris University, a master’s degree in instructional technology from Duquesne University, and a bachelor’s degree in elementary education from Indiana University of Pennsylvania. He is also a decorated veteran who served in the U.S. Army Infantry during Operation Desert Storm.

“The search for our new COO has been a very thorough journey,” said Ray W. Shook, executive director, AWS. “We feel good about the selection of Matt, and we are confident he will be a great addition in providing support to those areas where we have had rapid growth.”

FCA US Expands Commitment to U.S. Manufacturing with \$1 Billion New Investment

FCA (Fiat Chrysler Automobiles) US has confirmed the next phase of its industrialization plan, by devoting a \$1 bil-



Deonte Clark preps a Ram 1500 for EcoDiesel powertrain installation at the Warren Truck Assembly Plant. (Photo courtesy of FCA.)

lion investment to Michigan and Ohio plants, along with adding 2000 new American jobs.

The automaker will retool and modernize both the Warren Truck Assembly Plant in Michigan to produce the new Jeep® and Grand Wagoneers, and the south plant of the Toledo Assembly Complex in Ohio to build a new Jeep pickup truck. These actions are planned to be done by 2020. The Warren investment will also enable producing the Ram heavy-duty truck currently constructed in Mexico.

“The conversion of our industrial footprint completes this stage of our transformation as we respond to the shift in consumer tastes to trucks and SUVs, and as we continue to reinforce the U.S. as a global manufacturing hub for those vehicles at the heart of the SUV and truck market,” said Sergio Marchionne, CEO of FCA N.V.

GAWDA Begins Quarterly Economic Forecasts and Adds ITR Economics as a Consultant

The Gases and Welding Distributors Association (GAWDA), Hollywood, Fla., is offering its members industry-specific quarterly economic forecasts and market analysis reports provided by the firm ITR Economics. In addition, the association has named ITR Economics’ Principal and President, Alan Beaulieu, as its chief economist.

According to GAWDA Executive Director John Ospina, members will receive the initial quarterly market analysis and forecast reports in the first quarter of 2017. The material will be distributed through the association’s print and online publications along with its webinars and conferences.

Hiring ITR came from members’ interests in obtaining more industry-specific financial forecasting and market data to use in business decision making, noted Mark Raimy, GAWDA’s 2016–2017 president, who initiated the task.

Reports will be useful, Beaulieu added, “because ITR Economics is in the risk reduction business. If we can replace ‘think’ with ‘know’ in terms of what is coming along in the marketplace, and with a 95-percent confidence rating, that can help GAWDA members prepare before making decisions, and that can help members enhance profitability.” 



THIN & TOUGH



TIGER ULTRACUT 1MM THIN CUTTING WHEELS

Weiler's NEW UltraCut wheels deliver unmatched cutting performance and toughness with a TRUE 1 millimeter thickness. Proprietary SOLID CORE technology increases density of the wheels, resulting in longer life, reduced friction, and superior stability. From the first cut, operators will experience lightning fast, smooth cutting, and exceptional control for clean, precise cuts on thin sheet metal, profiles, and small diameter rods.

You can be thin and still be tough with Tiger UltraCut wheels.

Learn more and request a FREE sample at Weilercorp.com/UltraCut

PROPRIETARY
SOLID
CORE
TECHNOLOGY

800.835.9999 / weilercorp.com

For Info, go to aws.org/ad-index



AWS Training Facility Established in Indonesia



PT. Asian Welding Specialist, Lincoln Indoweld, and SMKN 2 representatives pose during the Oct. 15, 2016, memorandum of understanding and equipment donation gathering in Bandung, Indonesia.

PT. Asian Welding Specialist, an AWS Educational Institution Member and SENSE-participating organization, which provides welding certification for code welders, has opened for business in Bandung, Indonesia.

“It is imperative the local talent is developed, rather than utilizing imported labor, for the numerous infrastructure projects planned and currently underway, including 35 mW of power plant construction over the next two to five years, as well as numerous petrochemical expansion projects and more than 2000 km of pipeline projects,” stated AWS SCWI/CWE and Accredited Testing Facility (ATF) Supervisor Steven Synder.

The organization is operating from Bandung SMKN 2 Vocational Technical School and has partnered with other corporations, such as PT Lincoln Indoweld and Rigid Professional Tools, to provide the necessary equipment for conducting welder testing.

“This working agreement and memorandum of understanding allows us to work together, engaging local young developing talent to offer them the recognition and opportunity to train using SENSE guidelines and work toward achieving AWS Certified Welder status,” explained Managing Director and QA Manager Dina Septriana Snyder.

The organization is working on its next phase in acquiring AWS ATF certification.

RAMLAB Unveils Metal Printing Lab Designed for the Maritime Sector



From left are Vincent Wegener, RAMLAB managing director, and Allard Castelein, Port of Rotterdam CEO, during the grand opening of RAMLAB's 3D metal printing lab.

On Nov. 30, 2016, Rotterdam Additive Manufacturing Lab (RAMLAB) in the Port of Rotterdam in the Netherlands opened what is claimed as the world's first 3D metal print-

ing facility specifically for the maritime industry. Seventy people attended the grand opening, including the company's business partners and maritime representatives.

The event was centered around the unveiling of the company's newest wire arc additive manufacturing (WAAM) machine, which featured a talking robotic arm attached to an assembly line. Port of Rotterdam CEO Allard Castelein and RAMLAB Managing Director Vincent Wegener also showcased the WAAM machine's first printed object: a large propeller.

Italian Companies Sign Global Cooperation Agreement for Maintenance Systems

On Dec. 14, 2016, Engineering Ingegneria Informatica Spa and Comau Spa came together in Rome, Italy, to sign an international cooperation agreement to pursue the development and marketing of hardware and software systems for the predictive maintenance of machines. These seek to forecast machine malfunctions and intercept negative trends in production process quality.

The companies will focus on the manufacturing, automotive, industrial manufacturing, food and beverage, and pharmaceutical industries in accordance with the Industry 4.0 paradigm, a model based on computerized systems that monitor the processes of the factory and make decisions.

This collaboration “allows us to guide manufacturing companies toward changing production processes, with particular reference to the context of the so-called fourth industrial revolution,” explained Mauro Fenzi, CEO of Comau.

Sikorsky Agrees to Produce Helicopters for the Chilean Air Force



The S-70i is the newest model of Black Hawk, multimission helicopters produced by Sikorsky.

The Chilean Air Force (Fuerza Aérea de Chile) has contracted with Sikorsky, a Lockheed Martin company, for six S-70i™ Black Hawk helicopters, which are to be delivered in 2018.

The helicopters will be used for the service's medium-lift helicopter recapitalization program, which includes the acquisition of a logistical support package that will cover spare parts, pilot and maintenance specialist training, on-site technical assistance, and ground support equipment. They will also help Chile fulfill its requirements for the performance of military and humanitarian missions, including troop transport, search and rescue, and disaster relief.

“We are very pleased that the Fuerza Aérea de Chile has chosen the multirole Black Hawk helicopter following an intensive review of competing platforms,” said Adam Schierholz, Sikorsky regional executive for Latin America. [WJ](#)



Southwire®

ROYAL® EXCELENE®

Welding Cable



For Info, go to aws.org/ad-index

Royal® Excelene® Welding Cable has long been known as a leading brand in the welding marketplace. While the times have changed, we have not. We are still the same brand, with the same quality, produced in the same plant, by the same people you have entrusted throughout the years.

Some things never change. And that's a good thing.

For information, contact welding@southwire.com.



We're the wire.™



Southwire®

Major Water Infrastructure Bill Approved

The Water Resources Development Act of 2016, enacted into law in December, authorizes more than \$10 billion in federal spending to upgrade U.S. water infrastructure, including waterways, harbors, ports, channels, locks, and dams. The bill also authorizes the Army Corps of Engineers' recommendations to Congress for water resources infrastructure investment received since 2014; approves studies for future water resource improvements; strengthens process reforms for greater local participation in project selection; empowers nonfederal participation in construction, operation, and maintenance activities; accelerates and broadens reforms for the processing of infrastructure project permits; and requires timely approvals for nonfederal modifications to the Army Corps of Engineers projects.

Bill Introduced to Clarify Manufacturing Tax Rule

The Promoting More American Manufacturing Jobs Act has been introduced in the U.S. Senate to explain the domestic manufacturing tax deduction. This bipartisan legislation would clarify Congress's intent in enacting the domestic manufacturing deduction, section 199 of the federal tax code, in contract manufacturing situations. Any party to the arrangement that makes a substantial contribution through the activities of its U.S. employees to the manufacture of qualifying goods shall be entitled to claim the deduction.

Congress added the domestic manufacturing deduction to the tax code in 2004 to encourage the creation of manufacturing and domestic jobs. Application of the deduction to fully integrated manufacturers is relatively clear. However, the IRS has implemented and applied regulations relating to the domestic manufacturing deduction in a manner that does not benefit most manufacturers that rely on contract manufacturing, even though both types of domestic manufacturers make similar contributions to job creation. The bill would eliminate the different treatment of manufacturers with vertically integrated and nonvertically integrated supply chains.

Legislation Enacted for Manufacturing Universities

A new federal law has been approved authorizing the Department of Defense to support industry-relevant, manufacturing-focused engineering training at U.S. universities. Universities and other participating organizations would be selected through a competitive grant-based process and required to align their education programs with the needs of modern U.S. manufacturers, focusing engineering programs on the development of industry-relevant advanced manufacturing skills, building new partnerships with manufacturing firms, increasing hands-on training opportunities for students, and fostering manufacturing entrepreneurship.

The program will be governed by the Secretary of Defense, in consultation with other federal agencies, such as

the National Science Foundation, the National Institute of Standards and Technology, the Department of Energy, and the Department of Education.

Government Seeks to Expand Manufacturing Extension Partnerships

The Manufacturing Extension Partnership (MEP) Improvement Act seeks to expand and improve the MEP program to better serve small/medium-sized manufacturing companies. Of particular importance is an adjustment of the cost share. Previously, MEP centers were required to raise \$2 of nonfederal funds for every one federal dollar received after five years. This was higher than most other federal-matching grant programs and seen as a significant obstacle. This new law will permanently reduce the cost share to one nonfederal dollar for every one federal dollar received.

In addition, the law will strengthen and clarify the MEP center review process and require recompetition of MEP center awards every ten years; authorize MEP centers to support the development of manufacturing-related apprenticeship, internship, and industry-recognized certification programs; increase the MEP program authorization level to \$260 million per year through 2020; and require the MEP program to develop open-access resources describing best practices for America's small manufacturers.

Government R&D Efficiency Bolstered

The Research and Development (R&D) Efficiency Act, which is now law, requires the Office of Science and Technology Policy to establish an interagency working group to reduce administrative burdens on federally supported researchers and bolster transparency. Acting under the authority of the National Science and Technology Council, the interagency group will be responsible for reviewing federal regulations affecting research and research universities, as well as making recommendations on how to 1) harmonize, streamline, and eliminate duplicative federal regulations and reporting requirements; 2) minimize the regulatory burden on U.S. institutions of higher education performing federally funded research while maintaining accountability for federal tax dollars; and 3) identify and update specific regulations to refocus on performance-based goals, rather than on process, while still meeting the desired outcome.

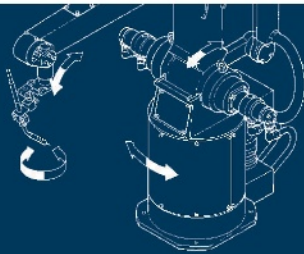
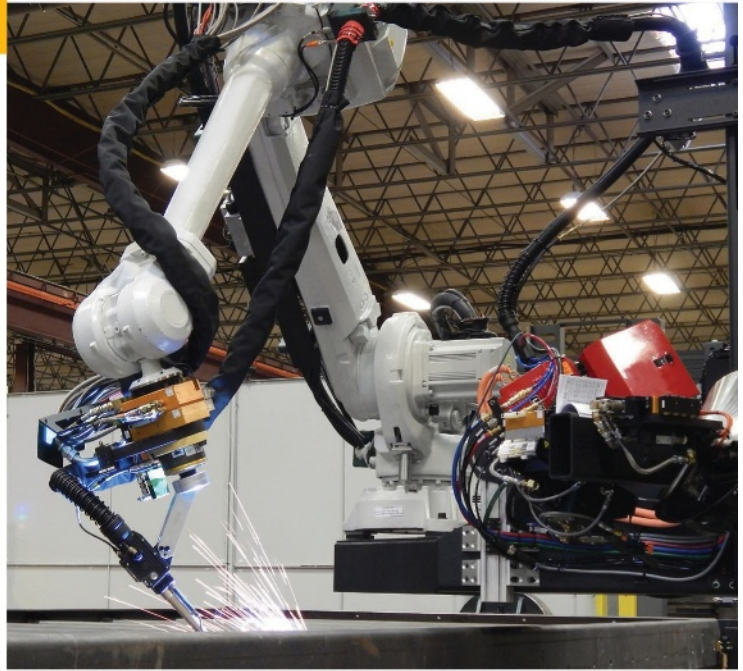
STEM Advisory Panel to be Established

Acting under a legislative mandate, the National Science Foundation will be establishing a science, technology, engineering, and mathematics (STEM) education advisory panel consisting of individuals from academic institutions, non-profit organizations, and industry. The primary role of the new panel will be to advise the National Science and Technology Council, a cabinet-level body that coordinates science and technology policies across the diverse entities that make up the federal research and development enterprise. 

National Robotic Welding Conference & Exhibition 2017

Tuesday, June 6
& Wednesday, June 7, 2017

with Bonus Tour on June 5



The Simple and Beyond

Data Driven, Flexible Manufacturing with One Robot or Many

Milwaukee, Wisconsin

This two-day event with a bonus day hosted by Miller Electric features two tours of companies utilizing robots in applications that range from the “Simple to Beyond.” On Tuesday, the conference features two tours for each conference attendee. One tour will be of Kohler Power Systems, a manufacturer of large fuel tanks for power generation. The second tour will be of Telsmith Inc., an Astec Industries Company. Telsmith Inc. has been providing the global mining and aggregate industries with crushing and vibrating equipment, modular and portable plants for over 100 years. On Wednesday the conference will feature a variety of industry leaders presenting on data driven flexible manufacturing with one robot or many, and how to optimize upstream processes. Proceeds fund the John F. Hinrichs Memorial Endowment, which provides scholarships to students in welding and engineering.

For more information or to register, contact: Karen Gilgenbach (262) 613-3790, Karen.gilgenbach@airgas.com
Or download more information: <http://www.aws.org/milwaukee-NRAWC-2017>



American Welding Society®
D16 COMMITTEE



KOHLER®



MATC is an Affirmative Action/Equal Opportunity Institution and complies with all requirements of the Americans With Disabilities Act. MATC is accredited by the Higher Learning Commission, Commission on Institutions of Higher Education, the national standard in accrediting colleges and schools for distinction in academics and student services.

For Info, go to aws.org/ad-index

Hobart Institute of Welding Technology Opens New Welder Training Facility



Hobart's new facility was designed to enhance the student experience for new welders and welders seeking continuing education/certifications, as well as corporate services training and testing.

The Hobart Institute of Welding Technology (HIWT) has opened the Next Generation Welder Learning Facility on its Troy, Ohio, campus. The new, more than 16,000-sq-ft building began hosting classes in late October and represents an addition to the 13-acre campus where more than 100,000 welders have been trained.

The facility features three technically advanced classrooms that seat up to 120 students and contain high-tech

audio-visual training aids. In addition, there is a nondestructive testing lab and classroom for hands-on liquid penetrant and magnetic particle inspection, along with a welder performance qualification lab for destructive testing.

"This expansion to our campus is an investment in its mission to serve our students and industry as HIWT is dedicated to welding training and education excellence...for those current and future Certified Welding Inspectors and Certified Welders looking to gain continuing education or acquire new certifications, this building is certainly designed to provide that successful environment," said Scott Mazzulla, HIWT president and CEO.

Aluminum Cracking Mitigation System Offers the Navy an Alternative to Replacing Plate

The Navy Metalworking Center (NMC), Johnstown, Pa., has led a project to address cracking in the aluminum superstructure of the CG 47 class cruisers. An integrated project team developed and demonstrated a portable heat-treatment system that reverses sensitization in Aluminum Alloy 5456. This will provide the Navy a low-cost alternative to cutting and replacing sensitized plate that can save virtually \$2.4 million per CG 47 ship availability, resulting in a cost avoidance of as much as \$43.2 million for 18 ships.

NMC conducted lab tests and finite element simulations to fabricate a prototype reverse sensitization unit that imparts heat treatment to the aluminum plate in the class

Invest to improve productivity, throughput and safety

The proper positioner will offer you a number of advantages:

- Positioners can boost your throughput 35% or more
- Improve ergonomics and safety
- Higher productivity and reduced consumables
- Higher throughput and **PROFITS**



Call 855.750.4295
or visit www.almmh.com

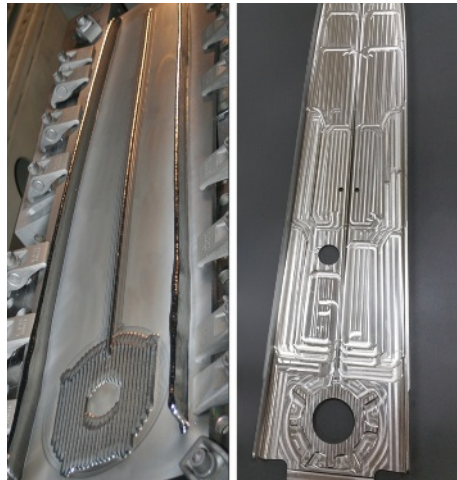


cruiser superstructure to mitigate sensitization. The final prototype system was transitioned to PMS 407 for further evaluation and use during maintenance intervals.

The new process was initiated in September 2016 with the equipment transition to Ingalls Shipbuilding, the planning yard for CG repairs.

Sciaky to Deliver Industrial-Scale Metal 3D Printer to Airbus

Sciaky, Inc., Chicago, Ill., has recently announced Airbus accepted delivery of an electron beam additive manufacturing (EBAM™) 110 system. The aircraft manufacturer will



These photos highlight two stages of an Airbus rear upper spar 3D printed in titanium with Sciaky's electron beam additive manufacturing process. The image to the left reflects the part in an early pre-form stage while the other portrays the finished part.

For info, go to aws.org/ad-index

WELDING AND CUTTING AUTOMATION

60 YEARS

AUTOMATE THE WELDING PROCESS

With 3 Industry Proven Products

www.GULLCO.com

KBM®
Plate Beveling Machine

KATBAK®
Ceramic Weld Backing

KAT®
Oscillation Weld Carriage

GULLCO INTERNATIONAL INC. - USA
21568 Alexander Rd. - Cleveland - Ohio - 44146
Tel: 440-439-8333 Fax: 440-439-3634 e-mail: ussales@gullco.com

Looking for 2% Thoriated Tungsten?

2% Thoriated Tungsten has been the welding industry standard for decades. Now, some tungsten suppliers will have you believe it won't be around much longer!

The Tungsten Electrode Experts™ at Diamond Ground Products have 2% Thoriated in stock and readily available, with no end in sight.

Call DGP today to get your **2% or 4% Thoriated Tungsten** or get a **FREE** sample of our other tungsten varieties such as Tri-Mix™ or Cryo-T. They are better options than cheap imitations claiming to be “new technology”.

Diamond Ground Products...
The Tungsten Electrode Experts

2651 Lavery Court • Newbury Park, CA 91320 • Tel: 805.498.3837 • sales@diamondground.com
diamondground.com

For info, go to aws.org/ad-index



TRIANGLE ENGINEERING, INC.
Services for the Welding Industry



Hydraulic Wrap Around Bender

Model# WTB-HRA/14

- ▶ Durable, industry tested design provides decades of reliability
- ▶ Uses wrap around bend testing method eliminating "undue stress"
- ▶ Specimens are formed to a uniform 180 degree bend
- ▶ Conveniently plugs into 110V wall outlet.
- ▶ 1-1/2" diameter die post included
- ▶ Additional die posts up to 3-1/2" available



Like us on facebook

6 Industrial Way, Hanover, MA 02339-2425
(781)878-1500 • (781)878-1374 • Fax(781)878-2547
www.trieng.com

For info, go to aws.org/ad-index

utilize the industrial-scale metal 3D printing system to produce large structural parts made of titanium. The process combines computer-aided design, additive manufacturing processing principles, and an electron beam heat source. In addition, a closed-loop control is the primary reason this 3D printing process enables consistent part geometry, mechanical properties, microstructure, and metal chemistry.

OSU Welding Engineering Students Begin to Heal after Tragedy

In response to the injuries sustained by several welding engineering (WE) students at The Ohio State University (OSU) during the November 28, 2016, attack on campus, its alumni group has stepped up to provide support.

OSU WE Alumni Society President Patrick Staunton reached out to the Department of Materials Science and Engineering (MSE). This move resulted in sponsoring the Buckeye Donuts Drop-In, organized by the MSE Department for WE students, and providing a therapy dog. Peter Anderson, chair, MSE Department, appreciated the support that funded these social events on the west and main campuses.

"A majority of the injured students were juniors in welding engineering who are taking my metals laboratory course, among others. The good news is that everyone will survive, but there were significant injuries...one of our students who tried to take the knife from the attacker was severely slashed in his hand and may incur permanent nerve damage," explained David Phillips, WE associate professor of practice. "I was told that another one of our WE students [Maxes Wieneke] shoved his fellow student out of the way of



WEMCO

An Association of Welding Manufacturers

Know a person or company who gives back to their community and makes the welding industry shine?

Nominate them for the 2017 awards!



NOMINATION CATEGORIES

(Please choose a category)

- | | |
|---|-------------------------------------|
| ● Individual | ● Educator |
| ● Small Business
(less than 200 employees) | ● Media |
| ● Large Business
(200+ employees) | ● Educational Facility |
| ● Section
(AWS local chapter) | ● Distributor
(welding products) |
| | ● Veterans |

Entry deadline is June 30, 2017

For more information and to submit a nomination form online, visit aws.org/excellenceinwelding or call 800-443-9353.

the attacker's car that was barreling into the Watts Hall courtyard, possibly saving his life."

Wieneke's bicycle was crushed, so students started a GoFundMe campaign, which raised \$1190. "I'm happy to report that Maxes' bike has already been replaced," said Nancy Porter, treasurer, OSU WE Alumni Society.

The Columbus Dispatch also listed these individuals as injured: Kaylee Hoffner (MSE senior); William Clark (emeritus professor); Kerri Strausbaugh; Anthony DiCocco (WE senior); Kristopher L. Waninger and Anderson Payne (WE juniors); Marc Coons; Katie Schultz; Pavel Sergeev; Theron Ellinger; and Elisabeth Sturges and Linda Rager (MSE juniors). Megan Daniels, MSE and WE undergraduate academic advisor, indicated WE Juniors Kate Namola, Andy Landis, and Stan Blados were hurt as well.

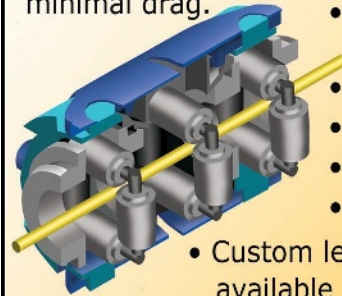
"In addition to the magnificent response of the OSU police officer who quickly ended the threat, it was absolutely amazing to see the entire city of Columbus pour onto campus with an amazing arsenal of police officers, sheriff's deputies, SWAT teams, etc.," Phillips concluded.

Motlow State Community College to Use \$5.5 Million Grant for Robotics Training Center

The Tennessee Higher Education Commission and the governor's office recently revealed that Motlow State Community College, Lynchburg, Tenn., has been awarded a \$5.5 million grant — the largest ever awarded to the educational institution — to build a robotics training center near its McMinnville campus, according to Fred Rascoe, dean of career and technical programs for the college.

Anti-Friction Conduit for Aluminum & Steel Electrode

When you want x-ray quality welds, you can count on Electron Beam's Anti-Friction Conduit to **carry your aluminum or steel electrode over long distances** with minimal drag.



- Ideal for a wide range of electrodes
- Corrosion resistant
- Kink resistant
- Dual insulated
- Quick connect
- Custom lengths available
- Adaptable to most feeder models and payoff systems



1275 Harvard Drive • Kankakee, IL 60901 USA
 Ph: 815-935-2211 • Fax: 815-935-8605
 ebtservice@electronbeam.com • www.electronbeam.com
 AFC-2

For info, go to aws.org/ad-index

The Tungsten Electrode Experts Since 1992

DGP is the industry leader in Tungsten and Tungsten preparation offering low-cost and high-quality Tungsten electrodes, Tungsten grinders & replacement diamond grinding wheels.

We have been dedicated to the improvement of weld quality and welder productivity since 1992.



Piranha II



Piranha III



DGP-2-V2



Raw Tungsten including Tri-Mix® & Cryo-T



Replacement Diamond Grinding Wheels for all Tungsten Grinders



Pre-ground Tungsten Electrodes



Welding Torches and parts Buy online!



"The Tungsten Electrode Experts"

Tel: 805.498.3837 • sales@diamondground.com
diamondground.com



TECHNICAL TRAINING

The Hobart Institute of Welding Technology offers our comprehensive Technical Training courses through the year. Upcoming start dates:

Preparation for AWS® Certified Welding Inspector/Educator (CWI/CWE®) Exam
Mar 13; Apr 10; May 8; Jun 19; Jul 17; Aug 14

Preparation for AWS® Certified Welding Supervisor (CWS®) Exam
Apr 24; Oct 9

Preparation for Recertification of AWS® CWI®
Mar 20; Apr 17; May 15; Jun 26; Jul 24; Aug 21

Arc Welding Inspection
Feb 2; Apr 3

Welding for the Non Welder
Mar 6; May 1; Jul 31

Weldability of Metals, Ferrous & Nonferrous
Feb 13, 20; Mar 13, 20; Apr 10, 17; May 8, 15

Liquid Penetrant & Magnetic Particle Inspection
Jan 30; May 22; Aug 28

Fundamentals of Visual Inspection
May 31; Sep 6



HOBART INSTITUTE
OF WELDING TECHNOLOGY

937-332-9500

or visit us at www.welding.org
for more information.

© 2016 Hobart Institute of Welding
Technology, Troy, Ohio
State of Ohio Reg. No. 70-12-0064HT

For info, go to aws.org/ad-index

“Currently, it is estimated there are more than 7000 robots in use within 75 miles of Motlow’s McMinnville campus, and that number will only grow,” said Rascoe. “Middle Tennessee is fast becoming a nationwide leader in advanced manufacturing, which uses robotic technology. Motlow State is vital in the process to train skilled workers to support these fast-paced industries.”

The new robotics training center will be on 4.5 acres, adjacent to the Tennessee College of Applied Technology and Motlow State McMinnville campus, donated to the college by the Warren County Commission.

Governor Bill Haslam’s office also indicated the grant as part of the Drive to 55 Capacity Fund, which is an initiative to support colleges and universities as enrollment increases since the launch of Tennessee Promise.

Great Bay Community College Starts Nondestructive Testing Certificate Program



An instructor demonstrates magnetic particle testing on a steel part as part of a class at Great Bay Community College. The institution’s Nondestructive Training certificate is new.

Great Bay Community College will begin offering a Non-destructive Training (NDT) certificate as part of its advanced materials manufacturing program. Designed in partnership with industry experts, this program aims to meet the hiring demands of businesses. It will be run out of the Rochester, N.H., campus where space is being built.

The liquid penetrant method will be taught to start, but as equipment funding becomes available, the college will add more methods including ultrasonic and radiography.

Safran Aerospace Composites, Rochester, N.H., is among the companies seeking qualified employees. NDT Supervisor Donald Chabot routinely sends employees to training facilities for meeting National Aerospace Standards; he expects to add 10–20 employees over the next year. Hitchiner Manufacturing Co., Inc., Milford, N.H., seeks skilled workers as well. “Great Bay’s new program will create a nice applicant pool for us, and will also allow us to offer training to our existing employees so they can further advance their skills while we cover the cost for them to do so,” said Quality Director Matt Wallace.

Industry Notes

• **Steffensmeier Welding & Manufacturing, Inc.**, Pilot Grove, Iowa, has been awarded the 2016 Best Development Award by **1000 Friends of Iowa** in the renewable energy

Original & Patented ROD GUARD®

PROUDLY MADE IN THE USA

The Total Welding Rod Protection System:
Airtight storage and inventory control for welding electrodes and filler metals with genuine Rod Guard® welding accessories.

- **Airtight** - Threaded cap with long-lasting Neoprene Seal
- **Reusable** - Constructed of High-Impact Polyethylene
- **Additional Colors Now Available** – Call for Details
- **Storage Racks** - Now Available for 36” & 1 meter cannisters
- **High-Temp Models** - Steel-lined, heat resistant to 450°
- **Chloride-Free**
- **Quality Guaranteed**

Quality and Excellence Since 1981

Available through your welding supply distributor; or contact us for more information:

Beware of Cheap Imitations --

INSIST ON

ROD GUARD®

--And ask for it by name!!

K.I.W.O.T.O., Inc.

P.O. Box 1526-WJ
Benton Harbor, MI 49023-1526
Phone: 269-944-1552 • Fax: 269-944-1536
www.rodguard.net

For info, go to aws.org/ad-index

category. Its solar field project — highlighted in the July 2016 *Welding Journal* feature article, Sunny Economics: Using Solar Power to Save Money — has adopted strategies to increase efficiency and spur growth. Five independent jurors from across the state picked the winning projects.

• **Workshops for Warriors**, San Diego, Calif., has received a \$75,000 commitment from **JPMorgan Chase & Co.** The funds will provide veterans with training and accredited STEM educational programs. “We’re helping veterans gain the skills they need in an effort to help fill the more than 2.3 million advanced manufacturing jobs in the U.S. These funds are crucial to helping us reach our goals,” said Hernán Luis y Prado, founder, Workshops for Warriors.

• **Digicom Electronics, Inc.**, Oakland, Calif., now generates its own nitrogen to use in the company’s solder reflow along with selective and hand soldering processes. The nitrogen is generated and piped to machine inputs/work areas at a prescribed volume and pressure to achieve optimized inert gas saturation.

• **Muza Metal Products**, Oshkosh, Wis., is working with **Fox Valley Technical College**, Appleton, Wis., to fill a need for skilled welders. Leaders serve on the college’s program advisory committee, helping to ensure graduates are well prepared, and works with Fox Valley to proactively promote welding careers in the K-12 education system.

• **Dengensha America** has opened a customer service and support branch office in Cincinnati, Ohio. The sales and service support center, established to provide a more timely response for resistance welding users in the southern territory, is staffed with a sales manager, service engineer, customer service, and support specialists.

• The welding technology program at **Clark College**, Vancouver, Wash., is offering its students certification tests approved by the **Washington Association of Building Officials** and required for welding professionals performing code work in the state. Tests for 3G Limited Certification and 3G and 4G Unlimited Certification can be taken by students and recent graduates at the college for reduced rates. Welding professionals in the community can also take the tests at Clark but are not eligible for student prices.

• **Solar Atmospheres** has been awarded Nadcap 18-month merit status for heat treating at the Souderton, Pa., facility. The company demonstrated its quality commitment by satisfying customer requirements and industry specifications.

• **Randolph Community College**, Asheboro, N.C., is offering a new basic fabrication course to enhance welding and fabrication skills, as they relate to industry, with an emphasis on structural welding techniques. The first course is being held twice a week, January 23 to March 29, at the Asheboro Campus.

• **MoviTHERM Advanced Thermography Systems**, Irvine, Calif., has expanded its U.S. sales channels for infrared nondestructive examination systems. This will be backed by **Composite Automation, LLC**, Collingswood, N.J., a company with more than 30 years of experience. **WJ**



WE CAN HELP YOU FIND THE RIGHT FIT

Make Donaldson your first call for replacement filters and parts—no matter the collector. We stock over 90,000 filters and replacement parts including:

- Cartridge filters
- Bag filters
- Pleated bag filters
- PowerCore® filter packs
- Panel filters
- Parts (hardware, motors, cages, rotary valves, ductwork, controls, fans, and more)

Live, expert service specialists can help you determine the size and style you need within minutes. Plus, our Ready 2 Ship program means your order is out the door within 24 hours.

Call now to order your replacement filters and parts.



For info, go to aws.org/ad-index



800.365.1331
Donaldson.com

© 2017 Donaldson Company, Inc.

TRUMPF Opens Technology and Laser Center in Silicon Valley



The new TRUMPF laboratory in Santa Clara, Calif., features up-to-date technology ranging from lasers to generators. Pictured is the optical arrangement in a TruMicro microma-chining laser. (Photo: TRUMPF.)

TRUMPF has opened a technology and laser center in Santa Clara, Calif., with continuous-wave, short, and ultrashort pulsed lasers as well as beam sources and generators. Its Silicon Valley location puts the facility close to users and associates from many industries, including companies from the consumer electronics and e-mobility sectors.

“Our new application laboratory for laser processing, micro applications, and coating technology places us firmly at the heart of the U.S. technology industry and brings us close to our customers and partners in this region,” said Peter Leibinger, vice chairman, managing board, TRUMPF Group and head of the laser technology/electronics division.

TransCanada to Proceed with \$655 Million Saddle West Natural Gas Project

TransCanada Corp.’s wholly owned subsidiary, NOVA Gas Transmission Ltd. (NGTL), is proceeding with an expansion of the Saddle West Project. This will increase the total natural gas transportation capacity on the northwest portion of the NGTL System — which is connected to one of the continent’s largest supply basins, the Western Canadian Sedimentary Basin — by approximately 355 million ft³/day. It is expected to be in service in 2019.

The project will include 29 km of 36-in. pipeline looping of existing mainlines, the addition of five compressor units at existing station sites, and new metering facilities.

Karl Johansson, executive vice president and president, natural gas pipelines, mentioned NGTL’s footprint enables meeting the increased transportation needs of customers in the Montney, Duvernay, and Deep Basin areas.

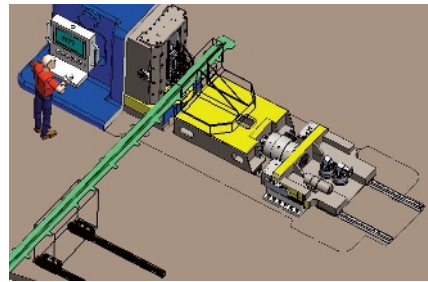
An application to construct and operate the project will be filed with the National Energy Board in the third quarter of 2017. Construction is expected to begin in 2018.

Arconic Signs More than \$450 Million in Agreements; Reinforces 3D Printing with Airbus

Arconic, Cleveland, Ohio, has signed more than \$450 million in long-term agreements over the past year with customers in North America, South America, Europe, and Asia for its forged aluminum wheels. The largest is with PACCAR, a manufacturer of light- to heavy-duty trucks. The company will supply forged aluminum Alcoa® wheels for

these trucks under the Kenworth and Peterbilt nameplates. Additionally, the company has entered into two agreements to supply Airbus 3D printed metal parts for the airplane maker’s commercial aircraft. It will supply 3D printed components made from high-temperature nickel superalloys and 3D printed titanium airframe parts under two separate agreements. The first parts under both agreements are expected to be delivered in the second quarter of 2017.

Manufacturing Technology Forms Partnership with LIFT to Deliver Large Linear Friction Welding Machine



This linear friction welding machine (displayed is a rendering) will use aerospace technology for full-size demonstrator parts in automotive and transportation industries.

Manufacturing Technology, Inc., South Bend, Ind., will develop what it claims is North America’s largest linear friction welding machine in terms of force capacity and tooling envelope. This will be delivered to LIFT (Lightweight Innovations for Tomorrow),

Detroit, Mich., for use in lightweight metals research and development projects.

The LF35-75 welding machine, currently under development and set for completion in spring 2018, will be housed in LIFT’s Corktown manufacturing center. It will bring the linear friction welding technology used in aerospace to achieve light weighting in blisks and integrally bladed rotors in aircraft engines to the automotive industry.

Acquiring this machine is part of LIFT’s recent \$50 million investment, with IACMI (The Composites Institute), in their shared Detroit facility. It will enable manufacturers to weld full-size demonstrator parts in the United States.

National Tooling and Machining Association Selected as National Partner to Grow Manufacturing Apprenticeships

The National Tooling and Machining Association (NTMA), Cleveland, Ohio, is partnering with the National Institute for Metalworking Skills (NIMS), Fairfax, Va., which has been selected by the United States Department of Labor as an industry intermediary to support expanding registered apprenticeships within manufacturing.

NTMA will work with NIMS to increase access to apprenticeships and assist employers in developing new programs. As part of this initiative, \$500,000 is available to support companies in establishing a registered apprenticeship program with the Department of Labor.

In addition, NTMA will help members establish and register apprenticeship programs with the Department of Labor utilizing its online training resource. [WJ](#)



INNOVATION TO WORK



MAY 2-4, 2017

CINTERMEX | MONTERREY, MEXICO



EXPERIENCE FABTECH MEXICO 2017

- More than **575** action-packed exhibits
- **140,000** nsf exhibit space
- Top-notch **education program**
- **Invaluable networking**
- More than **13,000** industry colleagues



**EXHIBIT, ATTEND OR
SPONSOR TODAY!**

Learn more at www.fabtechmexico.com



CO-SPONSORED BY:



Q: Filler metal selection for aluminum welding is a subject I receive many enquiries about. Therefore, I have compiled a selection of questions asked on a regular basis. These are associated with several applications using a variety of aluminum base metal types. I hope to highlight how the considerations relating to filler metal selection for aluminum welding are different from those used when selecting a filler metal for most other materials.

What aluminum filler metal would be the most appropriate for welding the following aluminum base metals used in the described applications, and why?

Question 1: A handrail made of 6061-T6 tubing that will be postweld anodized and required to have a good color match between the base metal and weld after anodizing. (Note: Anodizing is an electrochemical surface treatment that can be applied to aluminum to increase aluminum oxide thickness and provide improved surface characteristics in some applications.)

Answer 1: Tubing made from 6061-T6 can be welded with either 4xxx or 5xxx series filler metals. Filler metals 4043, 4943, and 5356 are often used to weld this popular base alloy. However, this is an application that will be postweld anodized, and using a 4xxx series (silicon based) filler metal will create a color match problem after the weldment is anodized. The silicon in the 4043 or 4943 will cause the weld to become very dark in contrast to the lighter colored base metal after anodizing. Any of the 5xxx series filler metals would be suitable for this application; 5356 filler is often the choice as it is most readily available and will provide a close color match.

Question 2: An aluminum bracket that is part of a heating system made from 6082-T6 base material. This component will be postweld anodized, is required to have a good color match after anodizing, and is to be used in an application with a sustained temperature of around 250°F. Should I use 4043 or 5356 filler metal?

Answer 2: Our choice for this application has become a little more

complicated than in question one, as we now have two important criteria. First, we have the anodized color match after welding requirement, and second, sustained service at an elevated temperature.

The definition of elevated temperature for aluminum is a temperature above 150°F. Prolonged exposures to temperatures between 150° and 350°F can have a detrimental effect on aluminum alloys that contain more than 3% magnesium (Mg); prolonged exposure of these materials to these temperatures can promote precipitates to form in the grain boundaries of the metal that are highly anodic to the aluminum-magnesium matrix. It is this grain boundary network of precipitates, produced over time, that can create susceptibility to stress corrosion cracking (SCC) and the potential for premature component failure.

The 5356 filler metal, which we may have chosen to obtain a good color match after anodizing, contains more than 3% Mg (it contains 4.7 to 5.5% Mg) and is therefore an unsuitable choice for this elevated temperature application. We cannot seriously consider the 4043 filler metal (suitable for elevated temperature service) because its silicon content will provide a very poor color match after anodizing.

For this application requiring color match after anodizing, and elevated temperature service, we should consider filler metal 5554. Filler metal 5554 has slightly lower strength when compared to 5356, but its Mg content is 2.4 to 3.0%, making this filler metal suitable for elevated temperature service. In addition, because it is an aluminum-magnesium alloy that does not contain intentionally added silicon, it will provide a reasonable color match after anodizing.

Question 3: An aluminum test fixture frame made from 6061-T4 base metal. This structure will be postweld artificially aged to strengthen the completed structure by taking it from the -T4 temper to the -T6 temper. The fillet welds must have optimum strength after postweld heat treatment (PWHT).

Answer 3: The primary consideration here is filler metal strength after PWHT. This base metal is most often welded in the -T6 temper (solution heat-treated and artificially aged condition); when welded in this temper,

the as-welded strength in the heat-affected zone (HAZ) is considerably reduced. One method of improving the HAZ strength in these heat-treatable alloys is to weld them in the -T4 temper (solution heat treated and naturally aged), which is a lower strength than the -T6 temper, and then to perform postweld artificial aging (typically around 350°F for 10 to 12 h) to increase the strength of the entire -T4 structure and to improve the strength of the HAZ.

This base metal is often welded with a 4xxx and 5xxx series filler metal. However, in this application, we would not select a 5xxx series filler metal such as 5356 as this type of filler is not suitable for PWHT. Therefore, we must consider one of the 4xxx series filler metals. The 4043 filler metal could be used for such an application; however, 4043 is not a heat-treatable filler alloy. That is, 4043 will not produce adequate strength to match the 6061-T6 base material in the -T6 condition. The obvious choice for this application is a filler alloy that will naturally respond to PWHT. Filler metal 4643 was developed by Alcoa in the 1960s specifically for this purpose. It is similar to 4043 but includes the addition of magnesium, which provides it with the ability to respond to strengthening through this form of PWHT. A second option for this application would be the more recently developed filler metal 4943. The 4943 filler metal was primarily designed to provide higher strength over 4043 in the as-welded condition, but it will also provide increased strength over 4643 in the postweld heat treated condition.

Figure 1 depicts a chart compiled from micro hardness testing conducted by NASA when comparing strength values of 4043, 4643, and 4943 filler metals. These tests were performed in preparation for the development of welding procedures for welding a 6061-T4 structure that was to be postweld heat treated and used on the James Webb Space Telescope (JWST) project.

Question 4: A complete joint penetration groove-weld procedure qualification test using ½-in.-thick 5083 base metal, which is required to meet the minimum transverse tensile strength specified by AWS D1.2, *Structural Welding Code — Aluminum*. Should I

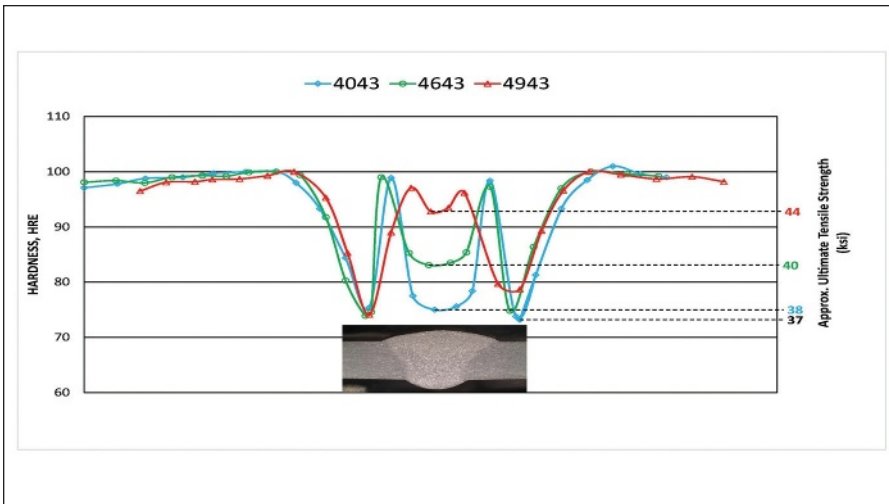


Fig. 1 — NASA test data showing comparison of the postweld aged strength for 4043, 4643, and 4943. The macro photograph of the groove weld below the three colored data point lines is added to assist in the physical location relating to the difference in strength as the test moves from -T6 base metal, into the HAZ, through the weld metal, second HAZ, and back to the -T6 condition. NASA's reason for this test is the data in the graph's center, which shows approximate comparative strengths of the three filler metals. The test was conducted to provide data that can be related to the weld strength of fillet welds. The postweld-aged filler metal tensile strength comparisons are approximate and calculated from the hardness values as follows: 4043 (38 ksi), 4643 (40 ksi), and 4943 (44 ksi). Based on the test data obtained by NASA, the 4943 filler metal was chosen for this project. (Graph sourced from James Webb Space Telescope (JWST) Project Space Environment Simulator (SES) Integration Frame (SIF) Welding Development Report June 7 2012.)

use 5356, 5183, or 5556 filler metal?

Answer 4: This is a selection that is primarily concerned with the strength of the filler metal and its ability to meet that of the base material in the as-welded condition. The minimum transverse tensile strength required for procedure qualification of complete joint penetration groove welds made with the (5xxx series) nonheat-treatable aluminum alloys is based on the annealed strength of the base metal being welded. If this were a fillet weld qualification test with 5083 base metal and not a complete joint penetration groove weld, the small differences in filler metal shear strength values may or may not be significant. Certainly, welding procedures for fillet welds made on 5083 base metal could be easily qualified with all three of these filler metals. However, when it comes to tensile strength requirements for complete joint penetration groove welds, there can be differences between these filler metals that may affect test results. In some cases, the strength differences between these filler metals, although quite small, can

POWERBALL®

TORCH PRODUCTS

HIGH PERFORMANCE MIG WELDING GUNS

PROUDLY MADE

NEW

- ▶ Maximum conductivity with superior cooling
- ▶ Long-life, energy efficient PowerBall® consumables reduce operating costs
- ▶ Rounded tip & reduced heat prevents spatter build-up and burn backs
- ▶ Durable ergonomic handle with comfort grip and adjustable trigger pull
- ▶ High performance semi-automatic & robotic torches available

WELDERS CAN FEEL, HEAR & SEE THE DIFFERENCE!

ELC ENTERPRISES, INC. 517-782-8040 • wire-wizard.com

For info, go to aws.org/ad-index

HDE Technologies, Inc.

Industrial Laser Applications

40
years
2016

916 - 714 - 4944

Laser Welding and AM* Technologies

*(introduction to Additive Manufacturing)

Comprehensive classroom training of key technologies

- Lasers and optics - characteristics and selection
- Metallurgy - selection of alloys and powders of alloys
- Metallurgy - compensation for changes in alloying
- Control of transient heat and solidification
- Porosity and voids
- Current standards related to laser welding

Schedule of classes for 2017

- Feb. 20 - 24, 2017, Phoenix, AZ
- June 5 - 9, 2017, Minneapolis, MN
- Oct. 9 - 13, 2017, Phoenix, AZ

On-site classes - may be scheduled as needed

Register NOW >>>>

www.laserweldtraining.com

www.hdetechologies.com

For info, go to aws.org/ad-index

WORK SMART



Model 200 Positioner
3 models available:
100 pound, 200 pound and
500 pound capacity.



Model 1200 Pipemate
Rotates pipe and tube
from 1 1/2" to 17" diameter,
up to 1200 pounds.

Smart Work Handling
Means
Increased Productivity



800-962-9353
www.atlaswelding.com

For info, go to aws.org/ad-index

mean the difference between passing and failing a procedure qualification transverse tensile test. Also, the strength of any one of these filler metal classifications can differ from one batch to another based on the actual magnesium content of the alloy and where it resides within the classification chemistry range limits.

The 5356 filler metal was developed for welding 5086 base metal and to match, or slightly exceed, its annealed tensile strength (35 ksi), which is lower than the annealed tensile strength of 5083 (40 ksi). Therefore, I would not recommend the 5356 filler for this application.

The 5556 filler metal was originally developed for welding 5456 base alloy to meet its tensile strength requirements (42 ksi), which is higher than 5083 (40 ksi). The 5556 filler metal will meet the minimum tensile strength requirements for 5083 base alloy, but it is not usually the filler metal of choice for 5083 base metal.

The 5183 filler metal was produced specifically to meet the tensile strength requirements on 5083 base materials and does so successfully when used in its mid-range chemistry. I recommend evaluation of 5183 filler metal for this application.

Question 5: I must weld an A356.0 aluminum casting to a 6061-T6 extruded section.

Answer 5: It is common to weld dissimilar aluminum base metals together. However, not all aluminum base metal combinations are suitable for welding to each other. The metal combinations to avoid are the high silicon to the high magnesium base alloys, and the high copper to the high magnesium base alloys. This particular combination, A356 to 6061, is not usually a problem. However, we must carefully consider the most appropriate filler metal to use. The 6061 base metal can be welded to itself with 4xxx or 5xxx filler metal, with the 4043 and 5356 filler metals as the most commonly used. However, the A356 casting has high silicon content (around 7% Si) and therefore should not be welded with a 5356 filler metal, which has a high magnesium content (around 5% Mg). Either the 4043 or 4943 silicon based filler metals would be good filler metals to evaluate for this application.

Question 6: I must repair a machined aluminum component made of 6262 base metal.

Answer 6: There are a small group of aluminum base alloys that were developed for their machinability characteristics and not for their weldability. One of these is alloy 6262 and another is 2011. These two base metals have lead, bismuth, and/or tin added in small quantities to facilitate their machinability. These small additions of low melting point metals seriously increase their solidification cracking tendency. Therefore, these base metals are typically mechanically fastened rather than welded.

Summary

Filler metal selection is perhaps one of the most significant challenges when developing welding procedures for various applications. These six examples illustrate not only the base material chemistry, but also that the application of the completed weldment, can strongly influence your choice in selecting the most appropriate filler metal for a given base metal in a specific application.

Fortunately, there are several excellent filler metal selection charts available to help you choose the most appropriate filler metal. Many of these provide ratings for filler metals on such characteristics as strength, crack sensitivity, ductility, color match after anodizing, corrosion resistance, elevated temperature service, toughness, and PWHT. Contact me if you would like a filler metal selection chart. I will send you one free of charge. [WJ](#)

TONY ANDERSON is director of aluminum technology, ITW Welding North America. He is a Fellow of the British Welding Institute (TWI), a Registered Chartered Engineer with the British Engineering Council, and holds numerous positions on AWS technical committees. He is chairman of the Aluminum Association Technical Advisory Committee for Welding and author of the book Welding Aluminum Questions and Answers currently available from the AWS. Questions may be sent to Mr. Anderson c/o Welding Journal, 8669 NW 36th St., #130, Miami, FL 33166-6672; tony.anderson@millerwelds.com.



American Welding Society®
MEMBERSHIP

SOMETHING
BIG
IS HERE



membersnetwork.aws.org

The AWS Member Network is a brand new online community exclusively for AWS Members.

- Discussion Groups – collaborate, ask questions, give answers & discuss hot topics
- Resource Library - share documents, presentations, videos, photos, and more
- Directory – connect with other members who have similar backgrounds and interests
- Wiki Glossary – find terms specific to the welding industry
- Event Calendars – view important AWS Member events and opportunities
- And much more

Visit: membersnetwork.aws.org



Q: We are going to braze 316 stainless steel parts for a device to work in an ITER reactor system. This means brazed joints may be irradiated by a fast neutron flux $\geq 2 \times 10^{20}$ n/cm², at 300–400°C. The assembly should preserve the performance characteristics permanently within the service life of ITER, which is ~30 years. We know radiation is a factor that may affect mechanical properties of large metal pieces, including those stainless steel ones. But we'd like to know if the radiation affects mechanical properties of brazed joint material, which is very thin. Also, because replacement in such places is difficult or impossible during reactor operation, how do we select a filler metal that should withstand possible damage?

A: Very little information is published pertaining to behavior of brazed joints in such application. Basic studies and tests were performed 40–50 years ago. Industry standards are based primarily on this experience. From these tests, two types of irradiation damage to the mechanical properties have been found: 1) atom displacements and 2) n , α -reactions (Ref. 1). Atom displacements are produced by fast neutrons. So this is your case.

These displacements increase strength of metals and produce a low work-hardening structure. This can result in lower ductility as measured by elongation at break using a tension test. This irradiation damage can be removed by post-irradiation annealing. For example, 1 h at 500°C (932°F) is sufficient to partially recover ductility of stainless steel irradiated at 50°C (122°F) by the neutron fluence of 10^{20} n/cm² (Ref. 1).

The second type of embrittlement is only observed when the metal is stressed at creep temperatures, such as at 40–50% of the melting point. Helium produced by both fast neutron or thermal reaction affects the process of intergranular fracture. Any grain boundary cracks appear easier and propagate faster in the irradiated alloy. In contrast to the atom displacement damage, the n , α -reactions do not affect yield strength of the alloy, while creep strength may be reduced. Also,

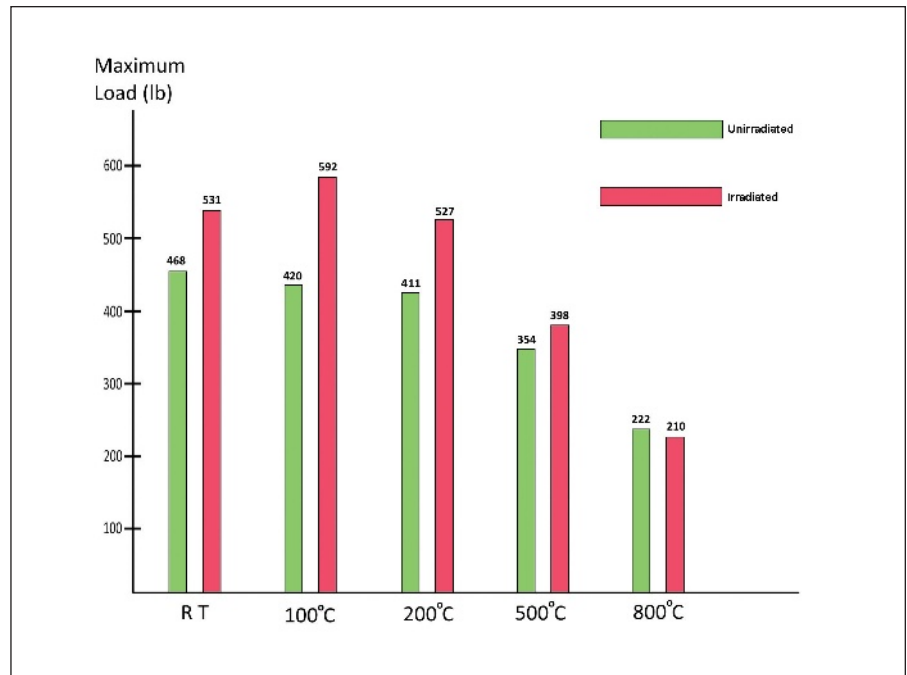


Fig. 1 — Load-carrying capacity of irradiated and unirradiated 304 stainless steel joints brazed by BNi-7 filler.

the defected structure cannot be improved by a post-irradiation annealing.

It was also found that contents of some alloy components such as boron and silver are critical and should be limited or avoided in welded or brazed alloys subjected to irradiation. The ^{10}B n , α -reaction is a principal source of helium in the thermal neutron range (Ref. 1). As boron is presented from 1.5 to 4 wt-% in some brazing filler metals of the BNi family typical for brazing stainless steels (such as BNi-2, BNi-5a, or BNi-9), these filler metals are not recommended for application. Such brazing alloys as BNi-5, BNi-7, or BNi-12 containing <0.03 wt-% of boron can be used after testing, while BNi-6 or BNi-8 are suitable for brazing stainless steel in reactor parts because they do not contain boron at all.

In general, the use of silver-containing alloys is also not recommended for reactor applications. It is estimated that during ITER life about 5% of silver can transmute into cadmium isotopes, mainly to ^{109}Cd that can cause a small effect of bonding properties (Refs. 2, 3). This means that silver-based filler metals of the BAg family, also typical for brazing stainless steel, are not recommended for your application.

The bottom line is you can choose the filler metal among the above me-

nioned BNi-6, BNi-8, BNi-5, BNi-7, or BNi-12 after appropriate testing according to conventional industrial specifications. The strength of the irradiated and unirradiated 304 stainless steel joints brazed by BNi-7 was studied in Ref. 1 in the range of temperatures from RT to 800°C (1472°F). The shear strengths of brazed joints at low temperatures were higher due to the fast neutron displacement damage (Fig. 1). At 500°C and above, holding for 30 min prior to the deformation was sufficient to remove the negative effect of irradiation. This test confirmed that irradiation did not result in degradation of strength of brazed joints.

At the same time, we have to remember that conditions of the base metal play a significant role in the strength of brazed joints. From this point of view, the post-irradiation annealing of stainless steel is recommended. Annealing at 400°C does not provide a positive effect on the steel with radiation defects and only slightly lowers the defect density. Besides, the martensitic phase was no longer observed in the irradiated stainless steel (Ref. 4). Annealing at 500°C effectively reduces the hardness, and recovers the ductility, of the irradiated stainless steel, as well as restores hard-

ening workability of this material. The intergranular fracture is significantly reduced after 3.5 h, and eliminated after 6 h of holding at 500°C (Ref. 4). **WJ**

References

1. Martin, W. R., and Slaughter, G. M. 1966. Irradiation embrittlement of welds and brazes at elevated temperatures. *Welding Journal* 45(9): 385-s to 391-s.
2. Loughlin, M. 2008. Nuclear issues for the ITER design. *Proc. of International Conference on Nuclear Energy for New Europe*. Eds. S. Rozman, T. Zagar, and B. Zefran. Portoroz, Slovenia.
3. Gusarov, A. 2013. Irradiation effects on the optical and mechanical performance of ITER prototype window assemblies. *Fusion Engineering and Design* 88: 1192-1195.
4. Van Renterghem, W., Al Mazouzi, A., and Van Dyck, S. 2011. Influence of post irradiation annealing on the mechanical properties and defect

structure of AISI 304 steel. *Journal of Nuclear Materials* 413: 95-102.

This column is written sequentially by TIM P. HIRTHER, ALEXANDER E. SHAPIRO, and DAN KAY. Hirthe and Shapiro are members of and Kay is an advisor to the C3 Committee on Brazing and Soldering. All three have contributed to the 5th edition of the AWS Brazing Handbook.

Hirthe (timhirthe@aol.com) currently serves as a BSMC vice chair and owns his own consulting business.

Shapiro (ashapiro@titanium-brazing.com) is brazing products manager at Titanium Brazing, Inc., Columbus, Ohio.

Kay (dan@kaybrazing.com), with 40 years of experience in the industry, operates his own brazing training and consulting business.

Readers are requested to post their questions for use in this column on the Brazing Forum section of the BSMC website brazingandsoldering.com.



SPECIALTY CORED WIRES
COATED ELECTRODES
SOLID WIRE MIG AND TIG



Manufacturing Flux Cored Welding Wire

- Cobalt
- Nickel
- Hardface
- Stainless
- Alloy Steel
- Tool Steel
- Maintenance
- Forge Alloys
- Custom Alloys



COR-MET, INC.

12500 Grand River Rd.
Brighton, MI 48116
PH: 800-848-2719
FAX: 810-227-9266

www.cor-met.com
sales@cor-met.com

For info, go to aws.org/ad-index

Take a look inside



The best kept secrets in the Welding Industry

- **Widest range of Hardfacing and Cladding wires**
 - Including a New all-position general hardfacing wire
- **Extensive line of Specialty Alloy Stainless Steel wires**
 - Including duplex super-duplex stainless, and controlled ferrite alloys
- **Complete line of Cobalt based wires**
 - Stelloy 1, 6 and 21 in-stock for immediate shipment
- **New line of Tubular Hardfacing Electrodes**
 - Allowing for lower heat input with less dilution, and high productivity

Call us first !

Welding Alloys
Tel: (859) 525-0165 • www.welding-alloys.com

For info, go to aws.org/ad-index

Report Provides Global Arc Welding Machine Market Outlook for 2016–2021

Manual Arc Welding Machine Market 2016 to 2021 — Analysis of Key Vendor and Market Status Overview evaluates worldwide markets for manual arc welding machines over a five-year pe-

riod. It provides market forecasts according to subsectors and region/country, including North America, Europe, Asia-Pacific, the Middle East, and Africa. Also covered are the factors affecting supply and demand; opportunities and challenges faced by industry participants; leading companies and their strategies; market trends; and technological developments. The

report spans 92 pages including tables and figures.

Market Study Report
marketstudyreport.com
 (866) 764-2150

Specially Formulated Abrasive Wheel Cuts Aluminum



The resin-bonded Magna-Cutter™ abrasive cut-off wheel cuts aluminum sheet, plate, tubing, and structural components. The product is available in 3- and 4-in. diameters, and formulated to cut aluminum fast, cool, and clean with no loading. The product also contains no ferrous materials for contaminant-free cutting.

Motor Guard Corp.
motorguardplasma.com
 (800) 227-2822

Flame-Resistant Welding Mat Designed for Safety

The SmashPad™ delivers a flame-resistant foam cushion that safeguards



STOP

(Using a crane to flip over large parts)

Start

Using Modular Rollover Fixtures

- ✓ Free Fixture Designs
- ✓ Reusable Tooling Kits

- ✓ In-Stock Delivery
- ✓ On-Site Training

- ✓ Rental Options
- ✓ Lifetime Warranty

BLUCO CORPORATION
 3500 Thayer Court - Aurora, IL 60504
www.BLUCO.com - 800-535-0135

For info, go to aws.org/ad-index

against sparks and spatter while providing comfort to alleviate the aches associated with kneeling, sitting, and leaning during welding. The 16 × 19-in. welding mat consists of a 15-oz fiberglass outer shell combined with a 30-oz silicone-coated top surface. The product also contains flame-resistant hooks and loop fasteners, allowing for two or more mats to be connected.

Black Stallion®
 blackstallion.com
 (800) 527-3826

GMAW Gun Handle Offers Ergonomic Benefits

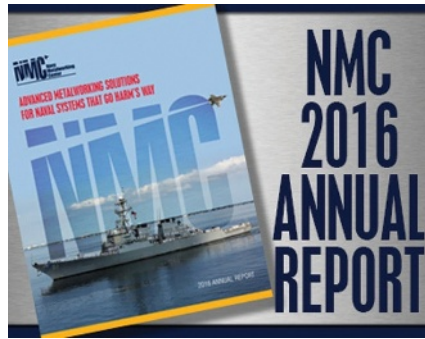


The GMAW gun C series straight handle delivers the same features as the earlier T series straight handle, plus additional ergonomic benefits including a handle overmold and rear swivel. The product is designed for the guns rated from 200 to 500 A in the BTB semiautomatic GMAW gun line. The product can be customized by visiting the online gun configurator and selecting the consumable series and trigger options.

Bernard
 bernardwelds.com
 (855) 644-9353

Navy Metalworking Center Unveils 2016 Annual Report

The 2016 *Navy Metalworking Center Annual Report* highlights the organization's current projects, as well as the development of advanced metalworking technologies for naval weapon systems. The report covers manufacturing tooling development, joining technologies, advanced metrology and inspection technologies, manufacturing



process optimization, and coatings application and removal.

Navy Metalworking Center
 nmc.ctc.com
 (800) 282-4392

Welding Gun Features Built-In Fume Extractor

The RoboVent Extractor™ combines a welding gun with an extraction sys-

Why settle for a weld like this?

When you could have this?

Save Time & Money While Improving Weld Quality!

Purge Monitors (Oxygen to 1ppm)

Assorted Purge Kits Available

INTERPURGE 1.800.665.6655
 www.InterPurge.com

For info, go to aws.org/ad-index

www.polysoude.com

A
S
T
R
O

A
R
C
POLYSOUDE

Orbital Welding
Automated Welding
Weld Overlay Cladding
Related Services

For info, go to aws.org/ad-index



tem that captures 90–95% of fumes at the source as soon as they are generated. The product employs a dust-collecting, high-vacuum filtration system to filter toxic fumes, which are collected in a package just slightly larger than a standard welding gun. Also featured is the product's lightweight and maneuverable handle combined with a streamlined nozzle designed for maximum visibility and control. The product is intended for GMAW and other welding processes that employ shielding gases.

RoboVent
robovent.com
(888) 762-6836

Flowmeter Regulators Deliver Increased Argon Capacities



The 20 series single-stage flowmeter regulators offer argon flow capabilities of up to 55 ft³/h coupled with self-centering flowball technology that provides accurate flowmeter readings even when tipped. Multiple scales are available for use with other shielding

gases to cover most GMAW and GTAW applications. Extra-long flow tubes make expanded scales easy to read and accurate within 5% of full-scale reading. An aluminum housing protects the flow tubes from damage, while also providing an unobstructed view of the flow reading.

Miller Electric Mfg. Co.
millerwelds.com
(800) 426-4553

Eyewear Fashioned for Women Provides In-Style Protection



The Erda eyewear line designed for female workers offers large-frame safety glasses in 34 color and lens combinations, as well as Fog-Off[®] antifog technology and polarized options. The product is softer and more rounded to prevent snagging in long hair while also providing four times the eye protection suggested by industry standards. An optional foam gasket insert safeguards against debris. It is easily removable to switch from safety to fashionable glasses.

Ergodyne
ergodyne.com
(800) 225-8238

Headsets Allow Communication while Blocking Unsafe Noises

The PELTOR[®] line headsets eliminate hazardous sounds without



impairing the user's ability to communicate or hear important warning sounds, such as alarms and signals. The product line has been expanded to include four new headsets: ProTac™ Hunter, ProTac™ Shooter, ProTac™ III, and WorkTunes™ Pro AM/FM Radio. These products provide noise-attenuating ear cups to provide safety in high-noise environments, user-friendly controls, and the option of connecting to a smart phone, radio, shoulder mic, or other external devices.

3M™
3M.com
(800) 328-1667

Website Launches 2016 Guide for Buying Welding Equipment

An updated guide for selecting proper welding equipment has been released on *welderworld.net*. It lists the latest welding trends, developments, and equipment along with product reviews and specifications, including input capacity, power capacity, amperage capacity, duty cycle, and portability. The product helps users pick equipment that suits their needs according to changing user reviews and testimonials from 2016.

Welder World
welderworld.net

Auto-Darkening Filter Safeguards Against Radiation

The X540V automatic darkening filter protects users from harmful ultraviolet and infrared rays in both light and dark states. The product offers a light shade of 4 along with a dark shade of 9–13, as well as a GTAW 10 rating, four sensors, and an Xtreme® viewing area of 12.6 in. The product also pairs with any of the company's Vision® welding helmets.



ArcOne®
arc1weldsafe.com
(800) 223-4685

WWW.COMMERCIALDIVINGACADEMY.COM 888.974.2232

WANT TO LAND A JOB AFTER GRADUATION?

Employers want commercial divers that are **internationally certified**.

CDA Technical Institute's Commercial Diver Program offers the internationally recognized DCBC Unrestricted Surface Supplied Divers Certification.

Start your career training in an internationally recognized Commercial Diving and Underwater Welding program.

Financial aid available for those who qualify • Approved for Veterans Benefits
For more information about graduation rates, the median debt of students who completed the program and other important information, visit www.cda.edu.

For info, go to aws.org/ad-index

For info, go to aws.org/ad-index

SKY'S THE LIMIT!

PROWRITE CLOUD

WELDERS eSIGNATURES
PQR | WPS | WPQ
ASME SEC. IX & AWS D1.1
INDUSTRY LEADING SOLUTION

Access your welding documents from virtually any system with almost zero IT overhead

THINKCEI.COM/PW
800-473-1976

Integrates with CEI's widely used DesignCalcs

For info, go to aws.org/ad-index

Preparing Aluminum before Welding

Different process options from thermal and mechanical cutting to oxide removal are examined

BY MIKAEL D. CARRIERE

Aluminum is being used more often for many different applications because of its material properties such as strength-to-weight ratios, corrosion resistance, the abundance of its raw form bauxite, and the relative ease of making aluminum.

With an increased use of aluminum comes the need to be able to weld the material with high quality. This article focuses on material preparation of aluminum prior to welding. When looking at the properties of aluminum that affect the quality of the welds, such as the high solubility of hydrogen in its

molten state, preparation of aluminum becomes a high priority.

Material Storage

Aluminum forms an oxide layer as soon as the material is subjected to oxygen. The rate at which the oxide grows highly depends on storage conditions such as temperature and relative humidity of the storage area. Aluminum oxide is porous and can become hydrated even when water is not in contact with the material. The best

practice is to store aluminum indoors to avoid weather elements. In some industries, indoor storage of aluminum plates is not practical, and in some cases, not possible. When aluminum is being stored outdoors, it should be stored vertically with space in between the sheets to allow rain water to flow freely off of the plates and to avoid wicking. Also, any interleaving should be removed to avoid water pocketing in between the interleaving and the aluminum plate.

Thermal Cutting Processes

Plasma Arc Cutting

Plasma arc cutting is the most widely used thermal cutting process for aluminum — Fig. 1. It is very quick on thin materials and can cut up to 6-in.-thick aluminum plate at slow cutting speeds. To achieve a quality cut, thickness and travel speeds must be set correctly. When the travel speed of cutting is faster than optimum, the quality of the cut can be sacrificed. Typically, air plasma cutting can be used for cutting material thicknesses up to $\frac{1}{4}$ in. When plasma cutting a plate thicker than $\frac{1}{4}$ in., it is recommended to use argon or nitrogen as a plasma gas to increase cutting capabilities.

Plasma cutting can be done manually or using a mechanized or automated cutting table. The disadvantages of plasma arc include high heat inputs that can cause microcracking at the cut

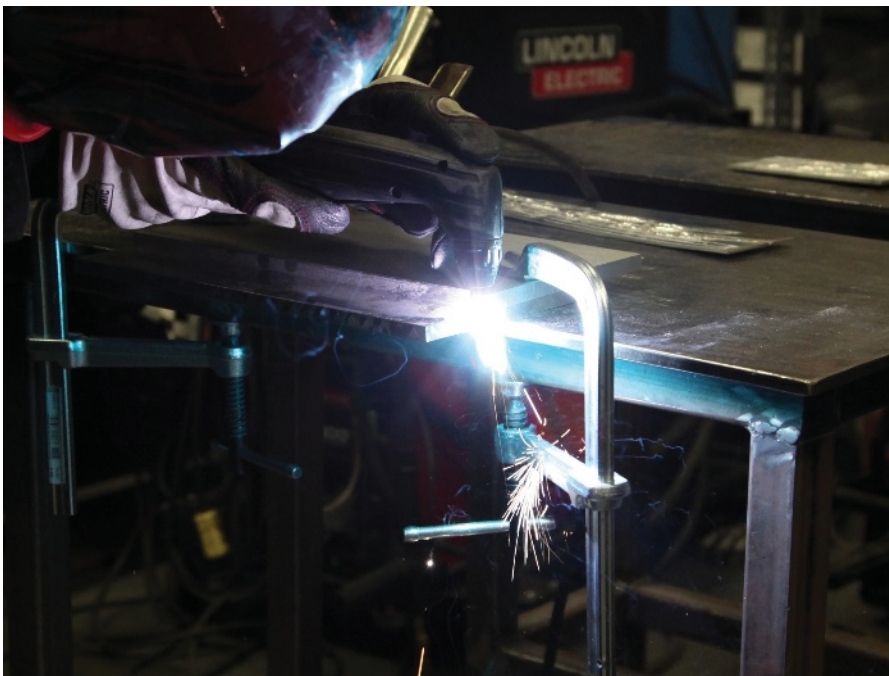


Fig. 1 — Plasma cutting aluminum using a hand-held system.



Fig. 2 — Gas tungsten arc welding showing an assortment of grinding and sanding discs.

interfaces. It is good practice to remove $\frac{1}{8}$ in. of the material from the cut edge to discard any cracking that may have occurred. In addition, the cut edge can have a kerf and slight roughness to it, and noise levels are high and may require hearing protection.

Laser Beam Cutting

Laser beam cutting technologies are used to cut aluminum as well. The advantages of laser beam cutting include the ability to cut thin material without causing distortion, less heat-affected zone, and kerf and cut surfaces are very smooth. One disadvantage is the thickness of material that can be cut is limited to about $\frac{3}{8}$ in. (~13 mm). Similar to plasma cutting, the laser cutting process can result in liquation cracking mainly in heat-treatable alloys. Laser

cutting is also more expensive than plasma cutting, it is not a portable process, and there is an increased amount of dross on the underside of the plate. High-power lasers are required for cutting due to the high reflectivity of aluminum, which can also decrease the life of the laser.

Mechanical Cutting

Mechanical cutting is very useful for the preparation of aluminum before welding. For the most part, the processes are very efficient and inexpensive. One thing that should be noted is the need for cutting lubricant is less than when cutting steels, but if it is used, ensure the oils are removed using the methods explained in the "Preparation of Aluminum before Welding" section.

High-Pressure Waterjet Cutting

Waterjet cutting utilizes high-pressure water with the addition of an abrasive garnet. Water pressures can reach up to 100 kilo-pounds per square inch (ksi) and the velocity of the water can reach speeds of Mach 3 or 2283 mph. Temperatures only reach 193°F, which allows the aluminum to be cut without causing liquation cracking like the thermal cutting processes. This process can cut aluminum up to 9.25 in. thick. There are, however, limitations. Cutting speeds are slower compared to plasma. For example, travel speeds may be as slow as 3.8 in./min when cutting aluminum with the thickness of 1.5 in. In addition to this, waterjet cutting systems are expensive and not portable.



Fig. 3 — A stainless steel wire brush can be used on aluminum to reduce the oxide thickness.

Machining

Machining of weld preparations can be performed using a variety of tools. Milling machines, bed planers, and shapers are commonly used with carbide cutting tools. It is recommended that any machining be performed without any cutting lubricants.

Sawing

Both band and circular saws are commonly used to make weld preparations. Higher blade speeds and finer teeth are required than when cutting steel. Recommended blade surface speeds are 3400–4200 surface ft/min for carbide circular saws and 3500 surface ft/min for band saws when cutting aluminum. Band saw blades should have no more than four teeth per inch. If circular saws are used, the cut quality can be good enough so that no further preparation is necessary. Band saws usually leave a coarse surface that must be sanded or ground.

Grinding and Sanding

All grinding and sanding discs use an organic binder to hold the abrasive material together — Fig. 2. This may introduce hydrocarbons into your weld causing porosity. Some manufacturers specify that the grinding or sanding disc is made specifically for aluminum. This simply means the abrasive used is

most effective at removing aluminum. To find out if a specific grinding or sanding disc is suitable for preparation of aluminum before welding, it is recommended to do the following simple destructive test.

- 1) Weld a 6–12 in. fillet weld using clean material.
- 2) Clamp the welded plate to a table and use a hammer to fold the weld face onto itself.
- 3) Check the fracture surface of the weld to see if it exhibits porosity.
- 4) Once you are sure that under normal conditions the welding process does not create porosity, use the grinding or sanding disc you would like to test to remove some aluminum from the area you will be welding to make the fillet weld.
- 5) Repeat steps 1 through 3.

Shearing

Shearing is very useful to cut sheets or plates to size. However, the edge quality is rarely acceptable for welding. It is relatively rough and has a lot of crevices that can trap oils, greases, etc. It is recommended that the edge be smoothed by machining, grinding, or sanding after shearing.

Routers and Carbide Burrs

Routers can be used for repairs and backgouging. Caution must be taken for a few reasons; if using an air-powered router, ensure that there is a dryer on the line to prevent moisture from getting on the workpiece. Ensure that when using for repair work or backgouging, the material is removed to sound metal to avoid weld defects.

Preparation of Aluminum before Welding

Oil and Grease

Because of aluminum's high hydrogen solubility in its molten state, it is recommended to remove any oil or grease from the area of welding to reduce or eliminate the possibility of porosity. Removal of oil and grease can be performed in several ways; for example, wiping with a clean rag saturated with a degreasing solvent. This method is very effective. When choosing a solvent, it is best to have a high threshold limit value (TLV) and a low flash point. For both of these reasons, it is best to consult with your environmental and safety representative.

Second, mild alkaline solutions make good degreasers. The part to be degreased can be sprayed with these solutions or dipped into a tank containing them. Since such cleaners are usually water based, it is important to thoroughly rinse and dry the part after degreasing.

Third, many suppliers sell acid-based cleaning solutions for cleaning aluminum. These are usually effective and also can remove excessive oxides. However, all are acidic and some contain hydrofluoric acid. Caution for use and disposal is required. Again, the piece must be thoroughly rinsed and dried before welding.

Whichever method is used, it is important to degrease the part to be welded before performing any of the oxide removal procedures outlined below. Otherwise the oil and grease will be spread by the oxide removal and will be difficult to remove.

Oxide Removal

Removal of the oxide layer is important before welding aluminum for a couple of different reasons. Alu-

minum oxide melts at a temperature significantly higher than that of aluminum. If welding on oxide that is excessive in thickness, oxide entrapment in the weld can occur. The oxide is porous and it has the tendency to draw in moisture in humid environments. This can lead to porosity in the weld if the material isn't properly prepared for welding.

Oxide removal can also be performed in several ways. The most common is to use a stainless steel wire brush — Fig. 3. The brush should be clean and not previously used on materials other than aluminum. The brush should be relatively flexible and used with light pressure to avoid unnecessarily roughening of the surface.

Oxide removal can also be performed by immersing the part in a strong alkaline solution. However, these solutions are very corrosive and can etch the surface of the aluminum; therefore, extreme care must be used.

In some industries, especially aerospace, final oxide removal is performed just before the joint is fit together by mechanically removing the oxide using a steel scraper (identical to those used in woodworking) or by draw filing. Once the cleaning is performed, the joint is fit together as soon as possible. These are very effective methods for oxide removal. However, they are time consuming, costly, and primarily used in industries where the demand for extremely high quality overrides the additional cost.

Conclusion

Using the guidelines outlined will surely increase the quality of aluminum welds for those who are new to welding aluminum, or for those who are having difficulty producing consistent, high-quality aluminum welds. 

MIKAEL D. CARRIERE (mikael_carriere@lincolnelectric.com) is applications manager – aluminum, Lincoln Electric Aluminum Solutions, Mississauga, Ont., Canada.

Base on a presentation at the 19th Annual AWS Aluminum Conference, Miami, Fla., Sept. 20–21, 2016.

For info, go to aws.org/ad-index

Capacitor Discharge Welder With Compact Design. Ideal For High-Strength Steel & Aluminum

With Dengensha America's compact new Capacitor Discharge Welder, you now have all the capability you need to achieve maximum part quality:

- Smaller footprint. Cost-efficient compact design.
- Weld current as high as 50kA, yet requiring only a small 6kVA power supply.
- Unique selectable current control modes enable you to fine-tune weld quality.
- High current in short bursts allows minimum heat transfer and workpiece distortion.
- Ideal for welding small projection parts on high-strength steel and aluminum.

Benefit from a broad new range of part production opportunities and potential.

Call: 440-439-8081 • Ask for Steve Andrassy
Web: dengensha.com

 **DENGENSHA AMERICA**

Engineering Resistance Welding Value★



The Midalloy Advantage



Technical Support

Global Supplier

Quality Consumables

**Stainless Steel
Nickel
Low Alloy
Flux Cored
Submerged Arc Flux
Welding Strip
Cryogenic Stainless**

Midalloy

St. Louis, Missouri
800-776-3300

Houston, Texas
866-790-9058

www.midalloy.com

For info, go to aws.org/ad-index

AWS Certification Program Update

Important changes to the CWI, CAWI, and SCWI certification programs are outlined

BY MARTY LUCIA

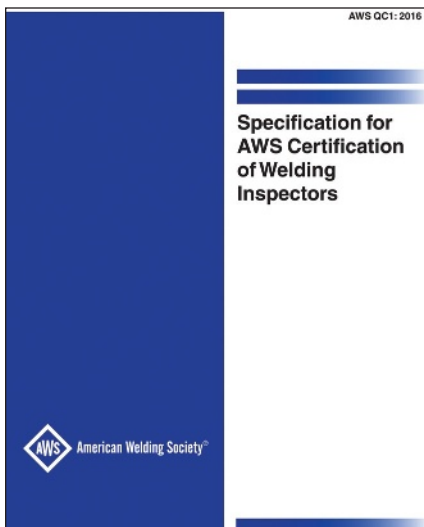


Fig. 1 — The latest version of AWS QC1 contains significant changes.

AWS QC1:2016, *Specification for AWS Certification of Welding Inspectors*, stands as the seminal certification standard for welding inspectors — Fig. 1. The Certified Welding Inspector (CWI) certification has been issued to more than 100,000 individuals worldwide since 1976. Since QC1 was last revised nine years ago, significant changes have been made to the 2016 edition that you need to know. As of January 2017, the American Welding Society (AWS) has initiated a phased implementation of QC1:2016.

The Certified Associate Welding Inspector (CAWI), the Certified Welding Inspector (CWI), and the Senior Certi-

fied Welding Inspector (SCWI) programs are directly impacted. It benefits you to know how these changes will apply to your initial application, three-year renewal, and nine-year recertification. Following are details on some of these changes.

B5.1 – QC1 Relationship

AWS B5.1, *Specification for the Qualification of Welding Inspectors*, establishes the requirements for qualification and defines the body of knowledge applicable to welding inspection personnel. AWS QC1 sets the certification requirements for the AWS Certified Welding Inspector program. Certification documents follow the standards established in the corresponding qualification documents; in this case, QC1:2016 reflects the changes in the B5.1:2013 document.

Endorsements for SCWI

New subclause 6.1.4 allows an alternative method for individuals to achieve the SCWI by earning endorsements. The CWI applicant can take an approved core of mandatory endorsement exams and a specified additional number of elective endorsement exams. Some of these endorsement exams exist today while others are under development. The AWS Qualification & Certification Committee will establish the details of this option at a later date.

It is important to note that the ten

current endorsement certifications only supplement inspection credentials (CWI and SCWI). Most of the mandatory and elective endorsements have yet to be created and approved. You cannot obtain a SCWI with the existing endorsements.

It was clarified in the definitions section that an endorsement is an indication of additional “knowledge,” “ability,” or “skill” beyond what the individual was originally tested for when earning his/her CWI or SCWI. The following endorsements are available: Structural Steel, Structural Aluminum, Bridge Welding, Railroad, Aerospace, API 1104 Pipeline, Structural Drawing Reading, Structural Bolting Inspection, ASME Pressure Piping B31.1 and B31.3, and ASME Pressure Vessel Section VIII, Div. 1.

CAWI Active Supervision

The Certified Associate Welding Inspector has always only been able to perform inspections under the direct supervision of a CWI/SCWI. However, in this edition, direct supervision has been clarified and defined as active supervision, meaning “direct on-site or readily available supervision” by a CWI or SCWI “in the form of necessary instructions to assure that the CAWI can perform specific evaluations as specified by the employer” (subclause 4.4). As in the past, the CWI or SCWI maintains the responsibility for determining final acceptance of the welds.

Education and Experience Requirements

Senior Certified Welding Inspector applicants are now able to draw from only the last eight years to meet the six-year minimum CWI certification status requirement (subclause 5.2). Previously, an individual who held a CWI for at least six years, then let it lapse for any duration of time (for example, 20 years), could apply and earn a SCWI without first reestablishing his or her CWI certification. The new rule limits the lapse of time to two years.

Exam Application Requirements

Subclause 5.3 calls for more specific information described in the relevant work experience including contact information for employers, description of the work performed, and employment dates. Applicants attest to the accuracy of the information provided, which is subject to review by the AWS Certification Department. It is important to note that false information is cause to reject the application and can disqualify the applicant from testing to be an AWS CAWI, CWI, or SCWI. This applies to the first three-year and second three-year renewals, as well as the nine-year recertifications.

Examination Requirements for SCWI and CWI

The minimum number of questions for Part B – Practical portion of the CWI exam allows for a decreased number of questions as per subclauses 6.2.2 and 7.1. This change allows more flexibility for the CWI exam developers. For example, more time intensive, but fewer, questions could be chosen to better differentiate candidates' abilities in the given testing period. There is no plan to reduce the Part B exam to fewer than the current 46 questions, but this option was deemed possible during the recent development of the new Part B exam so the option was included in this edition of QC1.

Retesting

A retest is the testing of a previously failed portion of the exam (Part A – Fundamentals, Part B – Practical, or Part C – Code Book). QC1:2016, sub-

clauses 6.2.5.1 and 6.2.5.2, differentiate the amount of additional hours of training required. If one or two parts of the exam need retesting, then 16 hours of qualifying training are required. If all three parts need to be re-taken, then 40 hours of training are needed before retesting. This better reflects the relationship between the necessary retraining required in proportion to the number of test portions and topics covered in the retest. The qualifying training must be documented as per subclause 6.2.5.2.

QC1 has been revised to clarify that applicants who fail to pass the Part C – Code Book portion of the CWI examination are required to use the same code used for the original examination (subclause 6.2.5.3).

A new subclause (6.2.6) describes a Certified Welding Educator (CWE) exemption: If the CWI applicant previously passed the CWE Parts A and B at or above the CWI level, then he/she need only take Part C and pass it at the CWI level.

Split Examination

During this revision of QC1, the Certification Committee considered changing the testing model of the CWI to require individuals to first pass Part A before being able to take Parts B and C (i.e., Part A would serve as a prerequisite). At the same time, AWS considered moving some of its testing to computer-based testing platforms, which would have helped facilitate this new testing model. Subclause 6.2.7 on 'Split Examinations' was added to allow AWS to implement this change when and if it chooses to do so. AWS is planning to move most of its exams to computer-based testing in 2017; however, moving to split exams as allowed by subclause 6.2.7 proved to be too challenging logistically and not practical at this time. So, although QC1 allows split exams per 6.2.7, the AWS Certification Department is not planning to implement them until the logistical and practical issues are resolved, which may take years.

AWS is planning to change its administration of CWI exams in mid-2017 by first requiring candidates to take the practical Part B exam at a typical AWS exam location, which usually follows a multiday preparatory course. Within a predetermined period of time, set by AWS, after taking the Part B exam, can-

didates must take Parts A and C at a computer-based training location. All three exam scores are then combined to determine if the candidate achieved the scores necessary to become a CWI. The rules for scoring and determination of certification are not changing from what they have been previously.

Although this new approach to administering exams appears to be split, it is only split in terms of timing, and not the split examination option described in subclause 6.2.7. This B then A and C method is being run under the existing rules found in subclauses 6.2.1 through 6.2.6. We understand this change to QC1 and our change in test administration might be confused with each other because in both instances there is some splitting of the exam; however, the subclause 6.2.7 testing model and the change in our administration of the exam are completely separate situations.

Achieving Certified Associate Welding Inspector Certification

New language cautions that CAWIs are limited on how they can practice inspection activities. For those who are unable to comply with these restrictions, it is recommended to surrender the CAWI certification and to continue to work uncertified.

Visual Acuity and Photo Requirements

QC1:2016 introduces the AWS Visual Acuity Form that a designated professional must complete for the SCWI, CWI, and CAWI. The visual acuity time period has changed from seven months to one year prior to the examination or certification expiration date. The (completed) visual acuity record is valid for up to one year from the exam date.

The time for the AWS Certification Department to receive the results of the Visual Acuity Form has been extended up to 60 days after the examination date in subclause 8.1.2. A new subclause (8.2) describes passport-style color photograph requirements and acceptance parameters.

Certification

New documentation language (sub-

clause 10.1) clarifies that certification becomes effective on the first day of the month following the date of examination. Note that this has been previously implemented. Also, the wallet card will include the photo of the person certified.

Verification requests of status and certification number of SCWIs, CWIs, and CAWIs will now include the certified person's photo, in addition to the certification number, date certified, expiration date, current status (current, revoked, etc.), and certification limitations (corrected vision, etc.) as per subclause 10.2. Remember, you can always verify current AWS Certification credentials using the AWS Certification Quickcheck at aws.org/certification/search.

Code of Ethics, Rules of Conduct, and Practice

Language has been added stating that the SCWI, CWI, and CAWI will not use the certification stamp or number connected to a lapsed or terminated SCWI, CWI, or CAWI status (subclause 11.2.3). This is an important ethical matter that directly affects one's livelihood. Following QC9, *Administrative Procedures for Alleged Violations of AWS Certification Programs*, a recent AWS Subcommittee on the Code of Ethics Hearing Panel ruled against a CWI for falsely representing his/her current status as a CWI; the penalty included having the CWI credential, which was active at that time, revoked for a significant period of time.

With the CAWI active supervision addition in subclause 4.4, the Code of Ethics in subclause 11.2.5 clarifies active supervision as one of the parameters in which an inspector can sign off work. Language has been modified in subclause 11.4.4 regarding conflict of interest conditions allowed for an inspector whose work is performed while being a public official. This is now allowed if this practice is expressly dictated by a job description or specification and all affected parties are notified.

Renewals

New language reaffirms that the CAWI certification is up to a three-year period with no renewals as per subclause 15.1, and that CAWI testing

for CWI status falls under CWI examination requirements (subclause 15.1.1).

Subclause 15.2.2 extends the period of time in which SCWI and CWI renewal applications are accepted by the AWS Certification Department — no earlier than 11 months prior to the certification expiration date. Previously, the time period was six months. This gives welding inspectors additional time to prepare and submit their documentation. If you should miss the renewal deadline, new subclause 15.3.2 allows renewals to be accepted after the 60-day grace period for up to one year of expiration; however, administrative late fees may be applied. SCWIs and CWIs are strongly advised to renew prior to the grace period since the SCWI and CWI certifications will be expired during this time. You cannot perform welding inspector work using an expired certification. See the Code of Ethics section of this article.

The SCWI and CWI certification renewal clarifies that continuous inactivity refers to work inactivity in subclause 15.4.

Nine-Year Recertification for SCWI and CWI

Consistent with the renewal application extension, subclause 16.1 extends the nine-year recertification application acceptance up to 11 months prior to the certification expiration date. A 60-day administrative extension is allowed; however, your certification will be expired during this time.

QC1:2016 references that the CWI may recertify by taking a Committee-approved endorsement and that the endorsement need not be current at the time of CWI recertification application (subclause 16.3.1). As of this writing, in addition to the ten existing endorsements cited in the Endorsement section of this article, there are additional endorsements pending development and approval by the Qualification & Certification Committee, as well as administrative implementation. For further information, go to aws.org/certification/page/cwi-scwi-endorsements.

Within training and teaching requirements, new language allows for broader course content relevant to subject or job functions in B5.1 (subclause 16.4.2). Earning Professional Develop-

ment Hours (PDHs) now reflect a wider parameter as stated in subclause 16.5.1. Wording in subclause 16.5.2 increases the maximum PDHs to 40 from the previous 20; also, proof of attendance was added as a form of verification. Subclause 16.5.3 clarifies that non-AWS conference PDHs are allowed if they address subjects in B5.1 and if proof of participation is provided. However, new subclause 16.5.9 allows PDHs for items not directly listed in B5.1 contingent upon AWS Certification Department approval.

New language has been added in subclause 16.7 to allow CWI nine-year recertification applicants to switch the recertification means (such as from Part B to an endorsement) if within the deadline. New subclause 16.7.1 specifies the instances in which all three exam Parts — A, B, and C — are required for CWI nine-year recertification. Individuals who take the exams but fail to pass are no longer certified once the certification expires and are then considered new applicants as described in subclause 16.7.2.

Conclusion

This article is not intended to serve as a complete depiction of all changes in QC1:2016, nor is it intended to replace your own review of the document. There are many nuances in the standard that cannot be fully reflected in this article. It is the responsibility of first-time applicants and renewing CWIs and SCWIs to carefully identify how these changes will affect themselves.

Should you have any questions or concerns, please feel free to contact the AWS Certification Department at (800) 443-9353, ext. 273. AWS QC1:2016 is available for free download at pubs.aws.org/t/freedownloads. 

MARTY LUCIA (mlucia@aws.org), PhD, is standards program manager, Certification Department, American Welding Society, Miami, Fla.



American Welding Society®

LEARNING

aws.org



IN YOUR CAREER, EXPERIENCE IS A FACTOR BUT KNOWLEDGE CAN SET YOU APART.



Whether you are currently employed or are looking for a career in welding, fundamental knowledge is the cornerstone in your career preparedness.

It is this fundamental knowledge that provides the backbone for and the ability to turn a skill into a marketable vocation.

Use these **AWS Online Learning** courses to keep you sharp; prepared for career opportunities that may come your way.

Courses to help brush up on your fundamental knowledge include:

- Welding Fundamentals I, II & III
- Understanding Welding Symbols
- Metallurgy for the Non-Metallurgist: Fundamentals
- Safety in Welding
- Fabrication Math

Visit go.aws.org/awsknowledge to learn more.

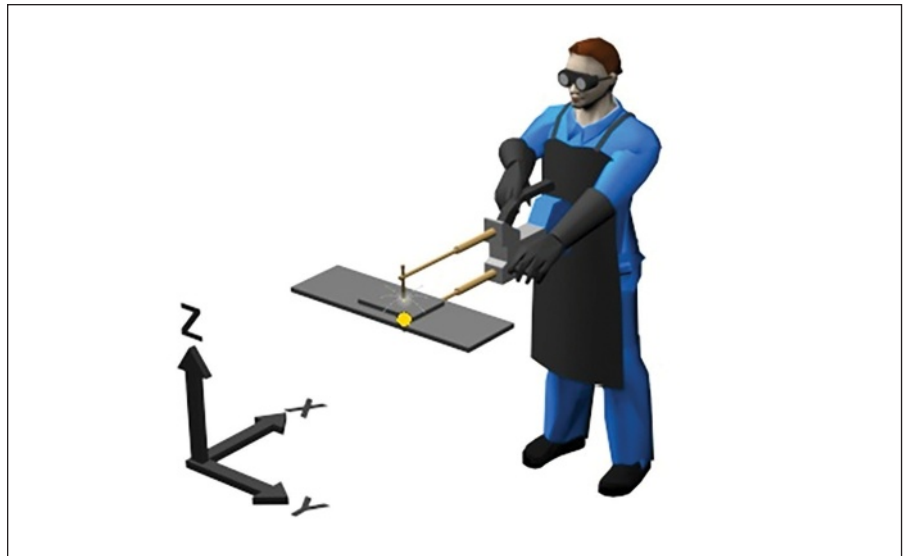
European Law Requires Assessment of Workers' Exposure to Electromagnetic Fields

A consortium of European organizations developed specialized software to assess this hazard

BY EURICO ASSUNÇÃO AND GEOFF MELTON

There are many hazards in the workplace, and as a result, many regulations to protect workers from harm. Most of the hazards in welding are well known. Welders can readily identify the need for personal protective equipment. For example, arc welding produces welding fumes, which can be smelled, and extremely bright light, which can be seen, while grinding creates noise, which can be heard. Assessment is usually straightforward: noise, for example, can be measured using a sound level meter. But not all hazards are that easy to measure.

A new European law (EU Directive 2013/35/EU) (Ref. 1) came into effect this July and now requires workers' exposure to electromagnetic fields (EMF) to be assessed. For most industrial processes, the levels of exposure will be low and no further action will be necessary. However, some welding processes produce high levels of EMF, which can lead to workers being exposed to fields higher than permitted.



Low Action Level (%)	High Action Level (%)	Limb Action Level (%)
72	58	174

Sensory Exposure Limit Value (%)	Health Exposure Limit Value (%)
Not Applicable	178

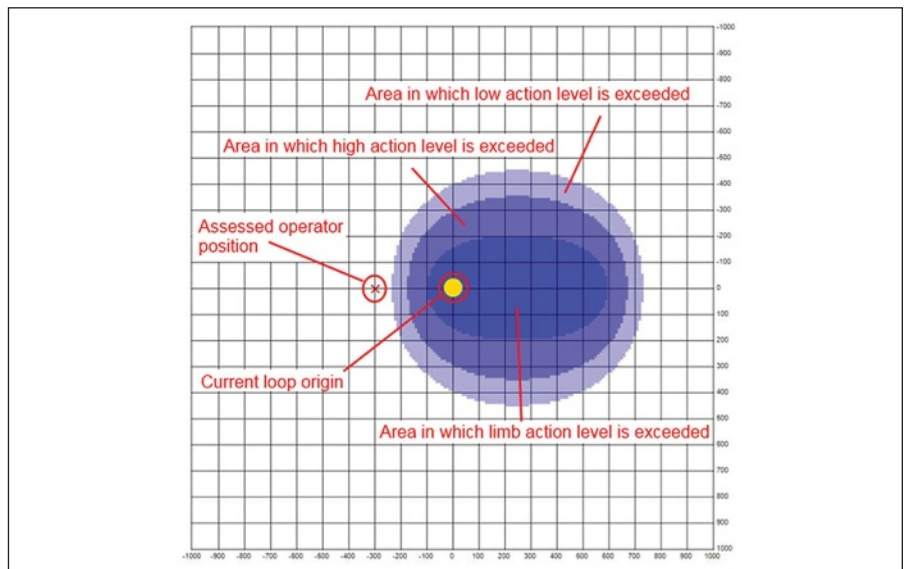


Fig. 1 — A map for a resistance welding process reveals exposure levels.

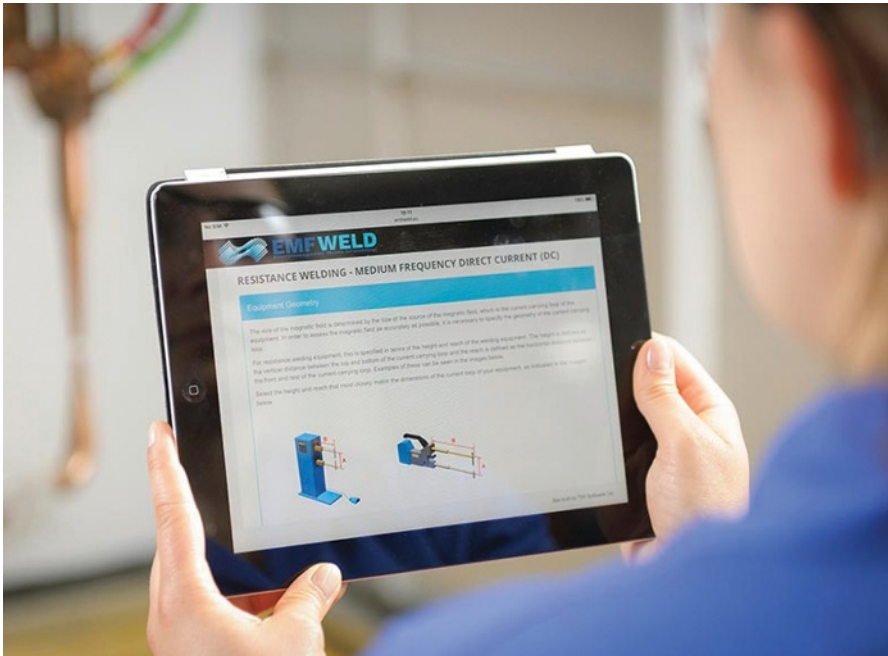


Fig. 2 — EMFWELD allows users to enter details of the equipment, welding parameters, and the operator position. The EMF exposure is then calculated based on an extensive database. (Photo courtesy of TWI.)

Electromagnetic fields cannot be seen or heard, so an assessment by measurement or calculation is required.

In the case of EMF, assessment is not straightforward. Exposure limit values are given for the field induced by the human body, but these are very difficult to assess. The directive also gives action levels of the field to which the worker is exposed, which can be measured directly. There are separate action levels for the body and limbs, and those levels are frequency dependent. The EMF needs to be assessed at various positions around the welder, and the frequency of the field needs to be taken into account. Most processes will generate multiple frequencies, and the field for each frequency component needs to be accounted for.

A number of processes typically found in production have been identified as producing high levels of EMF. These include the following:

- Resistance welding
- Some arc welding processes
- Induction heating
- Magnetic particle inspection.

The magnitude of the field to which the welder is exposed will depend on the type of equipment, the welding pa-

rameters, and the position of the welder. A separate assessment is therefore required for every type of equipment and operating procedure. This can be achieved by taking many measurements or by complex calculations.

To make assessment simpler for health and safety officers and supervisors, a consortium of European organizations has developed specialized software called *EMFWELD*.

EMFWELD is available online (emfweld.com) and requires no download or installation. The user enters details of the equipment, the welding parameters, and the operator position. The EMF exposure is then calculated based on an extensive database of results obtained from magnetic field waveforms from different processes and equipment. An assessment against the three action levels (low, high, and limb) in the directive is provided in the assessment report, which also includes exposure limit values where data are available.

In addition, *EMFWELD* generates a map of the field around the equipment, so it is easy to see where the exposure is below the action levels.

Figure 1 shows a map for a resistance welding process revealing that exposure is below the action levels where the operator is standing. It also shows that if the operator is holding a component, the hand exposure will be ex-

ceeded up to 150 mm from the electrodes. Also, for this equipment, exposure is higher at the side of the gun than in front of the electrodes.

Where exposures exceed the action levels, often only small changes are required to bring the process into conformance. For example, moving slightly farther away from the equipment or adjusting the position of handles and controls can produce a significant reduction in exposure.

Workers who are pregnant or fitted with implanted devices (e.g., pacemakers) will require a separate assessment based on levels for the general public.

Although the EMF directive applies only in Europe, the exposure limits and action levels are based on the International Committee for Non-Ionizing Radiation Protection (ICNIRP) guidelines for limiting exposure to EMF (Ref. 2). The low action levels in the directive are the equivalent of the reference levels in the ICNIRP guidelines, so *EMFWELD* can effectively be used for assessment against the ICNIRP guidelines in countries where the directive does not apply — Fig. 2.

EMFWELD has been developed by a consortium led by the European Federation for Welding, Cutting and Joining; the Council of European Employers of the Metal, Engineering and Technology-Based Industries; and TWI, a UK-based welding and joining research organization. 

References

1. Directive 2013/35/EU of the European Parliament and of the Council of June 26, 2013, on the minimum health and safety requirements regarding the exposure of workers to the risks arising from physical agents (electromagnetic fields) (20th individual Directive within the meaning of Article 16(1) of Directive 89/391/EEC) and repealing Directive 2004/40/EC.
2. ICNIRP Guidelines for limiting exposure to time-varying electric and magnetic fields (1 Hz to 100 kHz). 2010. *Health Physics* 99(6): 818–836.

EURICO ASSUNÇÃO (EGAssuncao@isq.pt) is deputy manager, EWF. GEOFF MELTON (geoff.melton@twi.co.uk) is consultant, Materials Group, TWI Ltd.

Newer Spot Welding Technology Works Well with Aluminum

A newer process reduces the difficulties encountered when spot welding aluminum

The growing requirement for reduced-weight structures has resulted in lightweight aluminum gaining prominence as an effective substitute for steel along with other materials like magnesium, titanium, and composites. Unfortunately, lower strength and ductility, as well as inconsistent weld integrity of welded aluminum alloy structures has hindered the use of aluminum alloys. In particular, durability of aluminum alloy welds produced with resistance spot welding (RSW) can be questionable.

Conventional Aluminum Welding: Issues and Challenges

The difficulties in welding aluminum alloys stem from three main issues.

1) Aluminum's good conductivity results in high temperatures in the heat-affected zones (HAZs). In heat-treated alloys, this results in excessive softening of the aluminum as well as generating corrosion-sensitive phases in some grades. The loss of strength per unit area is typically in the range of 40–70% of the original heat-treated strength. Because of this, thicker material is needed for load-bearing abilities, which negates much of the lightweight objectives for using aluminum.

2) In addition, many of the aluminum alloy grades are prone to cracking when spot welded. This is particularly seen with the higher strength aerospace alloys. Consequently, while the RSW process is an inexpensive welding process, it is difficult to use with confidence for the 2000 and 7000 series aerospace alloys. Also, RSW is difficult to use with confidence for all alloy grades due to electrode tip surface stability issues.

3) The aluminum oxides that form readily on aluminum surfaces also readily absorb moisture. This results in a variety of weld quality issues such

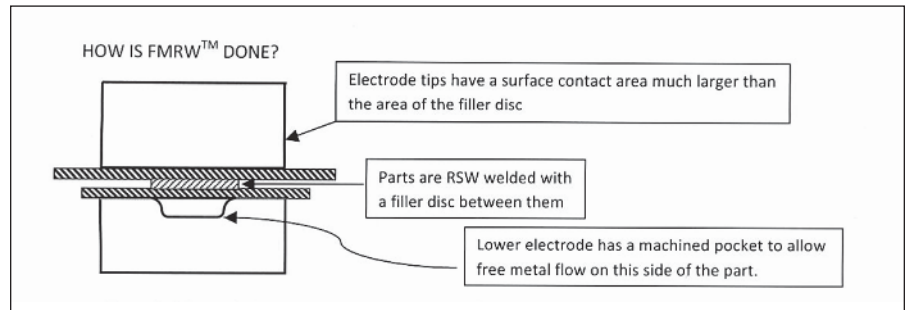


Fig. 1 — Schematic of a FMRW™ setup in a common aluminum resistance spot welding machine.

as porosity in arc welds and variable surface resistances resulting in variable heat-creation in RSW-produced nuggets. Also, the surface of the parts to be welded need to be free from objectionable films such as heavy oxides, scale, ink, grease, dirt, or surface conditions detrimental to the welding process as mentioned in AWS D17.2/D17.2M:2013, *Specification for Resistance Welding for Aerospace Applications*.

Surface cleaning is an important requirement for producing consistent-quality welds. For example, when a surface cleaning procedure is changed for welding aluminum alloys, the surface resistance (micro-ohms) average should be no more than 1.05 times that achieved by the replaced procedure. Due to moisture absorption, these resistances vary with time, particularly in damp conditions, to generate surface resistance uncertainty. This is easily observed when parts that are partly welded are welded again the next day without additional cleaning.

Desirable Features of a Welding Process for Aluminum Alloys

Any weld process, to be desirable, should use weld equipment suitable for large-volume manufacture that the industry is familiar with in buying, setting up, and maintaining globally.

The surfaces of parts welded should have a good appearance with no loss of thickness. When welding aluminum, the electrodes should deliver a repeatable input that is at least as stable as that found in RSW of steel over the entire production shift.

A good process should

- Enable rapid solidification of the weld metal under pressure.
- Permit the use of low-melting range fillers that enable the solidification of aerospace-grade alloy welds without solidification defects.
- Not soften hardness and strength values in the HAZ by more than 15% from heat-treated values.
- Help retain nonmelted microstructures on the outer surfaces with no intermetallic compounds for superior resistance to corrosive attacks in service.
- Permit the welding of thick-thin alloy combinations of thickness ratios up to 1:10, or even higher.

Such a weld process, due to the above characteristics, should enable proliferation of weight reduction without loss of strength, ductility, or physical appearance.

A New Technology

Innovative Weld Solutions Ltd., Dayton, Ohio, has developed a spot welding process that helps eliminate these problems. This process, Focused-



Fig. 2 — Typical microstructure of an FMRW™ weld nugget in an aluminum alloy. The weld nugget is about seven times larger in diameter than the sheet thickness. The outer layers of the sheets at the weld remain unmelted. The left side of the figure shows one of the mating sheets being torn in the peel test; the right side of the lower sheet is welded at its very edge with no adverse effects or expulsion.



Fig. 3 — A 0.6-mm-thick 6061-T6 sheet welded to a 5.0-mm-thick 6061-T6 plate to yield a weld button size in excess of 10 mm diameter in a peel test. The tensile-shear strengths of these welds were in the range of 800 to 1000 lb (3.5 to 4.4 kN).

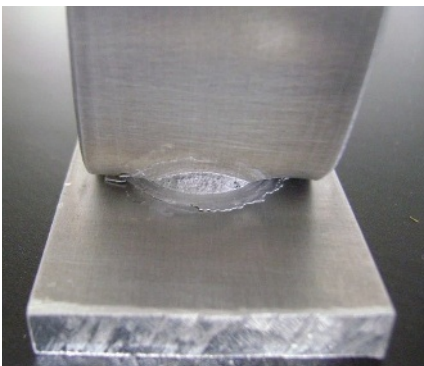


Fig. 4 — Peel tested FMRW™ spot weld of a 6.25-mm-thick 6061-T6 plate to a 6.25-mm-thick 5454-O plate. The process yielded a nearly 20-mm-diameter weld nugget close to the plate edges with good outer surface appearance. Weld shear-tensile strengths consistently exceeded a 5000-lb load (22 kN).



Fig. 5 — After a fatigue test specified by a flatbed manufacturer, the weld shows little indication of the test except for the grip marks on the sheet surfaces. The fatigue test conditions consisted of loading from 0 to a 1700-lb load (0–7.5 kN load) at 1 cycle/s for 30,000 cycles.

Melt Resistance Welding (FMRW™), is covered by U.S. and global Patent Cooperation Treaty (PCT) patents.

The process was designed, developed, and validated specifically to eliminate the traditional drawbacks of RSW aluminum.

How Is It Done?

The process uses an aluminum alloy filler disc to focus the weld current at the weld interface — Fig. 1. This causes the electrode-to-metal current densities to be an order of magnitude smaller than the actual weld current densities. With the electrode tips being water cooled as in a typical resistance welding machine, this helps maintain electrode surfaces, and the outer surfaces of parts welded stay relatively cool. The selectable filler size also helps select the weld size. This means nugget size is not limited by the sheet thickness.

Tooling that enables quick follow-through and forging at the end of the weld process results in defect-free weld microstructures as shown in Fig. 2.

One application of the technology is its capability for welding thick-to-thin combinations of aluminum alloy sheets and plates.

The advantages of the technology include long electrode life and stable process quality using existing RSW equipment. High-quality, reliable welds are produced with cosmetic outer surfaces. The scope for nondestructive examination is wide open due to the smooth outer surfaces and a well-identifiable melted-and-solidified weld nugget. HAZ softening is limited to around 15% of original values to produce weld strengths that are often more than three times the minimum specified weld strengths per AWS

D17.2. The weld size being selectable, coupled with these hard HAZ regions, lead to high load-bearing abilities and excellent joint fatigue life.

Reduced Surface Cleaning

The newer process helps eliminate the need for surface cleaning of the aluminum alloy components prior to welding, provided there is no heavy scale on the part surfaces. This process is not sensitive to other surface contaminants such as grease, light dirt, ink, light oxides that form naturally, and the moisture absorbed by such oxides. Also, electrode tip dressing once in every 250–300 welds is sufficient to result in reliable weld quality.

Welding Thick-Thin Combinations

One application of the technology is its capability for thick-to-thin combinations of aluminum alloy sheets and plates. Thickness ratios of 1:10 were readily welded with no thinning of the thinner member being welded — Fig. 3.

Thick, Fatigue-Resistant Welds

Thick aluminum plates can be successfully welded with considerably lower welding currents using the process — Fig. 4. Because of the fatigue test results, thick plates welded with this process would be useful for railroad, flatbed truck, and other heavy-duty applications requiring overall weight reduction — Fig. 5.

Welding Aerospace-Grade Aluminum

The use of low-melting-range filler

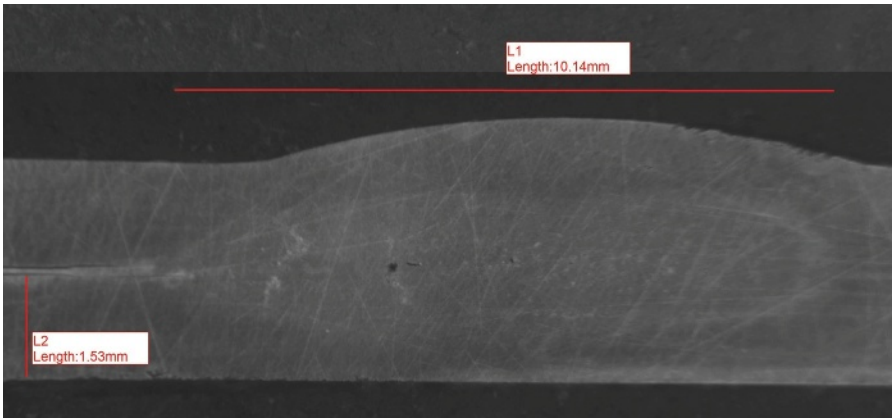


Fig. 6 — This 7075-T6 weld shows good weld macrostructure in the weld nugget.

metals of the 4000 and 6000 series makes aerospace grade alloys weldable with the newer technology. Figure 6 shows the results of a shear-tensile test on an aerospace alloy.

Dissimilar Metal Welds

The technology enables making high-quality welds of dissimilar materials, such as a dual-phase steel to an aluminum alloy, through diffusion-barrier interlayers. These diffusion-barrier layers do not melt and keep the molten steel and aluminum apart during welding. Both steel and aluminum are fused to this barrier layer generating a strong weld, as the process enables an independent selection of weld size. This method can also readily enable effective spot welding of aerospace grades of aluminum alloys such as 7075-T6 to 5000 or 6000 series aluminum alloy members.

Tube-to-tube welds of such dissimilar materials are also readily produced by this welding technology.

Conclusion

The FMRW™ process economically

produces high-strength, ductile, and reliable joints with good outer surface appearance using existing resistance welding equipment. **WJ**

V. (ANTHONY) ANANTHANARAYANAN
 (anthony@innovativeweldsolutions.com)
 is president, Innovative Weld Solutions Ltd.,
 Dayton, Ohio.

Change of Address? Moving?

Make sure delivery of your *Welding Journal* is not interrupted. Contact Maria Trujillo in the Membership Department with your new address information — (800) 443-9353, ext. 204; mtrujillo@aws.org.

WELDING Journal CUSTOM REPRINTS



Take Advantage of your Editorial Exposure.

Use reprints to maximize your marketing initiatives and strengthen your brand's value.

REPRINTS ARE IDEAL FOR:

- New Product Announcements
- Sales Aid For Your Field Force
- PR Materials & Media Kits
- Direct Mail Enclosures
- Customer & Prospect Communications/Presentations
- Trade Shows/Promotional Events
- Conferences & Speaking Engagements
- Recruitment & Training Packages

Reprints are a simple way to put information directly into the hands of your target audience. Having been featured in a well-respected publication adds the credibility of a third-party endorsement to your message.

For additional information, please contact Foster Printing Service, the official reprint provider for *Welding Journal*.



Call 866.879.9144
 or sales@fosterprinting.com



American Welding Society®
CORPORATE MEMBERSHIP

ENHANCE YOUR COMPANY'S POSITION WORLDWIDE

BEST VALUE



AWS Sustaining Company Membership

Sustaining Companies receive a choice of:

Complete AWS Standard eLibrary (a \$12,000 value):

- Nearly 160 AWS Standards accessible online
- 24/7 access via a single integrated environment
- Text searchable for quick information retrieval
- Multiple user access at single site with valid IP address
- User friendly interface, giving clickable access to resources
- Remote access via VPN or proxy server

OR

10 additional AWS Individual Memberships:
(Receive 20 memberships in total. A \$980 value).

If you're an organization who prioritizes continuous improvement and learning; collaborative connections with other leaders in the field; and the opportunity to shape the future of the welding industry; a Sustaining Company Membership is your most inclusive and influential level.

AWS Sustaining Company Members support their employees with extra benefits and savings that enhance their technical and career growth professionally, and provide excellent opportunities for them to connect with thousands of industry leaders.

Includes: **10 AWS INDIVIDUAL MEMBERSHIPS**

Visit us to learn more at Booth #C1700



AWS SUPPORTING COMPANY MEMBERSHIP

The AWS Supporting Company Membership is designed especially for companies who strive to maintain their team's expertise and professionalism.

Includes: **5 AWS INDIVIDUAL MEMBERSHIPS**



AWS WELDING DISTRIBUTOR MEMBERSHIP

As a welding distributor, AWS membership benefits you in two major ways: helping you boost your customer base and competitive market share. Put your company on

the AWS Welding Distributor Map.

Includes: **5 AWS INDIVIDUAL MEMBERSHIPS**



AWS EDUCATIONAL INSTITUTION MEMBERSHIP

Educational Institution Membership: reinforce your reputation for excellence. The Educational Institution Membership was designed especially for educational

leaders, faculty, staffs and students.

Includes: **3 AWS INDIVIDUAL MEMBERSHIPS**



AWS AFFILIATE COMPANY MEMBERSHIP

Get the critical tools, resources and guidance to boost revenue and results. Affiliate Company Membership is designed for the specific needs of independent welding

fabricating shops.

Includes: **1 AWS INDIVIDUAL MEMBERSHIP**

AWS-SPONSORED EVENTS

For more information on AWS conferences:
aws.org/w/a/conferences/index
 (800/305) 443-9353, ext. 455

Aluminum Welding Technology Seminar. March 8. Metairie, La. The AWS New Orleans Section will host a seminar covering aluminum welding processes, metallurgy, procedure development, weld quality, productivity, and application. Certificates of attendance will be provided for eight Professional Development Hours (PDHs) toward AWS CWI renewal. For more information, contact D. J. Berger at (504) 415-9165 or dj@nationalitc.com.

National Robotic Arc Welding Conference. June. Milwaukee, Wis. A call for papers has been issued for topics addressing robotic arc welding related challenges and successes through innovation in part design, tooling, process optimization, people skills, or other means. This conference is a joint effort between the AWS Milwaukee Section, AWS D16 Robotic and Automatic Welding Committee, and Milwaukee Area Technical College. All proceeds from the conference go toward the J. F. Hinrichs Scholarship fund. To submit a short abstract, contact Jeffrey Noruk, j.noruk@us.servorobot.com, or Jay Haynes, jay.haynes@wolfrobotics.com.

U.S., CANADA, MEXICO EVENTS

The 4th Lightweight Vehicle Manufacturing Summit 2017. February 22, 23. Detroit, Mich. An expert speaker panel including Honda, Volvo, FCA, GM, Ford, and others will discuss the latest innovations in adhesives, additive manufacturing, machine learning, joining methods, corrosion mitigation techniques, and more. Visit global-lightweight-vehicle-manufacturing.com.

INTERNATIONAL EVENTS

4th UKP Workshop: Ultrafast Laser Technology. April 26, 27. Fraunhofer Institute for Laser Technology, ILT, Aachen, Germany. More than 20 international speakers will report on the most recent developments in ultrafast laser beam sources and optical systems for ultrafast laser technology. The event is an opportunity for scientists, laser manufacturers, and users to come together. Visit ultrafast-laser.com.

BLECH India. April 27–29. Bombay Exhibition Center, Mumbai, India. Business platform for India's sheet metal working industry. Visit blechindia.com.

19th International Conference on Joining Materials. May 7–10. Konventum LO-Skolen, Helsingør, Denmark. The In-

stitute for the Joining of Materials (JOM) in association with the International Institute of Welding (IIW) present a conference dedicated to the advancement of joining and material technologies and fabrication techniques in all the key industries. Contact +45 48355458 or e-mail jom_aws@post10.tele.dk.

Schweissen & Schneiden. September 24–29. Düsseldorf, Germany. The meeting places for experts and top decision makers of the joining, cutting, and surfacing technology industries. Held every four years, the show offers a range of machinery, products, processes, and service. Visit schweissen-schneiden.com/joining-cutting-surfacing/.

China Chongqing Machine Tool Show. Nov. 13–16. Chongqing International Expo Center, Yubei, Chongqing, China. The Association for Manufacturing Technology and the China Machine Tool and Tool Builders' Association present this expo to showcase the latest manufacturing technology and bring buyers and sellers together from all over the world. Visit imts.com.

EDUCATIONAL OPPORTUNITIES

ASME Section IX Seminar. Apr. 3–5, San Francisco, Calif., and June 12–14, Houston, Tex. Visit asme.org and search "PD 190" or contact Marian Hess, hessm@asme.org; (212) 591-7161.

Brazing Training Seminars. Three-day intensive training programs in all aspects of brazing from fundamentals to advanced concepts. Covers furnace, torch, induction, and dip brazing of aluminum, titanium, superalloys, and ceramics. Classes held April 11–13, Simsbury, Conn.; May 16–18, Los Angeles, Calif.; October 3–5, South Carolina; and November 14–16, Simsbury, Conn. Contact Kay & Associates at dan.kay@kaybrazing.com or call (860) 651-5595.

Business Electronics Soldering Technology. Classes held in Chicago, Ill., Detroit, Mich., Minneapolis, Minn., Cleveland, Ohio, Huntsville, Ala., or can be coordinated onsite at your facility. Contact BEST at (847) 797-9250 to register.

Certified Welding Inspector/Educator Prep Courses and Endorsement Seminars. Allentown, Pa. Six-day prep courses begin Feb. 13, May 1, July 31, and Nov. 13. Single-day bolting endorsements begin Feb. 10 and July 28. Single-day D1.1/D1.5/API endorsements begin Feb. 16, May 4, Aug. 3, and Nov. 16. CWI/CWE and endorsement exams given Feb. 19, May 7, Aug. 6, and Nov. 19. Contact Welder Training and Testing Institute, Tracy Wiswesser, (610) 820-9551, ext. 204; wtti.com.

Clean Air Academy. April 18, 19. A two-day course developed by RoboVent and designed to give engineers, facility managers, and maintenance staff a solid foundation in the science of air quality management. For more information, e-mail kristen.hughes@robovent.com or info@robovent.com.

E-Courses in Destructive and Nondestructive Testing of Welds and Other Welding-Related Topics. Online video courses taken at one's own pace offer certificates of completion and continuing education units. Contact Hobart Institute of Welding Technology; (800) 332-9448; welding.org/product-category/online-courses/.

ESAB Welding and Cutting Distributor Instructor Lead Training. Year-round training at Denton, Tex.; West Lebanon, N.H.; Traverse City, Mich.; Hanover, Pa.; and Salt Lake City, Utah. Online eLearning training available at training.victortechologies.com, e-mail trainingteam@esab.com.

GE Industrial Computed Tomography (CT) Operator Course. Learn to operate the 3D technology that is becoming more prominent in industrial quality control and metrology. Lewistown, Pa., (315) 554-2039; geinspectionacademy.com.

Hypertherm Cutting Institute Online. Includes video tutorials, interactive e-learning courses, discussion forums, webinars, and blogs. Visit hypertherm.com; hyperthermcuttinginstitute.com.

Industrial Laser Training. Technical training and support offered for users of industrial lasers in manufacturing, education, and research. Regularly scheduled classes in laser welding and laser cutting and drilling. HDE Technologies, Inc.; (916) 714-4944; laserweldtraining.com, laser-cutting-drilling-training.com.

INTEG Courses. Courses in NDE disciplines to meet certifications to Canadian General Standards Board or Canadian Nuclear Safety Commission. The Canadian Welding Bureau; (800) 844-6790; cwbgroup.org.

Laser Safety Online Courses. Courses include Medical Laser Safety Officer, Laser Safety Training for Physicians, Industrial Laser Safety, and Laser Safety in Educational Institutions. Laser Institute of America; (800) 345-2737; lia.org.

Laser Safety Training Courses. Courses based on ANSI Z136.1, *Safe Use of Lasers*. Orlando, Fla., or customer's site. Laser Institute of America; (800) 345-2737; lia.org.

Laser U — Online Education Portal. Offers practical information to use on the job. Topics range from 3D printing to drilling, welding, wireless and optical product requirements, and many others. Visit Laser Institute of America; lia.org/laseru.

Laser Vision Seminars. Two-day classes, offered monthly and on request, include tutorials and practical training. Presented at Servo-Robot, Inc., St. Bruno, QC, Canada. For schedule, cost, and availability, e-mail info@servorobot.com.

Laser Welding Technology Classes. Classes begin February 20–24, Phoenix, Ariz.; May 15–19, Minneapolis, Minn.; and October 9–13, Phoenix, Ariz. Visit laserweldtraining.com.

— continued on page 75



BE A PART OF THE FUTURE IN RESISTANCE WELDING

Over 75 companies within the resistance welding industry make up what is known as RWMA.

This alliance of resistance welding professionals supports research, education and the overall promotion of resistance welding as a viable industry. If you want to be a part of resistance welding's future join us at aws.org/rwma

canaweld
200 AMPS IN A COMPACT DESIGN
TIG/MIG/STICK
MADE IN CANADA
MORE POWERFUL, PORTABLE, & LIGHTER THAN ANY OTHER IN ITS CLASS
f /Canaweld in /Company/Canaweld-Inc t /CanaweldInc y /CanaweldInc
www.canaweld.com

For info, go to aws.org/ad-index

Note: The 2017 schedule for all certifications is posted online at aws.org/w/a/registrations/prices_schedules.html.

Certified Welding Inspector (CWI)

Location	Seminar Dates	Exam Date
Houston, TX	Feb. 26–March 3	March 4
Kansas City, MO	Feb. 26–March 3	March 4
Norfolk, VA	Feb. 26–March 3	March 4
Boston, MA	March 5–10	March 11
Sacramento, CA	March 5–10	March 11
Salt Lake City, UT	March 5–10	March 11
Orlando, FL	March 5–10	March 11
Perrysburg, OH	Exam only	March 11
Chicago, IL	March 12–17	March 18
San Antonio, TX	March 12–17	March 18
Miami, FL	Exam only	March 24
York, PA	Exam only	March 25
Springfield, MO	March 19–24	March 25
Portland, OR	March 19–24	March 25
Las Vegas, NV	March 19–24	March 25
Dallas, TX	March 26–31	April 1
Minneapolis, MN	March 26–31	April 1
Pittsburgh, PA	March 26–31	April 1
Atlanta, GA	April 2–7	April 8
San Francisco, CA	April 2–7	April 8
Detroit, MI	April 2–7	April 8
St. Louis, MO	Exam only	April 8
Miami, FL	Exam only	April 21
Nashville, TN	April 23–28	April 29
Syracuse, NY	April 23–28	April 29
Pittsburgh, PA	May 7–12	May 13
Orlando, FL	May 7–12	May 13
Tulsa, OK	May 7–12	May 13
Biloxi, MS	May 7–12	May 13
Des Moines, IA	May 7–12	May 13
Houston, TX	May 14–19	May 20
Cleveland, OH	May 14–19	May 20
Los Angeles, CA	May 14–19	May 20
Charlotte, NC	May 14–19	May 20
Miami, FL	Exam only	June 9
New Orleans, LA	June 4–9	June 10
Kansas City, MO	June 4–9	June 10
Denver, CO	June 11–16	June 17
Milwaukee, WI	June 11–16	June 17
Huntsville, AL	June 11–16	June 17
Newark, NJ	June 11–16	June 17
Beaumont, TX	June 25–30	July 1
Duluth, MN	June 25–30	July 1
Waco, TX	July 9–14	July 15
Sacramento, CA	July 9–14	July 15
Houston, TX	July 9–14	July 15
Miami, FL	Exam only	July 22
Louisville, KY	July 16–21	July 22
Atlanta, GA	July 16–21	July 22

9-Year Recertification Seminar for CWI/SCWI

For current CWIs and SCWIs needing to meet education requirements without taking the exam. The exam can be taken at any site listed under Certified Welding Inspector.

Location	Seminar Dates
Denver, CO	Feb. 26–March 3
Dallas, TX	March 5–10
Miami, FL	March 5–10
Sacramento, CA	April 2–7
Charlotte, NC	May 7–12
Pittsburgh, PA	May 14–19
Kansas City, MO	June 4–9
Miami, FL	July 23–28

Certified Welding Educator (CWE)

Seminar and exam are given at all sites listed under Certified Welding Inspector. Seminar attendees will not attend the Code Clinic portion of the seminar (usually the first two days).

Certified Welding Sales Representative (CWSR)

CWSR exams are given at Prometric testing centers. More information at aws.org/certification/detail/certified-welding-sales-representative.

Certified Welding Supervisor (CWS)

CWS exams are given at Prometric testing centers. More information at aws.org/certification/detail/certified-welding-supervisor.

Certified Radiographic Interpreter (CRI)

The CRI certification can be a stand-alone credential or can exempt you from your next 9-Year Recertification.

Location	Seminar Dates	Exam Date
Seattle, WA	Feb. 27–March 3	March 4
Houston, TX	March 13–17	March 18
San Francisco, CA	April 10–14	April 15
Las Vegas, NV	May 1–5	May 6
Cleveland, OH	June 5–9	June 10
Dallas, TX	July 17–21	July 22
Miami, FL	Exam only	Aug. 4
Kansas City, MO	Aug. 21–25	Aug. 26
Chicago, IL	Sept. 11–15	Sept. 16
Pittsburgh, PA	Oct. 9–13	Oct. 14

Certified Robotic Arc Welding (CRAW)

ABB, Inc., Auburn Hills, MI; (248) 391-8421
 OTC Daihen, Inc., Tipp City, OH; (937) 667-0800, ext. 218
 Lincoln Electric Co., Cleveland, OH; (216) 383-8542
 Genesis-Systems Group, Davenport, IA; (563) 445-5688
 Wolf Robotics, Fort Collins, CO; (970) 225-7736
 On request at MATC, Milwaukee, WI; (414) 456-5454

IMPORTANT: This schedule is subject to change. Please verify your event dates with the Certification Dept. to confirm your course status before making travel plans. Applications are to be received at least **six weeks** prior to the seminar/exam or exam. Applications received after that time will be assessed a \$350 Fast Track fee. Please verify application deadline dates by visiting our website aws.org/certification/docs/schedules.html. For information on AWS seminars and certification programs, or to register online, visit aws.org/certification or call (800/305) 443-9353, ext. 273, for Certification; or ext. 455 for Seminars.

Industry Leaders Recognized at FABTECH



The AWS 2017 board of directors assembled at FABTECH in Las Vegas, Nev.

Class of 2016 Counselors and Fellows Announced

The 2016 classes of AWS Fellows and Counselors were recognized during FABTECH in Las Vegas, Nev.

The Fellows are John A. Goldak, Leijun Li, Anatol Rabinkin, Estela S. Surian, and Hongyan Zhang. The Counselors are Robert G. Pali, Robert F. Purvis, Kenneth R. Stockton, and George A. Young.

AWS Fellows are cited for “*servicing the welding community and industry with great distinction as individuals whose careers have contributed significantly to the knowledge, science, and application of welding.*”

John A. Goldak is recognized for his contributions to computational weld mechanics, including the seminal development of the “double ellipsoid heat source.” He is also cited for developing and applying state-of-the-art computational models in practice and in high responsibility situations.

Leijun Li is recognized for his efforts to secure research and instrument grants. He has established a welding research group that attracts students and postdoctoral researchers. He has also made contributions to the science and technology of austenitic stainless steels, laser deposition and laser processing of materials, bond formation for ultrasonic welding, and phase transformations in advanced alloys.

Anatol Rabinkin is recognized for his accomplishments in the area of filler metal development, including fundamental mechanical and physical properties, as well as braze joint

performance and brazing technology. His inventions of the amorphous alloy have been used for pollution control in diesel trucks and equipment.

Estela S. Surian is recognized for her contribution to the



From top left are Fellows Hongyan Zhang, Anatol Rabinkin, Estela S. Surian, John A. Goldak, and Leijun Li. From bottom left are Counselors Robert G. Pali, Robert F. Purvis, Kenneth R. Stockton, and George A. Young.

design and development of consumables in the areas of covered electrodes, cored wires for semiautomatic and automatic welding, and fluxes for submerged arc welding. She has also developed welding-related courses in the United States, Argentina, Brazil, and Switzerland.

Hongyan Zhang is recognized for his contributions to the joining of aluminum and other lightweight materials, especially for automotive applications.

AWS Counselors are recognized for “serving the welding community and industry with distinction and organization-

al leadership that has enhanced the image and impact of the welding industry.”

Robert G. Pali is recognized for devoting more than 50 years to the welding industry. He served the American Welding Society as treasurer from 2010–2015, and is currently an AWS Foundation trustee.

Robert F. Purvis is currently a vocational instructor at the California Department of Corrections and Rehabilitation for Folsom State Prison. He pioneered the vocational curriculum for the department and wrote a complete set of weld procedure specifications for Clark-Pacific Construction.

Kenneth R. Stockton is recognized for his design and development of a portable welding training facility, which has minimized the training infrastructure and allowed more efficient training and upgrading of welders.

George A. Young is recognized for his work in explosion welded components and their application in the petroleum, power generation, marine, and primary metals industries. He has served the American Welding Society for 45 years.

Achievement Awards Presented at FABTECH



Paul T. Vianco



Wei Zhang



Scottie C. Smith



Branden Otto



Dashuang S. Liu

Comfort A. Adams Lecture Award

This award is presented to an outstanding scientist or engineer for a lecture describing a new or distinctive development in the field of welding. The lecture is presented during FABTECH.

“Understanding the Reliability of Solder Joints Used in Advanced Structural and Electronics Applications”

Paul T. Vianco, an AWS Fellow, has been a Distinguished Member of the technical staff at Sandia National Laboratories since 1987. Vianco has authored more than 100 peer-reviewed journal articles, eight book chapters, and two books. Vianco also coauthored a solder fatigue software and holds five patents.

Adams Memorial Membership Award

This award recognizes educators for outstanding teaching activities in undergraduate and postgraduate engineering institutions.

Wei Zhang is an associate professor at the Department of Materials

Science and Engineering in The Ohio State University, where he also contributes to the Simulation Innovation and Modeling Center as well as teaches welding design and computational weld modeling.

Howard E. Adkins Memorial Instructor Membership Award

This award recognizes instructors for outstanding teaching accomplishments at the high school, trade school, technical institute, and community college levels.

Scottie C. Smith, a welding instructor at Northwest Florida State College, helped implement a welding program under a grant from the U.S. Department of Labor, and built a welding lab from the ground up.

Branden Otto, an AWS CWI and CWE, is a welding instructor at Iowa Central Community College. He is also an industrial trainer, AWS accredited testing facility manager, and test supervisor.

Robert J. Conkling Memorial Award

This award is presented to the schools that trained the two first-place winners in the SkillsUSA welding competition.

2016 SkillsUSA Championships Gold Medalist First-Place Schools

High School: Willoughby-Eastlake Tech Center, Willoughby, Ohio

Postsecondary School: Central New Mexico Community College, Albuquerque, N.Mex.

A. F. Davis Silver Medal Award

This award recognizes authors of papers published in the Welding Journal during the previous calendar year that represent the best contributions to the progress of welding in the categories of machine design, maintenance and surfacing, and structure design.

Maintenance and Surfacing

“Properties of Silicon-Added, Iron-Based, Slag-Free, Self-Shielded Flux-Cored Wire”

Dashuang S. Liu is a lecturer on management in the Department of Welding Technology and Engineering



Ping Wei



Jay D. Blom



Brian Griffith



Behrooz Beidokhti



Rasoul Pouriamanesh

at the School of Material Science & Engineering at the Jiangsu University of Science and Technology. He has published more than 20 articles.

Ping Wei is a research associate at the School of Naval Architecture and Ocean Engineering at Jiangsu University of Science and Technology. She has published more than ten articles.

Distinguished Welder Award

This award recognizes individuals who have exceptional welding skills and experience related to all aspects of the art of welding.

Jay D. Blom, an engineering technician at Vermeer Corp., began his welding career 22 years ago. He was a top welder at the company in 2005, 2007, and 2013, and ranked fifth place at the 2005 AWS Professional Welder competition.

Dalton E. Hamilton Memorial CWI of the Year Award

This award recognizes AWS members participating in the SCWI/CWI programs whose inspection, Society, and civic activities have enhanced public awareness of the Society and the CWI program or who have otherwise made an outstanding contribution to the science of welding inspection.

Brian Griffith is a CWI and CWE who also holds ASNT Level III nondestructive testing certifications in multiple methods. He is manager of Engineering Services at Van Gorp Corp., Pella, Iowa, and chair of the AWS Iowa Section.

W. H. Hobart Memorial Award

This award is presented to the authors of the paper published in the Welding Journal during the previous calendar year that describes the best contribution to pipe welding, the struc-

tural use of pipe, or similar applications, excluding the manufacture of pipe.

“Effect of Filler Metal on Mechanical Properties of HSLA Welds”

Behrooz Beidokhti is an assistant professor in the Materials and Metallurgical Engineering Department at the Ferdowsi University of Mashhad.

Rasoul Pouriamanesh is a PhD candidate in metallurgical and materials engineering at the Amirkabir University of Technology.

Honorary Membership Award

This award is presented to a person of acknowledged eminence in the welding profession or who is credited with exceptional accomplishments in the industry.

Sindo Kou, a Fellow of AWS and ASM International, has served as professor at the University of Wisconsin since 1983.

Robert F. Purvis (see bio under Class of 2016 Counselors and Fellows).

International Meritorious Certificate Award

This certificate recognizes an individual who has made significant contributions to benefit the worldwide welding industry.

Kendall Ymker is an engineering manager at RoMan Mfg., Inc. He has been involved with AWS technical committees for 20 years.

William Irrgang Memorial Award

This award recognizes the individual who has done the most to enhance the American Welding Society’s goal of advancing the science and technology of welding over the last five years.

Thomas J. Lienert, AWS Fellow and CWE, is currently an AWS vice president. He holds various positions on AWS committees, and serves as lead principal reviewer for the *Welding*

Journal. He is also a technical staff member for R&D at Los Alamos National Laboratory.

Charles H. Jennings Memorial Award

This award is presented for the most valuable paper written by a college student or faculty representative published in the Welding Journal during the previous calendar year.

“Primary Chromium Carbide Fraction Control with Variable Polarity SAW”

Ivan Le Gall is a welding engineer at Saipem S.A. He has previously worked for the Subsea Department specializing in offshore projects.

Patricio F. Mendez, an AWS Fellow, is the Weldco/Industry chair in Welding and Joining and director of the Canadian Centre for Welding and Joining at the University of Alberta. He has 59 indexed publications and nine patents.

Steven Borle holds a master of science from the Canadian Centre for Welding and Joining at the University of Alberta.

James F. Lincoln Gold Medal Award

This award is presented for the paper with a single author that represents the best original contribution to the advancement and use of welding published in the Welding Journal during the previous calendar year.

“A Simple Index for Predicting the Susceptibility to Solidification Cracking”

Sindo Kou (see bio under Honorary Membership Award).

McKay-Helm Award

This award is presented for the best contribution to the advancement of knowledge of low-alloy steel, stainless steel, or surfacing welding metals involving the use, development, or testing of



Sindo Kou



Robert F. Purvis



Kendall Ymker



Thomas J. Lienert



Ivan Le Gall



Patricio F. Mendez



Steven Borle



Holly D. Carlton



John W. Elmer



Randolph Pong

these materials, as represented by articles published in the *Welding Journal* during the previous calendar year.

“The Effect of Ar and N₂ Shielding Gas on Laser Weld Porosity in Steel, Stainless Steels, and Nickel”

Holly D. Carlton is a materials scientist at Lawrence Livermore National Laboratory, where she started in 2012 as a postdoctoral research scientist.

John W. Elmer, an AWS Fellow and Honary Member, serves on several committees for the American Welding Society, ASM International, The Metallurgical Society, and Institute of Electrical and Electronics Engineers. He also serves on the editorial review board for several publications.

Randolph Pong, a retired engineer, has recently accepted a position to return as a contractor for Lawrence Livermore National Laboratory serving as a consulting welding SME and AWS CWI for various laboratory programs.

Jay Vaja has been a member of TWI’s Research Members Board since 2009. He has more than 27 years’ experience in the field of laser material processing and has written and coauthored numerous technical reports and papers.

Professor Koichi Masubuchi Award

This award is presented to an individ-

ual who has made significant contributions to the advancement of science and technology of materials joining through research and development.

Adrian Gerlich is associate professor at the University of Waterloo, where he is also the appointed NSERC/TransCanada industrial research chair in welding for energy infrastructure.

Samuel Wylie Miller Memorial Medal Award

This medal is awarded for meritorious achievements that have contributed conspicuously to the advancement of the art and science of welding and cutting.

Richard P. Martukanitz has served on the board of directors for the Laser Institute of America, holds five patents, and is currently on the editorial board of *Additive Manufacturing*. He is also a Life Member of the American Welding Society and serves as the chair of the C7C Subcommittee on Laser Beam Welding and Cutting.

National Meritorious Award

This award recognizes good counsel, loyalty, and devotion to the affairs of the Society, and for promoting cordial relations with industry and other organizations.

Joseph Stricker was a member of

the International Thermal Spray Association for 28 years, while holding several positions on its executive board. He also served on the AWS C2 technical committee on Thermal Spray and has contributed to the recent revision of the Materials section of the original *AWS Thermal Spray Handbook*.

Muralidhar Tumuluru, an AWS Fellow, is a member of several AWS committees and the American Council of International Institute of Welding. He is also a principal reviewer for the *Welding Journal* and a peer reviewer for several other leading journals.

Robert L. Peaslee Memorial Brazing Award

*This award recognizes the paper considered to be the best contribution to the science or technology of brazing published in the *Welding Journal* during the previous calendar year.*

“Interfacial Microstructure of Laser Brazed AZ31B Magnesium to Sn-Plated Steel Sheet”

Ali M. Nasiri is an assistant professor of mechanical engineering at the Memorial University of Newfoundland.

David C. Weckman is a professor in the Department of Mechanical and Mechatronics Engineering at the University of Waterloo, where he is also



Jay Vaja



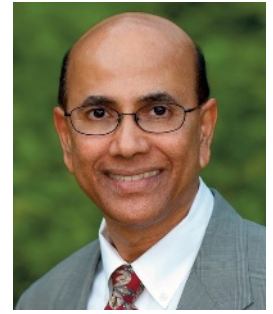
Adrian Gerlich



Richard P. Martukanitz



Joseph Stricker



Muralidhar Tumuluru



Ali M. Nasiri



David C. Weckman



Y. (Norman) Zhou



Scott L. Burdige



George T. Rolla

the coordinator of the undergraduate Welding and Joining Specialization.

Yunhong (Norman) Zhou, an AWS Fellow, is a university research chair and director of the Centre for Advanced Materials Joining in the University of Waterloo. He has published more than 270 peer-reviewed papers and several books.

Plummer Memorial Education Lecture Award

This award recognizes outstanding contributions to the national education lectures presented at the AWS Annual Welding Show and Convention.

“Making Advisory Boards Work through Industry Partnerships”

Scott L. Burdige teaches welding/metal fabrication to grades 11 and 12 at R. G. Drage Career Technical Center. He also sits on the National Visiting Committee as a representative of the National Science Foundation for WELD-ED, and serves as president of the Stark County Area Vocational Educators.

Private Sector Instructor Membership Award

This award honors educators in the welding community who teach in private facilities and have, in the opinion of the AWS Education Committee, advanced the

knowledge of welding to their students through apprenticeship programs, internal corporate training programs, and similar nonpublic education activities.

George T. Rolla created a unique teaching program in Lake Elsinore, Calif., where the goal is to help people launch successful careers in welding within two months. He also consults for companies in the industry by training and certifying welding employees, troubleshooting, and providing advice.

Warren F. Savage Memorial Award

This award recognizes the paper published in the Welding Journal Research Supplement the previous calendar year that best represents innovative research resulting in a better understanding of the metallurgical principles related to welding.

“Transformation and Tempering Behavior of the Heat-Affected Zone of 2.25Cr-1Mo Steel”

David K. Hodgson works for General Electric Aviation in Cincinnati, Ohio, as the lead joining engineer.

John C. Lippold, an AWS Fellow, has served on the faculty of the Welding Engineering program at The Ohio State University since 1995. He has also coauthored three textbooks and published more than 250 technical papers. He is coeditor of *Welding in the World*, published by the International

Institute of Welding.

Tao Dai is a PhD candidate in the Welding Engineering program at The Ohio State University. He is scheduled to receive his degree this summer.

William Spraragen Memorial Award

This award recognizes the best paper published in the Welding Journal Research Supplement during the previous calendar year.

“Creep Rupture Performance of Welds of P91 Pipe Steel”

Mario Amata has been an electrode development engineer at Hobart Brothers Co. for the last ten years.

Sudarsanam Suresh Babu, an AWS Fellow, is the appointed chair of Advanced Manufacturing at the University of Tennessee, Knoxville. He has published more than 140 peer-reviewed papers and numerous conference proceedings.

Joseph C. Bundy has served the Hobart Brothers Co. for almost 30 years. He holds five patents in the area of tubular welding electrode formulations. He has also published several articles in the *Welding Journal* and other publications.

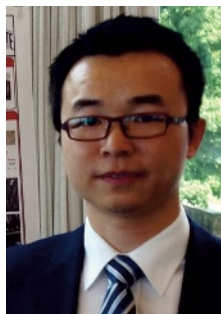
Xiao Chai is a metallurgical scientist at Novelis Global Technology and Research Center in Kennesaw, Ga., where he focuses on joining techniques



David K. Hodgson



John C. Lippold



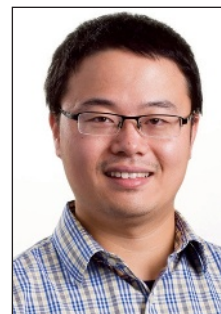
Tao Dai



S. Suresh Babu



Joseph C. Bundy



Xiao Chai



Shuanglin Chen



Chuan Zhang



Fan Zhang



David R. Miller



Donald F. Maatz Jr.



Donald D. Rager

for aluminum alloys.

Shuanglin Chen helped develop a user-friendly phase diagram calculation software for the U.S. Air Force, which led to the formation of CompuTherm, LLC. He also developed PanEngine, a thermodynamic calculation engine.

Sindo Kou (see bio under Honorary Membership Award).

Chuan Zhang is involved in software and database development at CompuTherm, LLC. He has authored and coauthored more than 50 published scientific articles.

Fan Zhang is the president of CompuTherm, LLC. She also serves as associate editor of the *Journal of Phase Equilibria and Diffusion*, and chairs several technical committees of the TMS Society.

R. D. Thomas Memorial Award

This award recognizes a member of

the American Council of the International Institute of Welding (IIW) or an AWS member who has made a substantial contribution to the IIW activities.

David R. Miller has served ABS Shanghai, where he troubleshoots a variety of shipyard, foundry, and fabrication problems. He also serves on the AWS welding consumables committees and subcommittees.

Elihu Thomson Resistance Welding Award

This award recognizes an outstanding contribution to the technology and application of resistance welding, including equipment innovations, unique applications in production, a published paper, or other activity of merit.

Donald F. Maatz Jr., a CWI, serves on the D8 and D8D Automotive Welding Committees, the D8.1 and D8.9 Automotive Welding Subcommittees, and is an advisor to the C1 Resistance

Welding Committee. He is also an instructor for the RWMA Welding School, and vice chairman of the Certified Resistance Welding Technician working group.

George E. Willis Award

This award recognizes an individual for promoting the advancement of welding internationally, by fostering cooperative participation in areas such as technology transfer, standards rationalization, and promotion of industrial goodwill.

Donald D. Rager, an AWS counselor and Life Member, is a Professional Engineer in Ohio, and a registered and licensed Professional Engineer in Virginia. He is also the president of Rager Consulting, Inc., founded in 2000, and serves on various AWS technical committees. [WJ](#)

Candidates Sought to Receive the MIT Masubuchi Award

The Prof. Koichi Masubuchi award, with a \$5000 honorarium, is presented to one person, 40 or younger, who has made significant contributions to the advancement of materials joining

through research and development. Send a list of your candidate's experience, publications, honors, awards, and at least three letters of recommendation from fellow researchers to Prof.

Todd Palmer, tap103@psu.edu. This award is sponsored annually by the Massachusetts Institute of Technology, Dept. of Ocean Engineering.

Member Service Anniversaries Recognized at FABTECH



AWS 2016 President David McQuaid (far left) is shown with Gold Members celebrating 50 years of service to the Society — (from left) Phillip Schmidt, Riley Turpin, Ray Wilsdorf, and Victor Matthews.



Life Members, with 35 years of service to the Society, included Larry Anderson, David Bennett, Kevin Disney, Rick Henson (accepting for him was Randy Polito), James Hoffman, Paul Goodale, Melton Kemp, Stephen Liu, John Moore, Randee Munns, Craig Newell, Rick Polanin, Raymond Shehata, Ray Shook, Keith Steelman, Kurt Trarbach, Chris Trumbull, Michael Urioste, and Phil Zammit. Not everyone is pictured. AWS 2016 President David McQuaid is at the far left in both photos.



Silver Members celebrating 25 years of membership included David Baron, Micky Bradican, Mike Bumgarner, Ken Caratelli, Richard Cook, Mary Ruth Johnsen, Kenneth Karwowski, Ron Lynn, Fred Martelli, Paul Ruess, Salvatore Russomanno, Joel Sims, Jeff Straham, John Tiemann, Russell Wahrman, David Webber, and Joseph Zawodny. Not everyone is pictured. AWS 2016 President David McQuaid is at the far left in both photos.

Sections Recognized for Sponsoring Welding Scholarships



Representing the Sections sponsoring new scholarships are Mike Skiles (Central Louisiana), Bob Wilcox (Central Michigan), J Jones (Central and East Texas), Randy Emery (Central Valley), Stewart Harris (accepting for Greg Frederick, Charlotte), Josh Burgess (Chattanooga and Greater Huntsville), John Willard (Chicago), J. T. Mahoney (Columbia), and Dan Roland (Fox Valley and Lakeshore). Not everyone is pictured. AWS Foundation Board of Trustees Chair William Rice is at the far right.



Representing the Sections sponsoring new scholarships are Josh Burgess (Nashville); Harland Thompson (New York); Paul Stanglin, Ernest Levert, Steve Hatten, Terri Barbeau, and Mike Barbeau (North Texas); J Jones (Oklahoma and Ozark); Dan Zabel, Shannon Hansen, and Chase Einspahr (Southeast Nebraska); and Stewart Harris and Jay Manning (Triangle). Not everyone is pictured. AWS Foundation Board of Trustees Chair William Rice is at the far right.

TECH TOPICS

Opportunities to Contribute to AWS Technical Committees

The following committees welcome new members. Some committees are recruiting members with specific interests in regard to the committee's scope, as marked below: Producers (P), General Interest (G), Educators (E), Consultants (C), and Users (U). For more information, contact the staff member listed or visit aws.org/library/doclib/Technical-Committee-Application.pdf.

S. Borrero, sborrero@aws.org, ext. 334. **Definitions and symbols**, A2 Committee (E). **Titanium and zirconium filler metals**, A5K Subcommittee. **Piping and tubing**, D10 Committee (C, E, U). **Welding practices and procedures for austenitic steels**, D10C Subcommittee. **Aluminum piping**, D10H Subcommittee. **Chromium molybdenum steel piping**, D10I Subcommittee. **Welding of titanium piping**, D10K Subcommittee. **Purging and root pass welding**, D10S Subcommittee. **Low-carbon steel pipe**, D10T Subcommittee. **Orbital pipe welding**, D10U Subcommittee. **Duplex pipe welding**, D10Y Subcommittee. **Joining metals and alloys**, G2 Committee (E,

G, U). **Reactive alloys**, G2D Subcommittee (G).

R. Gupta, ext. 301, gupta@aws.org. **Filler metals and allied materials**, A5 Committee (E). **Magnesium alloy filler metals**, A5L Subcommittee.

P. Portela, pportela@aws.org, ext. 311. **High energy beam welding and cutting**, C7 Committee (C, E, G). **Hybrid welding**, C7D Subcommittee (G). **Robotic and automatic welding**, D16 Committee (C, E). **Welding in sanitary applications**, D18 Committee (C, E, G). **Additive manufacturing**, D20 Committee (C, E, G).

J. Molin, ext. 304, jmolin@aws.org. **Structural welding**, D1 Committee (E). **Sheet metal welding**, D9 Committee (C, G).

J. Douglass, jdouglass@aws.org, ext. 306. **Methods of weld inspection**, B1 Committee (C, E). **Brazing and soldering**, C3 Committee (C, E, G). **Welding in marine construction**, D3 Committee (C, E, G, U). **Welding of machinery and equipment**, D14 Committee (C, E, G, U).

A. Babinski, ababinski@aws.org, ext. 310. **Resistance welding**, C1 Committee (C, E, G, U). **Friction welding**, C6 Committee (C, E). **Automotive welding**, D8 Committee (C, E, G, U). **Resistance welding equipment**, J1 Committee (C, E, G, U). **Welding in the aircraft and aerospace industry**, D17 Subcommittee (C, E, G).

S. Hedrick, steveh@aws.org, ext. 305. **Metric practice**, A1 Committee (C, E). **Mechanical testing of welds**, B4 Committee (E, G, P). **Joining of plastics and composites**, G1 Committee (C, E, G). **Personal & facilities qualification**, PFQC Committee (C, E, G). **Safety and health committee**, SHC Committee (E, G).

J. Rosario, jrosario@aws.org, ext. 308. **Procedure and performance qualification**, B2 Committee (E, G). **Thermal spraying**, C2 Committee (C, E, G, U). **Oxyfuel gas welding and cutting**, C4 Committee (C, E, G). **Welding iron castings**, D11 (C, E, G, P, U). **Railroad welding**, D15 (C, E, G, U).

Technical Committee Meetings

All AWS technical committee meetings are open to the public. Contact staff members listed below or call (800/305) 443-9353 for information.

Feb. 7. B2F Subcommittee on Plastic Welding Qualification. Miami, Fla. Contact: S. P. Hedrick, stevenh@aws.org, ext. 305.

Feb. 7. G1A Subcommittee on Hot Gas Welding and Extrusion Welding. Miami, Fla. Contact: S. P. Hedrick, ext. 305, stevenh@aws.org.

Feb. 7. D15D Subcommittee on Resistance Welding for Railroad Applications. Nashville, Tenn. Contact: J. Rosario, ext. 308, jrosario@aws.org.

Feb. 8. D15 Committee on Railroad Welding. Nashville, Tenn. Contact: J. Rosario, ext. 308, jrosario@aws.org.

Feb. 8. D15A Subcommittee on Cars and Locomotives. Nashville, Tenn. Contact: J. Rosario, jrosario@aws.org,

ext. 308.

Feb. 23. D3B Subcommittee on Underwater Welding. New Orleans, La. Contact: J. Douglass, jdouglass@aws.org, ext. 306.

New Standards Project

Development work has begun on the following new or revised standards. Affected individuals are invited to contribute to their development. Participation on AWS Technical committees is open to all persons.

A1.1:20XX, *Metric Practice Guide for the Welding Industry*. This metric practice guide is based on the International System of Units (SI) as defined in the U.S. Federal Register notice of July 28, 1998, "Metric System of Measurement: Interpretation of the International System of Units for the United States." This guide contains specifications of SI

base units, derived units, prefixes, and rules for their use in AWS documents. It also contains factors and rules for converting from U.S. customary units to SI units, as well as recommendations to industry for managing the transition. Stakeholders: Welders, manufacturers, and welding engineers. Revised Standard. Contact: S. P. Hedrick, stevenh@aws.org, ext. 305.

B4.0:20XX, *Standard Method for the Mechanical Testing of Welds*. This specification establishes standard methods for mechanical testing of welds. It also describes the significance of each test, test apparatus, test specimen preparation, and test procedure. Sample test results sheets are provided. Stakeholders: Welding industry, test laboratories, and users of welding processes. Revised Standard. Contact: S. P. Hedrick, stevenh@aws.org, ext. 305.

G1.10M:20XX, *Guide for the Evaluation of Thermoplastic Welds*. This stan-

standard lists and describes flaws and defects in hot gas, hot gas extrusion, heated tool butt fusion, socket fusion, electrofusion, and flow fusion welded joints in thermoplastics. Its intent is to make possible a generally valid evaluation by giving consideration to graded quality requirements. Included are tables illustrating cracks, voids, solid inclusions, incomplete fusion, flaws and defects of shape, and other flaws and defects in thermoplastic welds. Flaw and defect features with descriptions and illustrations are compiled into tables to aid in the evaluation of welds. Stakeholders: Welders, welding engineers, and users of thermoplastic welding. Revised Standard. Contact: S. P. Hedrick, stevenh@aws.org, ext. 305.

Standards for Public Review

AWS was approved as an accredited

standards-preparing organization by the American National Standards Institute (ANSI) in 1979. AWS rules, as approved by ANSI, require that all standards be open to public review for comment during the approval process. This column also advises of ANSI approval of documents.

The following standards are submitted for public review. A draft copy may be obtained by contacting the staff secretary of the committee as listed below at AWS, Standards Development, 8669 NW 36 St., #130, Miami, FL 33166-6672; (800/305) 443-9353.

C2.16/C2.16M:201X, *Guide for Thermal Spray Operator Qualification Programs*. Revised Standard. \$31.50. ANSI public review expires 2/6/17. Contact: J. Rosario, jrosario@aws.org, ext. 308.

C7.4/C7.4M:201X, *Process Specification and Operator Qualification for Laser Beam Welding*. Revised Standard. \$68.00. ANSI public review expires

2/13/17. Contact: P. Portela, ext. 311, pportela@aws.org.

Revised Standard Approved by ANSI

A5.9/A5.9M:2017, *Welding Consumables — Wire Electrodes, Strip Electrodes, Wires and Rods for Arc Welding of Stainless and Heat Resisting Steels — Classification*. Approval Date: 12/9/2016.

A5.10/A5.10M-2016, *Welding Consumables — Wire Electrodes, Wires and Rods for Welding of Aluminum and Aluminum-Alloys — Classification*. Approval Date: 11/22/2016.

MEMBERSHIP ACTIVITIES

AWS Member Counts

January 1, 2017

Sustaining.....	591
Supporting	347
Educational.....	765
Affiliate	704
Welding Distributor	60
Total Corporate	2467
Individual	59,807
Student + Transitional	12,490
Total Members	72,297

New AWS Supporters

Sustaining Members

Dean's Certified Welding, Inc.
27645 Commerce Center Dr.
Temecula, CA 92590
deanswelding.com

Unlimited Welding, Inc.
235 Old Sanford Oviedo Rd.
Winter Springs, FL 32708
unlimitedwelding.com

Affiliate Companies

Aerial Access Solutions

22 SE 7th Ave.
Deerfield Beach, FL 33441

CRRC MA Corp.

100 Summer St.
Suite 1603
Boston, MA 02110

CT & C Fabrication

P.O. Box 973
Grantsville, UT 84029

Clover Field Services, LLC

81 Low Rd.
Ashland, PA 17921

Cyclone Welding

186 Timerline Rd.
Unit B-3
Clarksboro, NJ 08085

Damen Shipyards Sharjah-Albwardy Marine

Plot Hd-22, Hamriyah Freezone
P.O. Box 52125, Sharjah Sharjah 971
United Arab Emirates

Engineered Parts & Services

P.O. Box 1899
Vega Alta, PR 00692

FJ Propeller Miami Corp.

2185 NW 34th Ave.
Miami, FL 33142

Fabex Engineering

B-69, MIDC, Ambad
Nashik, Maharashtra
422010, India

GM Rogers QA/QC Consulting Services

1748 N. Linn Lane
Las Vegas, NV 89156

Golden Manufacturing, Inc.

17611 East St.
N. Fort Myers, FL 33917

McPherson Enterprises, Inc.

3341 New McEver Rd.
Acworth, GA 30101

McWhirter Steel, Inc.

41004 41 St. West
Palmdale, CA 93551

Montesco, S. A.

Sector 1
Puerta del Llano del Pinal
Quetzaltenango, Quetzaltenango
0901 Guatemala

North East Wisconsin Welding

1200 Blackwell St.
Kaukauna, WI 54130

Oestec De México S.A. De C.V.

Las Torres 807
Col. Villa Hogar
Toluca 50170, Mexico

Reynolds Iron Works

157 Palmer Industrial Rd.
Williamsport, PA 17701

Southern Tank, Inc.

182 Union Rd. 293
El Dorado, AR 71730

Trinweld Contracting Services, Ltd.

No. 24 IDC Estate
Harmony Hall
San Fernando, Marabella
Trinidad and Tobago

West Metal Works, Inc.

68 Hayes Pl.
Buffalo, NY 14210

Wildcat Steel & Fabricating

P.O. Box 1429
Hardeeville, SC 29927

Educational Institutions**AKS East Africa, Ltd.**

34711 Nairobi
Nairobi 00100, Kenya

Amaze Weld Tech Private, Ltd.

11/3, 4th Cross, Magad
Bangalore, Karnataka 560023
India

Centro De Formacion De EM

Avenida Manzanares A5
Urbanizacion Manuel Prado
Cusco, 51 Peru

CNI Pacific Co., Ltd.

174/80 T. Pla.
A. Banchang, Thailand

Local 520 JATC

7193 Jonestown Rd.
Harris, PA 17112



CK Worldwide, an AWS Sustaining Member, donated \$1000 worth of toys to the local fire department for the Toys for Tots charity. Wearing Santa hats from left to right are Jeff Sharpe, CK Worldwide president, and Bonnie Sims, secretary-treasurer.

Mukwonago Area School District

605 W. School Rd.
Mukwonago, WI 53149

Peter the Great St. Peters

29, Polytechnicheskaya St.
St. Petersburg, 195251 Russia

Polk County College & Career Academy

167 Frank Lott Dr.
Cedarown, GA 30125

Southwest Mississippi Comm. College

1156 College Dr.
Summit, MS 39666

Waverly-Shell Rock High School

1405 4 Ave. SW
Waverly, IA 50677

Supporting Company Members**Alloy Coating Supply**

22820 IH45 North Bldg. 6
Spring, TX 77373

Bolt Construction, Inc.

10422 S. Ave.
Youngstown, OH 44514

Clearwater Contracting

2618 Bannock Ave.
Nampa, ID 83686

Fabrineering

1035-D Mecklenburg Hwy.
Mooresville, NC 28115

MD Merrett, Inc.

P.O. Box 380, Carefree, AZ 85377

Member-Get-A-Member Campaign

Listed here are the members participating in the 2016 Member-Get-a-Member campaign. The campaign runs from Jan. 1 to Dec. 31, 2016. Members receive 5 points for each Individual Member and 1 point for every Student Member recruited.

For campaign rules and a prize list, please see page 65 of this *Welding Journal*. Standings as of December 21. Call the AWS Membership Dept. at (800) 443-9353, ext. 480, for more information.

J. W. Morris, Mobile — 135
G. Bieniecki, Cleveland — 128
M. Krupnicki, Rochester — 65
D. A. Saunders, Lakeshore — 47
D. J. Ebenhoe, Kern — 45
J. W. Fregia, Houston — 43
G. L. Gammill, NE Mississippi — 43
D. P. Thompson, SW Virginia — 43
J. G. Knapp, Tulsa — 40
R. Riggs, Tulsa — 40
A. D. Stute, Madison-Beloit — 40
G. J. Smith, Lehigh Valley — 38
B. P. Brandmeir, Lehigh Valley — 38
B. M. Scherer, Cincinnati — 37
D. M. Box, Pascagoula — 35
H. H. Hughes, Mahoning Valley — 32
D. Lesik, Alberta — 30
G. G. Schroeter, Nebraska — 30
T. Geisler, Pittsburgh — 26
J. J. Russell, Fox Valley — 26
R. F. Purvis, Sacramento — 25
S. P. Siviski, Maine — 26
R. D. Zabel, SE Nebraska — 26
C. L. Claycomb, Kansas City — 25
K. Conway, Cleveland — 25
R. F. Purvis, Sacramento — 25
S. R. Ulrich, Mississippi Valley — 25

M. J. Wilson, Wyoming — 25
 B. A. Cheatham, Columbia — 21
 C. A. Donnell, NW Ohio — 21
 S. Gambill, Detroit — 20
 D. J. Larson, Northern Plains — 20
 C. A. Galbavy, Idaho/Montana — 19
 C. D. Spitzer, Tri-State — 19
 J. A. Gentry Sr., Sangamon Valley — 18
 A. I. Duron, New Orleans — 17
 J. N. Carney, Western Michigan — 17
 C. A. Renfro, Chattanooga — 17
 R. L. Richwine, Indiana — 17

D. S. Beecher, San Diego — 16
 T. A. Harris, Johnstown-Altoona — 16
 C. J. Bridwell, Ozark — 15
 E. J. Hinojosa, Johnstown-Altoona — 15
 R. D. Irving, Spokane — 15
 K. Koch, Fox Valley — 15
 Y. Lopez, International — 15
 C. Parsons, Holston Valley — 15
 J. D. Schlarb, Portland — 15
 M. D. Stein, Detroit — 15
 J. Upton, Houston — 15

J. C. McClung, Cincinnati — 14
 R. A. Ray, Tri-River — 14
 T. E. Buckler Sr., Columbus — 13
 M. J. Haggard, Inland Empire — 13
 L. J. Palm, San Diego — 13
 L. M. Roat, Sacramento — 13
 C. Baker, Philadelphia — 12
 O. N. Boylan, Cleveland — 11
 E. Cooper, Indiana — 11

WEMCO Holds Meet and Greet at FABTECH

For a third consecutive year, WEMCO, an association of welding manufacturers, and a standing committee of the American Welding Society, brought together key players of the industry for a meet and greet cocktail reception at FABTECH in Las Vegas, Nev., on Nov. 17, 2016.

Those in attendance included WEMCO members, prospects, and AWS staff. Approximately 60 attendees

enjoyed the two-hour networking event, as well as the opportunity to nurture existing relationships and forge new friendships.

The 2017 WEMCO Annual Meeting will take place Feb. 22–24 at Loews Coronado Bay Resort in Coronado, Calif. Online registration is open until February 20th. It is also open to nonmembers. Visit wemco.org for more information.



From left are David Lambert, vice president of North American Sales, Miller Electric Mfg.; Keila DeMoraes, AWS WEMCO program manager; and Jeff Deckrow, Hypertherm vice president of North America.



From left are Bob Ranc, director of sales, Weldcoa; David Sullivan, WEMCO chair and welding national sales manager, 3M Speedglas; and Chris Westlake, director of sales, MK Products.

AWS Attends Weld India and the Golden Jubilee Ceremony

Several AWS representatives traveled to Kolkata, India, for Weld India, the 11th International Welding Technology Exhibition that took place Dec. 15–17 at the Chennai Trade Centre. The event was organized by the Indian Institute of Welding (IIW India), a member society of the International Institute of Welding.

AWS members also attended the Golden Jubilee Year ceremony celebrating the Indian Institute of Welding's 50th anniversary, where they made speeches and gave presentations. AWS 2016 President David McQuaid presented IIW India with an award honoring its momentous milestone. AWS Executive Director Ray Shook received an award from IIW India for his contributions to welding internationally.



Ray Shook (left), AWS executive director, and David McQuaid, AWS 2016 president, visit Kolkata, India, for the Weld India Show.

District 1

Douglas A. Desrochers, director
(508) 763-8011
dadaws@comcast.net

MONTREAL November 25

Location: Barbie's Restaurant and Bar, Montreal, Quebec, Canada
Summary: Executive committee members got together to discuss Section financial details, membership status, and upcoming 2017 meetings.

District 2

Ken Temme, director
(856) 264-8377
kentemme@matrixnac.com

NEW JERSEY November 16

Location: Pantagis, Scotch Plains, N.J.
Presenter: Seann Bradley, senior sales engineer, Lincoln Electric Co.
Summary: Bradley spoke to members about the latest in Lincoln Electric robotics. Section awards were also given out to members.

PHILADELPHIA November 9

Location: Miller Electric Welding Technology Center, Swedesboro, N.J.
Presenter: Michael Novak, welding engineer, Miller Electric Co.
Summary: The Miller LiveArc™ welding performance management system was introduced to meeting attendees. Afterward, Novak answered questions and gave advice about welding problems members in the audience had encountered while welding.

District 3

Michael Sebergandio, director
(717) 471-2065
drweld13@gmail.com

READING December 15

Location: Osgood's, Robeson, Pa.
Summary: Section members enjoyed dinner and discussed upcoming events including a Zumba fundraiser in February, a student welding contest in mid-March, and a banquet in April.

District 4

Stewart A. Harris, director
(919) 824-0520
stewart.harris@altec.com

CHARLOTTE December 1

Location: Charlotte, N.C.
Presenter: Ray Sosko, welding instructor and faculty advisor for AWS student chapter, Central Piedmont Community College
Summary: Welding students and members were inducted into the National Technical Honor Society.

SOUTHWEST VIRGINIA September 22

Location: Lynchburg, Va.
Summary: 2016 AWS President David McQuaid shared his experiences as president. Following, members were given a plant tour of AREVA NP, Inc., hosted by Pete Strubhar and members of the AREVA training facility staff.



MONTREAL — Section Vice Chair and Treasurer Gil Trigo, District 1 Director Douglas A. Desrochers, and Section Chairman Michel Marier discussed Section activities.



NEW JERSEY — Section Chair Vince Murray (left) posed with speaker Seann Bradley.



NEW JERSEY — Victor Rhodes (right) received his 25-year member award from Chair Vince Murray.



PHILADELPHIA — Guest speaker Michael Novak (left) and Chairman Michael Chomin after the meeting.



READING — Seen (from left to right) are Past Chair Francis Butkus, Chevelle Houser, Past Chair Tracy Davenport, Past Chair Marilyn McLaughlin, Past Chair and current Treasurer David Hibshman, Secretary Sharon Bally, Chair Richard Heisey, and Randy Jacobs. The photo was taken by support person Mike McLaughlin.



CHARLOTTE — Faculty advisors and members posed for a photo after National Technical Honor Society inductions. Shown are Patrick McElhone, Shawn Spigner, John Burke, Ray Sosko, Ed Jones, Josh Armstrong, Collin Fanelli, Rich Davis, and John McPherson.



SOUTHWEST VIRGINIA — 2016 AWS President David McQuaid visited Section members before taking a tour of AREVA NP, Inc.



ATLANTA — Patrick Sands of Kia Motors (front left, holding plaque) gathered with Section members and students after accepting a gift of appreciation from Chair René Engeron.

District 5

Joseph T. "J. T." Mahoney, director
(352) 727-0366
Joseph.jt.mahoney@gmail.com

ATLANTA

November 15

Location: Lagrange, Ga.

Presenter: Patrick R. Sands, public relations, Kia Manufacturing Motors Group

Summary: Sands gave members a historical presentation about Kia Motors' fully automated assembly lines, safety benefits, and teamwork. Afterward, attendees were given a plant tour to see metal stamping and finishing product assembly. Attendees learned that assembly line employees change jobs every 15 min to learn all positions. Kia Motors was presented a plaque for hosting the meeting.

December 16

Location: Duluth, Ga.

Summary: The executive committee met with District Director J. T. Mahoney. New CWI exam proctors were elected and members discussed a college student trip to Germany, the Georgia Skills competition in March, and upcoming meetings. New member Jessica Plaunt was welcomed into the advisory committee.

FLORIDA WEST COAST

December 6

Location: Erwin Technical College Welding Department, Tampa, Fla.
 Presenter: Joseph "J. T." Mahoney, District 5 director

Topic: American Welding Society and the welding student

Summary: Mahoney advised students about the numerous ways AWS can assist them in their pursuit of a welding career. In addition, the Section raffled prizes and paid a one-year AWS student membership for all students in attendance.

District 6

Michael Krupnicki, director
 (585) 705-1764
mkrup@mahanyweld.com

NORTHERN NEW YORK

December 6

Location: Philips Healthcare, Latham, N.Y.

Presenters: Suellen Mallatte, Kevin Jordan, and Briant Carlo, tour guides, Philips Healthcare

Summary: Section members toured the Philips Healthcare welding shop where superconducting magnets are made.

District 7

Uwe Aschemeier, director
 (786) 473-9540
uwe@sgsdiving.com

COLUMBUS

December 8

Location: ASNT Center for Excellence, Dublin, Ohio

Presenter: James Bennett, chief technical officer, American Society of Nondestructive Testing (ASNT)

Summary: Bennett is responsible for

the certification, quality, and technical services provided by ASNT. AWS Section members learned about his career experience, received an overview of ASNT, and toured the new ASNT Center for Excellence.

District 8

D. Joshua Burgess, director
 (931) 260-7039
djoshuaburgess@gmail.com

CHATTANOOGA

November 29

Location: Tennessee Valley Authority Central Lab, Chattanooga, Tenn.

Presenters: Jesse Johnston, supervisor, metallurgy and boiler inspection, Tennessee Valley Authority (TVA)
 Topic: Inspection, testing, monitoring, and analysis

Summary: Johnston gave an overview of the services offered at the TVA laboratory and guided a tour of the lab. The highlight of the tour was the 3D scanning electron microscope.



NORTHERN NEW YORK — Section Secretary and Treasurer Dave Parker (right) thanked Suellen Mallatte for the Philips Healthcare tour.



COLUMBUS — Section Chairman Jim Worman (left) and speaker James Bennett of ASNT are pictured.



ATLANTA — Seen at their December meeting are (from left front to back) Greg Engeron, René Engeron, Tom Flynn, Tom Rieger, and Carl Matricardi. On the right (from back to front) are Jessica Plaunt, Bria Aguayo, Jay Maughon, Doug Rouner, and J. T. Mahoney.



FLORIDA WEST COAST — District Director J. T. Mahoney joined students at Erwin Technical College for AWS Information Day.

GREATER HUNTSVILLE

December 6

Location: Alabama Robotics Technology Park, Tanner, Ala.

Summary: Alabama Senator Arthur Orr visited Alabama Robotics Technology Park on the day of its grand opening ceremony. The AWS Skills Competition Committee's SkillsUSA WorldTeam Stage 2 U.S. Weld Trials and the Robotic Competition Committee's Student Robotic Welding Competition also took place that day. Additionally, Brewer High School welding instructor Brandon Jarrett received the Howard E. Adkins Memorial Instructor District Award.

December 7

Location: Wallace State Community College, Hanceville, Ala.

Summary: Roger Landers was presented the Dalton E. Hamilton Memorial CWI of the Year Section Award by Section Chairman and fellow Wallace State Community College Welding Instructor, Randy Hammond.



GREATER HUNTSVILLE — Brandon Jarrett (right) received the Howard E. Adkins Memorial Instructor District Award from Section Chair Randy Hammond.

NORTHEAST TENNESSEE

October 25

Location: Triple-S Steel, Knoxville, Tenn.

Summary: Members toured the Knoxville facility. Triple-S employees demonstrated the facility's shearing, cutting, and processing services as a



GREATER HUNTSVILLE — Alabama Senator Arthur Orr (left) and Rick Maroney, second vice chair of Section and director of Alabama Robotics Technology Park.

local distributor of structural and decorative steel. In addition to the tour, Paul Pipkin and Maneel Bharadwaj were recognized with District awards.

December 2

Location: University of Tennessee, Knoxville, Tenn.

Summary: The Materials Joining Group hosted students from Sequoyah High School for a tour. Students led by Maneel Bharadwaj, John Bohling, and Will Hoskins toured undergraduate laboratories, the welding research laboratory, and microscopy laboratories. Students also met with the leader



NORTHEAST TENNESSEE — Maneel Bharadwaj (right) received a District award from Joshua Burgess.



GREATER HUNTSVILLE — Roger Landers (left) was presented the Dalton E. Hamilton Memorial CWI of the Year Section Award by Chairman Randy Hammond.



NORTHEAST TENNESSEE — Joshua Burgess (left) presented Paul Pipkin with a District Service Award.



CHATTANOOGA — Thomas Platt, Jake Parish, Chris Renfro, Hannah McDonald, Jesse Johnston, Don Harvey, Jason West, Dusti Jones, and Thomas Atkinson toured Tennessee Valley Authority Central Lab.



American Welding Society®
MEMBERSHIP

EARN PRIZES WHEN YOU SPONSOR NEW MEMBERS

THE AWS 2017 MEMBER-GET-A-MEMBER CAMPAIGN



CAMPAIGN RULES

**RECRUIT NEW AWS MEMBERS FROM
JANUARY 1, 2017 TO DECEMBER 31, 2017 TO WIN.**

You receive points for each AWS Member you recruit:
5 Points for every AWS Individual Member you recruit
1 Point for every AWS Student Member you recruit

CAMPAIGN PRIZES

PRIZE CATEGORIES*

Earn 10-24 points.....	AWS Cap
Earn 25-34 points.....	AWS Polo Shirt
Earn 35+ points.....	AWS Jacket
Top Point Earner Wins.....	\$500 VISA Gift Card

*Prizes will be issued at the end of the campaign, based on total points earned.

To recruit new Members, use the application on the reverse:

All AWS members in good standing may participate and are eligible to win. In order to be eligible to win the drawing, the referring member must be an active AWS member at the time the campaign ends 12/31/17. AWS staff members are not eligible to participate. Providers of commercial educational programs that include an AWS membership in the program's pricing structure are not eligible to participate in this campaign. Participants' eligibility is also determined at the sole discretion of the campaign's administrators. The campaign period runs from January 1, 2017 through December 31, 2017.



AWS MEMBERSHIP APPLICATION

Join or Renew:



Mail: Form with your payment, to AWS



Call: Membership Department at (800) 443-9353, ext. 480



Fax: Completed form to (305) 443-5647



Online: www.aws.org/membership



American Welding Society

8669 NW 36 St, # 130
Miami, FL 33166-6672
Telephone (800) 443-9353
FAX (305) 443-5647
Visit our website: www.aws.org

CONTACT INFORMATION

New Member Renewal

Mr. Ms. Mrs. Dr.

Please print • Duplicate this page as needed

Last Name: _____

First Name: _____ M.I.: _____

Birthdate: _____ E-Mail: _____

Cell Phone () _____ Secondary Phone () _____

Were you ever an AWS Member? YES NO If "YES," give year _____ and Member #: _____

Company (if applicable): _____

Address: _____

City: _____ State/Province: _____

Zip/Postal Code: _____ Country: _____

<p>1 Who pays your dues?: <input type="checkbox"/> Company <input type="checkbox"/> Self-paid <input checked="" type="checkbox"/> Sex: <input type="checkbox"/> Male <input type="checkbox"/> Female</p> <p>2 Education level: <input type="checkbox"/> High school diploma <input type="checkbox"/> Associate's <input type="checkbox"/> Bachelor's <input type="checkbox"/> Master's <input type="checkbox"/> Doctoral</p> <p><input type="checkbox"/> Check here if you learned of the Society through an AWS Member? Member's name: _____ Member's # (if known): _____</p> <p><input type="checkbox"/> Check here if you would prefer not to receive email updates on AWS programs, new Member benefits, savings opportunities and events.</p>
--

INDIVIDUAL MEMBERSHIP

→ Please check each box that applies to the Membership or service you'd like, and then add the cost together to get your Total Payment.

- AWS INDIVIDUAL MEMBERSHIP (One Year)**.....\$88
- AWS INDIVIDUAL MEMBERSHIP (Two Years) SAVE \$25 New Members Only**.....\$151
- New Member Initiation Fee\$12

OPTIONS AVAILABLE TO AWS INDIVIDUAL MEMBERS ONLY:

A.) OPTIONAL **Book Selection** (Choose from 25 titles; up to a \$192 value; includes shipping & handling)

- Individual Members in the U.S.....\$35
- Individual Members outside the U.S (includes International shipping).....\$85

ONLY ONE SELECTION PLEASE. For more book choices visit <https://app.aws.org/membership/books>

- Jefferson's Welding Encyc.* (CD-ROM only) *Design & Planning Manual for Cost-Effective Welding* *Welding Metallurgy* *Welding Inspection Handbook*
- Welding Handbook Selections:* *WHB* (9th Ed., Vol. 5) *WHB* (9th Ed., Vol. 4) *WHB* (9th Ed., Vol. 3) *WHB* (9th Ed., Vol. 2) *WH* (9th Ed., Vol. 1)
- Pocket Handbook Selections:* *PHB-1* (Arc Welding Steel) *PHB-2* (Visual Inspection) *PHB-4* (GMAW / FCAW)

B.) OPTIONAL **Welding Journal Hard Copy** (for Members outside North America)

- Individual Members outside North America (note: digital delivery of WJ is standard).....\$50

INDIVIDUAL MEMBERSHIP TOTAL PAYMENT\$ _____

NOTE: Dues include \$17.30 for *Welding Journal* subscription and \$4.00 for the AWS Foundation.

STUDENT MEMBERSHIP

- AWS STUDENT MEMBERSHIP (with digital *Welding Journal* magazine)**.....\$15
- AWS STUDENT MEMBERSHIP (with hard copy *Welding Journal* magazine)**.....\$35
Option available only to students in U.S., Canada & Mexico.

PAYMENT INFORMATION

Payment can be made (in U.S. dollars) by check or money order (international or foreign), payable to the American Welding Society, or by charge card.

Check Money Order AMEX Diners Club MasterCard Visa Discover Other

CC#: _____ / _____ / _____ / _____ Expiration Date (mm/yy) _____ / _____

Signature of Applicant: _____ Application Date: _____

OFFICE USE ONLY	Check #: _____	Account # _____
Source Code: WJ	Date: _____	Amount: _____

REV. 11/16

Type of Business (Check ONE only)

- A Contract construction
- B Chemicals & allied products
- C Petroleum & coal industries
- D Primary metal industries
- E Fabricated metal products
- F Machinery except elect. (incl. gas welding)
- G Electrical equip., supplies, electrodes
- H Transportation equip. — air, aerospace
- I Transportation equip. — automotive
- J Transportation equip. — boats, ships
- K Transportation equip. — railroad
- L Utilities
- M Welding distributors & retail trade
- N Misc. repair services (incl. welding shops)
- O Educational Services (univ., libraries, schools)
- P Engineering & architectural services (incl. assns.)
- Q Misc. business services (incl. commercial labs)
- R Government (federal, state, local)
- S Other

Job Classification (Check ONE only)

- 01 President, owner, partner, officer
- 02 Manager, director, superintendent (or assistant)
- 03 Sales
- 04 Purchasing
- 05 Engineer — welding
- 20 Engineer — design
- 21 Engineer — manufacturing
- 06 Engineer — other
- 10 Architect designer
- 12 Metallurgist
- 13 Research & development
- 22 Quality control
- 07 Inspector, tester
- 08 Supervisor, foreman
- 14 Technician
- 09 Welder, welding or cutting operator
- 11 Consultant
- 15 Educator
- 17 Librarian
- 16 Student
- 18 Customer Service
- 19 Other

Technical Interests (Check all that apply)

- A Ferrous metals
- B Aluminum
- C Nonferrous metals except aluminum
- D Advanced materials/Intermetallics
- E Ceramics
- F High energy beam processes
- G Arc welding
- H Brazing and soldering
- I Resistance welding
- J Thermal spray
- K Cutting
- L NDT
- M Safety and health
- N Bending and shearing
- O Roll forming
- P Stamping and punching
- Q Aerospace
- R Automotive
- S Machinery
- T Marine
- U Piping and tubing
- V Pressure vessels and tanks
- W Sheet metal
- X Structures
- Y Other
- Z Automation
- 1 Robotics
- 2 Computerization of Welding

of the Materials Joining Group, Dr. Carl Lundin, over lunch provided by the Materials Science Department.

District 9

Michael Skiles, director
(337) 501-0304
michaelskiles@cox.net

AUBURN-OPELIKA

November 3

Location: Sejong Georgia, Lagrange, Ga.

Summary: Members toured Sejong Georgia. Company employees gave a presentation about its product line and welding methods used. The tour guide then showed attendees the assembly line of exhaust systems produced for Kia.

NEW ORLEANS

November 8

Location: Boh Bros. Construction Co., New Orleans, La.

Topic: "Why the World Needs Welders"

Summary: Boh Bros. sponsored the Section's November general meeting at its facility. The construction staff gave a presentation on the need for welders, career paths, and opportunities available in the industry. Attendees were engaged with challenging questions. Door prizes were donated by the company, and there was also a 60/40 raffle with proceeds dedicated to Section student activity.



NORTHEAST TENNESSEE — Triple-S Steel's Knoxville branch welcomed Section members for a facility tour.



NORTHEAST TENNESSEE — Seen are the individuals who participated in the tour of the University of Tennessee's facilities. From left are John Bohling, Dr. Carl Lundin, six students from Sequoyah High School, Dr. Maneel Bharadwaj, Welding Instructor Chris Renfro, and Will Hoskins.



NEW ORLEANS — Speaker/sponsor recognition award recipients posed for a photo. Shown are (from left) Tri Le, project manager; Richard Tamor, piledriver foreman; Aldo Duron, Section secretary; Brigitte Toups, Boh Bros. craft coordinator; William "Trey" St. John, Boh Bros. quality control manager; and Vincent Rabalais, Boh Bros. assistant general superintendent, pile and marine department.

CENTRAL LOUISIANA

December 1

Location: Central Louisiana Technical Community College (CLTCC), Winnfield, La.

Summary: The Section held its first High School Welding Competition, which included ten high schools from three parishes. The Section plans to hold the event annually. CLTCC Chancellor Jimmy Sawtelle addressed students about the importance of continuing their education in the community college system. Lincoln Electric Co. supplied placement prizes for all winning contestants, and the Section provided t-shirts to all attendees.

District 10

Mike Sherman, director
(216) 570-9348
mike@shermanswelding.com

District 11

Phillip Temple, director
(734) 546-4298
nwcllc_ptemple@att.net

District 12

Daniel J. Roland, director
(920) 241-1542
daniel.roland@airgas.com

RACINE-KENOSHA

December 5

Location: Milwaukee, Wis.

Presenter: Kent Knapp, owner, Milwaukee Blacksmith

Summary: Milwaukee Blacksmith, which was recently featured on the History Channel, hosted Section members and students from Gateway Technical College Elkhorn Campus for a facility tour and demonstrations by company owner Kent Knapp and his sons Miles and Oscar.



CENTRAL LOUISIANA — Central Louisiana Section 509's first High School Welding Competition participants and instructors.



RACINE-KENOSHA — Section members and Gateway Technical College students enjoyed a visit to Milwaukee Blacksmith and meeting Kent, Miles, and Oscar Knapp. The shop was recently featured on the History Channel.

District 13

John Willard, director
(815) 954-4838
kustom_bilt@msn.com

District 14

Tony Brosio, director
(765) 215-7506
tbrosio@yahoo.com

INDIANA

November 16

Location: Las Vegas Convention Center, Las Vegas, Nev.

Summary: Several Section members attended the Excellence in Welding Awards ceremony to receive the 2016 Section Award.

November 28

Location: Indiana Pipe Trades Local 440 Union Hall/Training Center, Indianapolis, Ind.

Summary: The Section's annual student night was held at the Indiana Pipe

Trades facility. More than 100 students and teachers were in attendance for the meeting and dinner. After dinner, there was a facility tour and a drawing was held for door prizes.

Summary: Members gathered for their annual Christmas get together where they enjoyed lunch with their families, worked on upcoming meetings and events for the year, and exchanged gifts.

December 10

Location: Turkey Run State Park, Indianapolis, Ind.



INDIANA — Several Section members attended the Excellence in Welding Awards to receive the 2016 Section category award.



INDIANA — Section members and their families enjoyed an annual Christmas gathering at Turkey Run Inn.



INDIANA — Students enjoyed a pizza dinner at the Indiana Pipe Trades Local 440 Union Hall/Training Center as part of the Indiana Section's annual student night.

LEXINGTON

December 8

Location: Hendrickson Trailer Systems, Inc., Somerset, Ky.

Summary: Section members participated in a Hendrickson product orientation and plant tour.

District 15

David Lynnes, director
(701) 893-2295
dave@learntoweld.com

District 16

Karl Fogleman, director
(402) 677-2490
fogleman3@cox.net

KANSAS CITY

December 10

Location: Crider's Institute of Welding Technology, Grain Valley, Mo.

Presenter: Stan Crider, owner, head instructor, Crider's Institute of Welding Technology

Summary: Crider's hosted Boy Scout Troop 286, Odessa, Mo., for a Welding Merit Badge clinic. The boys learned about different welding jobs, safety procedures, welding equipment, and welding terminology. They also received hands-on instruction and were able to weld a bead tracing their initials, cover a plate with beads, tack and weld two plates together in a square groove butt joint, tack and weld a T-joint, and tack and weld a lap joint.



LEXINGTON — Hendrickson Production Managers Chad Gates (left) and Keith White (right) welcomed Section Chairman Coy Hall (center) to the company's facilities for a tour.

EASTERN IOWA

October 13

Location: SSAB Research and Development Center, Muscatine, Iowa

Presenter: Dr. Erik Soderstrom

Topic: Welding metallurgy with sample preparation and testing demonstrations

Summary: Dr. Soderstrom gave members a technical presentation on welding metallurgy and how alloys affect the base material, electrode selection, and welding procedures. Samples were then prepared for metallography, microhardness, tensile, and impact testing. In conclusion, demonstrations of the proper testing techniques using the prepared samples were tested and the results compared with the code or

material requirements. Professional Development Hour (PDH) certificates were earned by those in attendance.

November 10

Location: Henderson Products, Inc., Manchester, Iowa

Presenters: Gary Adams and Garret White

Summary: Section members received a plant tour of Henderson Products, Inc. The company builds snow plows, utility boxes, and a variety of other equipment. Work ethics, engineering, and commitment to quality products were seen throughout the plant in the workforce and manufacturing processes. The tour showcased why welding is so critical to manufacturing.



KANSAS CITY — Crider's Institute of Welding Technology introduced Boy Scout Troop 286 to welding in an effort to help the boys earn Welding Merit Badges.

District 17

J Jones, director
(832) 506-5986
jjones6@lincolnelectric.com

EAST TEXAS

December 6

Location: Papacita's Restaurant, Longview, Tex.
Presenter: J Jones, AWS District 17 director, and district manager, Harris Products Group

Summary: The Section hosted the East Texas Section Annual Toys for Tots Dinner. Dinner was provided to all members who brought a new unwrapped toy donation of \$10 or more. Recognition was given to the Section's scholarship recipients and a review of the many AWS scholarship opportunities available for the coming year were announced.

TULSA

November 29

Location: Oklahoma Joe's Bar-B-Que, Tulsa, Okla.
Presenter: Ralph Johnson, Section 34 advisor

Topic: ASME Welding Qualifications
Summary: Johnson explained how to qualify welders and welding procedures using ASME Section IX.

District 18

John Stoll, director
(713) 724-2350
John.Stoll@voestalpine.com

District 19

Shawn McDaniel, director
(509) 793-5182
shawnm@bigbend.edu

District 20

Pierrette H. Gorman, director
(505) 284-9644
phgorma@sandia.gov

District 21

Sam Lindsey, director
(858) 740-1917
slindsey@sandiego.gov

District 22

Kerry E. Shatell, director
(925) 866-5434
kesi@pge.com



TULSA — Prize winners Bob Steinhart (left) and Brenda Randall (right) with Section Chair Travis Weber (second from left) and guest speaker and Board Advisor Ralph Johnson.



EASTERN IOWA — Members during a plant tour of Henderson Products, Inc.



EASTERN IOWA — SSAB Research and Development Center welcomed Section members for a technical presentation.



EAST TEXAS — Section members with the toys they donated during their Annual Toys for Tots Dinner.

SECTION EVENTS CALENDAR

*Please note events are subject to change.
Reach out to the listed contact to confirm.*

Colorado

February 10
Downtown Aquarium, Denver, Colo.
Annual Ladies' Night

March 10
Denver, Colo.
8th Annual "Welding the Rockies
Symposium" Metallurgy of Welding

April 13
Presentation on welding and driving
NASCAR racing cars

May 11
Denver, Colo.
Annual awards dinner with 2016
AWS President David McQuaid

*Contact Bob Teuscher for more information
about Colorado events at (303) 893-
3602 or by e-mail at bobteuscher@
hotmail.com.*

Drake Well

February 9
Local facility tour

April 11
AWS/Venango Technology Center
joint meeting

May TBD
District meeting

August 4
Meadville, Pa.
Annual golf outing

*Contact Robert Fugate for more infor-
mation about Drake Well events at
rfugate@vtc1.org.*

Florida West Coast

February 7
Pinellas Technical College Welding
Department, Clearwater, Fla.
Presentation on AWS and the welding
student

*Contact Alan Shissler for more informa-
tion about Florida West Coast events at
(813) 245-9328 or by e-mail at
alan@shissler.org.*

New Orleans

Meetings are usually the third Tuesday
of each of the following months: Sept.,
Oct., Nov., Jan., Feb., March, April, and
May.

March 8
Landmark Hotel, Metairie, La.
Aluminum Welding Seminar

*Contact D. J. Berger for more information
about New Orleans events at (504) 415-
9165, or by e-mail at
dj@nationalitc.com.*

Detroit

March 25
The Royal Park Hotel, Rochester,
Mich.
Ladies' Night

*Contact John Bohr for more information
at (734) 751-7226 or by e-mail at
johnc.bohr@gmail.com.*

North Texas

Meetings are the third Tuesday of each
month: dinner at 6:30 pm, program at
7 pm
Humperdinks, 700 Six Flags,
Arlington, Tex.
Bring three canned goods for the
North Texas Food Bank and receive a
door prize ticket.

*Contact Paul Stanglin for more
information about North Texas
events by e-mail at
pstangli@cityofirving.org.*

Guide to AWS Services

American Welding Society®

8669 NW 36th St., #130
Miami, FL 33166-6672
(800/305) 443-9353; Fax: (305) 443-7559
Phone extensions are in parentheses.

AWS PRESIDENT

John Bray...*sales@affiliatedmachinery.com*
Affiliated Machinery, Inc.
3008 South Main Street, Pearland, TX 77581

ADMINISTRATION

Executive Director

Ray Shook...*rshook@aws.org*(210)

Chief Operating Officer

Matt Miller...*mmiller@aws.org*(207)

Senior Associate Executive Directors

Cassie Burrell...*cburrell@aws.org*(253)

John Gayler...*gayler@aws.org*(472)

Chief Financial Officer/Chief Administrative Officer

Gesana Villegas...*gvillegas@aws.org*(252)

Chief Information Officer

Emilio Del Riego...*edelriego@aws.org*(247)

Board and Executive Director Services

Associate Director

Alex Diaz...*adiaz@aws.org*(294)

AWS Awards, Fellows, Counselors

Board and Executive Director Services

Program Manager

Chelsea Steel...*csteel@aws.org*(293)

Coordinates AWS awards and Fellow and Counselor nominations.

Administrative Services

Corporate Director

Hidail Nuñez...*hidail@aws.org*(287)

HUMAN RESOURCES

Director

Gricelda Manalich...*gricelda@aws.org*(208)

INTERNATIONAL INSTITUTE OF WELDING

Senior Coordinator

Sissibeth Lopez...*sissi@aws.org*(319)

Liaison services with other national and international societies and standards organizations.

GOVERNMENT LIAISON SERVICES

Hugh Webster...*hwebster@wc-b.com*

Webster, Chamberlain & Bean, Washington, D.C.
(202) 785-9500; F: (202) 835-0243.

Monitors federal issues of importance to the industry.

CONVENTION AND EXPOSITIONS

Director, Convention and Meeting Services

Matthew Rubin...*mrubin@aws.org*(239)

ITSA — INTERNATIONAL THERMAL

SPRAY ASSOCIATION

Program Manager

Alfred Nieves...*anieves@aws.org*(467)

RWMA — RESISTANCE WELDING MANUFACTURING

ALLIANCE

Program Manager

Adrian Bustillo...*abustillo@aws.org*(295)

WEMCO — ASSOCIATION OF WELDING

MANUFACTURERS

Program Manager

Keila DeMoraes...*kdemoraes@aws.org*(444)

INTERNATIONAL SALES

Managing Director of North American Sales

Joe Krall...*jkral@aws.org*(297)

Learning Sales Representative

Efram Abrams...*eabrams@aws.org*(307)

Corporate Director, Global Sales

Jeff Kamentz...*jkamentz@aws.org*(233)

Oversees international business activities; certification, publications, and membership.

PUBLICATION SERVICES

Dept. information(275)

Welding Journal

Publisher/Editor

Mary Ruth Johnsen...*mjohnsen@aws.org*(238)

Society News Editor

Katie Pacheco...*kpacheco@aws.org*(275)

Section News Editor

Cindy Weihl...*cweihl@aws.org*(256)

Inspection Trends Editor

Carlos Guzman...*cguzman@aws.org*(348)

Welding Handbook Editor

Kathy Sinnes...*ksinnes@aws.org*(255)

MARKETING COMMUNICATIONS

Chief Marketing Officer (interim)

Michael Walsh...*mwash@aws.org*(350)

MEMBER SERVICES

Dept. information(480)

Senior Associate Executive Director

Cassie Burrell...*cburrell@aws.org*(253)

Corporate Director

Rhenda Kenny...*rhenda@aws.org*(260)

Serves as a liaison between members and AWS headquarters.

CERTIFICATION SERVICES

Dept. information(273)

Managing Director

Judy Manso...*jmanso@aws.org*(281)

Director of Agency Representation

Terry Perez...*tperez@aws.org*(470)

EDUCATION SERVICES

Corporate Director

Patrick Henry...*pHenry@aws.org*(226)

Director, Development and Systems

David Hernandez...*dhernandez@aws.org*(219)

TECHNICAL STANDARDS SALES

Managing Director

Michael Walsh...*mwash@aws.org*(350)

AWS Bookstore, Subscription Sales, and AWS

Reseller Management

Customer Service...*customerservice@aws.org* ... (280)

STANDARDS DEVELOPMENT

Dept. information(340)

Managing Director — Standards Development

Annette Alonso...*aalonso@aws.org*(299)

Technical Committee Activities, Additive Manufacturing, Welding Qualification

Director — International Activities

Andrew Davis...*adavis@aws.org*(466)

International Standards Activities, American Council of the International Institute of Welding

Manager, Safety and Health

Stephen Hedrick...*stevveh@aws.org*(305)

Metric Practice, Safety and Health, Joining of Plastics and Composites, Personnel and Facilities Qualification, Mechanical Testing of Welds

Program Managers II

Stephen Borrero...*sborrero@aws.org*(334)

Definitions and Symbols, Structural Subcommittees on Reinforcing Steel and Stainless Steel, Joining of Metals and Alloys, Piping and Tubing

Rakesh Gupta...*gupta@aws.org*(301)

Filler Metals and Allied Materials, International Filler Metals, UNS Numbers Assignment, Arc Welding and Cutting Processes, Computational Weld Mechanics

Jennifer Molin...*jmolin@aws.org*(304)

Structural Welding, Sheet Metal Welding

Program Managers

Annik Babinski...*ababinski@aws.org*(310)

Automotive, Friction Welding, Resistance Welding, Resistance Welding Equipment, Welding and Brazing in Aerospace

John Douglass...*jdouglass@aws.org*(306)

Brazing and Soldering, Methods of Weld Inspection, Welding in Marine Construction, Welding of Machinery and Equipment

Peter Portela...*pportela@aws.org*(311)

High-Energy Beam Welding, Robotics Welding, Welding in Sanitary Applications, Additive Manufacturing, Structural Subcommittees on Bridge Welding and Titanium

Jennifer Rosario...*jrosario@aws.org*(308)

Oxyfuel Gas Welding and Cutting, Railroad Welding, Thermal Spraying, Welding Iron Castings, Welding Qualification

CUSTOMER OPERATIONS

Program Specialists

Vivian Pupo(362)

Vanessa Vasquez(361)

Answer customer questions about AWS.

AWS FOUNDATION, INC.

aws.org/w/a/foundation

General Information

(800/305) 443-9353, ext. 212, *vpinsky@aws.org*

Chairman, Board of Trustees

William A. Rice...*brice@oki-bering.com*

Executive Director, Foundation

Sam Gentry...*sgentry@aws.org*(331)

Corporate Director, Workforce Development

Monica Pfarr...*mpfarr@aws.org*(461)

Associate Director of Scholarships

Vicki Pinsky...*vpinsky@aws.org*(212)

The AWS Foundation is a not-for-profit 501(c)(3) charitable organization established to provide support for the educational and scientific endeavors of the American Welding Society. Promote the Foundation's work with your financial support.

AWS Promotes Diversity

AWS values diversity, advocates equitable and inclusive practices, and engages its members and stakeholders in establishing a culture in the welding community that welcomes, learns from and celebrates differences among people. AWS recognizes that a commitment to diversity, equity, and inclusion is essential to achieving excellence for the Association, its members and employees.

Simonds Saw Appoints New President



David Miles

Simonds Saw LLC, Fitchburg, Ma., has named David Miles president. The saw manufacturer was formed by Simonds International in 2014 as a separate company under the same management team. Miles previously served as vice president of sales and marketing for Simonds International. He succeeds Ray Martino in the role of president. Martino will continue to serve as CEO of Simonds Saw and as president and CEO of Simonds International.

ISA Welcomes President



Steven W. Pflantz

The International Society of Automation (ISA), Research Triangle Park, N.C., has welcomed Steven W. Pflantz as its 2017 president. In this role, Pflantz will work with the organization's leaders and staff to increase awareness of the value and relevance of the company brand. A long-time ISA member and leader, he served as vice president of the professional development department in 2012–2013. He has also served on ISA's executive board and as an ISA district vice president.

Lincoln Electric General Counsel to Retire, Successor Named

Lincoln Electric Holdings, Inc., Cleveland, Ohio, has announced that Frederick G. Stueber will retire as the company's executive vice president, general counsel, and secretary in April after 22 years with the company. Upon his retirement, Jennifer I. Ansberry will be promoted to executive vice pres-



Jennifer I. Ansberry

ident, general counsel, and secretary, and she will serve as an officer of the company. Ansberry has been with Lincoln Electric since 2004 and currently serves as vice president, deputy general counsel. She also leads the company's environmental, health, and safety organization.

Camfil APC Americas Names Vice President

Camfil Air Pollution Control (APC), Jonesboro, Ark., has appointed Graeme Bell to the position of vice president, Camfil APC Americas. His most recent title was vice president, Camfil APC Europe, where he handled the UK, German, and Czech operations including manufacturing sites as well as strategic growth responsibility for Europe. Bell will relocate from Europe to Camfil corporate headquarters in Jonesboro.

TransCanada Designates Chairman of the Board

TransCanada Corp., Calgary, Alberta, has announced that Siim A. Vanaselja has been designated as the company's next chair. Vanaselja has been a TransCanada board member since May 2014 and serves as the chair of the company's audit committee. Vanaselja's appointment succeeds S. Barry Jackson who has retired. Jackson will continue to be a board member subject to his reelection at TransCanada's annual meeting of shareholders.

ASTM Chairman Begins Term

ASTM International, W. Conshohocken, Pa., has revealed that D. Thomas Marsh has started his term as 2017 chairman of the ASTM board of directors. Marsh is president and CEO of Centrotrade, Chesapeake, Va., and has been an ASTM International member since 1990.

Cincinnati Incorporated Appoints Regional Sales Engineer



Kristina Frontino

Cincinnati Incorporated, Harrison, Ohio, has named Kristina Frontino regional sales manager for northern California, Nevada, Utah, and southern Idaho. She replaces Mike Malatesta, who after covering the territory for 30 years, is retiring. Frontino brings more than five years of experience in project management and holds a bachelor of science degree in civil engineering from the University of Nevada, Reno.

Mathey Dearman Restructures Sales Force

Mathey Dearman, Tulsa, Okla., has restructured its sales organization. The team is made up of Brandon Boyd, director of sales; Josh Wilson, area sales manager for the western U.S. and



Josh Wilson



Mike Brace



Svatopluk Jezek



Al Smith

western Canada; Mike Brace, area sales manager for the eastern U.S. and eastern Canada; Svatopluk (Sevy) Jezek, European sales manager; and Al Smith, training and product coordinator.

Two Laboratory Testing Employees Retire

Laboratory Testing, Inc., Philadelphia, Pa., honored the retirement of Gary Doerfer, chemistry technician, and Frank Peszka, director of quality. Doerfer was with the company since July 1986 and Peszka joined the company in 2004. The two men were honored for their service during the company's holiday luncheon in December.

Obituaries

Joseph R. Crisci

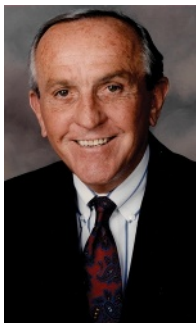


Joseph R. Crisci

Joseph R. Crisci, Murrells Inlet, S.C., passed away October 8. Born in Brooklyn, N.Y., he graduated from Brooklyn Polytechnic University (now the engineering school for New York University) with both bachelor and master degrees in metallurgical engineering. He had a distinguished 42-year career as a naval engineer for the U.S. Government, becoming a leading expert in the development of welding technologies for naval vessels and attained numerous patents for these technologies. He was a member of the American Welding Society (AWS) for 39 years and served on the B4 Committee on Mechanical Testing of Welds since 1990, where he served as chair from 1990 to 2001.

Donald F. Hastings

Donald F. Hastings, Naples, Fla., passed away on December 27. Hastings is best known for his 44-year career at The Lincoln Electric Co. After



Donald F. Hastings

graduating from Harvard Business school, Hastings began his career at Lincoln as a sales trainee and rose to become CEO and chairman of the board. He was a Life Member of AWS having joined the organization in 1959. From 1997 to 2003, he served as an AWS Foundation Trustee and was named an AWS Counselor in 2001. As an advocate for advanced welding education, he helped endow the Donald F. Hastings Scholarship in 1996. The scholarship provides financial assistance to individuals interested in pursuing a career in welding engineering. A second scholarship, the Donald and Shirley Hastings Scholarship, was endowed in 2003. More than \$70,000 has been awarded to date between the two scholarships.

Richard Trillwood



Richard Trillwood

Richard Trillwood, Santa Ana, Calif., died on December 6 after a battle with kidney cancer. Trillwood was the founder and CEO of Electron Beam Engineering, Inc. In 1968, he designed and built the world's first small chamber electron beam welder and was an expert in the field. Trillwood had been an AWS member since 1982. [WJ](#)

An Important Event on Its Way?

Send information on upcoming events to the Welding Journal Dept., 8669 N.W. 36th St., Suite #130, Miami, FL 33166. Items can also be sent via FAX to (305) 443-7404 or by e-mail to cweihl@aws.org.

COMING EVENTS

— continued from page 47

Machine Safeguarding Seminars.

Rockford Systems, Inc.; (800) 922-7533; rockfordsystems.com.

NDE Classes. Moraine Valley Community College, Palos Hills, Ill., offers NDE classes in PT, MT, UT, RT, radiation safety, and eddy current, as well as API 510 exam prep and weld inspection. Contact (708) 974-5735; wcds@morainevalley.edu; morainevalley.edu/NDE.

NDT Courses and Exams. Brea, Calif., and customers' locations. Level I and II and refresher courses in PA, UT, MP, radiation safety, radiography, visual, etc. Test NDT, LLC; (714) 255-1500; testndt.com.

Offsite Resistance Welder Seminars.

Presented by T. J. Snow. Classes begin Mar. 22, Harlingen, Tex.; Apr. 12, Florence, Ky.; Apr. 26, Cleveland, Ohio; May 10, Minneapolis, Minn.; May 24, Phoenix, Ariz.; June 6-7, Chattanooga, Tenn.; July 19, Spartanburg, S.C.; Aug. 23, Tulsa, Okla.; Sept. 20, Birmingham, Ala.; Oct. 11, Lebanon, Tenn.; and Oct. 25, Columbus, Ohio. Contact (423) 894-6234; tjsnow.com.

Online Education Courses. Topics include Introduction to Die Casting (\$99), Metal Melting and Handling (\$99), Product Design (\$59), Energy Training (\$19), Dross Training (\$19), Managing Dust Hazards (\$19), and Safety (free). North American Die Casting Assoc.; (847) 808-3161; diecasting.org/education/online.

Plastics Welding School. A two-day course for certification to European plastics welding standards. Malcom Hot Air Systems; plasticweldingtools.com.

Protective Coatings Training and Certification Courses. At various locations and online. The Society for Protective Coatings; (877) 281-7772; sspc.org.

Robotics Operator Training. Presented by ABB University at 13 locations nationwide. For course titles and locations: (800) 435-7365, opt. 2, opt. 4; abb.us/abbuniversity. [WJ](#)

An Introduction to Pulsed GMAW

This process provides directional control over the weld pool, quick wire feed and travel speeds, and reduced spatter

BY ERIK BROWN



Fig. 1 — Pulsed GMAW may be a good option for companies looking to boost their efficiencies, especially because it can help improve the quality of welds across varying welding operator skill levels.

Companies are always looking for ways to become more productive, create higher quality parts, and generate greater profitability. In some cases, reaching these goals is a matter of improving operator training, implementing lean practices, or taking on other continuous improvement initiatives. Changing welding processes can make a significant difference.

While not new to the industry,

pulsed gas metal arc welding (GMAW-P) is still being adopted for the first time by many companies as a means to drive improvements in the welding operation. The process is an excellent alternative to constant voltage GMAW, and may be a good option for companies looking to boost their efficiencies, especially because it can help improve the quality of welds across varying welding operator skill levels — Fig. 1.

Why the Hesitation?

In some cases, companies have been slow to adopt GMAW-P in their operations for various reasons.

It may be that companies are simply unfamiliar with the process, or welding supervisors or operators are hesitant to change technologies because they fear extensive training may be involved. Some companies may be

concerned that the cost will be significantly higher.

Fortunately, the transition from a spray process to learning GMAW-P is not difficult. Changing from a standard GMAW or a short circuit transfer process requires operator training, but the learning curve is typically much shorter than expected. It is true, however, that the process produces a different sound, which may be unsettling or intimidating to some, and the technology often costs more.

The long-term benefits the process offers, however, can produce a solid return on investment, and a bit of practice and knowledge can easily put common concerns to rest.

How It Works

Pulsed GMAW is a modified spray transfer process in which the power source switches between a high peak current or voltage and a low background current or voltage between 30 to 400 times per second. During this switch, the peak current pinches off a droplet of wire and propels it to the weld joint. At the same time, the background current maintains the arc but produces such a low heat input that metal transfer can't occur, allowing the weld pool to freeze slightly and to help prevent melt-through.

This action differs from a traditional spray transfer process, which continuously transfers tiny droplets of molten metal into the weld joint.

Synergic vs. Nonsynergic

There are two different types of GMAW-P processes: synergic and nonsynergic. In a synergic GMAW-P system, the power level automatically adjusts to the wire speed as it changes. This is the most common method in welding equipment today, as it is the easiest for welding operators to set and achieve good welding parameters.

For example, if the wire feed speed changes from 200 to 400 in./min, the arc length or power on the wire will remain the same relative to the power level that was on the 200 in./min setting.

On the other hand, using a nonsynergic GMAW-P process requires the welding operator to adjust the power to match the wire feed speed.

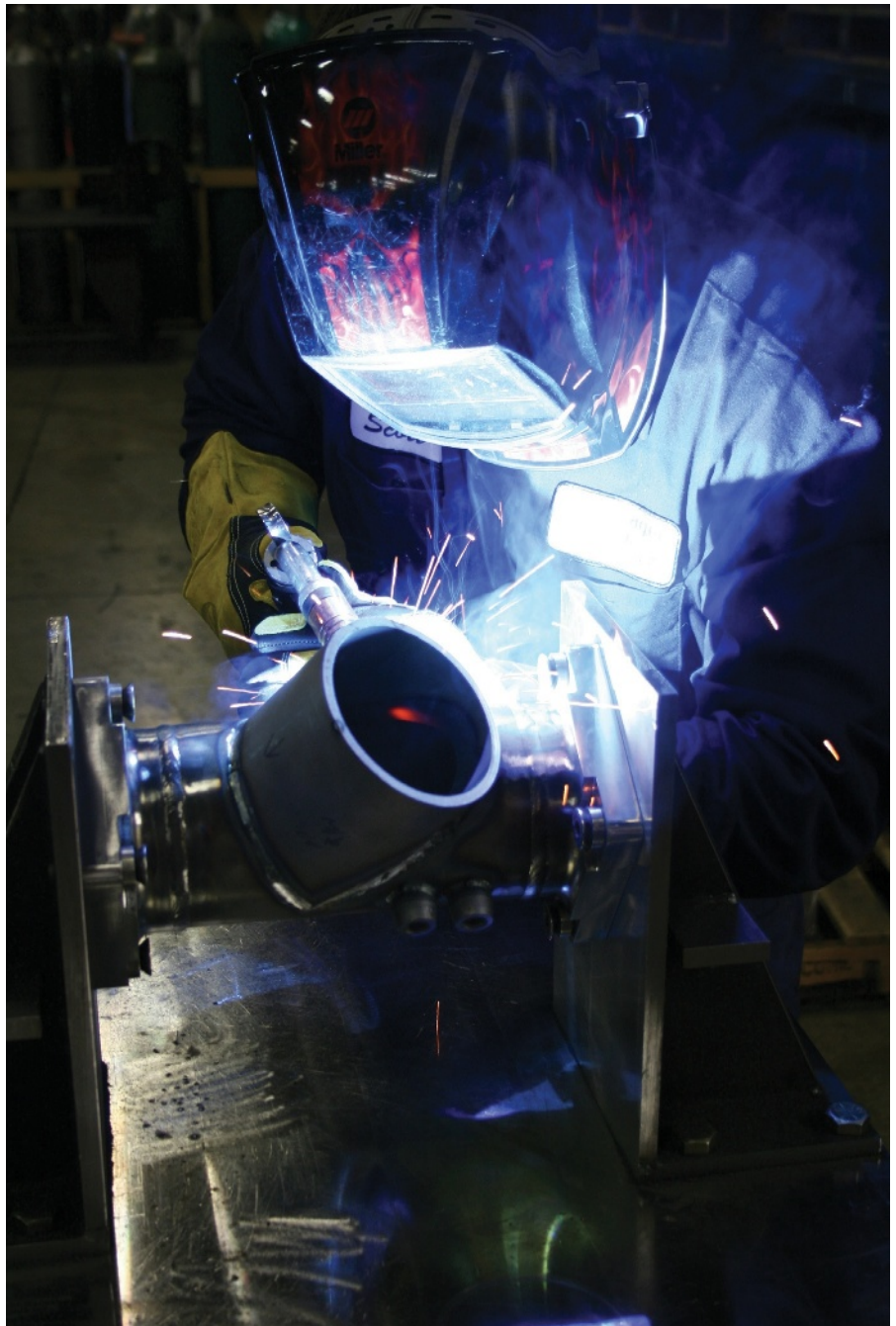


Fig. 2 — Pulsed GMAW provides advantages such as improved control over arc starts and stops, faster travel speeds, lower spatter, and a reduction in overwelding and incomplete fusion compared to constant voltage GMAW.

The Advantages

Using GMAW-P offers users key benefits — Fig. 2. Consider these positive factors impacting productivity, quality, and ease of use.

- Exceptional directional control over the weld pool makes it easier for new welding operators to learn the GMAW-P process and create welds with good bead appearance. In addition,

most pulsed waveforms have a built-in “adaptive function” technology that allows more inexperienced welding operators with less steady hands to produce more consistent welds.

- Improved control over arc starts and stops helps reduce weld defects and improve appearance. When the welding operator initiates the arc, the process delivers higher energy, which

offers good fusion. It then reduces the amount of energy going into the weld to prevent melt-through and provide greater control over the weld bead appearance. When stopping the arc, a GMAW-P process with a crater function is ideal, as it allows the operator to ramp down to a cooler welding parameter to fill in the crater at the end. This helps eliminate the potential for termination cracking that can easily occur when welding materials such as aluminum.

- Faster wire feed and travel speeds can occur in many applications with GMAW-P. This helps increase productivity while simultaneously reducing heat input, to decrease residual stress and reduce the opportunity for distortion or melt-through. Consider stainless steel. This material cannot handle too much heat or the welding operator may burn the chromium and nickel out of the base material. As a result, the weld metal and surrounding joint turn into mild steel, which lacks corrosion resistance and toughness. Pulsed GMAW is a good solution for welding this material and avoiding such pitfalls.

- Some GMAW-P power sources allow welding operators to adjust the width of the arc cone, which helps them tailor the bead profile to the application. This helps prevent overwelding and poor fusion. Wider beads help improve tie-in on both sides of a joint, while narrower beads provide good fusion at the joint's root.

- Reduced spatter generated during the GMAW-P process results in reduced time and money spent on associated grinding and postweld cleanup.

- Simple process setup means the welding operator uses a single knob to set the wire feed speed. Because the arc length number or voltage automatically adjusts with GMAW-P, the arc becomes longer or shorter accordingly, for greater ease of use and productivity.

The Applications

Applications that are prone to weld defects such as incomplete fusion or porosity, or problems like melt-through, spatter, or warping are good candidates for GMAW-P. The lower heat input generated by the process offers similar advantages as found when using a process like gas tungsten arc

welding (GTAW), along with the good penetration, deposition, and fusion associated with a traditional spray transfer process.

Pulsed GMAW can be used to weld thick or thin materials. On thicker sections, it helps minimize downtime for repositioning parts because it generates a cooler weld pool than a traditional spray transfer process, which makes it usable in all positions. On thinner sections, it minimizes the opportunity for melt-through and reduces the risk of warping by controlling the heat input. This control often allows operators to use a larger diameter wire (up to $\frac{3}{4}$ in.), which in turn increases deposition rates and productivity. It also allows the welding operator to put more weld metal in the joint in less time without the risk of adding excessive amounts of heat.

Common Mistakes

Welding operators who are new to GMAW-P should be aware of a few pitfalls and common mistakes, the most common of which is assuming the arc length is the same as the voltage.

In fact, on a GMAW-P power source, the arc length is a function of voltage, but the actual number is arbitrary. These power sources often have a zero to 100 scale that is nominal 50. If the welding operator wants less power, for example, he or she would adjust below 50 and then adjust above 50 for more power.

Taking a limited look at the possibilities of GMAW-P is another common pitfall. There are advanced GMAW-P processes available with multiple programs, each of which possesses different attributes. Welding operators should always check to make sure they have the right program for the job to achieve the best results.

As always, companies should consult with a trusted welding distributor with questions about GMAW-P to determine the best power source for the application and to ensure they gain the best results. [WJ](#)

ERIK BROWN is a welding engineer and AWS CWI, industrial equipment, Miller Electric Mfg. Co. (millerwelds.com), Appleton, Wis.

CAN WE TALK?

The *Welding Journal* staff encourages an exchange of ideas with you, our readers. If you'd like to ask a question, share an idea, or voice an opinion, you can call, write, e-mail, or fax. Staff e-mail addresses are listed below, along with a guide to help you interact with the right person.

Publisher/Editor

Mary Ruth Johnsen
mjohnsen@aws.org, Ext. 238
 General Management,
 Reprint Permission,
 Copyright Issues

Sr. Editor

Cindy Weihl
cweihl@aws.org, Ext. 256
 Section News

Production Manager

Zaida Chavez
zaida@aws.org, Ext. 265
 Design and Production

Manager of International Periodicals and Electronic Media

Carlos Guzman
cguzman@aws.org, Ext. 348
 Design and Production

Sr. Advertising Sales Executives

Sandra Jorgensen
sjorgensen@aws.org, Ext. 254
 Advertising Sales
 Annette Delagrange
adelagrange@aws.org, Ext. 332
 Advertising Sales

Sr. Advertising Production Manager

Frank Wilson
fwilson@aws.org, Ext. 465
 Advertising Production

Manager of Sales Operations

Lea Owen
lea@aws.org, Ext. 220
 Production and Promotion

Subscriptions

Evelyn Andino
eandino@aws.org, Ext. 258
 Subscriptions Representative

Welding Journal Dept.
 8669 NW 36 St., #130
 Miami, FL 33166
 (800) 443-9353;
 FAX (305) 443-7404

Measuring the Effective Throat of Groove Welds

A programmable methodology determines the minimum total effective throat of a combined flare-bevel-groove weld with a reinforcing fillet weld in a T-joint

BY GLENN R. FRAZEE

The use of flare-bevel-groove T-joint welds is widespread for steel structures using hollow structural sections (HSS). These welds are qualified based on a maximum allowable effective throat, which is specified in the American Welding Society's (AWS) D1.1/D1.1M:2015, *Structural Welding Code — Steel*. This weld detail provides an AWS prequalified

weld joint with well-established welding procedures and predictable weld strength.

In certain cases, the effective throat of a flare-bevel weld may be insufficient to provide the necessary strength for the welded connection. In instances of a T-joint, it may be possible to strengthen this flare-bevel weld with a reinforcing fillet weld.

As noted in D1.1, Section 2.4.2.7, Reinforcing Fillet Welds, “The effective throat of a combination of PJP flare bevel groove weld and a fillet weld shall be the shortest distance from the joint root to the weld face of the diagrammatic weld minus the deduction for incomplete joint penetration (see Table 2.1, Figure 3.2, and Annex A).”

Given the somewhat complex



A welder performing shielded metal arc welding attaches a platform frame to a steel base plate at Calvert Cliffs Nuclear Power Plant, Lusby, Md. (Photo courtesy of Glenn R. Frazee.)

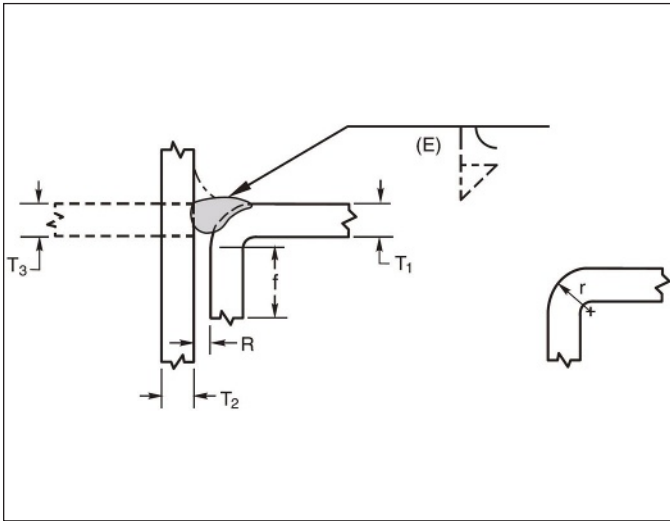


Fig. 1 — A flare-bevel-groove weld. (Sourced from AWS D1.1, Fig. 3.2, p. 72.)

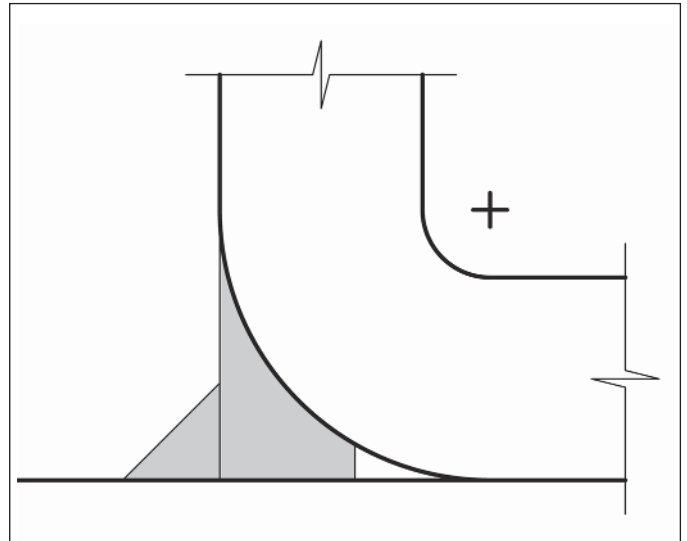


Fig. 2 — Simplified weld geometry is highlighted here.

geometry of this weld combination, the shortest distance from the weld root to the weld face may not be immediately obvious nor easy to quantify. This article aims to provide a formulaic methodology to determine the effective throat of such a connection.

Assumptions and Design Considerations

AWS recognizes that a flare-bevel weld will resemble that shown in Fig. 1 (D1.1, Fig. 3.2, prequalified PJP groove welded joint details). One will

notice that the filler metal for the weld extends convexly beyond the top flat face of the curved member. The reinforcing fillet weld is shown in a dashed line as well.

Recognizing that AWS does not consider the convexity of a weld to account for its effective throat, the flare-bevel with reinforcing fillet is simplified — Fig. 2. This simplification assumes the weld profiles for both the flare-bevel and fillet meet the requirements of AWS (D1.1, Fig. 3.2, as noted before, and Fig. 5.4, requirements for weld profiles). Additionally, the opening between the two mating pieces is

assumed to be zero, which is conservative given that a larger opening allows a greater effective throat during the welding process.

Finally, the methodology presented in this article assumes the two pieces joined are perpendicular to each other.

Case 1: Undersized Fillet Weld

The first case considered is one where the fillet weld is undersized to the point of being ineffective. Figure 3 illustrates this weld combination. This

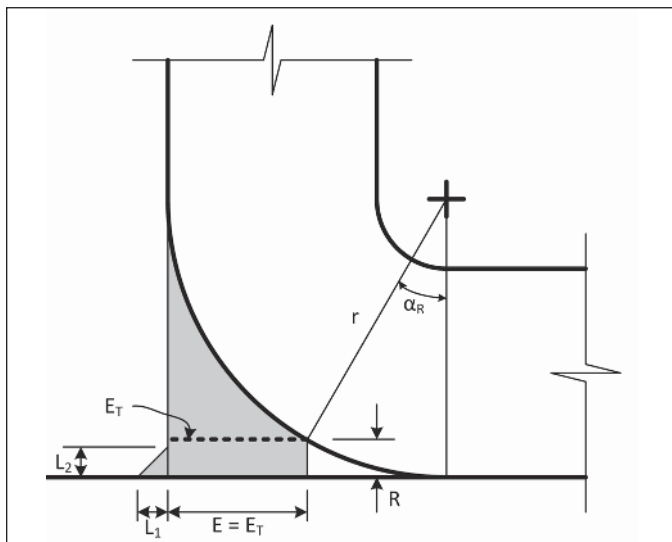


Fig. 3 — The weld configuration for case 1.

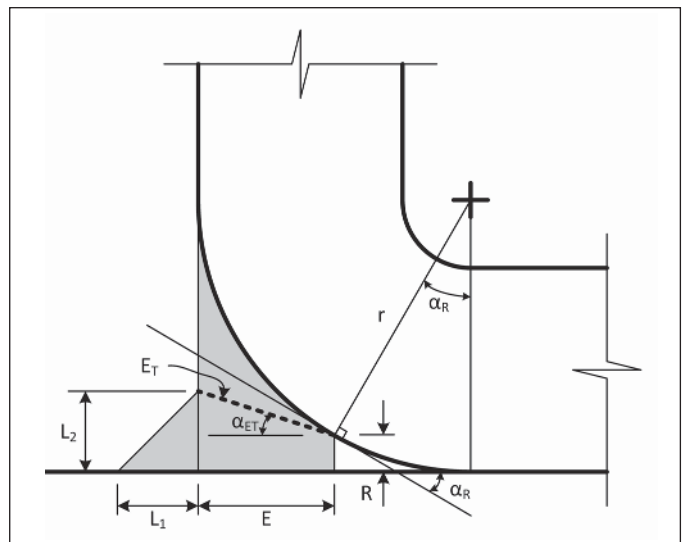


Fig. 4 — The weld configuration for case 2.

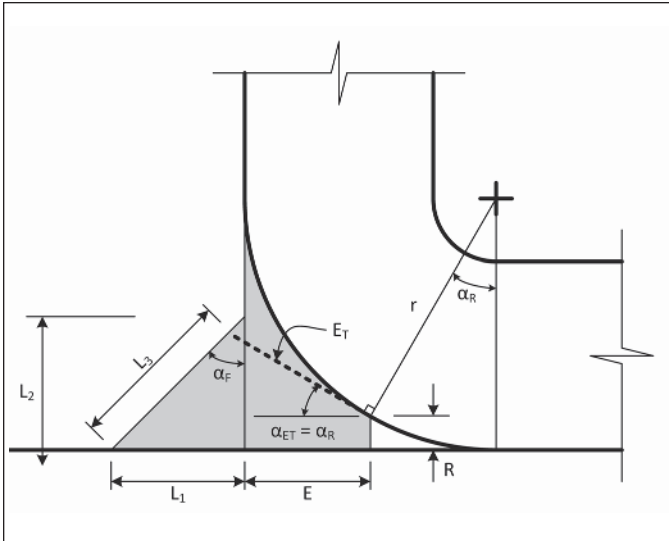


Fig. 5 — The weld configuration for case 3.

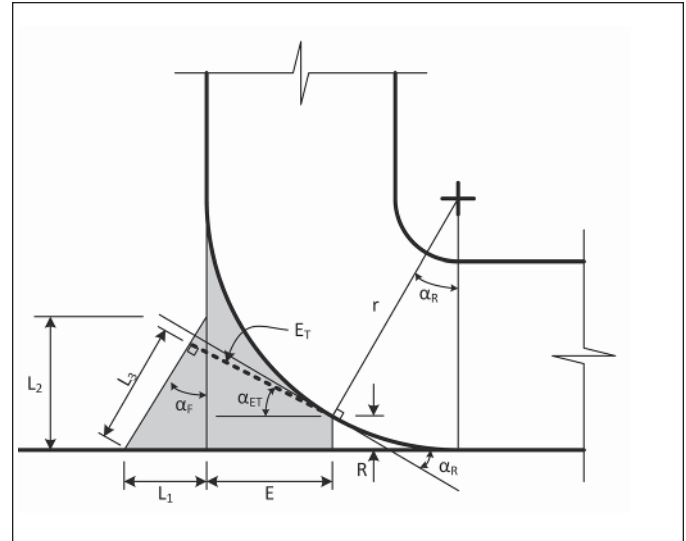


Fig. 6 — The weld configuration for case 4.

weld should be avoided because it increases the cost to construct the joint without adding any benefit to the strength.

To determine if the fillet weld is undersized, one must first determine several parameters of the connection. The effective throat of the flare-bevel, E ; the fillet weld legs, L_1 and L_2 ; and the outer radius of the curve, r , are specified by the engineer or given based on the material. Knowing these, the first quantity to be determined is the angle of the root opening, called α_R in Fig. 3. This is

$$\alpha_R = \sin^{-1}[(r - E)/r]. \quad (1)$$

From here, one may solve for R , the size of the weld root opening, by

$$R = r [1 - \cos(\alpha_R)]. \quad (2)$$

Because the vertical leg of the fillet weld, L_2 , is known, the weld is undersized if $L_2 \leq R$, and therefore

$$E_T = E. \quad (3)$$

Case 2: Medium Fillet Weld

The second case is one where the fillet weld is large enough to increase the minimum total effective throat, or E_T , of the connection, yet small enough that the minimum total effective throat still only passes through

the flare-bevel weld metal. Figure 4 illustrates this case.

Several of the parameters in Fig. 4 were already solved for in the previous section. The reader will notice that the angle α_R is now shown for the tangent line at the weld root. The minimum total effective throat is now the line connecting the weld root to the intersection of the top toe of the fillet weld and flare-bevel face. This is found as

$$E_T = \sqrt{E^2 + (L_2 - R)^2}. \quad (4)$$

Thus, it can be shown that case 2 is applicable when $R < L_2 \leq R + E \tan(\alpha_R)$.

The angle of the minimum total effective throat is the one between the line E_T and horizontal plane, and it has the value

$$\alpha_{ET} = \cos^{-1}(E/E_T). \quad (5)$$

However, this quantity is not immediately useful for design because E_T must first be determined.

Case 3: Large Fillet Weld, Minimum Total Effective Throat Line Nonperpendicular to the Fillet Face

In the third case, the fillet weld is large enough that the minimum total

effective throat, E_T , of the connection passes through part of the fillet weld itself, and the weld face is the outer face of the fillet weld. In this case, the angle of the fillet weld, called α_F , is obtuse enough that the line of E_T cannot intersect with it at a perpendicular angle without passing through the curved base metal, thus $\alpha_{ET} = \alpha_R$. Figure 5 illustrates this case.

The new variable α_F is determined by

$$\alpha_F = \tan^{-1}(L_1/L_2). \quad (6)$$

To solve for E_T , first a system of equations is set up as follows:

$$\begin{cases} L_3 \sin(\alpha_F) + E_T \cos(\alpha_R) = L_1 + E \\ L_3 \cos(\alpha_F) = E_T \sin(\alpha_R) + R. \end{cases} \quad (7)$$

By solving Equation 7 for E_T , one finds that

$$E_T = \frac{L_1 + E - R \tan(\alpha_F)}{\sin(\alpha_R) \tan(\alpha_F) + \cos(\alpha_R)}. \quad (8)$$

With an equal-leg fillet weld ($\alpha_F = \pi/4 = 45 \text{ deg}$), Equation 8 simplifies to

$$E_T = \frac{L_1 + E - R}{\sin(\alpha_R) + \cos(\alpha_R)}. \quad (8a)$$

Case 4: Large Fillet Weld, Minimum Total Effective Throat Line Perpendicular to the Fillet Face

In case 3, the vertical leg of the fillet weld is large enough that the minimum total effective throat, E_T , of the connection passes through part of the fillet weld itself, and the weld face is the outer face of the fillet weld. However, in case 4, α_F is acute enough that the line of E_T intersects with it at a perpendicular angle without passing through the curved base metal ($\alpha_{ET} < \alpha_R$). Figure 6 illustrates this case.

Note that this condition does not necessarily require an unequal-leg fillet weld and can happen if E is small, making $\alpha_R \geq \pi/4 = 45$ deg. This would, however, require a small enough E value that instead of adding a reinforcing fillet, one would be better served by increasing the flare-bevel effective throat instead.

It can be shown that $\alpha_F = \alpha_{ET}$ in this case because the fillet weld face is perpendicular to the line of E_T . Thus, reconfiguring Equation 8,

$$E_T = \frac{L_1 + E - R \tan(\alpha_F)}{\sin(\alpha_F) \tan(\alpha_F) + \cos(\alpha_F)},$$

which simplifies to

$$E_T = [L_1 + E - R \tan(\alpha_F)] \cos(\alpha_F). \quad (9)$$

Also, if $\alpha_F = \pi/4 = 45$ deg,

$$E_T = \frac{L_1 + E - R}{\sqrt{2}}. \quad (9a)$$

Conclusions

By summarizing the equations in the previous sections, one may establish a case that may be programmed into a computer-aided engineering software package for rapid iteration of results. Thus, the minimum total effective throat of a flare-bevel groove weld with a reinforcing fillet is found generically as

$$E_T = \begin{cases} E & \text{if } L_2 \leq R \\ \sqrt{E^2 + (L_2 - R)^2} & \text{if } R < L_2 \leq R + E \tan(\alpha_R) \\ \frac{L_1 + E - R \tan(\alpha_F)}{\sin(\alpha_R) \tan(\alpha_F) + \cos(\alpha_R)} & \text{if } L_2 > R + E \tan(\alpha_R) \\ & \text{and } \alpha_R \geq \alpha_F \\ [L_1 + E - R \tan(\alpha_F)] \cos(\alpha_F) & \text{if } L_2 > R + E \tan(\alpha_R) \\ & \text{and } \alpha_R < \alpha_F. \end{cases} \quad (10)$$

Given an equal-leg fillet weld, the case above can be simplified as

$$E_T = \begin{cases} E & \text{if } L_1 \leq R \\ \sqrt{E^2 + (L_1 - R)^2} & \text{if } R < L_1 \leq R + E \tan(\alpha_R) \\ \frac{L_1 + E - R}{\sin(\alpha_R) + \cos(\alpha_R)} & \text{if } L_1 > R + E \tan(\alpha_R) \\ & \text{and } \alpha_R \geq 45 \text{ deg} \\ \frac{L_1 + E - R}{\sqrt{2}} & \text{if } L_1 > R + E \tan(\alpha_R) \\ & \text{and } \alpha_R < 45 \text{ deg}. \end{cases} \quad (10a)$$

These cases can be programmed into a computer-aided engineering software package with relative ease and allow the engineer to rapidly iterate to find the optimum weld sizes. Or, if the weld geometry is known, the strength of the weld can easily be determined.

Given the current effective throat limitations of a flare-bevel-groove weld per AWS D1.1 (Table 2.1, effective size of flare-groove welds filled flush, and Fig. 3.2, as previously noted), Equations 10 and 10a may be further simplified for shielded metal arc welding, shielded flux cored arc welding, and submerged arc welding as

$$E_T = \begin{cases} \frac{5}{16}r & \text{if } L_2 \leq 0.274r \\ \sqrt{0.098r^2 + (L_2 - 0.274r)^2} & \text{if } 0.274r < L_2 \leq 0.570r \\ \frac{L_1 + \frac{5}{16}r - 0.274r \tan(\alpha_F)}{0.688 \tan(\alpha_F) + 0.726} & \text{if } L_2 < 0.570r \text{ and} \\ & \alpha_F \geq 43.43 \text{ deg} \\ [L_1 + \frac{5}{16}r - 0.274r \tan(\alpha_F)] \cos(\alpha_F) & \text{if } L_2 < 0.570r \\ & \text{and } \alpha_F < 43.43 \text{ deg}, \end{cases} \quad (11)$$

and for an equal-leg fillet weld,

$$E_T = \begin{cases} \frac{5}{16}r & \text{if } L_1 \leq 0.274r \\ \sqrt{0.098r^2 + (L_1 - 0.274r)^2} & \text{if } 0.274r < L_1 \leq 0.570r \\ \frac{L_1 + 0.039r}{1.414} & \text{if } L_1 < 0.570r. \end{cases} \quad (11b)$$

For gas metal arc welding and gas flux cored arc welding, Equations 10 and 10a may be further simplified as

$$E_T = \begin{cases} \frac{5}{8}r & \text{if } L_2 \leq 0.073r \\ \sqrt{0.391r^2 + (L_2 - 0.073r)^2} & \text{if } 0.073r < L_2 \leq 0.326r \\ \frac{L_1 + \frac{5}{8}r - 0.073r \tan(\alpha_F)}{0.375 \tan(\alpha_F) + 0.927} & \text{if } L_2 < 0.326r \text{ and} \\ & \alpha_F \geq 22.02 \text{ deg} \\ [L_1 + \frac{5}{8}r - 0.073r \tan(\alpha_F)] \cos(\alpha_F) & \text{if } L_2 < 0.326r \\ & \text{and } \alpha_F < 22.02 \text{ deg}, \end{cases} \quad (12)$$

and for an equal-leg fillet weld,

$$E_T = \begin{cases} \frac{5}{8}r & \text{if } L_1 \leq 0.073r \\ \sqrt{0.391r^2 + (L_1 - 0.073r)^2} & \text{if } 0.073r < L_1 \leq 0.326r \\ \frac{L_1 + 0.552r}{1.302} & \text{if } L_1 > 0.326r. \end{cases} \quad (12a)$$



Acknowledgment

The author would like to thank his colleague, Karl R. Anderson III, for his help and guidance in refining the methodology for this article.

Nomenclature

- E = Effective throat of flare-bevel-groove weld
- E_T = Minimum total effective throat of combined flare-bevel-groove and reinforcing fillet weld joint
- L_1 = Length of fillet weld leg (not touching flare-bevel weld)
- L_2 = Length of fillet weld leg (touching flare-bevel weld)
- L_3 = Diagonal length of fillet weld from its toe to its intersection with the line of E_T
- r = Outer radius of the curved item
- R = Root opening at the back side of the flare-bevel weld
- α_{ET} = Angle of the minimum total effective throat
- α_F = Angle of the fillet weld
- α_R = Angle of the root opening

GLENN R. FRAZEE (grfrazee@gmail.com), PE, is a senior structural associate at Sargent & Lundy, LLC, Chicago, Ill.

Journalist Trades Pen for a Welding Torch

How the welding program at Wallace State Community College is helping a longtime journalist transition into a new career

BY MELANIE PATTERSON

As someone starting a new career later in life, welding at first was a bit of a mystery. I had worked as a journalist for 20 years, deciding in my early 40s that it was time for a change. After exploring the options available at Wallace State Community College (WSCC), Hanceville, Ala., I decided welding would be my new career.

Studying Surprises

At the time, I had never welded before, or even seen it performed. My first surprise came when I learned the welding program is five semesters long. What could possibly take that long? Welding can't be that hard, right?

My second surprise came as the answer to that question. I was unprepared for the welding program to be so academic. Not only do we have to spend time in the welding shop, but we also have to take theory classes because welding incorporates many other fields of study, such as chemistry and physics. For example, welding students at WSCC learn about the different types of filler metals and when to use them; various shielding gases and their properties; why and when to pre-

heat or postheat base metal to prevent it from cracking; characteristics of metals (e.g., tensile strength, yield strength, ductility, hardness, and toughness); and much more.

We are also learning many of the American Welding Society (AWS) codes for acceptable welds, because the instructors use AWS standards to determine whether our welds pass or fail. All students learn to use fillet weld gauges and other tools employed by welding inspectors to assess their welds. We also incorporate nondestructive examination (visual and ultrasonic) and destructive testing (bend test) — Fig. 1.

All of these academic classes are in addition to learning how to actually weld. The WSCC program teaches the basic processes used in industry today: shielded metal arc welding, gas metal arc welding, flux cored arc welding, and gas tungsten arc welding — Fig. 2.

In addition to welding, WSCC students learn to carbon arc gouge, cut metal using plasma and oxyfuel torches, properly utilize gas cylinders for welding and cutting, and use grinders and other hand tools. Safety is incorporated into every aspect of the program — Fig. 3.

Teachers 'Weld' the Way

The WSCC welding program's standards are high. This is because the instructors care about the success of their students. Jim Thompson, head instructor of the welding program, continually reminds students that he



Fig. 1 — Instructor Randy Hammond (right) shows student Victor Andrade the result of a cross section acid etching test, which checks the root penetration of a fillet weld.

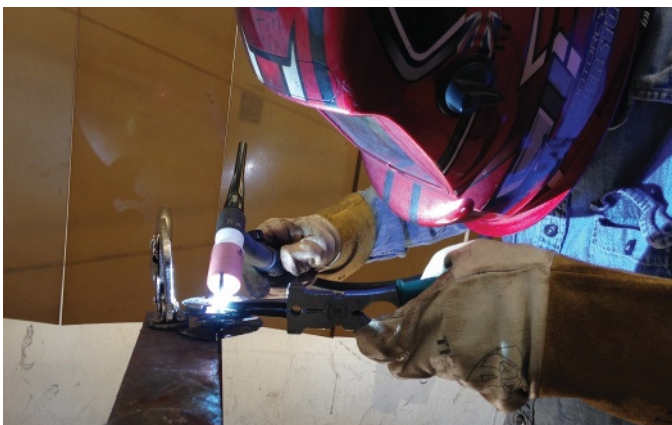


Fig. 2 — Student Austin Perkins uses gas tungsten arc welding to create a school project.



Fig. 3 — Instructor Randy Hammond (left) monitors students as they weld using an oxyfuel torch. The program does not teach this process because it is not commonly used in industry, but Hammond insists that students see how the process works.



Fig. 4 — Students try their hand at virtual welding during an April 2016 visit to the Alabama Robotics Technology Park in Tanner, Ala.

is preparing them for the “real world” in industry. “It’s a different world out there, and we want you to be ready,” said Thompson. “Employers do not play. They want a fair day’s work for a day’s pay. And we’re here to get you ready for that.”

One way the instructors help prepare students is to take them on facility tours so they can see first-hand what the welding industry is like — Fig. 4. We have visited several welding shops in north Alabama, including a NASA welding site at Redstone Arsenal in Huntsville and fabrication plants in Steele and Arab.

The welding program offers two courses of study — a certificate and an associate degree. Although it is up to each student to choose which program is right for him or her, Thompson strongly encourages students to earn their associate degree, which requires more classes than the certificate program. He believes in as much education as possible, and frequently takes classes himself, including a recent course in which he became certified to conduct ultrasonic testing.

All three welding instructors at WSCC are AWS Certified Welding Inspectors, and they all have many years of experience working in the welding industry. It is through that experience and training that they guide students to do their best.

Instructor Roger Landers, who has more than 40 years of experience in welding, explained that welding is not

even the most important thing we need to learn.

“Students need to have soft skills,” affirmed Landers, such as being on time, having a good work ethic, being a team player, and having a good attitude. “If you show up on time every day, you stay here all day, and you work hard through our program, you’re going to be successful. If you get a job and lay out or don’t show up on time, you’re not going to have a job no matter how good of a welder you are.”

For that reason, the WSCC program requires students in the welding and other technical programs to pass a workplace essential skills course that teaches those important soft skills.

Welding instructor Randy Hammond agrees that soft skills are crucial for success in any job. “If students don’t already have a good work ethic, we try to instill a good work ethic into them,” he said. “This is a key thing. Most employees will not always be supervised at all times, so they have to stay busy. As a supervisor, I could always tell the ones who were trying to pull the wool over my eyes and those who were trying to do well.”

WSCC to Train More Welders

With about 85 students in the welding program, including day, night, and high school fast-track students, the instructors have a big job. The daytime program is capped at 50 students because there are only 50 welding

booths. With the welding industry booming right now, the school had to turn students away for the Fall 2016 semester.

The good news is WSCC has plans to build a new \$4 million facility for the welding program. Jimmy Hodges, dean of applied technologies at WSCC, said the school has approved preliminary drawings and is hoping to break ground on the facility this year. It will feature 75 welding booths, as well as plenty of space for both advanced welding, including robotics, and weld testing that will likely provide partnership opportunities with various companies.

“In the state of Alabama, we’ve been very fortunate to have recruited the automotive industry and all of the other companies that come along with that,” Hodges explained. “We also have aerospace and shipbuilding. There is a huge demand in the state for welders. I feel like we’re doing our part.”

Yes, I Can Make It

With plans to graduate from the WSCC welding program in May 2017, it’s unlikely I’ll get the opportunity to train in the new building. However, I’m excited that such a facility will exist in the area for future students.

When I first enrolled in the welding program, my plans were to simply try it out for a semester and go from there, as I had no idea whether I would like it. I also had no idea if I could make it as a welder. More than a year later, I’ve learned that, yes, I like welding very much, and, yes, I can make it.

Although I have worked hard, others share the credit for the multitude of new skills I’ve acquired. The WSCC welding program is extremely well-rounded, providing rigorous hands-on training. That training is strongly supported by the theory of why we do what we do.

“Anybody can make it sparkle,” explained Hammond, “but we’re going to make you into welders.” **WJ**

MELANIE PATTERSON (mkpatte@gmail.com) is a longtime journalist and welding student at Wallace State Community College, Hanceville, Ala. She also took the photos shown in Figs. 1–4.



Friends and Colleagues:

The American Welding Society established the honor of Counselor of the Society to recognize members for a career of distinguished leadership contributions in the advancement of welding science and technology. Election as a Counselor is based upon an individual's career of outstanding achievements and accomplishments. The selection committee is seeking qualified individuals who can demonstrate their leadership in the welding industry as evidenced by:

- Sustained service and performance in the advancement of welding science and technology
- Publication of papers, articles and books which enhance knowledge of welding
- Innovative development of welding technology
- Society, National and Section contributions
- Professional recognition
- Leadership in AWS or other corporate levels, particularly as it impacts the advancement of welding technology
- Facilitating others to participate as a volunteer in the advancement of welding technology

For specifics on the nomination requirements, please contact Chelsea Steel at csteel@aws.org at AWS headquarters in Miami, or simply follow the instructions on the Counselor nomination form located at www.aws.org/counselor. Please remember, we all benefit in the honoring of those who have made major contributions to our chosen profession and livelihood. The deadline for submission is July 1, 2017. The Counselor Committee looks forward to receiving numerous Counselor nominations for 2018 consideration.

Sincerely,

Lee Kvidahl
Chair, Counselor Committee



AWS COUNSELOR APPLICATION GUIDELINES

Nomination packages for AWS Counselor should clearly demonstrate the candidate's outstanding contribution to the advancement of welding science and technology. In order for the Counselor Selection Committee to fairly assess the candidate's qualifications, the nomination package must list and clearly describe the candidate's specific accomplishments, how they contributed to the advancements of welding technology and that these contributions were sustained. Essential in demonstrating the candidate's impact are the following:

1. Description of significant technical advancements. This should be a brief summary of the candidate's most significant contributions to the advancement of welding science and technology
2. Publication of books, papers, articles or other significant works
3. Inventions and patents
4. Professional recognition including awards and honors from AWS, other professional organizations, industry or other recognized body
5. Meaningful participation in AWS committees, Sections or other AWS voluntary contributions
6. Contributions to handbooks and standards
7. Presentations made at technical sessions, including Section meetings
8. Consultancy in technical matters or welding industry business matters
9. Leadership in AWS or other corporate levels, particularly as it impacts the advancement of welding technology
10. Participation on organizing committees for technical programs
11. Advocacy in support of AWS through institutional, political or other means
12. Facilitating others to participate as a volunteer in the advancement of welding technology

Note, packages for nominees that do not show participation in several of the activities above will have a low probability of success.

SUPPORTING LETTERS

Letters of support from individuals knowledgeable of the candidates and his/her contributions are encouraged. These letters should address the metrics listed above and provide personal insight into the contribution and stature of the candidate. Letters of support that simply endorse the candidate will have little impact on the selection process.

SUBMISSION DEADLINE JULY 1, 2017



Nomination of AWS Counselor

I. HISTORY AND BACKGROUND

In 1999, the American Welding Society established the honor of Counselor to recognize individual members for a career of distinguished organizational leadership that has enhanced the image and impact of the welding industry. Election as a Counselor shall be based on an individual's career of outstanding accomplishments.

To be eligible for appointment, an individual shall have demonstrated his or her leadership in the welding industry as evidenced by:

- Sustained service and performance in the advancement of welding science and technology
- Publication of papers, articles and books which enhance knowledge of welding
- Innovative development of welding technology
- Society, National and Section contributions
- Professional recognition

II. RULES

- A. Candidates for Counselor shall have at least 10 years of AWS membership
- B. Each candidate shall be nominated by at least five members of AWS
- C. Nominations shall be submitted on the official form, available from AWS Headquarters
- D. Nominations must be submitted to AWS headquarters no later than July 1 of the year prior to that in which the award will be presented
- E. Nominations shall remain valid for three years
- F. All information on nominees will be held in strict confidence
- G. All required mandatory information is to be included in the nomination package or the package will be returned and not considered by the Selection Committee
- H. Candidates who have been selected as Fellows of AWS shall not be eligible for selection as Counselors. Counselors may not be nominated for both of these awards at the same time.

III. NUMBER OF COUNSELORS TO BE SELECTED

Maximum of 10 Counselors selected each year

Return completed Counselor nomination package to:

Chelsea L. Steel
Program Manager, Board and
Executive Director Services
8669 NW 36th Street, # 130
Miami, FL 33166

Email: csteel@aws.org
Telephone: 305-443-9353 Ext. 293
800-443-9353 Ext. 293
Fax: 305-445-1809



American Welding Society

CLASS OF 2018 COUNSELOR NOMINATION FORM

Date _____ Name of Candidate _____
 AWS Member Number _____ Years of Membership _____
 Home Address _____
 City _____ State _____ Zip Code _____ Phone _____
 Email _____
 Present Employer _____
 Title/Position _____
 Business Address _____
 City _____ State _____ Zip Code _____ Phone _____
 Academic Background, As Applicable _____
 Institution _____ Major/Minor _____
 Degree/Certification/Year _____

IT IS **MANDATORY** THAT A CITATION (50 TO 100 WORDS) BE INCLUDED. USE SEPARATE SHEET INDICATING WHY THE NOMINEE SHOULD BE SELECTED AS AN AWS COUNSELOR. THE CITATION IS TO BE A PART OF THE NOMINATION PACKAGE.

ESSENTIAL FOR THE NOMINATION PACKAGE

The Counselor Selection Committee criteria are strongly based upon and extracted from the categories indicated on the second page of this application. It is strongly recommended that the nominator prepare a complete summary of the nominee's history as an attachment to this application to ensure that the committee has sufficient information to deliberate and make the appropriate selections of Counselor nominees.

SUBMITTED BY: _____
 PROPOSER: _____
 AWS Member Number: _____

The proposer will serve as the contact if the Selection Committee requires further information. The proposer is encouraged to include a detailed biography of the candidate and letters of recommendation from individuals describing the specific accomplishments of the candidate. Signatures on the nominating form, or supporting letters from each nominator, are required from four AWS members in addition to the proposer. Signatures may be acquired by photocopying the original application and transmitting to each nominating member. Once the signatures are secured the total package should be submitted.

NOMINATING MEMBER _____ Print name _____
 AWS Member Number _____
 NOMINATING MEMBER _____ Print name _____
 AWS Member Number _____
 NOMINATING MEMBER _____ Print name _____
 AWS Member Number _____
 NOMINATING MEMBER _____ Print name _____
 AWS Member Number _____

SUBMISSION DEADLINE IS JULY 1, 2017



Friends and Colleagues:

The American Welding Society, in 1990, established the honor of Fellow of the Society to recognize members for distinguished contributions to the field of welding science and technology, and for promoting and sustaining the professional stature of the field. Election as a Fellow of the Society is based on outstanding accomplishments and the technical impact of the individual. Such accomplishments will have advanced the science, technology and application of welding, as evidenced by:

- Sustained service and performance in the advancement of welding science and technology
- Publication of papers, articles and books which enhance knowledge of welding
- Innovative development of welding technology
- Society and Section contributions
- Professional recognitions

I want to encourage you to submit nomination packages for those individuals whom you feel have a history of accomplishments and contributions to our profession consistent with the standards set by the existing *AWS Fellows*. In particular, I would make a special request that, in considering members for nomination, you look to the most senior members of your Section or District. In many cases, the colleagues and peers of these individuals who are the most familiar with their contributions, and who would normally nominate the candidate, are no longer with us. I want to be sure that we make the extra effort required to ensure that those truly worthy are not overlooked because no obvious individual was available to start the nominating process.

For specifics on nomination requirements, please contact Chelsea Steel at csteel@aws.org at AWS headquarters in Miami, or simply follow the instructions on the Fellow nomination form located at www.aws.org/fellow. Please remember, we all benefit in the honoring of those who have made major contributions to our chosen profession and livelihood. The deadline for submission is August 1, 2017. The Fellows Committee looks forward to receiving numerous Fellow nominations for 2018 consideration.

Sincerely,

Dr. Charles V. Robino
Chair, AWS Fellows Committee

Safe Practices for Welding Aluminum

When working with aluminum, welders should follow the general safe practices outlined in ANSI Z49.1, *Safety in Welding, Cutting, and Allied Processes*, and other safety and health standards.

In addition, because most welding processes use enough heat to produce molten filler and base metal to accomplish welding, the following conditions warrant safety precautions in welding aluminum alloys:

1. High levels of fumes may be produced when welding any aluminum alloy; however, welding the 5XXX series aluminum alloys tends to produce higher fume levels.
2. Welding aluminum and aluminum alloys tends to utilize argon-based or helium-based shielding gases, which produce an intense arc and very little visible fume. The arc produces ultraviolet radiation that reacts with oxygen in the surrounding atmosphere to produce ozone. Aluminum's high reflectivity tends to exacerbate the problem. While ozone may be produced during any arc welding process, the particular features associated with welding aluminum make it more of a concern. Adequate ventilation should always be used, and air sampling should always be performed to ensure ozone does not exceed permissible exposure limits.

Ozone is produced as a result of the action of the arc on oxygen in the surrounding atmosphere. While it may be worse with argon-rich blends, it will occur to some degree with any shielding gas. Higher fume-producing gases and processes will produce more visible fume, which helps to shield the atmosphere from the arc rays. Processes that produce an intense arc and little fume such as gas metal arc and gas tungsten arc welding will produce more ozone. Also, because aluminum is very reflective, the production of ozone tends to be higher.

If it is determined personnel are exposed to excessive pollutants, the use of filtering masks or air-supplied respirators are required.

As with any welding process, the work area should be kept clean of any paper, wood, rags, or other combustible materials that can be ignited by flying sparks.

Surface Preparation

Preparing a surface for welding, brazing, and other joining processes requires removal of all grease, oil, dirt, paint, and other contaminants that can generate hydrogen.

The cleaning and welding areas must be well ventilated. If chlorinated solvents are used for degreasing, this should take place at a location remote from the welding area. Highly toxic phosgene gas can result from the dissociation of the vapors of chlorinated hydrocarbons by arc radiation.

Petroleum-based solvents, such as acetone, leave little residue and are nontoxic when used in a well-ventilated welding area, but these solvents have low flash points and require special storage and handling. Instructions for the use of the solvent provided by the manufacturer in the safety data sheet should be carefully followed.

Due to the reaction between aluminum and certain sol-

vents and cleaners, caution must be observed. Instructions for the use of the solvent provided by the manufacturer in the safety data sheet should be carefully followed.

If acid cleaning or etching of the aluminum surface is required, it should be recognized that all acids used in cleaning and etching solutions have the potential to be extremely hazardous. Personnel using them should be thoroughly familiar with all chemicals involved, and adequate safety equipment should be used.

Plasma Arc Cutting

Voluminous fumes are evolved when cutting aluminum with this process, therefore, a water table and exhaust hood are recommended for operator safety. When cutting close to a water surface, hydrogen will be generated if molten aluminum reacts with the water. A cross flow of air is required to prevent a buildup of an explosive atmosphere. When cutting under water, a perforated air line should be used to bubble air through the water to reduce hydrogen concentrations.

Resistance Welding

The main hazards that may be encountered with resistance welding processes and equipment are the following:

1. Electric shock from contact with high-voltage terminals or components
2. Ejection of small particles of molten metal from the weld
3. Crushing of some part of the body between the electrodes or other moving components of the machine.

High-frequency generators must be equipped with safety interlocks on access doors and automatic safety grounding devices to prevent operation of the equipment when access doors are open. The equipment should not be operated when panels or high-voltage covers have been removed or when interlocks and grounding devices are blocked.

Stud Welding

Personnel operating stud welding equipment should be provided with face and skin protection to guard against burns from spatter. Eye protection in the form of safety glasses with side shields or a face shield with a No. 3 filter lens should be worn to protect against arc radiation.

When an inert gas is used to shield aluminum stud welding, proper procedures for handling, storing, refilling and using the gas storage cylinders should be observed. Capacitor-discharge stud welding is characterized by a sharp noise when the arc disintegrates the stud tip. Continual exposure to this elevated noise level can damage hearing, so the use of hearing protection is advised. Operators with pacemakers should not operate stud welding equipment or come near the welding vicinity. [WJ](#)

Excerpted from the *Welding Handbook*, Ninth Edition, Volume 5, Materials and Applications, Part 2.

FOR SALE OR RENT

MITROWSKI RENTS

Made in U.S.A.

Welding Positioners
1-Ton thru 60-Ton
Tank Turning Rolls



Used Equipment for Sale
www.mitrowskiwelding.com



sales@mitrowskiwelding.com
(800) 218-9620
(713) 943-8032

**Red-D-Arc
Welderrentals**
reddarc.com

Rentals, Lease and Sales



Welders



Weld
Automation



Generators

1-866-733-3272

ORDER ONLINE
MARKINGPENDEPOT.COM

MFD

MARKING PEN DEPOT
The World's Biggest Selection of Markers

FREE Samples Available
...Millions of Markers!

The World's
Largest Selection
of Markers for the
Welding Trade

Distributor of
Markal, Dykem, Nissen, Tempil,
Unipaint and Arro markers.

FREE SHIPPING AT \$50

888.906.9370
ORDER BY PHONE



TRAINING



CWI/CWE PREPARATORY COURSE

FUNDAMENTALS, CODE, PLUS 5 DAYS ON PART B.
PLENTY OF SELF STUDY FOR NIGHTS & WEEKEND

Houston, TX March 27–April 7, April 24–May 5
Houston, TX March 13–17 (Part B Only)
Marksville, LA June 5–16
Ardmore, OK July 10–21
Ellijay, GA May 8–19, Aug. 28–Sept. 8
Pascagoula, MS April 10–21, May 29–June 9
Searcy, AR Feb. 27–March 10
Port Arthur, TX May 22–June 2

VISUAL INSPECTION COURSE

LEARN HOW TO DO THE JOB START TO FINISH
HANDS-ON TRAINING FOR NEW CWI INSPECTORS!

Ellijay, GA Feb. 20–24, Sept. 4–8

CALL OR E-MAIL

1-228-762-2890

info@realeducational.com

Also Offering: RT Film Interpretation,
Welding Procedure Fundamentals,
CWS, SCWI, 80-Hour CWI Renewal

**INDUSTRIAL PLASMA MACHINES
FOR FABRICATORS**

Profile Cutting Systems USA

A Veteran Owned Business



John E. Zuehlke
jz@pcsusa.pro

1-800-757-8250
US: www.pcsmachines.com
AU: www.profilecuttingsystems.com



JOE FULLER LLC

We manufacture tank turning rolls

3-ton through 120-ton rolls

www.joefuller.com



email: joe@joefuller.com

Phone: (979) 277-8343

Fax: (281) 290-6184

Our products are made in the USA

SERVICES

SEEKING GROWTH?

Global Welding Technologies, LLC. (GWT) announces the launch of its international consulting business.

Whether you're a welding products manufacturer seeking entry or growth in North America or a distributor seeking to develop private label initiatives, GWT can help develop the customized strategies and deliver the commercial results.

Web: www.gwt-consulting.com



Contact: David Wilton
dwilton.gwt@outlook.com
+1 314 609 6203

ALM Positioners almmh.com	14 (855) 750-4295
Arcos Industries, LLC arcos.us	Inside Back Cover (800) 233-8460
Astro Arc Polysoude polysoude.com	30 (661) 702-0141
Atlas Welding Accessories, Inc. atlaswelding.com	24 (800) 962-9353
AWS Education Services aws.org/education	39 (800) 443-9353, ext. 455
AWS Member Services aws.org/membership	25, 45 (800) 443-9353, ext. 480
Bluco Corp. bluco.com	28 (800) 535-0135
Camfil Air Pollution Control camfilapc.com	2 (800) 479-6801
Canaweld, Inc. canaweld.com	47 (416) 548-5650
CDA Technical Institute commercialdivingacademy.com	31 (888) 974-2232
CEI thinkcei.com/pw	31 (800) 473-1976
Cor-Met cor-met.com	27 (800) 848-2719
Dengensha America dengensha.com	35 (440) 439-8081
Diamond Ground Products, Inc. diamondground.com	15, 17 (805) 498-3837
Donaldson Filtration Systems donaldson.com	19 (800) 365-1331
Elco Enterprises, Inc./Wire Wizard Welding Products wire-wizard.com	23 (517) 782-8040
Electron Beam Technologies, Inc. electronbeam.com	17 (815) 935-2211
FABTECH MEXICO 2017 fabtechmexico.com	21 52 (81) 8369-6969
Gullco International, Inc., U.S.A. gullco.com	15 (440) 439-8333
HDE Technologies, Inc. hdetechnologies.com	23 (916) 714-4944
Hobart Institute of Welding Technology welding.org	18 (800) 332-9448
Hodgson Custom Rolling, Inc. hcrsteel.com	5 (905) 356-6025
Intercon Enterprises, Inc. intercon1978.com	29 (800) 665-6655
K.I.W.O.T.O., Inc. rodguard.net	18 (269) 944-1552
Lincoln Electric Co. lincolnelectric.com	Outside Back Cover (216) 481-8100
Midalloy midalloy.com	35 (800) 776-3300

National Robotic Welding Conference & Exhibition 2017 aws.org/milwaukee-NRAWC-2017	13 (262) 613-3790
RWMA/Resistance Welding Manufacturing Alliance www.aws.org/rwma	47 (800) 443-9353, ext. 295
Select-Arc, Inc. select-arc.com	Inside Front Cover (937) 295-5215
Southwire Co., LLC southwire.com	11 (800) 444-1700
Triangle Engineering, Inc. trieng.com	16 (781) 878-1500
TRUMPF us.trumpf.com	7 web contact only
Voestalpine Bohler Welding USA, Inc. voestalpine.com/welding	1 (800) 527-0791
Weiler Corp. weilercorp.com/ultracut	9 (800) 835-9999
Welding Alloys welding-alloys.com	27 (859) 525-0165
WEMCO/Welding Equipment Manufacturers Committee aws.org/wemco	16 (800) 443-9353, ext. 444

Visit our Interactive Ad Index: aws.org/ad-index



Creating Bonds - Changing Lives
Freedom Guide Dogs provides independence to the visually impaired by placing quality guide dogs through their Hometown Training™ program - at no charge to the client.

www.freedomguidedogs.org



Understanding the Reliability of Solder Joints Used in Advanced Structural and Electronics Applications: Part 1 — Filler Metal Properties and the Soldering Process

The effects of filler metal properties and the soldering process on joint reliability were examined

BY PAUL T. VIANCO

ABSTRACT

Soldering technology has made tremendous strides in the past half-century. Whether structural or electronic, all solder joints must provide a level of reliability that is required by the application. This Part 1 report examines the effects of filler metal properties and the soldering process on joint reliability. Solder alloy composition must have the appropriate melting and mechanical properties that suit the product's assembly process(es) and use environment. The filler metal must also optimize solderability (wetting and spreading) to realize the proper joint geometry. The soldering process also affects joint reliability. The choice of flux and thermal profile support the solderability performance of the molten filler metal to successfully fill the joint clearance and complete the fillet. Base material and/or surface finish dissolution can alter the filler metal composition, which together with the interface reaction, affect the long-term mechanical performance of the solder joint. A second report, Part 2, explores the factors that explicitly affect solder joint reliability, including solid-state growth of the solder/base material reaction layer as well as solder joint fatigue under cyclic loading environments.

ing materials properties, process optimization, and reliability analyses, can also be applied to structural applications (Ref. 1) — Fig. 1B.

The reliability requirements placed on solder joints are determined by their specific function(s) and the use conditions. Performance metrics include mechanical strength, both monotonic and cyclic, as well as conductivity in the case of electrical or electronic products. Solder joints may also be called upon to provide a hermetic seal between base materials. This Part 1 report begins by examining the effect of filler metal properties, which are often in a synergistic role with the properties of the base materials and surface finishes, on the latter. The melting properties of the filler metal, specifically, the solidus temperature (T_s) and liquidus temperature (T_l) must be well below the maximum service temperature and minimum process temperature, respectively. The bulk mechanical properties of the filler metal affect reliability performance; however, the contribution is often overwhelmed by the configuration of the solder joint, especially the joint clearance and surfaces for fillet development. Filler metal composition affects its solderability and is instrumental in

KEYWORDS

• Solder • Joint Reliability • Filler Metal Properties • Processing Effects

Introduction

The past half-century has seen a revolution in the miniaturization and increased functionality of electronics. Whether such products are portable electronic devices (PEDs) marketed within the consumer electronics sector, or advanced radar and autonomous flight systems used in high-

reliability military hardware, soldering technology has enabled these advances, beginning at the component level, through subassemblies, and on to the final system architecture. Advances in soldering technology have taken place primarily within the electronics industry — Fig. 1A. However, the fundamental knowledge base that has supported progress there, includ-

PAUL T. VIANCO (ptvianc@sandia.gov) is with Sandia National Laboratories, Albuquerque, N.Mex. Based on the 2016 AWS Comfort A. Adams Lecture delivered during FABTECH in Las Vegas, Nev.

achieving the optimum solder joint geometry, which also impacts reliability.

The base material affects solder joint reliability primarily by its support of solderability performance. Because solder alloys are usually weaker than most base materials, the latter's mechanical properties do not impact reliability except in a few instances. Base material solderability, which is often augmented by the use of surface finishes, controls the final geometry of the joint — filling the gap and fillet formation — that determine the solder joint mechanical properties.

Reliability is also affected by the soldering process used to form the joint. As noted above, maximizing solderability leads to an optimum joint geometry. Additional factors, which are relevant to the soldering process, include

- a) base material dissolution;
- b) in-situ changes to the molten solder composition; and
- c) formation of the interface reaction layers.

This Part 1 report examines the roles of materials properties, primarily those of the filler metal, and soldering processes on the long-term reliability of solder joints, whether the application is electronic or structural in nature. The factors that address, explicitly, solder joint reliability, such as solid-state interface reactions and fatigue performance, are discussed further in Part 2.

Material Properties

Solderability Performance

A discussion of the solderability begins by considering the T_s and T_l of the filler metal. The values of T_s and T_l are the same for pure (elemental) metals and eutectic compositions (whether binary or of higher order). A *solder* is defined as a metal or alloy having a liquidus temperature that is less than 450°C (842°F) (Ref. 2)¹. Several of the more common solder alloys are shown in Fig. 2 as a function of T_l . The 52In-48Sn (wt-%) and 58Bi-42Sn solders are often referred to as the “fusible” alloys. There are also alloys that are combinations of gallium (Ga), In, Cd,

1. Those alloys having T_l values greater than 450°C are designated as brazing filler metals.

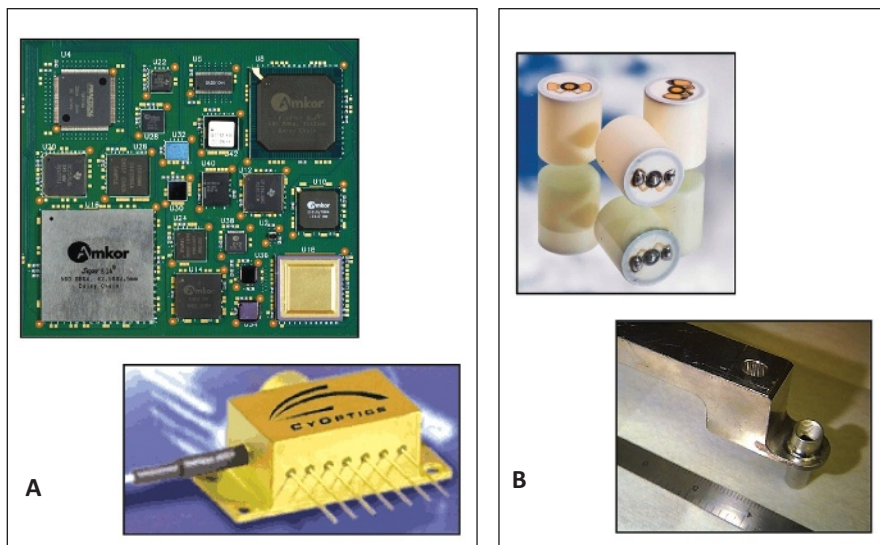


Fig. 1 — Solder interconnections are critical to advanced electronic and structural applications: A — Printed wiring assemblies and opto-electronic packages; B — microsampling device for atmospheric studies or the joining of large structural members.

and other elements with T_l values that are less than room temperature. The Sn-based solders form a majority of filler metals, having T_l values in the range of 183°C (63Sn-37Pb) to 240°C (95Sn-5Sb). The high lead (Pb) alloys, e.g., 95Pb-5Sn ($T_s = T_l = 312^\circ\text{C}$), are used in step soldering processes so that those joints do not melt when subsequent soldering operations are performed with filler metals having reduced melting temperatures, e.g., the commonly used, 63Sn-37Pb alloy. The Au-based (eutectic) solders, 80Au-20Sn ($T_s = T_l = 280^\circ\text{C}$), and 88Au-12Ge ($T_s = T_l = 356^\circ\text{C}$) are used to provide hermetic seals for electronic packages, or to attach the silicon microprocessor die to a ceramic package. Based upon the same step-soldering methodology, the Au-Sn or Au-Ge bond will not reflow when the package is soldered to the printed circuit boards with any of the high-Sn solders.

The 1986 amendment to the Clean Water Act required that Pb-bearing filler metals be replaced with Pb-free compositions for potable water systems and food handling equipment. Additional rule-making, both onshore and overseas, has now driven the conversion from 63Sn-37Pb eutectic solder to Pb-free alloys in consumer electronics. The supporting research and development activities have been costly. More importantly, the transition has generated an important philosophical change among design and

process engineers that rely upon soldering technology. The old premise was that all applications should be fitted to one solder, namely the traditional 63Sn-37Pb alloy. Today, both the structural and electronics soldering communities recognize the advantages of engineering new filler metals having properties that are optimized to the specific application. The consequence has been the development of alternative solder compositions having physical and mechanical properties that are engineered to optimize the soldering process as well as for the product to meet its reliability requirements with adequate margin.

The discussion now turns to *solderability*. There are three *functional conditions* that describe the solderability performance of a molten filler metal on a base material surface:

- a) Wetting;
- b) Nonwetting; and
- c) Dewetting.

These three conditions are illustrated in Fig. 3. The schematic diagrams reflect the respective photographs below them, which were obtained from a study that examined the solderability of 60Sn-40Pb alloy on bare Kovar™ base material (Refs. 3, 4). *Wetting* refers to the achievement of a uniform solder layer over the base material — Fig. 3A. The edge of the solder film is characterized as having a contact angle, θ_c , that is less than 90 deg, preferably in the range of 0–30 deg.

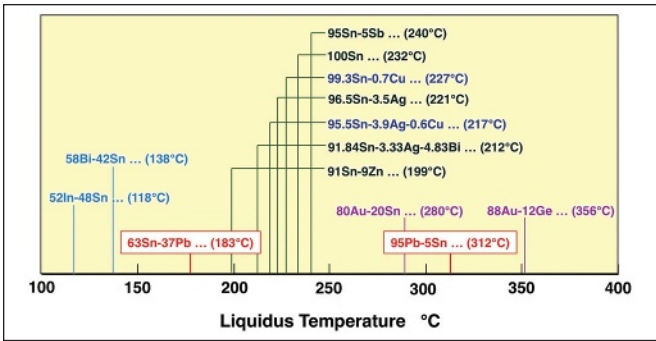


Fig. 2 — The graph shows the common solder alloys as a function of liquidus temperature (T).

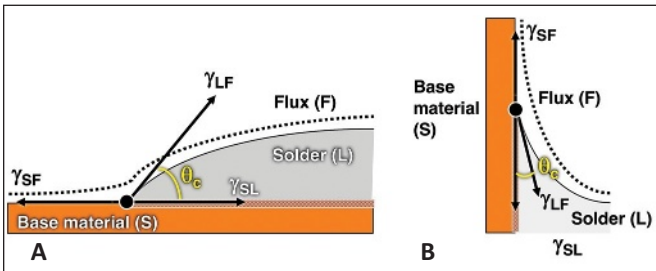


Fig. 4 — Schematic diagrams show the two horizontal and vertical configurations for solder wetting and spreading activity: A — Sessile drop; B — fillet rise, respectively. The interfacial tensions, γ_{ij} ($i,j = SF, SL, \text{ and } LF$) and contact angle, θ_c , are indicated in the diagrams.

The nonwetting condition is illustrated in Fig. 3B. The solder alloy has “balled up,” leaving large areas of exposed base material. The contact angle is greater than 90 deg. Theoretically, the solidified solder will fall off the base material surface. However, on some occasions, the solder is frozen onto the base material surface and appears to have formed a joint. However, adhesion strength is very low and the joint will come apart under minimal test or service loads.

The third solderability condition, which is observed primarily in soldering and not so much in brazing, is *dewetting*. This behavior is illustrated in Fig. 3C; the schematic diagram is particularly important to illustrate this phenomenon. Dewetting occurs when the molten solder initially wets and spreads over the base material. Then, during the soldering process, the molten film retracts into isolated mounds surrounded by a thin solder coating or exposed base material.

The dewetting behavior takes place when there is a dynamic change to the solderability of the overall base material/flux/(molten) solder system. Most often, the change occurs to the base

material. If there are small areas that are nonwetable by the filler metal, then as the molten film thins out near the completion of a soldering process, it can no longer cover those nonwetable areas and retracts away from them,

leaving either a very thin coating or none at all across them. Solderability is measured by the contact angle, θ_c , at the edge of the molten solder as shown by the schematic diagrams in Fig. 4. The horizontal and vertical base material orientations, which form the sessile drop and fillet configurations, respectively, are shown as gravity has a role in the molten solder profile. Contact angle is determined by the equilibrium balance of the interfacial tensions, γ_{SF} , γ_{SL} , and γ_{LF} , which are defined as follows:

- γ_{SF} , base material (S)/flux (F) interface
- γ_{SL} , base material (S)/liquid solder (L) interface, which actually has the base material replaced with the reaction layer, and
- γ_{LF} , liquid solder (L)/flux (F) interface.

That balance of interfacial tensions at equilibrium is expressed through Young’s equation:

$$\gamma_{SF} - \gamma_{SL} = \gamma_{LF} \cos\theta_c \quad (1)$$

Solderability is optimized by minimizing the value of θ_c . The value of θ_c is reduced by maximizing the difference,

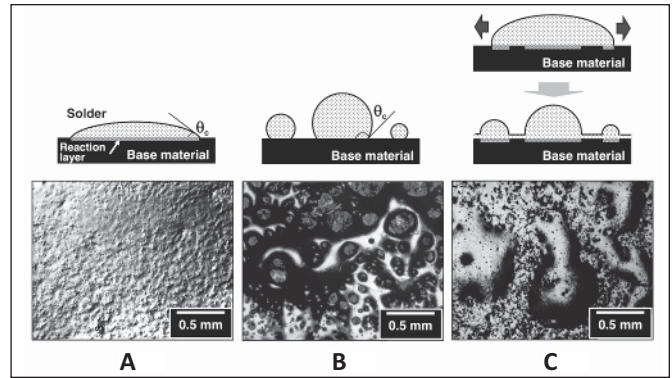


Fig. 3 — Optical photographs and schematic diagrams illustrate the three functional conditions of solderability: A — Wetting; B — nonwetting; C — dewetting. The contact angle is θ_c .

material. If there are small areas that are nonwetable by the filler metal, then as the molten film thins out near the completion of a soldering process, it can no longer cover those nonwetable areas and retracts away from them,

$\gamma_{SF} - \gamma_{SL}$. That difference is increased by increasing γ_{SF} , which is precisely the result of eliminating the oxide surface from base material surfaces by using a flux. The value of γ_{SL} is controlled by the details of the reaction layer at the solder/base material interface. The reaction layer chemistry is primarily a function of the solder and base material compositions and, secondarily, determined by the soldering time and temperature. Lastly, the value of θ_c can also be reduced by minimizing γ_{LF} . Reducing the surface tension of the liquid solder is a critical, if often unrecognized, role of the flux.

The value of θ_c is measured by the meniscometer/wetting balance technique (Ref. 5). This method is illustrated in Fig. 5A. The meniscometer measures the meniscus rise, H , and the wetting balance determines the meniscus weight, W . The wetting balance produces the wetting curve shown in Fig. 5B. The meniscus weight is output as a function of time, which allows for determining the wetting time and wetting rate metrics shown in the plot. The values of θ_c and γ_{LF} are calculated from W and H , by means of Equations 2 and 3, respectively:

$$\theta_c = \arcsin\{[4W^2 - (\rho gPH^2)^2] / [4W^2 + (\rho gPH^2)^2]\} \quad (2)$$

$$\gamma_{LF} = (\rho g/2)\{[4W^2/(\rho gPH^2)^2] + H^2\} \quad (3)$$

The additional parameters in Equations 2 and 3 are ρ , the solder density; g , the acceleration due to gravity; and P , the sample perimeter. The values of θ_c and γ_{LF} are shown in Table 1 for commonly used solder alloys (Refs. 5, 6). The contact angle and solder/flux

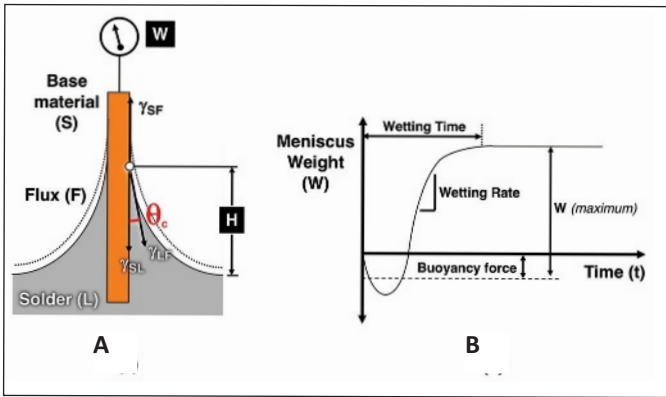


Fig. 5 — A — The schematic illustrates the meniscometer/wetting balance technique for determining the contact angle, θ_c , of the molten solder/flux/base material system. The measured parameters are the meniscus weight, W , and the meniscus height, H . B — The output of the wetting balance is the wetting force as a function of time. The wetting time and wetting rate provided comparative metrics of the wetting “kinetics.”

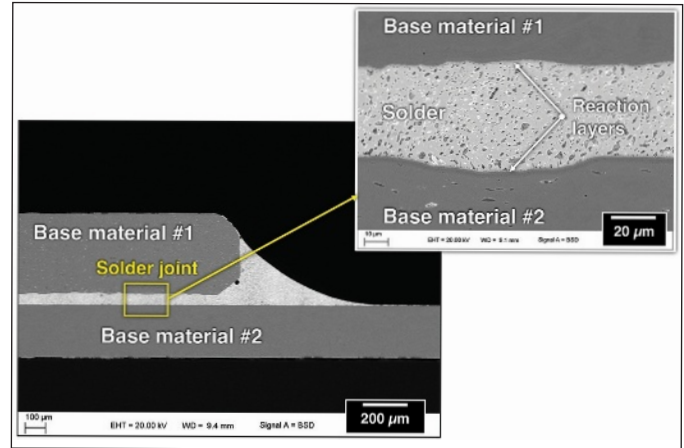


Fig. 6 — SEM images show the base materials, filler metal (solder), and reaction layers that comprise the “solder joint system.”

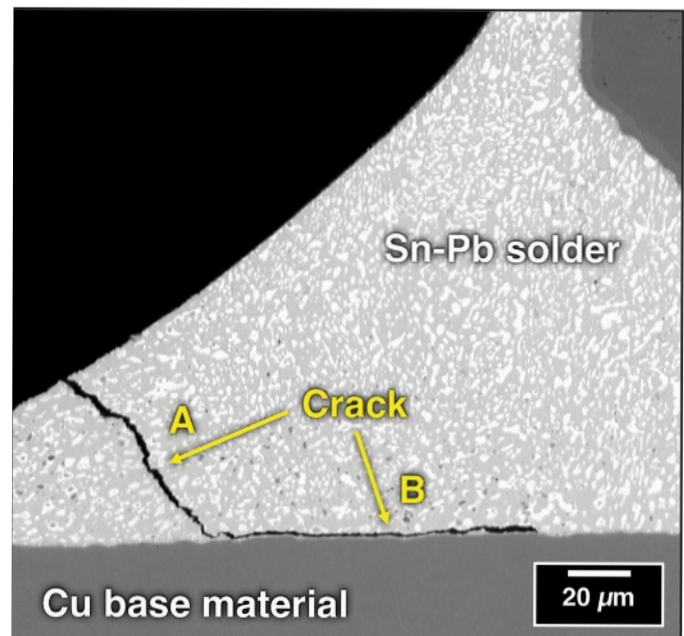


Fig. 7 — Crack propagation in a solder joint typically follows a path in the solder (A) or along the solder/base material interface (B). Both pathways are illustrated in this single SEM image.

interfacial tension are sensitive to temperature only for those off-eutectic solders having a large pasty range, or when the soldering temperature is outside the operating range of the flux, either below its activation temperature, or so high as to exceed its decomposition temperature. Lead (Pb) and bismuth (Bi) additions tend to reduce the surface tension of the molten solder. However, this trend does not necessarily prevail for the higher order solder compositions.

Mechanical Performance

The mechanical properties of the solder filler metal are critical factors in the overall performance and reliability of the joint. However, it is important to appreciate the fact that, at room temperature, solder alloys are performing under temperature conditions that are equivalent to those experienced by Ni-based superalloys inside of the combustion chamber of an operating jet engine. This scenario is owed to the relatively low solidus temperature of these filler metals (Ref. 7). Therefore, processes such as creep and dynamic recrystallization readily take place even at room temperature.

Although the (bulk) mechanical properties of the filler metal have a significant role in the strength of the solder joint, they are not always the only controlling factor. An understanding of the mechanical performance of the solder joint begins by con-

sidering it to be a system comprised of the base material(s), the filler metal, and the reaction layers — Fig. 6. By and large, the base materials are stronger than the filler metals, so solder joints typically fail in the filler metal or along one of the interfaces. The combination of both paths is illustrated by the SEM photograph in Fig. 7: “A,” the bulk solder and “B,” the solder/base material interface. When the solder alloy is very strong, e.g., the high-Au alloys shown in Fig. 2, and combined with a ceramic base material, it is possible to drive a crack in the latter rather than through the solder or associated interface reaction layers, particularly under very high loads (e.g., mechanical shock).

Because solder alloys are performing at high temperatures, corresponding physical metallurgy principles can be used to optimize mechanical performance. The development of the 91.84Sn-3.33Ag-4.83Bi (Sn-Ag-Bi) alloy illustrates the use of precipitation

hardening and solid-solution strengthening methodologies (Refs. 8, 9). The microstructure of the solder is shown in Fig. 8A. Precipitation hardening was obtained by the Ag_3Sn particles, which originated from the solidification event, and a lesser contribution by the 100Bi particles that precipitated in the Sn-rich matrix. The matrix phase was a solid solution of 96Sn-4.0Bi.

The relative contributions of these two strengthening mechanisms could be discerned by comparing the shear strengths between the Sn-Ag-Bi solder joints and two other alloys using the ring-and-plug test method depicted at

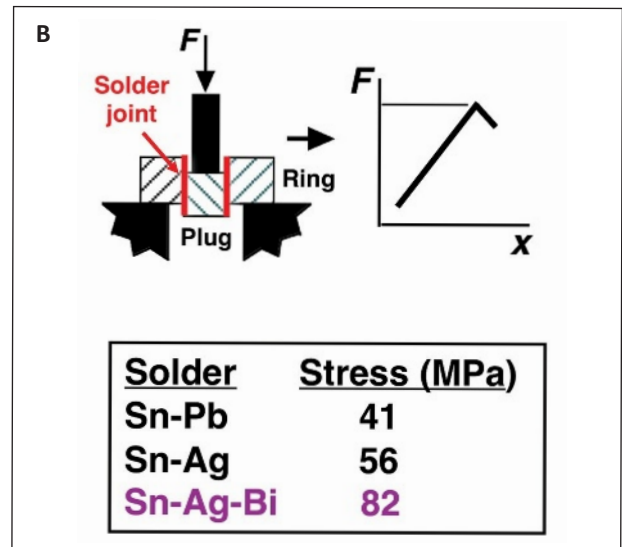
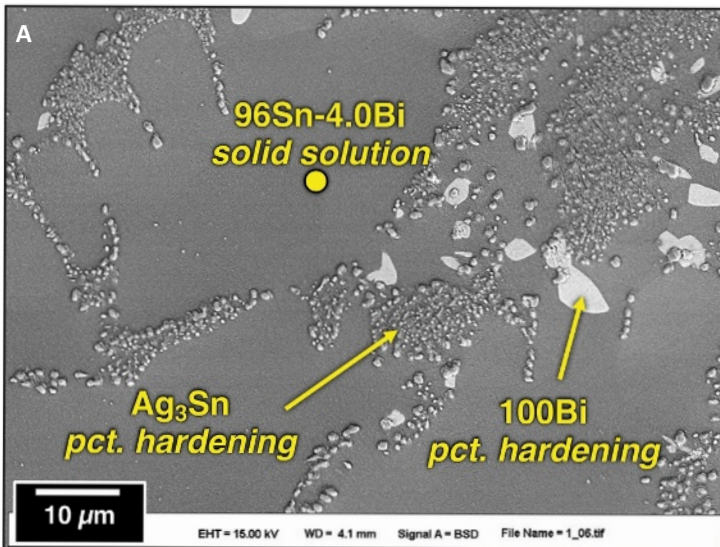


Fig. 8 — A — SEM image shows the microstructure of the 91.84Sn-3.33Ag-4.83Bi. There are two particle phases: Ag_3Sn intermetallic compound and 100Bi. The matrix is solid solution of phase 96Sn-4.0Bi. B — Schematic diagram shows the ring-and-plug shear test and corresponding force (F) – displacement (x) curve. The maximum load, together with the joint geometry, are used to calculate the failure stress. Failure stresses are shown for the Sn-Pb, Sn-Ag, and Sn-Ag-Bi solders in the table.

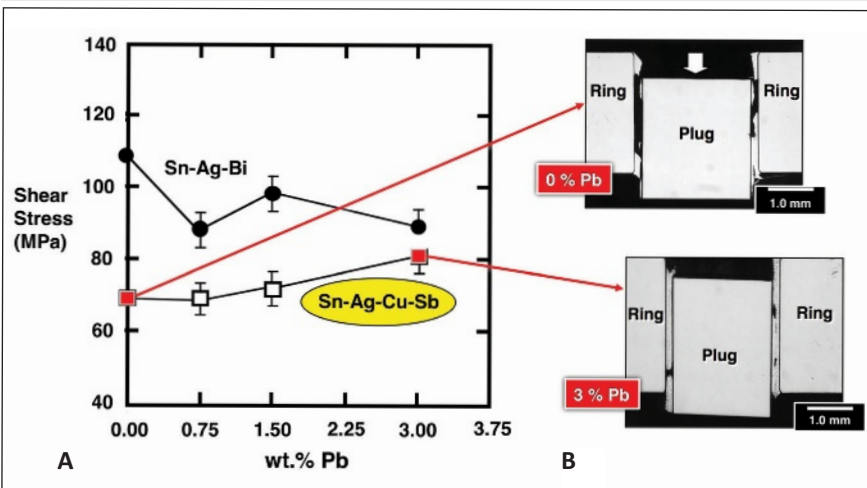


Fig. 9 — A — Ring-and-plug shear stress is plotted as a function of Pb additions for the two solders, Sn-Ag-Cu-Sb and Sn-Ag-Bi. The tests were performed at room temperature (10 mm/min displacement rate). B — The optical micrographs illustrate the failure modes for the Sn-Ag-Cu-Sb filler metal at zero and 3 wt-% Pb additions.

Table 1 — Solderability Parameters γ_{LF} and θ_c as a function of Solder Temperature and Composition as Determined on Copper Sheet Samples

Solder (wt-%)	Temp. (°C)	γ_{LF} (dyne/cm)	θ_c (deg)
95.5Sn-3.9Ag-0.6Cu	260	497 ± 16	40 ± 1.0
	245	444 ± 17	39 ± 1.0
	230	485 ± 27	42 ± 1.4
96.5Sn-3.5Ag	260	460 ± 30	36 ± 3
60Sn-40Pb	260	380 ± 10	17 ± 4
58Bi-42Sn	215	310 ± 50	37 ± 7

Substrate: OFHC Cu; Flux: RMA, 1:1 IPOH.

the top of Fig. 8B. The solder joint, which was made between the plug and the ring with a joint clearance thickness of 19 μm , was tested in shear by applying a load (F) to the plug. The displacement rate was 10 mm/min and the tests were performed at room temperature. The shear stress was calculated at the maximum value of F. The table is located at the bottom of Fig. 8B, which shows the maximum stresses for the three Sn-based solders: 63Sn-37Pb (Sn-Pb), 96.5Sn-3.5Ag (Sn-Ag), and the Sn-Ag-Bi alloy. The Sn-Pb solder joints had a mean strength of 41 MPa. Its microstructure has comparable volume percentages of Sn- and Pb-rich phase, both of which readily support deformation, so that neither strengthening mechanism is relatively strong during the deformation. By comparison, the Sn-Ag alloy has the Ag_3Sn particles that provide a precipitation-hardening effect, which results in a higher strength of 56 MPa. The Sn-Ag-Bi solder exhibited the highest shear stress of 82 MPa. Although the Sn-Ag-Bi alloys also benefited from Ag_3Sn precipitation hardening, its performance was further enhanced by the solution-strengthening mechanism.

Elemental additions can alter the mechanical properties of the solder filler metal, but in entirely different manners for different, higher-order alloy compositions. This point is illustrated by considering the effects of Pb

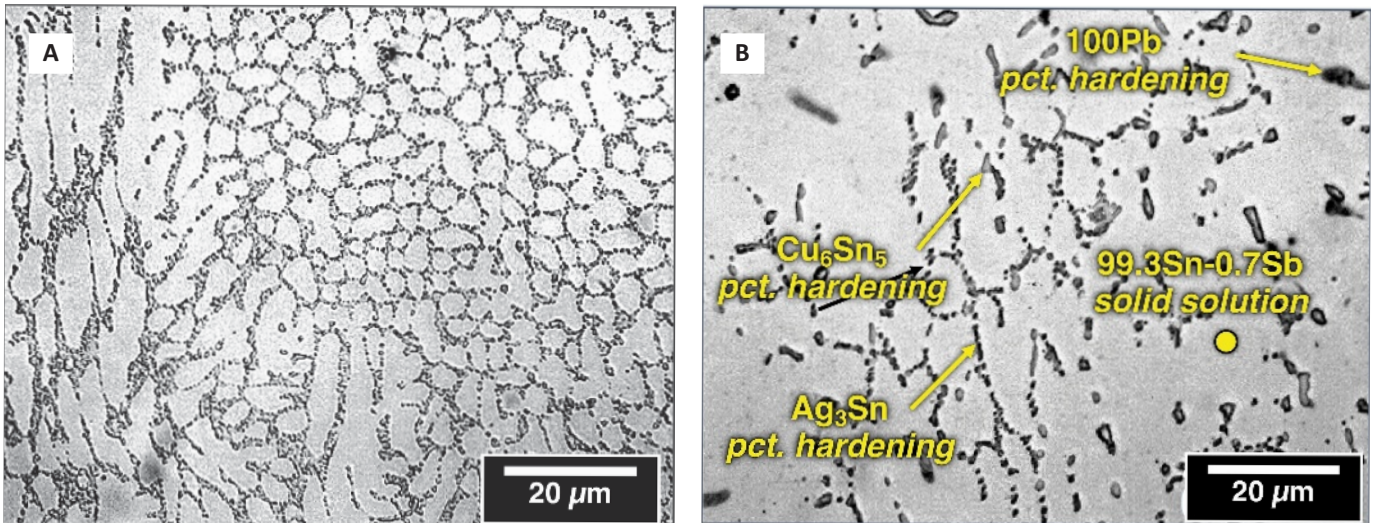


Fig. 10 — Optical photographs represent the microstructure of the Sn-Ag-Cu-Sb alloy as a function of Pb additions: A — 0 wt-%; B — 3 wt-%. The various phases have been identified along with their strengthening mode.

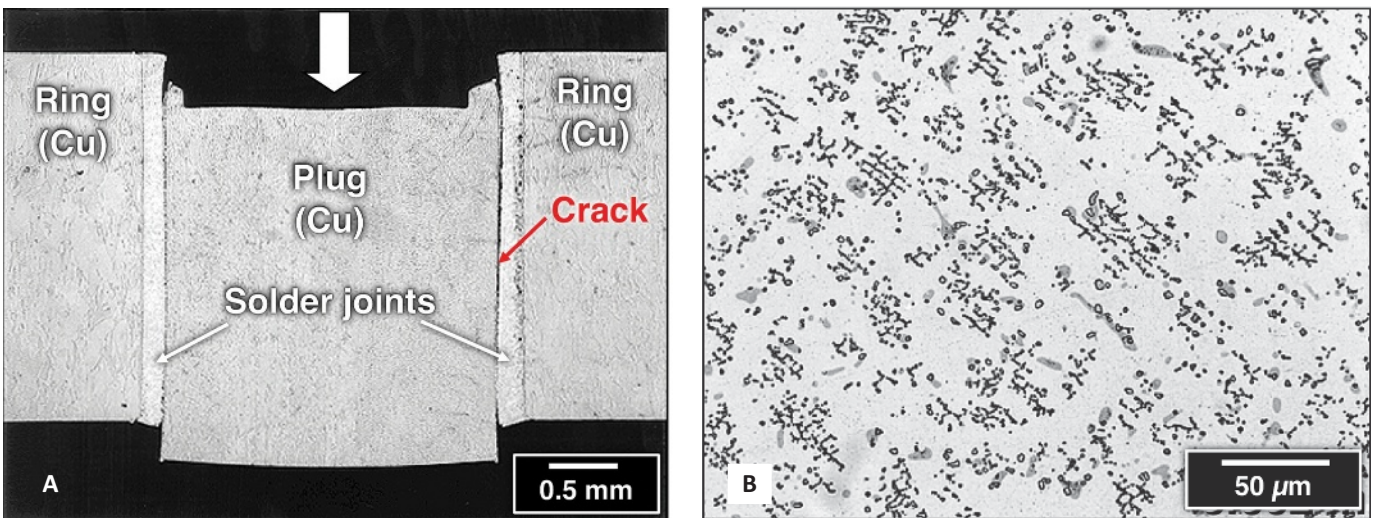


Fig. 11 — Optical micrographs showing the following: A — A post-test, Sn-Ag-Bi ring-and-plug specimen having a 3 wt-% Pb addition; B — the large-scale microstructure of the same alloy.

additions (0–3.75 wt-%) made to two alloys: 96.2Sn-2.5Ag-0.8Cu-0.5Sb (wt-%, Sn-Ag-Cu-Sb) and 91.84Sn-3.33Ag-4.83Bi (Sn-Ag-Bi). Shown in Fig. 9A is a plot of ring-and-plug shear stress as a function of Pb addition. The tests were performed at room temperature². A greater solution-strengthening effect of 4.0Bi in the Sn-Ag-Bi alloy is reflected by its generally higher failure stress than is obtained by the Sn-Ag-Cu-Sb alloy with its 0.7Sb content. The Sn-Ag-Cu-Sb filler metal experienced a

small, but significant, increase of shear stress with Pb additions. The optical micrographs in Fig. 9B represent the failure modes of the Sn-Ag-Cu-Sb solder joints at the two extremes of Pb content. In the absence of a Pb addition, the crack path is a mixture of bulk solder and interface failure. However, when 3 wt-% Pb was added to the alloy, the strength increase was accompanied by a transition to entirely an interface failure mode.

A microstructure/mechanical properties correlation was sought to explain the trends observed in Fig. 9. The SEM images are shown in Fig. 10A, B, and correspond to the 0 and 3 wt-% Pb additions, respectively, made to the Sn-Ag-Cu-Sb alloy. A “lacey”

network of Ag₃Sn particles formed in the absence of the Pb as shown in Fig. 10A. The addition of 3 wt-% Pb broke up that lacy network as shown in Fig. 10B. The greater dispersion of Ag₃Sn particles allows them to more efficiently interfere with dislocation movement in the material, hence the increase in joint strength. The phases and strengthening roles are identified in Fig. 10B. The precipitation hardening came about primarily from the Ag₃Sn particles. Lesser contributions came from Cu₆Sn₅ particles (that are too few in number) and 100-Pb particles (which deform under an applied stress). A nominal solid-solution strengthening was provided by the 0.7 wt-% Sb in the Sn-rich matrix.

2. Note that the 0-Pb content values are higher than those in Fig. 8B. This difference was due to the reduced solder joint gap of 12 vs. 19 microns in the case of Fig. 8B.

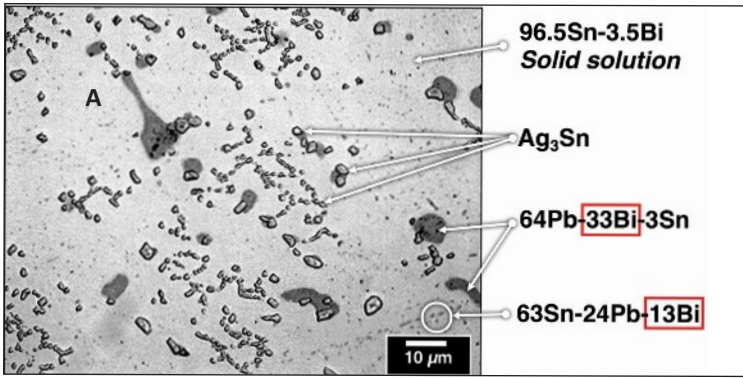


Fig. 12 — Optical micrograph shows the microstructure of the Sn-Ag-Bi solder that contained 3 wt-% Pb addition. The respective phase compositions are also shown in the image, which were determined by electron probe microanalysis (EPMA).

Referring back to Fig. 9A, Pb additions caused a small strength loss for the Sn-Ag-Bi alloy. The same failure mode, which is crack propagation along the solder/base material (plug) interface (Fig. 11A), was observed at all Pb contents because the joint strengths were consistently greater than approximately 80 MPa. The microstructure of the Sn-Ag-Bi plus 3 wt-% Pb alloy (Fig. 11B) appears nearly identical at this magnification to those observed with lesser Pb additions.

However, at a much smaller size scale, there were significant changes to the elemental distributions in the Sn-Ag-Bi microstructure. An optical micrograph is provided in Fig. 12 that illustrates the effects of 3 wt-% Pb addition. Most notably, the Pb has drawn Bi from the solid-solution, Sn-rich matrix and created Pb-Bi-Sn particles. The electron probe microanalysis (EPMA) detected a drop from 4.0 to 3.5 wt-% Bi in the Sn-rich matrix. The EPMA technique identified the two Pb-Bi-Sn compositions as 64Pb-33Bi-3Sn and 63Sn-24Pb-13Bi. The formation of these two particle types and any associated precipitation hardening did not compensate for the loss of solution strengthening caused by the removal of Bi from the Sn-rich matrix. The net consequence was the decrease of solder joint strength observed in Fig. 9A.

The mechanical and physical metallurgy data indicated the loss of strength experienced by the Sn-Ag-Bi solder joint with increasing Pb content was caused primarily by a loss of the solid-solution mechanism. This conclusion was validated by testing ring-

and-plug solder joints made from these two alloys: Sn-Ag-3Bi and Sn-Ag-2Bi. These alloys recreated the reduced Bi, solid-solution phases, but without the 64Pb-33Bi-3Sn and 63Sn-24Pb-13Bi precipitates. The resulting shear strengths of the ring-and-plug tests were 102 and 94 MPa for the Sn-Ag-3Bi and Sn-Ag-2Bi filler metals, respectively. These results validated the magnitude and trend of the proposed decrease in shear strength being attributed to a loss of the solid-solution strengthening mechanism and confirmed the limited role the two Pb-Sn-Bi particle phases had on strengthening the alloy strength.

The strength of a solder joint, whether in shear, tension, compression, or a combination of these deformation modes (multi-axial case) does not always correlate directly with the bulk strength of the solder. This discrepancy stems from the additional role of the joint clearance on deformation. As the joint clearance becomes thinner for a given faying surface area, the plastic deformation in the solder becomes increasingly more constrained — in effect, the solder appears to be stronger than would be predicted from its (unconstrained) bulk properties. This trend is referred to as the *plain strain effect*. As the solder joint clearance becomes thicker, the deformation transitions from plain strain back to

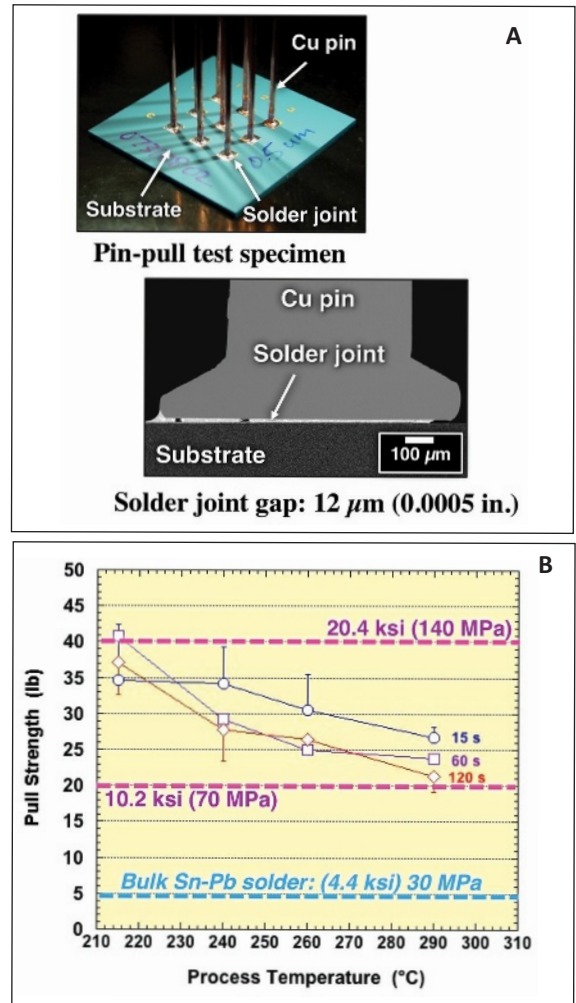


Fig. 13 — A — Photograph shows the pin pull test specimen (nine solder joints). The SEM image was taken of the cross sections of a pin's Sn-Pb solder joint; the joint clearance was 12 μm (0.0005 in.). B — Plot of pin pull strength as a function of soldering process temperature (abscissa) and soldering time (different symbols). The latter data were in a band of 70–140 MPa (10.2–20.4 ksi). The bulk tensile strength of Sn-Pb solder is 30 MPa (4.4 ksi).

plane stress and the joint strength approaches that calculated, based on the bulk solder properties.

The magnitude of the plain strain effect is illustrated with the pin pull (tensile) test. The test specimen is shown at the top of Fig. 13A. Nine pins are soldered to thin film pads that were deposited on a low-temperature, co-fired ceramic (LTCC) base material. The joints were made using the 63Sn-37Pb solder (Ref. 10). An SEM image is provided at the bottom of Fig. 13A that shows the solder joint. The joint clearance is 0.012 mm (0.0005 in.) thick over an area of 1.3 mm² (0.002 in.²), clearly a plain strain condition. The pins

were pull tested at 10 mm/min (0.4 in./min). The graph in Fig. 13B shows the pull strength (lb) as a function of processing temperature and time. The pull strengths are in the range of 70 to 140 MPa (10.2–20.4 ksi), which are considerably higher than the bulk tensile strength of Sn-Pb solder, which is 30 MPa (4.4 ksi) (Ref. 11).

Processing

The SEM images in Fig. 3 exemplified the three functional categories of solderability behavior. The discussion now considers in greater detail the fundamental aspects of wetting-and-spreading behavior that define a filler metal's solderability performance and the scenarios whereby the latter affects solder joint reliability.

Solderability refers to the capacity for the molten filler metal to wet and spread on the faying surface(s). The wetting process is the formation of a metallurgical bond between the solder and base material that joins the two together after solidification. Spreading describes the spontaneous flow of molten solder that is required to fill the joint clearance as well as form a fillet on the exterior surfaces.

Beside the effect of solder joint geometry, three phenomena take place during wetting-and-spreading activity that impact solder joint reliability:

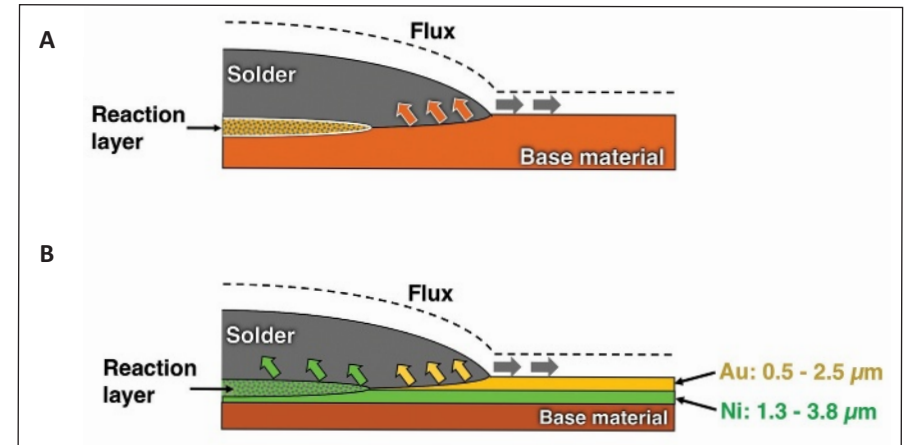


Fig. 14 — Schematics show the effects of the wetting-and-spreading activity by a molten solder within the course of a soldering process: A — Molten filler metal wetting directly to the base material; B — the sequence of steps when the molten solder wets and spreads over a surface finish — in this case, Au protective layer and Ni solderable layer. Typical layer thicknesses are shown here.

- Base material dissolution,
- Changing the solder alloy composition, and
- Formation of the interface reaction layer.

The schematic in Fig. 14A illustrates these three phenomena. Base material dissolution reduces the thickness of the base material. The magnitude of dissolution determines the second phenomenon, which is a change to the solder alloy composition caused by the incorporation of base material into the molten filler metal. Altering the

molten solder composition can lead to processing-related defects. In addition, base material dissolution and associated chemistry changes can degrade the mechanical properties of the solidified solder and, thus, those of the joint. Lastly, the soldering process affects the reaction layer that forms at the solder/base material interface. Although each of these three factors is discussed separately, the solder joint is a system (Fig. 6), and synergistic effects between the three factors will further affect the long-term reliability

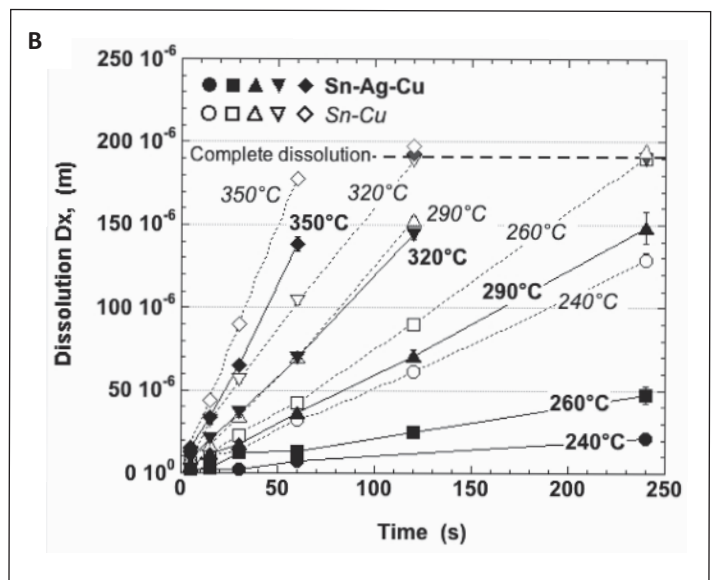
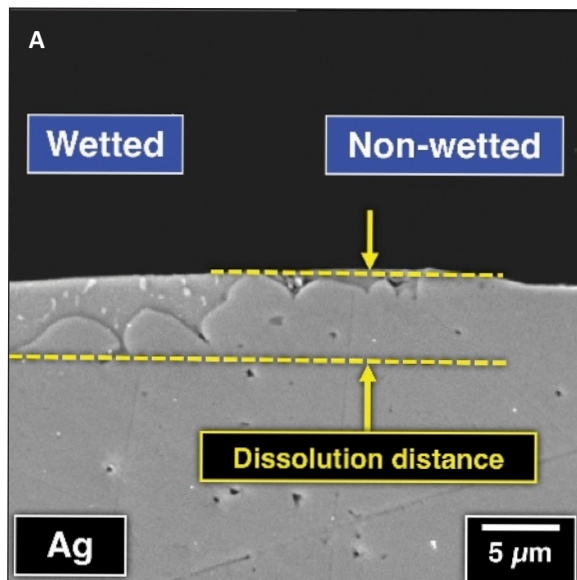


Fig. 15 — A — SEM image shows the extent of dissolution of Ag base material caused by exposure to molten 95.5Sn-3.9Ag-0.6Cu (Sn-Ag-Cu) solder at a temperature of 290°C. The exposure time was 60 s. B — Plot shows dissolution (D_x) of Ag as a function of exposure time for the two solder alloys: Sn-Ag-Cu (closed symbols) and 99.7Sn-0.3Cu (Sn-Cu, open symbols). The molten filler metal temperatures were 240°, 260°, 290°, 320°, and 350°C.

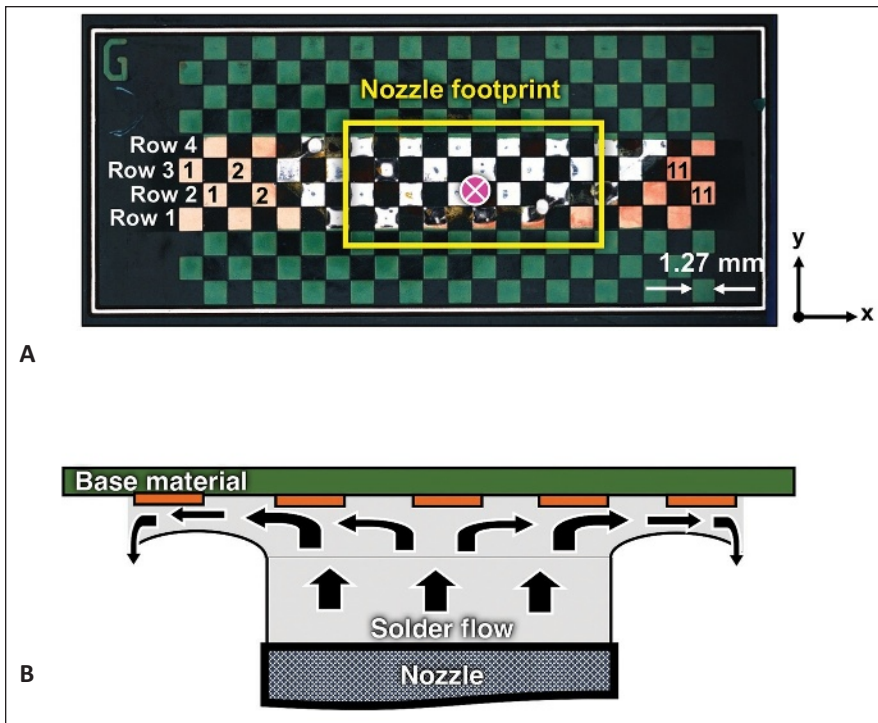


Fig. 16 — A — Printed circuit board test vehicle used to examine the fluid flow effects of an impinging solder fountain on molten solder contact with the Cu pads. The solder fountain nozzle footprint is outlined in yellow. The center point of impingement is indicated by the white outlined, magenta circle/cross. B — Schematic shows the flow pattern of the molten solder as it impinges on the test vehicle.

of the solder joint.

Surface finishes are frequently used to enhance the soldering process, particularly when the joint includes difficult-to-solder base materials such as aluminum, refractory metals, glasses, and ceramics (Ref. 12). Referring to Fig. 14B, the most common surface finish methodology begins with the Ni solderable layer, which is deposited directly on the base material. The metallurgical bond (wetting) of the solder is made to the solderable layer. Clearly, the solderable layer must also have good adhesion to the base material. On top of the solderable layer is the protective layer, which as the term implies, protects the solderability of the solderable layer's surface. Gold is the typical protective layer because it lacks significant oxidation activity. Customary Ni and Au thicknesses are shown in Fig. 14B for electroplated and electroless (conversion) finishes.

The schematic diagram in Fig. 14B also depicts the aftermath of the solderable and protective layers during the soldering process. The molten solder initially wets the protective layer

— so it cannot be heavily contaminated or oxidized — which is then completely dissolved into the molten filler metal. The solder wets to the exposed solderable layer, creating the important metallurgical bond. The consequence of this sequence is that the molten solder has the protective layer dissolved into it and, to a lesser degree, a portion of the solderable layer. The effects of these steps are correlated to the second bullet. Dissolution of the protective layer changes the molten solder composition, which potentially affects solder joint reliability.

Base Material Dissolution

The development of a soldering process must address the dissolution of base material by the molten solder. The dissolution of pure Ag base material by 95.5Sn-3.9Ag-0.6Cu solder is shown through the SEM image in Fig. 15A (Ref. 13). The solder temperature was 290°C and the time duration was 60 s. Approximately 5–6 μm of Ag was lost to the molten solder. Base material dissolution is an explicit function of

the molten solder composition and temperature as well as the base material composition and exposure time between them. Quantitative dissolution data are shown in Fig. 15B. The extent of Ag dissolution, D_x , is plotted as a function of solder temperature and exposure time for two filler metal compositions: 95.5Sn-3.9Ag-0.6Cu (Sn-Ag-Cu) and 99.3Sn-0.7Cu (Sn-Cu). The respective liquidus temperatures were 217° and 227°C. The presence of Ag in the Sn-Ag-Cu solder caused a reduction of Ag base material dissolution. The effect was strongest at the lower soldering temperatures, e.g., 240° and 260°C; it became less significant at the higher temperatures. The Ag component of the ternary alloy reduced the driving force for Ag base material to be dissolved into the molten filler metal, despite a greater temperature difference between the solder temperature and liquidus point that would be expected to enhance the dissolution process.

Numerous innovations have been made in electronics manufacturing that have significantly increased both production rates and product quality. As is often the case, new techniques bring about unexpected challenges. The application of wave soldering highlighted the need to recognize the role of *fluid flow mechanics* in the process (Ref. 14). Solder skips — areas where the solder did not wet the base material — were observed on the Cu pads of a printed circuit board product that had undergone a wave soldering process. Experiments confirmed the fault did not rest with the solderability of the pad surfaces. Therefore, a study was initiated to examine the contact between a molten 63Sn-37Pb (271°C) solder wave and a grid of Cu pads on a printed circuit board test sample — Fig. 16A. The metric of such contact was the extent of Cu pad dissolution. The impingement point (cross circle) and fountain footprint are superimposed on the photograph. The schematic in Fig. 16B illustrates the general, molten solder flow profile.

The profiles of the Cu pads are shown in Fig. 17 following 20-, 60-, and 90-s exposures to the molten solder. The spaces between the pads were eliminated for clarity. The dashed lines and accompanying numbers are the starting thickness of the Cu pads in

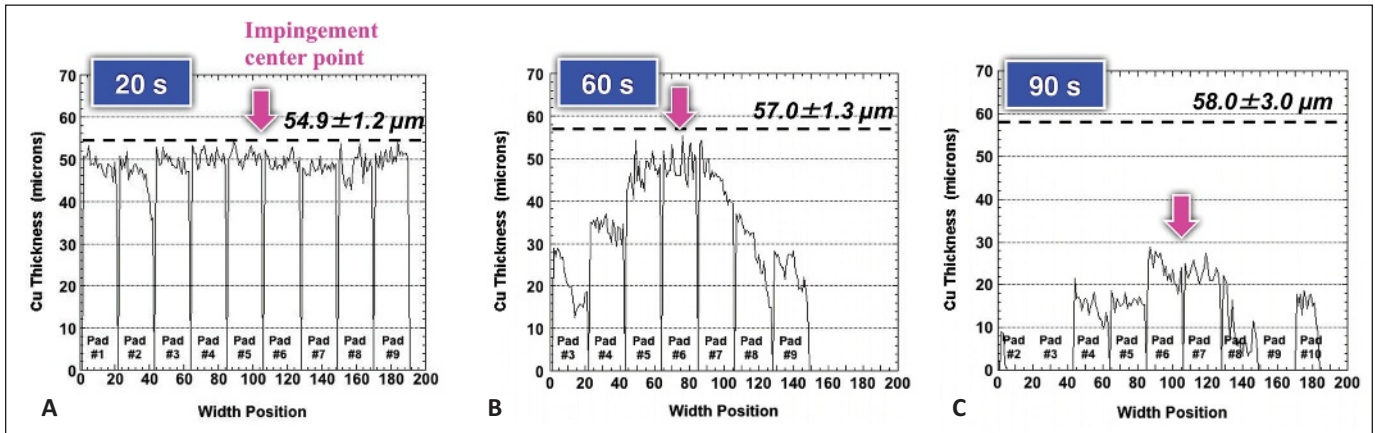


Fig. 17 — Graphs show Cu (pad) dissolution as a function of width position over the solder fountain. The filler metal was the 63Sn-37Pb alloy (271°C). The exposure times were as follows: A — 20 s; B — 60 s; C — 90 s. The magenta arrows indicate the center point of the impingement footprint. The dashed lines and accompanying numbers are the starting thickness of the Cu pads in that row.

that row. The absolute error was ± 1 micron. The increased extent of erosion to either side of the impingement point (magenta arrows) was due to the accelerated flow of molten solder in the lateral (x) direction — Fig. 16B.

The dissolution behavior showed two size scales. The larger size scale of ≈ 10 mm reflects dissolution behavior between pads within the solder fountain footprint. The dissolution data were separated into that belonging to the outer pads, which experienced a greater dissolution due to increased lateral flow, and the inner pads near to the impingement point where the vertical (y) flow was at the greatest velocity. The corresponding plots are shown in Fig. 18A. The impinging solder

caused less dissolution, which implies a greater likelihood that solder skips within this region of predominantly vertical flow vs. the outer pads that experienced a greater component of lateral flow.

Variations of Cu thickness were observed across the surface of each pad that were greater than the absolute error. Their smaller-size scale (≈ 0.5 mm) is illustrated by the optical micrograph in Fig. 18B. The image shows pad #8 of row 2 on the test vehicle exposed for 60 s. A comparison between the three colored arrow sets demonstrates the small-scale variations of Cu thickness caused by the dissolution process. Moreover, the image illustrates the capacity for the solder flow to create a “skip” defect on

the pad, even in the presence of a significant lateral flow component.

Changes to the Solder Alloy Composition

The second phenomenon associated with soldering processes that affects reliability are changes to the solder composition during wetting-and-spread activity. The solder composition is modified by the dissolution of base material or by dissolution of a protective finish. The immediate consequence, which occurs during the soldering process, is *constitutional solidification*. This term refers to the premature solidification of the filler metal due to the incorporation of elemental

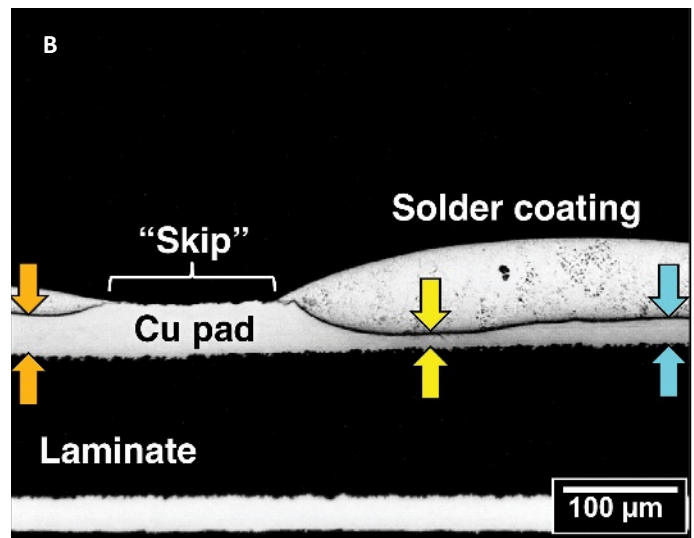
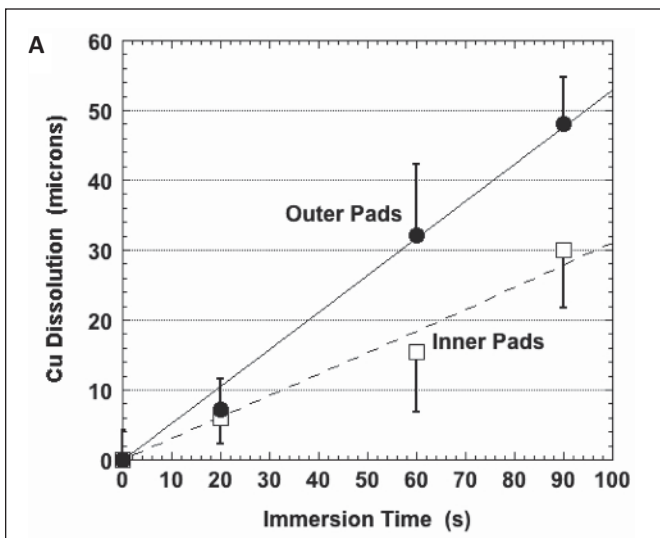


Fig. 18 — A — Plot shows the extent of Cu dissolution as a function of exposure time that represents the large-scale effect (≈ 10 mm). Data were separated into “outer pads” and “inner pads.” B — Optical micrograph illustrates the extent of small-scale variations (≈ 0.5 mm): yellow vs. cyan arrows as well as the nonwetted pad surface.

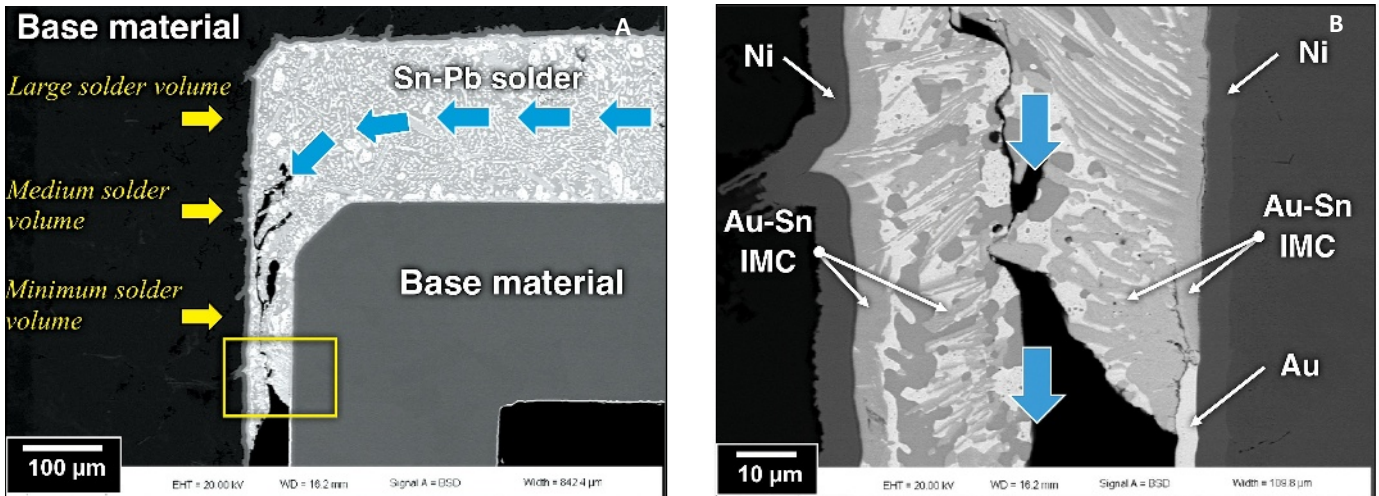


Fig. 19 — A — SEM image shows a solder joint that experienced constitutional solidification due to the dissolution of the Au protective finish present on both faying surfaces. The blue arrows indicate the flow of the solder through the gap. The local volume of molten solder decreased in the order: large, medium, and small. B — High magnification photograph shows the solder front that “froze” prior to completely filling the joint clearance.

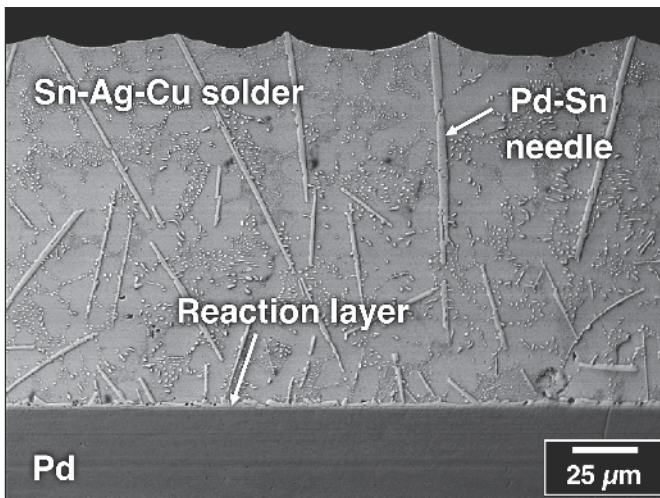


Fig. 20 — SEM image shows the microstructure of the 95.5Sn-3.9Ag-0.6Cu (Sn-Ag-Cu) solder on a pure Pd base material. The soldering conditions were 350°C and 5 s.

species that raise its liquidus temperature (T_l) to a value that is *greater than* the process temperature. Complete solidification occurs if the solidus temperature (T_s) is also made to exceed the process temperature.

The SEM photographs in Fig. 19 illustrate this phenomenon. Figure 19A shows the flow of the 63Sn-37Pb solder in the direction of the blue arrows. As the molten solder moves through the gap, it dissolves the Au protective finish that was present on both faying surfaces. As the volume of molten solder decreased, its local Au concentration increased until the solder solidified, prematurely. The resulting solder

Additional phases can form in the solder. This effect is illustrated in Fig. 20 (Ref. 15). The molten 95.5Sn-3.9Ag-0.6Cu (Sn-Ag-Cu) solder (350°C) was in contact with the pure Pd base material for 5 s. The Pd, which dissolved into the solder, then formed Pd-Sn needles upon solidification. These needles support a precipitation hardening mechanism that can potentially increase the yield and tensile strengths of a joint. Depending upon the loading conditions of the application, such large particles can also serve as crack initiation sites that reduce solder joint reliability.

joint microstructure, which is shown in Fig. 19B, was comprised of largely Au-Sn intermetallic compound (IMC) as the interface reaction layer and as particles within the remaining Sn- and Pb-rich phases.

Even when solderability goes unaffected by base material dissolution, the latter can also impact the mechanical properties of the solidified solder joint.

Formation of the Interface Reaction Layer

The third processing phenomenon that affects solder joint reliability is the reaction layer that forms at the solder/base material interface. These layers are generally intermetallic compounds (IMCs) having covalently bonded structures, causing them to be relatively brittle when compared to the solder and most metallic base materials. Interfaces are considered nonequilibrium structures so that the reaction layer is sensitive to solder composition as well as the solder temperature and time exposure, but not always in a predictable manner. These points are illustrated in Fig. 21. Figure 21A shows the reaction layer that developed between molten 95.5Sn-3.9Ag-0.6Cu (Sn-Ag-Cu) solder and pure Pd base material (Ref. 15). The Sn-Ag-Cu temperature was 350°C ($T_l = 217^\circ\text{C}$) and the Pd base material was exposed to the solder for 5 s. The reaction layer remained less than 5 μm , which poses a relatively low risk of degrading the solder joint's mechanical performance, even under shock loads. On the other hand, a considerably thicker Pd-Sn reaction layer developed between the 63Sn-37Pb solder and the same Pd base material as shown in Fig. 21B despite a reduced solder temperature of 290°C for the same duration of 5 s (Ref. 16). By exceeding the 5 μm thickness, this interface microstructure can potentially degrade solder joint reliability, again depending upon the loading

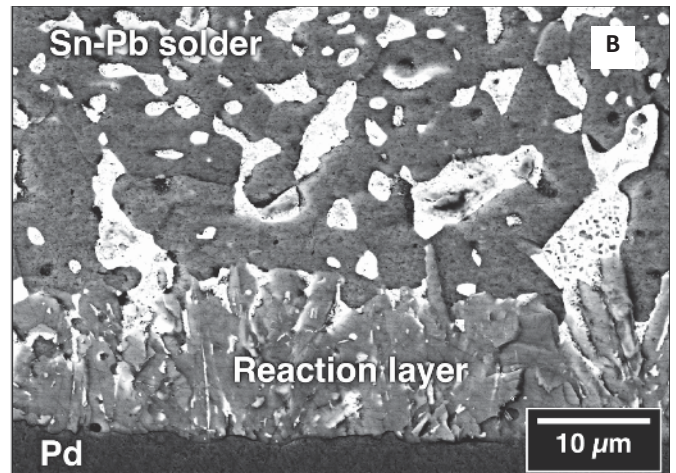
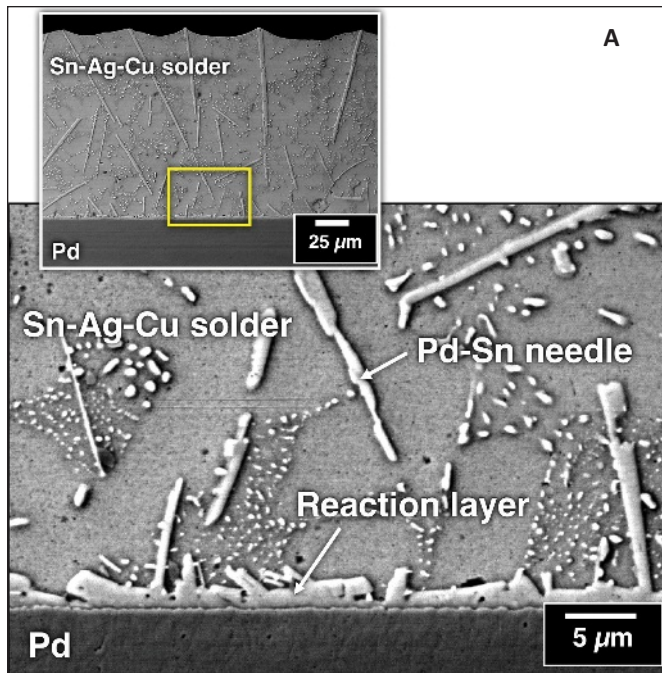


Fig. 21 — A — Reaction (IMC) layer is shown that formed between the 95.5Sn-3.9Ag-0.6Cu (Sn-Ag-Cu) solder and Pd base material. The processing conditions were 350°C and 5 s. The inset image identifies the location of the higher magnification picture. B — SEM photograph shows the reaction layer that formed between 63Sn-37Pb (Sn-Pb) solder (290°C) and Pd after an exposure of 5 s.

condition. Also, Pd-Sn needles were not observed in the Sn-Pb solder above the interface, unlike the Sn-Ag-Cu solder/Pd case.

The electron probe microanalysis (EPMA) technique provides *quantitative* reaction layer compositions. In the case of the Sn-Ag-Cu solder (e.g., Fig. 21A), the reaction layer exhibited a $(\text{Pd}, \text{Cu})\text{Sn}_4$ stoichiometry with 0–2 at.-% Cu. The composition was largely unchanged as a function of soldering process parameters. The Sn-Pb solder reaction layer (Fig. 21B) was predominantly the PdSn_4 phase, but having a small amount PdSn_3 phase. In Fig. 21B, elemental Pb, which was rejected by the reaction between Pd and Sn, located itself as “pockets” within the IMC layer as well as between the IMC layer and the Sn-Pb solder.

These “liquid-state aging” experiments provided critical data for determining the rate kinetics of reaction layer development at the solder/Pd interface. The data sets are shown in Fig. 22 for the Sn-Ag-Cu/Pd and Sn-Pb/Pd couples (Refs. 15, 16). The Sn-Ag-Cu/Pd data (Fig. 22A) is representative of most high-Sn alloys whereby the IMC layer experiences a fast, initial growth rate that quickly levels off to a steady-state thickness that increases with solder temperature. The fact that the IMC reaction layer remained less than 5 μm under all conditions implies that Sn-Ag-Cu solder joints made to Pd will not pose a reliability concern

over a process window represented by these test parameters.

An altogether different response was observed for the Sn-Pb/Pd system — Fig. 22B. First, the ordinate scale is nearly two orders of magnitude greater than that of the Sn-Ag-Cu/Pd plot in Fig. 22A, indicating a substantially faster growth rate at the Sn-Pb/Pd interface. Second, IMC layer development did not show a consistent, asymptotic effect as a function of soldering time. Third, the reaction layer thickness exhibited an unusual behavior at 320°C (red oval) when it became negligible for all time durations. Concurrently, the nearly absent interface reaction layer was accompanied by Pd-Sn needles in the solder. This latter behavior poses an important reminder that the nonequilibrium nature of interfaces can give rise to unexpected phenomenon.

The point was made earlier that solderability must also consider spontaneous spreading by the molten filler metal. A single printed wiring assembly may have upward of 10,000 solder joints, all of which must be formed satisfactorily within a single, 45–90 s soldering time, to be assured of a reliable product. Under these manufacturing constraints, spontaneous spreading is a critical property of the solder/flux/base material system.

Lastly, the soldering process requires two contributing activities within the wetting-and-spreading be-

havior of molten filler metal. This point is illustrated in Fig. 23, beginning with the placement of filler metal in Fig. 23A (and the faying surfaces coated with a suitable flux). The spreading process is shown in Fig. 23B. First, the molten solder must fill the joint clearance, which includes an assistance by capillary action. Secondly, fillet formation requires that the molten solder readily spread upward over the base material surface. These two activities are enhanced by following a few simple design rules for the base material structure(s) (Ref. 17). For example, adding chamfers at sharp corners (yellow arrow, Fig. 23) facilitates the flow of molten solder into the gap.

Summary

Soldering technology has made tremendous strides in the past half century. It has supported the further miniaturization and increased functionality of high-technology consumer electronics as well as opened many avenues for the use of soldering in advanced structural applications. Whether structural or electronic, all solder joints must provide a necessary level of reliability for the application.

Solder joint reliability begins with the selection of a proper solder filler metal. Its solidus temperature must provide a sufficient margin above the maximum service temperature to pre-

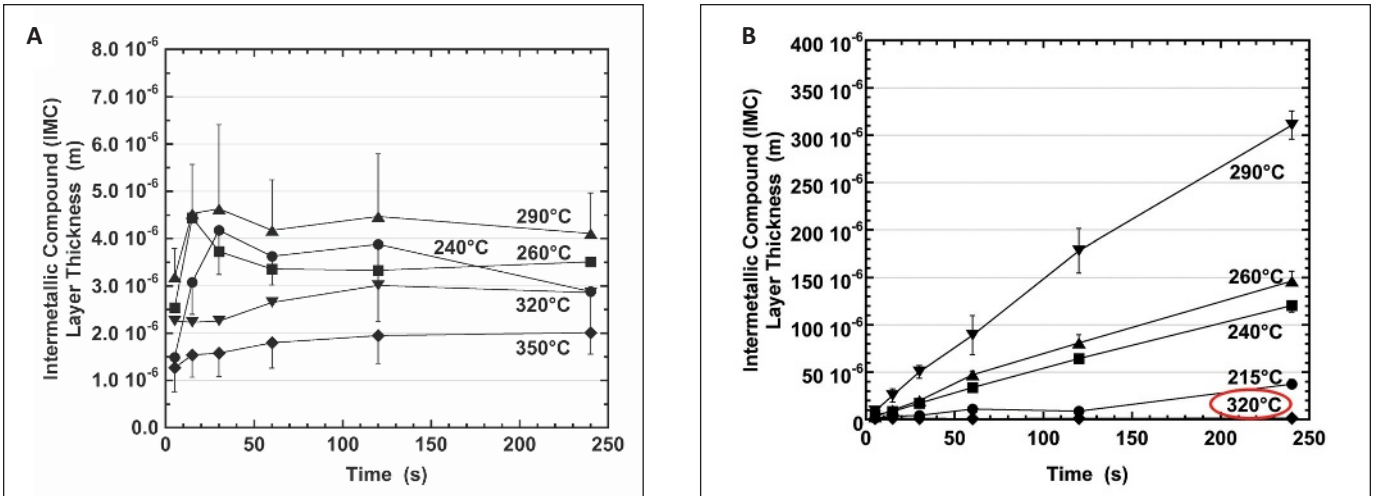


Fig. 22 — Plots show the rate kinetics of reaction (IMC) layer growth as a function of exposure time and solder temperature for these two solders on pure Pd: A — 95.5Sn-3.9Ag-0.6Cu (Sn-Ag-Cu) alloy; B — 63Sn-37Pb (Sn-Pb) alloy.

vent softening or even melting that would compromise the joint. The liquidus temperature must be sufficiently low to support wetting and spreading activity during the soldering process without thermal damage to the base material(s). The solder composition is also selected to have the optimum mechanical properties for the application.

The soldering process affects joint reliability. The flux and heating profile support wetting and spreading by the molten filler metal so that the latter fills the joint clearance and completes formation of the fillet. Base material and surface finish dissolution can alter solder composition, which together with the interface reactions, will directly impact the long-term mechanical performance of the solder joint.

Acknowledgments

The author wishes to acknowledge the contributions of these persons of his nearly 30 years in soldering technology (alphabetical order): W. Buttry, R. Grant, J. Grazier, P. Hlava, A. Kilgo, B. McKenzie, M. Neilsen, J. Rejent, and G. Zender, as well as other, countless individuals, who in many ways, supported the work and performed the work, the results of which, are reported here. The author wishes to thank Don Susan for his review of the manuscript. Sandia is a multiprogram laboratory operated by Sandia Corp., a Lockheed Martin Company, for the United States Department

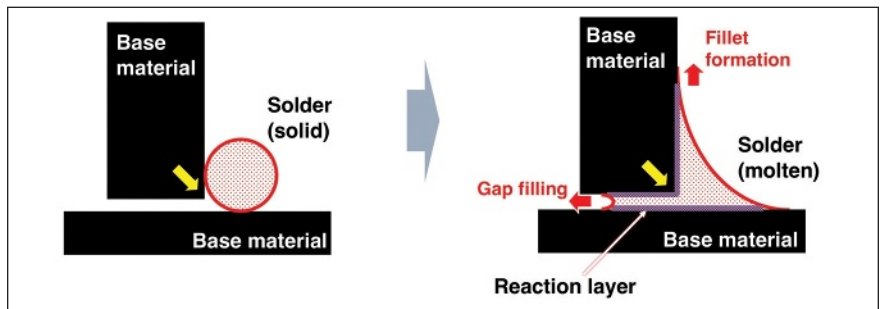


Fig. 23 — Schematics show the joint clearance filling and fillet formation activities by molten solder during wetting and spreading. A — Starting condition has a solder preform at the opening to the joint clearance. B — Final joint configuration includes formation of a fillet and the filling of the joint clearance. The yellow arrows indicate the location to place a chamfer to facilitate solder flow into the joint clearance.

of Energy’s National Nuclear Security Administration under Contract No. DE-AC04-94AL85000.

References

1. Manginell, R., Moorman, M., Rejent, J., Vianco, P., Grazier, M., Wroblewski, B., and Mowry, C. 2012. A materials investigation of a phase changer, micro-valve for greenhouse gas collection and other applications. *Rev. Sci. Inst.* 83: DOI: 030101.
2. Vianco, P. 2000. *Soldering Handbook*. Miami, Fla.: American Welding Society.
3. Vianco, P., Hosking, F., and Rejent, J. 1990. Solderability testing of Kovar with 60Sn-40Pb solder and organic fluxes. *Welding Journal* 69(6): 230-s to 240-s.
4. Kovar™ is a trademark of Carpenter Technologies, Reading, Pa.
5. Vianco, P. 1991. An overview of the meniscometer/wetting balance technique for wettability measurements. *The Metal Science of Joining*, ed. M. Cieslak, et al. pp. 265–284. Warrendale, Pa.: TMS.

6. Artaki, I, Finley, D., Jackson, A., Ray, U., and Vianco, P., 1995. Wave soldering with lead free solders. *Proc. SMTI*. pp. 495–510. Surface Mount Technology Association.

7. The homologous temperature, T_h , is defined as the ratio of the absolute temperature of the use condition over the absolute temperature of the solidus point. For example, 63Sn-37Pb solder has a solidus temperature of 183°C (456K). At 25°C (298K), the T_h is 298/456 K, which equals 0.65. By comparison, a T_h of 0.65 would be equivalent to 814°C for a nickel-based alloy having a solidus temperature of 1400°C (1673 K), hence, the analogy with the jet engine application.

8. Vianco, P., and Rejent, J. 1999. Properties of ternary Sn-Ag-Bi solder alloys: Part I – Thermal properties and microstructural analysis. *J. Electr. Mater.* 28: 1127–1137.

9. Vianco, P., and Rejent, J. 1999. Properties of ternary Sn-Ag-Bi solder alloys: Part II – Wettability and mechanical properties. *J. Electr. Mater.* 28: 1138–1143.

10. Vianco, P., Rejent, J., Grazier, M., Kilgo, A., McKenzie, B., and Allen, A. 2012. Establishing a Ti-Cu-Pt-Au thin film on-low temperature co-fired ceramic LTCC technology for high temperature electronics. *Proc. Surf. Mount Tech. Assoc. Inter.* CD-ROM Surface Mount Technology Association.

11. Siewert, T., Liu, S., Smith, D., and Madeni, J.-C. 2002. Properties of lead-free solders – Release 4.0. *Database of Solder Properties with Emphasis on New Lead-free Solders*. Boulder, Colo.: National Institute of Standards and Technology.

12. Vianco, P. 1998. An overview of surface finishes and their role in printed cir-

cuit board solderability and solder joint performance. *Circuit World* 25: 6–24.

13. Vianco, P., Martin, J., Wright, R., and Hlava, P. 2006. Dissolution and interface reactions between the 95.5Sn-3.9Ag-0.6Cu, 99.3Sn-0.7Cu, and 63Sn-37Pb solders and silver base metal. *Metallurgical and Materials Transactions A* 37A: 1551–1561.

14. Vianco, P., Rejent, J., Kilgo, A., and Garrett, S. 2014. Sensitivity of copper dissolution to the flow behavior of molten Sn-Pb solder. *Proc. Surf. Mount Tech. Assoc. Inter.* CD-ROM Surface Mount Technology Association.

15. Vianco, P., Rejent, J., Zender, G., and Hlava, P. 2010. Dissolution and interface reactions between palladium and tin (Sn)-based solders: Part I – 95.5Sn-3.9Ag-0.6Cu alloy. *Metall. and Mater. Trans. A* 41A: 3042–3052.

16. Vianco, P., Rejent, J., Zender, G., and Hlava, P. 2010. Dissolution and interface reactions between palladium and tin (Sn)-based solders: Part II – 63Sn-37Pb alloy. *Metall. and Mater. Trans. A* 41A: 3053–3064.

17. Vianco, P. 2016. *Guidelines for Hand Soldering*. Miami, Fla.: American Welding Society.

Call for Papers 2017 AWS Professional Program

November 6–9, 2017 (Monday–Thursday)
McCormick Place, Chicago, Ill.

The American Welding Society (AWS) will hold the 2017 Professional Program, in Chicago, Ill., from Monday, November 6 through Thursday, November 9. Please submit abstracts before March 17 at <http://awo.aws.org/professional-program-abstract-form/>.

Authors with accepted abstracts will be required to give oral presentations at the Professional Program. Presentations are welcome on novel developments and research areas related to materials joining including surfacing and additive manufacturing. Topics include but are not limited to

- Additive Manufacturing – Sponsored by the AWS D20 Committee
- Welding in Battery and Energy Systems
- Modeling and Numerical Analysis Related to Welding
- Sensors, Controls and Robotics for Welding Applications
- Surfacing, Overlay, and Repair
- Welding Processes/Methods including
 - o arc welding
 - o high-energy-density welding (LBW & EBW) – Sponsored by the AWS C7 Committee
 - o laser hybrid welding – Sponsored by the AWS C7 Committee
 - o solid-state welding – Sponsored by the AWS C6 Committee
- Weldability and Welding Metallurgy
- Properties and Performance of Welded Joints in Service (Corrosion, Creep, Fatigue)
- Industrial Applications and Technologies

The Professional Program will also include

- An Honorary Symposium for and a Plenary Presentation by Prof. T. DebRoy, Department of Materials Science and Engineering, The Pennsylvania State University;
- An Honorary Symposium for and a Plenary Presentation by Dr. Stan David, Oak Ridge National Laboratory.

In addition, please also plan to attend these related events

- The AWS Annual Meeting on Monday morning (November 6) where the new AWS Fellows and Counselors will be inducted;
- The Comfort Adams Lecture following the AWS Annual Meeting on Monday morning.

Registration for the Professional Program authors is complimentary to speakers and provides free access to FABTECH, which is the largest metal forming, fabrication, welding, and finishing event in North America.

Full papers are not required for the Professional Program, but authors are encouraged to submit to the *Welding Journal* at editorialmanager.com/wj for possible publication, before or after the presentation.

Influence of Welding Pressure on Diffusion Welded Joints Using Interlayer

Considering diffusion welding for superior performances

BY G. THIRUNAVUKARASU, B. MURUGAN, S. CHATTERJEE, AND S. KUNDU

ABSTRACT

The present study focused on elucidating the extent of influence of welding pressure on the evolution of interfacial microstructure, mechanical properties, and fracture morphologies of solid-state diffusion-welded joints (DWJs) of Ti-6Al-4V (TiA) and 304 stainless steel (SS) using 200- μ m-thick nickel (Ni) as an interlayer processed in vacuum at 750°C for 60 min using welding pressure in the range of 2 to 10 MPa in step of 2 MPa. Layer wise Ni-Ti-based intermetallic phase(s) were revealed at the TiA|Ni interface, whereas the Ni|SS interface showed solid solution behavior. From the surface property of the DWJs, it was sensed that the effect of work hardening occurred when the welding was processed at 4 MPa and above welding pressures. Exponential growth in the bulging property of the DWJs with the increase in the welding pressure was spotted. The study indicated the significant influence of welding pressure over the welded assemblies' tensile properties; however, tensile properties behaved asymptotic when the DWJs were processed beyond 6-MPa welding pressure. To understand the fracture characteristic of the DWJs, fracture path and fractography were evaluated. Thermal stresses induced on the materials diffusion welded were calculated.

strength/weight ratios of titanium and its family of alloys make them an attractive prospect for use in offshore oil and gas platforms. Ti-alloy armor is being incorporated into the design of some combat vehicles in order to save weight (Ref. 3).

Although Ti alloys are nonmagnetic, their high electrical resistivity is used in the manufacture of electromagnetic cookware. In addition to the capability of electromagnetic cooking, titanium's light weight, low heating capacity, and good corrosion resistance are the favorable properties of these cookwares (Ref. 4).

Austenitic stainless steels (ASSs) are the most common and familiar type of stainless steels. They are recognized as nonmagnetic. They are extremely formable and weldable, and successfully used from cryogenic to red-hot temperatures. ASSs have exceptional toughness and a combination of strength and corrosion resistance at elevated temperatures. ASSs are the most creep resistant of the stainless steels. Lean austenitic alloys constitute the largest portion of all stainless steels (SSs) produced. These are principally 201, 301, and 304 grades. Alloys with less than 20% Cr and 14% Ni fall into this unofficial category (Ref. 5). Highly efficient and reliable joints of corrosion-resisting-steels with titanium alloys find the greatest inevitable need in nuclear power engineering (Ref. 6).

In a satellite cooling system, Ti-6Al-4V is joined to stainless steel

KEYWORDS

- Diffusion Welding • Ti Alloys • Stainless Steels • Intermetallics
- Mechanical Properties

Introduction

Diffusion welding (DW) is a high-temperature solid-state joining process that permanently joins mating surfaces by simultaneous application of pressure and heat. It does not involve macroscopic deformation, melting, or relative motion of the parts welded. A solid filler metal (diffusion aid) may be inserted between the facing surfaces (Ref. 1). DW has demonstrated its uniqueness by finding application in the processes and products of front line areas of science and technology. DW is actually gaining mo-

mentum of applicability from the days of conception due to the inappropriateness of other joining techniques.

In the past quarter-century, Ti alloys have been successfully used in aircrafts, rockets, and biomedical implants, among other products, as key structural materials. Ti alloys derive their excellent properties from a combination of two ductile phases (hcp and bcc allotropic modifications) of Ti. Several key features of these phases independently and dependently determine the plasticity and fracture behavior of the family of Ti-alloys (Ref. 2). Both the high corrosion resistance and the good

G. THIRUNAVUKARASU, B. MURUGAN, S. CHATTERJEE, and S. KUNDU (skundu@metal.iests.ac.in) are with the Department of Metallurgy and Materials Engineering, Indian Institute of Engineering Science and Technology, Shibpur, India.

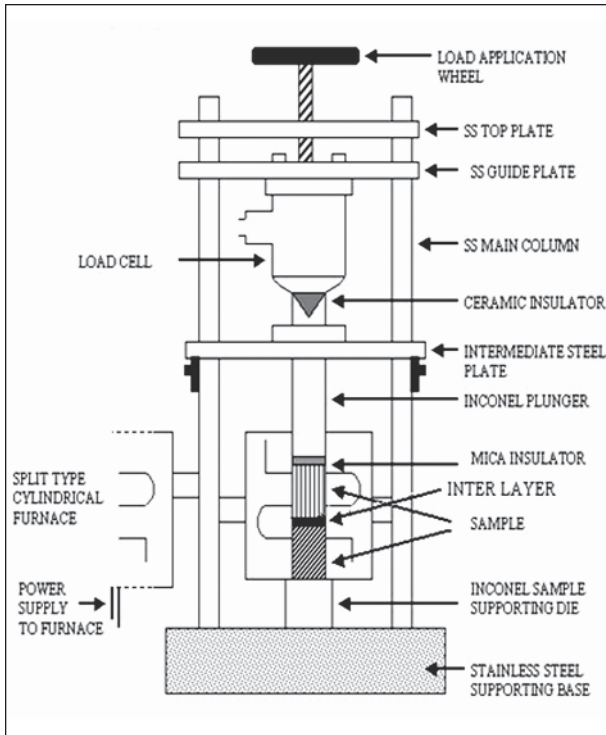


Fig. 1 — Schematic diagram of the indigenous fixture used for processing DWJs.

(1Cr18Ni9Ti) (Ref. 7). Joints of Ti alloy and Type 304 ASS are used in fuel tanks of satellite launch vehicles (Ref. 8); hence, joints of Ti-based alloy and SS using different welding techniques are undertaken as sponsored research by different agencies and institutes to know the details of optimal levels of operating parameters to achieve far better performance.

Table 1 shows the physical properties of Ti-6Al-4V and 304 SS (Ref. 9). It is readily seen that large property differences exist between the metals. The large variation of these and other properties provide an attractive source for the choice of materials for special service conditions and environments; however, the large differences in physical properties also yield difficulties in joining these metals together. A large difference in the melting temperature

between two metals makes the conventional fusion-welding processes inapplicable due to the segregation of low-melting eutectics, which can cause hot cracking. Large differences in thermal expansion will lead to the formation of large residual stresses and this leads to the formation of microcracks at the welded region; and thus reduce the joint strength and cause fatigue problems. A difference in the thermal conductivity of two metals easily causes uneven heat dissipation. Furthermore, chemical mismatches in dissimilar-metal joints can result in the formation of brittle phases and the diffusion of particular elements. These will adversely affect the service

properties of the joints, and are the main reasons why dissimilar-metal joining is normally more complex than similar-metal joining in many respects. Consequently, a solid-state joining method, viz., DW of these two materials using an interlayer, has gained more importance than other conventional welding methodologies. During welding, Ti alloys pick up oxygen and nitrogen from the atmosphere very easily (Refs. 10, 11). For this reason, DW in a vacuum or inert gas atmosphere is suggested.

One of the necessary conditions to considering a material as a potential interlayer to join the base metal(s) is that it reduces the chemical heterogeneity and improves the thermodynamic stability of the diffusion zone at the interface of the welded joints. Zeer et al. (Ref. 12) proposed a method to

classify interlayers for DW of dissimilar materials and discussed the role and contribution of the interlayers in the formation of the diffusion welded joints (DWJs) in different stages of welding. They advised using interlayers made from alloys or pure metals, usually with high ductility, such as nickel, copper, cobalt, zirconium, vanadium, Permalloy, silver and gold. The interlayers were used in the form of foil, film, or coatings and deposited on one or both sides of the to-be-welded surfaces by electroplating or thermal spraying, rolling of powders, and in the combined form of spraying and foil. Nickel was considered as a potential candidate for the interlayer due to its corrosion resistance for application at high temperature and substantial solid solubility with iron. Ni-Ti binary phase diagram suggested that intermetallics formation changes from NiTi₂ to Ni₃Ti via NiTi with increasing Ni (Refs. 13, 14). He et al. (Ref. 15) reported Ni-Ti intermetallics have higher plasticity than Fe-Ti intermetallics.

The success or failure of the DW process depends on welding pressure, temperature, and time (Ref. 16). In the past, most literature reported either the effect of temperature or time on the DWJs' microstructure and mechanical properties. The present authors along with Professor Mishra carried out two separate investigations on DWJs of TiA and SS using 200- μ m-thick Ni as an interlayer. To first optimize the welding temperature (Ref. 17), DWJs were prepared in the temperature range from 700° to 800°C in steps of 25°C using 3-MPa pressure for 60 min. A maximum tensile strength of ~206 MPa along with a ductility of ~2.9% was obtained for the DWJs processed at 750°C. Secondly, to optimize the welding time (Ref. 18), DWJs were processed using 4-MPa pressure at 750°C by varying the time from 30 to 120 min in steps of 15 min. Maximum tensile strength of ~382 MPa along with elongation of ~3.7% was observed for the DWJs processed for 60 min. Although it is universally accepted that welding pressure is a very important variable in the solid-state DW process, up until now there existed no sufficient, well-established empirical study/proof to back up such a hypothesis.

In view of limited studies, the present research work described in this pa-

Table 1 — Physical Properties of Base Metals

Metal	Melting Point (°C)	Density (g/cc)	Thermal Conductivity (W/m-K)	Coefficient of Thermal Expansion (μ m/m-°C), linear 250°C
304 SS	1400-1455	8	16.2	17.8
Ti-6Al-4V	1604-1660	4.43	6.7	9.2

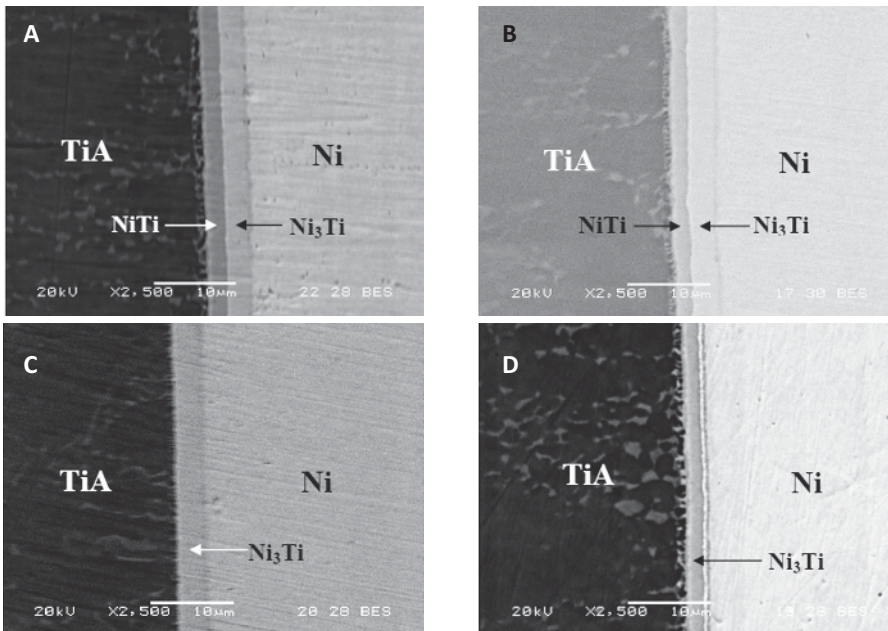


Fig. 2 — SEM-BSE images of TiAl/Ni interface of DWJs processed at 750°C for 60 min using A — 2 MPa; B — 4 MPa; C — 6 MPa; D — 8 MPa.

per was undertaken by the researchers in an attempt to know the extent of significant influence of pressure variation over intermetallics formation at the diffusion zone, the lateral plastic deformation, the room-temperature mechanical properties (tensile properties and hardness), and the fracture geographies of DWJs and to provide information about the possible causes. As this work is in continuation of the previous works (Refs. 17, 18), the optimized temperature of 750°C and the optimized time of 60 min were chosen from the respective literature sources (Refs. 17, 18). Choosing higher welding temperature and longer welding time deteriorated the DWJs' strength due to the formation of a large volume of Ni-Ti-based intermetallics at the TiAl/Ni interface (Refs. 17, 18). Even higher temperature and longer time will lead to the formation of Fe-Ti-based intermetallics that are more detrimental to the mechanical properties of the DWJs. Herein, the experimental investigation of influence of welding pressure on the evolution of interfacial microstructure and the mechanical properties of solid-state diffusion welded joints of Ti-6Al-4V (TiAl) and 304 stainless steel (SS) using 200- μ m-thick Ni as an interlayer was processed in vacuum at 750°C (welding temperature) for 60 min (welding time) using welding pressure in the range of 2 to 10 MPa in steps of 2 MPa.

Experimental Procedures

Base metals: Ti-6Al-4V wt-% [a.k.a. TiAl] and Fe-18Cr-8Ni wt-% [a.k.a. SS] and interlayer: 99.5 wt-% Ni ($\sim 200 \pm 10 \mu\text{m}$), were used in this investigation. Mating surfaces of base metals and interlayer were polished using diamond paste (1 μm) after grinding by hand using eleven series of SiC emery papers (grit sizes 40# to 1600#) to reduce surface roughness. Before DW, the mating surfaces were cleaned with acetone and dried using a portable hair dryer. In this study, DWJs were processed using a special fixture (Fig. 1) designed and manufactured indigenously. The fixture design is capable of processing only one DW experiment at a given point in time; hence, the DW experiments are time consuming by nature and by design. Mica of $\sim 1\text{-mm}$ thick was kept on the supporting die (Inconel) of the fixture — Fig. 1. The TiAl/Ni/SS assembly was placed over the mica. Mica avoids the interfacial contact between the assembly and the supporting die. Over the assembly, mica was again placed to avoid the interfacial welding between the plunger (Inconel) and the assembly. A ceramic-type insulator was used in between load cell and plunger to prevent metal-metal contact. Over the load cell, screw threaded wheel (of stainless steel) for load application was mounted. After

positioning all the above items in-line, a load cell (capacity: 500 kg) was connected to the load indicator, and the required welding pressure (2–10 MPa) was applied along the centerline of the assembly using the threaded wheel that acts over the load cell and the to-be-diffusion-welded assembly. This threaded wheel is used to control the welding pressure applied on the assembly. The welding pressure applied was measured at room temperature. The fixture with the assembly was inserted inside a vacuum chamber, with one end of the vacuum chamber sealed using nuts and bolts and the other end connected to a vacuum unit. After reaching enough vacuum ($\sim 6\text{--}8 \times 10^{-3}$ Pa), temperature was increased from 32°C (room temperature) to 750°C (welding temperature) at the rate of $0.24^\circ\text{C s}^{-1}$. The TiAl/Ni/SS assemblies were held for 60 min (welding interval) at 750°C. Power supply to the welding furnace was switched off after 60 min. At each level of the welding pressure factor, three separate experiments were conducted to process three samples of DWJs.

In this study, experiments were performed at five different levels (2, 4, 6, 8, and 10 MPa) of welding pressure factor; hence, there are a total of 15 individual, independent, and random experiments (three experiments repeated at each level of the welding-pressure factor).

After the DW process, DWJs were sectioned perpendicular to the mating surface and the surfaces were prepared by metallurgical polishing techniques. Polished surfaces of DWJs were examined in an SEM (JSM-5510, JEOL) in backscattered electron mode (SEM-BSE) to obtain finer microstructural features of diffusion zone. Chemical composition of the reaction layers were determined by energy dispersive spectroscopy (SEM-EDS, Thermo Electron Corporation-Noran System Six C10018) using a SiLi detector. Tensile properties of DWJs were evaluated with an Instron 4204 at a cross-head speed of 8.33×10^{-4} mms^{-1} . Cylindrical tensile specimens (gauge diameter: 4 mm, gauge length: 20 mm) were machined as per ASTM specification E8M-11 (Ref. 19). The average of the tensile properties of three DWJs processed at each pressure level along with the associated errors were reported here.

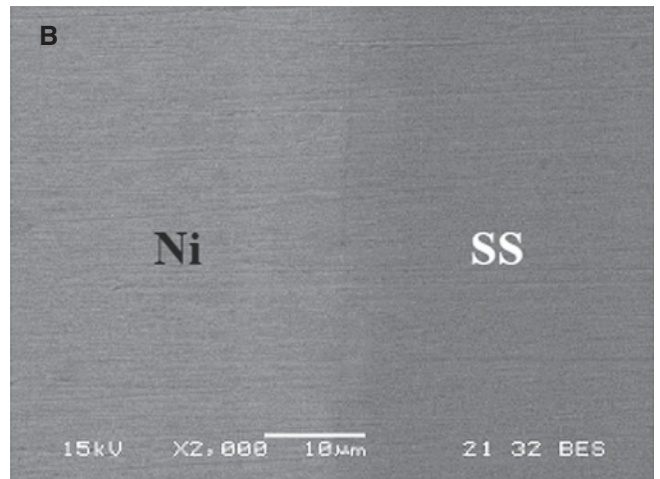
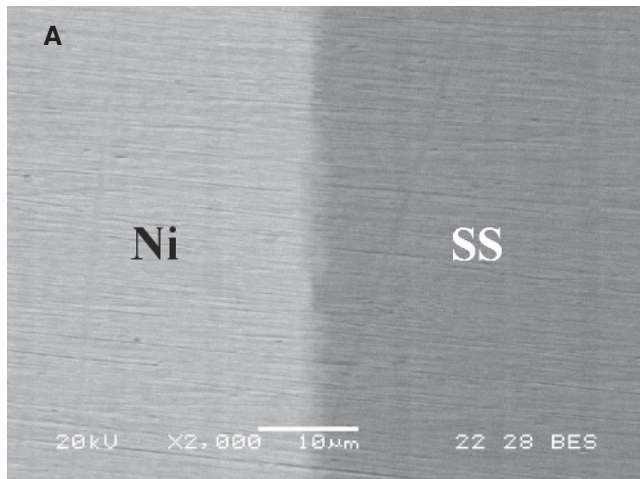


Fig. 3 — SEM-BSE images of Ni|SS of DWJs processed using welding pressure of A — 2 MPa; B — 10 MPa.

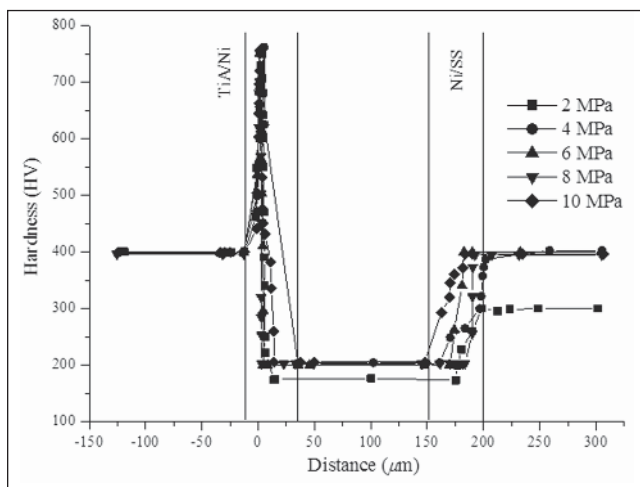


Fig. 4 — Microhardness profile along the interfaces of DWJs processed using various welding pressures.

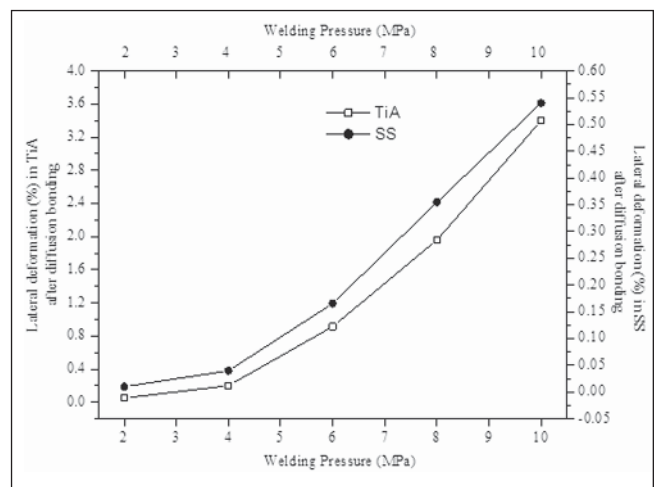


Fig. 5 — Variation of lateral deformation (%) in TiA and SS of DWJs with respect to the welding pressure applied.

Microhardness measurements were carried out on the polished surface of DWJs using Vickers diamond indenter (Leica VMHT) with a load of 25 gram force for 20 s dwelling time. Five measurements were carried out at each section and the respective average was mentioned in this study. Fracture surfaces of DWJs were observed in secondary electron mode using the SEM-EDS to reveal the nature and most possible location through which failure was initiated during tensile loading. SEM-BSE observations were also made to study the location of the fracture path, while fractography examination was carried out using secondary electrons of SEM.

Results

Absence of discontinuities and voids at both the interfaces (both TiA|Ni and

Ni|SS in Figs. 2, 3, respectively) was revealed, which established the superior contact of the mating surfaces with process parameters; hence, DWJs were efficacious. Layer wise intermetallics were observed at the TiA|Ni interface (Fig. 2), whereas the Ni|SS interface (Fig. 3) revealed solid-solution behavior. It was observed that the TiA|Ni interfaces (Fig. 2) of the DWJs processed using 6 and 8 MPa had only a light-shaded reaction layer. The light-shaded reaction layer on an average consisted of Ti (~27 at.-%) and Ni (~70 at.-%); hence, the Ni-Ti binary phase diagram indicated the realization of Ni₃Ti intermetallic (Refs. 13, 14).

The TiA|Ni interface of the DWJs processed using 2, 4, and 10 MPa had two reaction layers. The deep-shaded reaction layer observed adjacent to the TiA matrix consisted of Ti (~50 at.-%

and Ni (~45 at.-%); hence, the Ni-Ti phase diagram indicated the possibility of realization of NiTi intermetallic (Refs. 13, 14). The reaction layer adjacent to the Ni matrix was light shaded Ni₃Ti intermetallic. In general, for all DWJs, the width of Ni₃Ti intermetallic was wider compared to the NiTi intermetallic at the reaction zone (Ref. 18). The formation of the similar Ni-Ti-based reaction products were also observed in the literature (Refs. 20, 21).

It was observed, the hardness of the TiA side (Fig. 4) of the DWJs was ~400 HV irrespective of the welding pressure adopted during the experiments. The hardness of the other base metal side (SS side) of the DWJs was witnessed to be ~300 HV for the DWJs processed at 2 MPa, whereas the surface hardness of the SS side was ~400 HV for the DWJs processed from

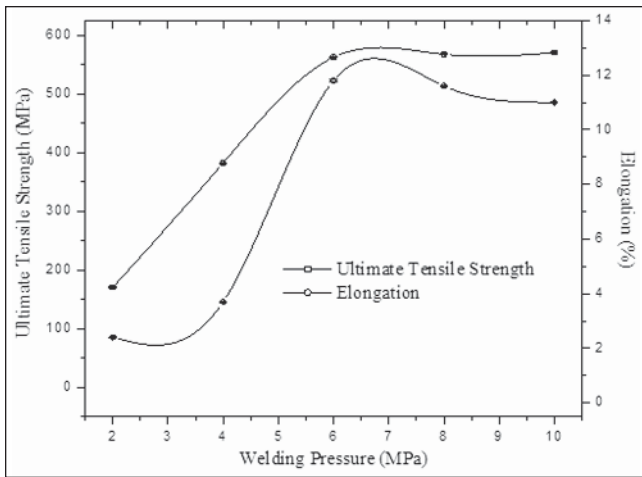


Fig. 6 — Tensile strength (MPa) and breaking strain (%) of DWJs processed at different levels of welding pressure.

4 to 10 MPa. In the same way, the hardness of the interlayer zone (Ni) of the DWJs was found to be ~175 HV for the DWJs processed at 2 MPa, whereas it was ~200 HV for the DWJs processed from 4 to 10 MPa. It was observed that the increase in the welding pressure had a significant influence in increasing the bulk property (hardness) of the SS side and Ni zone but such phenomenon was not observed in the case of the TiA-side.

The materials that were diffusion welded underwent serious changes in shape, i.e., geometry. In reality, whenever a force is applied to a solid object, a stress is produced within the object. The physical effect/manifestation of this stress is that the object experiences some form and amount of deformation, a strain. As the DWJs were prepared at five different levels of the welding-pressure factor, it was decided to observe the lateral deformation of the DWJs. The lateral deformation (Equation 1) of the DWJs is defined as follows:

$$\text{Lateral deformation (\%)} = \frac{(d_2 - d_1)}{d_1} \times 100 \quad (1)$$

d_1 : (diameter of base metal section) before diffusion-bonding

d_2 : (diameter of base metal section) after diffusion-bonding

The details of the lateral deformation of TiA and SS are given in Fig. 5. The lateral deformation of the TiA side of the DWJs was much higher than that

of the lateral deformation of the SS side of the respective DWJs. The reason for the significant differences in the lateral deformation of TiA side and SS side needs to be figured out.

Both tensile strength and elongation (Fig. 6) increased with the increase in the welding pressure from 2 to 6 MPa. Increase in the strength and elongation of the DWJs with the increase in pressure was presumably due to the improvement in the coalescence of the mating surfaces of the DWJs. There was no significant difference in the tensile strength of DWJs processed above 6 MPa. The tensile curve was more or less flat for the DWJs processed above 6 MPa. Elongation dropped insignificantly for the DWJs processed above 6 MPa. A slight drop in the elongation of DWJs with the increase in the welding pressure from 6 to 10 MPa is due to the work hardening effect (Ref. 22) experienced by DWJs. DWJs processed at 6 MPa achieved the optimal strength of ~560 MPa with substantial elongation of ~12%. In this work, dissimilar metal joints of Ti-6Al-4V and 304 SS achieved the highest strength of ~560 MPa, which is also the best performance of the joints processed to date in other routes reported in literature (Refs. 23–29). Shanmugarajan et al. (Ref. 23) achieved

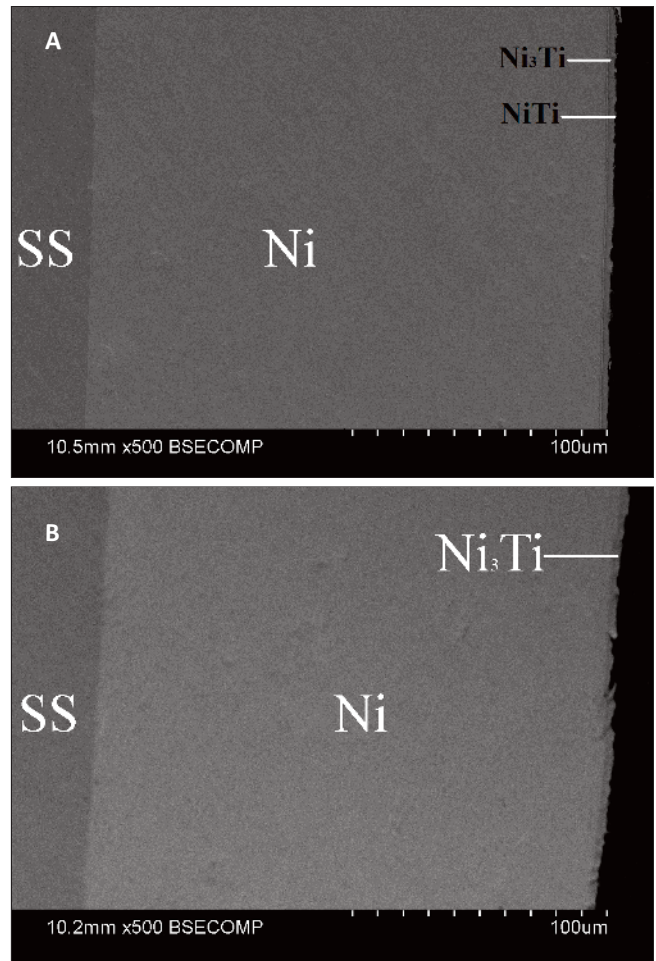


Fig. 7 — Fracture path of DWJs processed at A — 2 MPa—SS side; B — 6 MPa—SS side.

~40 MPa for the laser welded joints of Ti and SS using Ta as an interlayer. Wang et al. (Ref. 24) were able to reach ~124 and ~234 MPa for the electron beam welding of titanium alloy to SS using Ni and Cu filler metal, respectively. Balasubramanian (Refs. 25, 26) achieved ~158 MPa for DWJs of Ti-6Al-4V and 304 SS using an Ag interlayer. Tomashchuk et al. (Ref. 27) reached ~350 MPa for electron beam welded joints of Ti alloy and SS via copper as interlayer. Norouzi et al. (Ref. 28) achieved ~374 MPa for transient liquid phase (TLP) welded joints of Ti-6Al-4V and AISI 304 austenitic SS using Cu interlayer. Kumar et al. (Ref. 29) accomplished the highest tensile strength of ~523 MPa for the dissimilar metal joints of Ti-6Al-4V and SS304L with Cu as interlayer through friction welding technique. This work proved DW is a promising route to process dissimilar metal joints with far better mechanical properties.

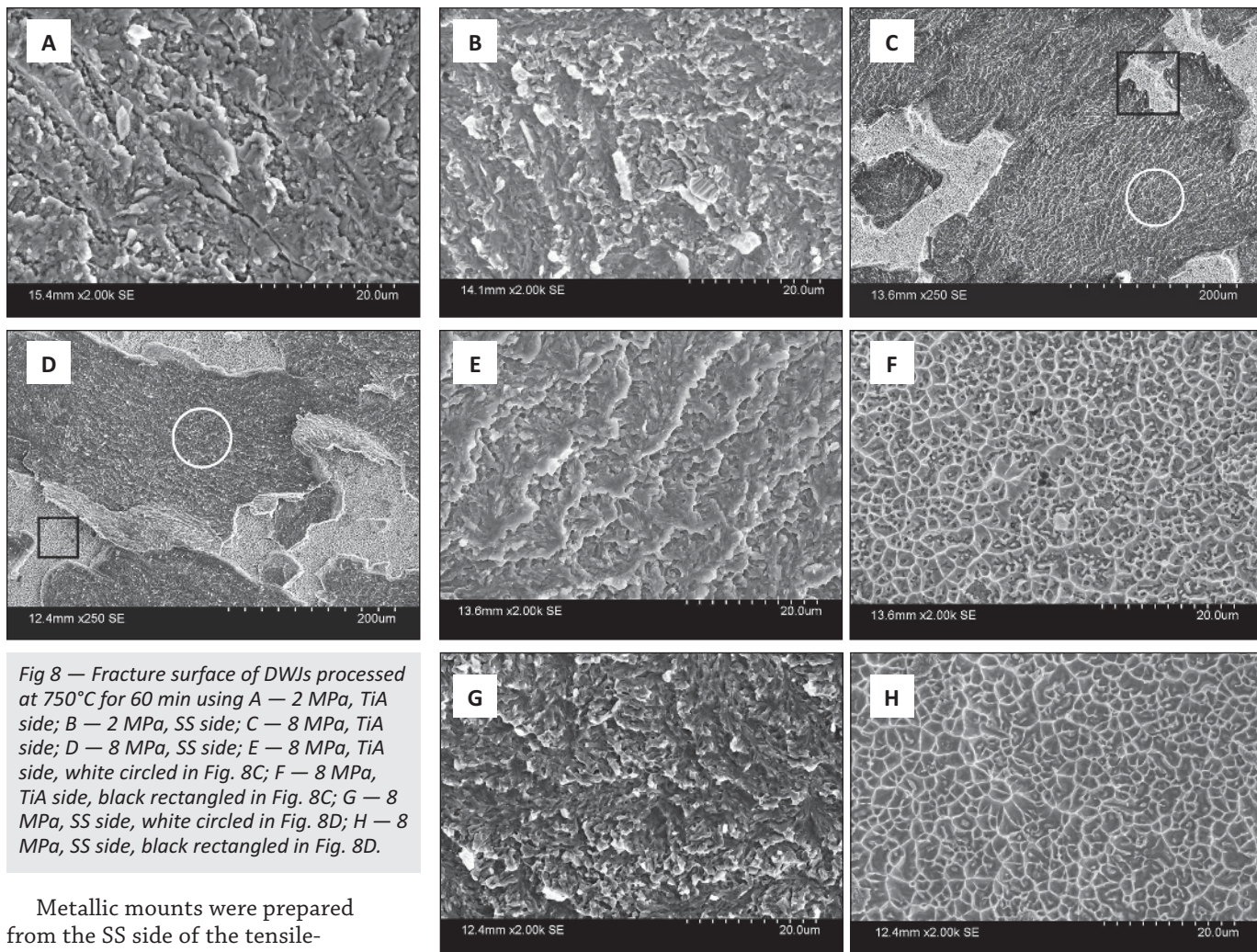


Fig 8 — Fracture surface of DWJs processed at 750°C for 60 min using A — 2 MPa, TiA side; B — 2 MPa, SS side; C — 8 MPa, TiA side; D — 8 MPa, SS side; E — 8 MPa, TiA side, white circled in Fig. 8C; F — 8 MPa, TiA side, black rectangled in Fig. 8C; G — 8 MPa, SS side, white circled in Fig. 8D; H — 8 MPa, SS side, black rectangled in Fig. 8D.

Metallic mounts were prepared from the SS side of the tensile-fractured DWJs. The SS side (Fig. 7A) of the fractured DWJ processed at 2 MPa revealed ample Ni interlayer; hence, the SEM micrographs of the metallic mounts suggested that the lower welding pressure functionally favored the fracture along the TiA | Ni interface with the intermetallics (Ni_3Ti and NiTi) completely cleaved off the TiA matrix. The fracture path (Fig. 7B) of the DWJ processed using 6 MPa exposed the full length of the Ni layer. It was observed that the DWJ processed using 6 MPa had proofs of Ni_3Ti intermetallic attached to the edge of Ni foil; therefore, the electron micrographs of the metallic mounts recommended that DWJs processed at higher welding pressure also preferred to fracture along the TiA | Ni interface with the intermetallic (Ni_3Ti) completely hewed off the TiA matrix. In brief, the fracture path (Fig. 7) observation yielded valuable information that the TiA | Ni | SS DWJs fractured along the TiA | Ni in-

terface regardless of the welding pressure chosen.

Selective tensile fractured samples along the TiA side and SS side of DWJs processed at 2 and 8 MPa were shown in Fig. 8. Both the fracture features of the TiA side (Fig. 8A) and SS side (Fig. 8B) of DWJ processed at 2 MPa did not show any sign of dimpled-rupture (ductile) mode of failure; but showed the noted “river marks.” Both the fractographs (Figs. 8A and B) had typical slightly faceted appearances principally because of the changes in the orientation of the cleavage planes operating from grain to grain; hence, it was established that the DWJs processed at 2 MPa had undergone a majorly brittle fracture of intergranular mode apparently through the TiA | Ni interface during tensile loading.

Both the fracture structures of the TiA side (Fig. 8C) and SS side (Fig. 8D) of the DWJ processed at 8 MPa detected two distinct regions. Firstly, the

zones identified as white circles were faceted river-pattern rupture (brittle) mode of failure; secondly, the zones identified using black rectangles were dimpled-rupture (ductile) mode of failure. Although the faceted river patterns were more in volume as compared to the other feature in the fractographs (Figs. 8C and D), it could be comfortably claimed that the DWJs processed using 8 MPa had undergone a mixed mode of failure. For better visualization and understanding, the details of the zone identified as white circles in Figs. 8C and D were shown in Figs. 8E and G, respectively. Similarly, the details of the zone identified as black rectangles in Figs. 8C and D were shown in Figs. 8F and H, respectively. In general, it was learned that the lowest welding pressure (2 MPa) yielded brittle fracture morphologies; and finally, the higher welding pressure (8 MPa) yielded mixed mode fractural features.

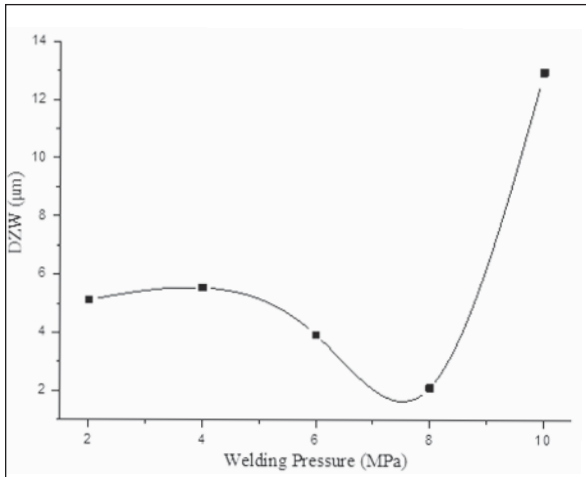


Fig. 9 — Diffusion zone width (DZW) at TiA|Ni interface of DWJs processed at different welding pressures.

Discussion

Sensible reasons for the presence of the layer-wise Ni-Ti-based intermetallics at the TiA|Ni interface and the solid-solution behavior at the Ni|SS interface could be explained using Hume-Rothery rules and the principle of electronegativity (Ref. 18). At the interfaces, the atoms from both sides diffuse in the opposite direction, but there is an effective diffusion of atoms at each interface that is more predominant than the other direction. At the TiA|Ni interface, Ni atoms diffused deeper into the TiA matrix as compared to the diffusing capability of Ti atoms into the Ni matrix. Similarly, net flux of Ni atoms past the interface in one direction were faster than the flux of atoms in SS in the opposite direction; hence, the effect proposed by Kirkendall was observed at Ni|SS interface for all DWJs (Ref. 18).

As DWJs fractured at the TiA|Ni interface due to the presence of intermetallics at the interfacial reaction (diffusion) zone, the diffusion zone width (DZW) of the TiA|Ni interface was measured. The DZW (Fig. 9) at the interface of the DWJs processed at 2 and 4 MPa have negligible significant differences. The DZW decreased with the increase in the welding pressure from 4 to 8 MPa. The DZW increased with the increase in the welding pressure from 8 to 10 MPa. A decrease in the DZW with an increase in the welding pressure, from 4 to 8 MPa, indicated there was a decrease in the net activity (diffusivity) of atoms at the TiA|Ni interfaces. A decrease in

the net activity of atoms with an increase in welding pressure shows an inverse relationship.

Most of our engineering materials are polycrystalline so that grain boundary diffusion is far more important than surface diffusion. Deformation forces the dislocations that exist in a polycrystalline metal to move up and pile up at the grain boundaries, and new dislocations to be generated. Consequently, the increase in pressure hinders the grain boundary diffusion, which affects the surface diffusion phenomenon. Hence, interfacial activity was affected (Refs. 30–32). At 10 MPa, diffusion along the free surfaces is a dominant diffusion path. A free surface is associated with more open structure, and experiments showed that the jump frequency for atoms diffusing along this defect is higher than for diffusion in lattice and grain boundaries (Ref. 31). With an increase in the welding pressure to 10 MPa, effective free surface for contact of the mating surfaces was increased, thus the effective atomic mobility increased. Hence, DZW increases with welding pressure from 8 to 10 MPa.

The increase in the hardness of the Ni and SS with the increase in welding pressure could be attributed to the effect of work hardening. When material is deformed, work hardening occurs resulting in an increase in the hard-

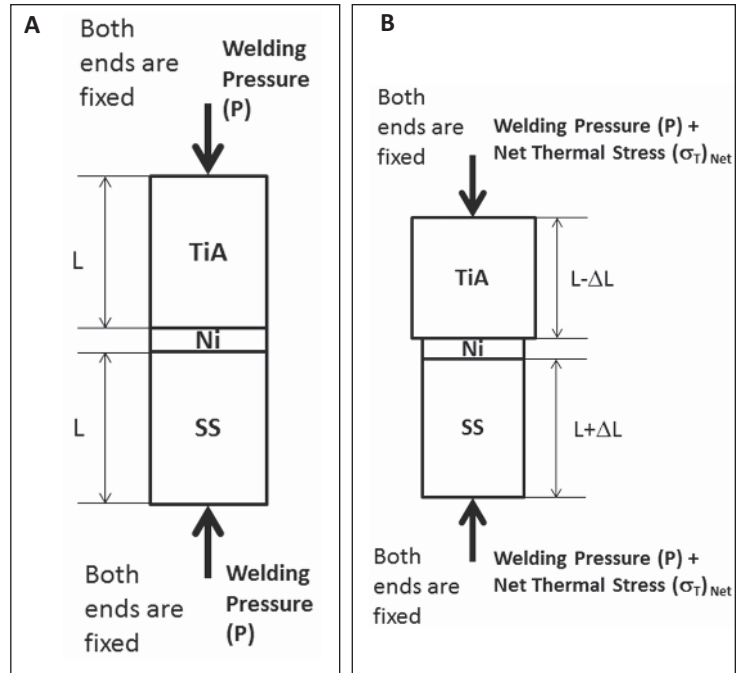


Fig. 10 — Line sketch of the materials assembled in the DW fixture when furnace temperature was at A — 32°C (ambient temperature); B — 750°C (welding temperature).

ness of the material. In general, the rate of work hardening is lower for hcp metals than for cubic metals. TiA is being hcp metal whereas that of Ni and SS are cubic metals. The hardness of Ni and SS were increased significantly with the increase in the welding pressure from 2 to 4 MPa and above, while the hardness of TiA (hcp metal) doesn't change with the welding pressure (Ref. 33). Along the Ni|SS interface, the hardness increased from Ni to SS and the observed hardness was ~220 HV for the DWJs processed at 2 MPa, whereas it was ~330 HV for 4 MPa and above welding pressures. Along the TiA|Ni diffusion zone, the hardness increased initially till it reached a maximum value and dropped toward Ni. The hardness of NiTi intermetallic and Ni₃Ti intermetallic was ~550 and ~750 HV, respectively. The hardness at NiTi/Ni₃Ti interface was ~650 HV. It was also noticed that the fracture was expected to occur apparently near the TiA|Ni interface because the hardness at the TiA|Ni interface (~750 HV) was much higher than the hardness at the Ni|SS interface (~330 HV), thus the TiA|Ni interface was more brittle as compared to the Ni|SS interface. Sam et al. (Ref. 19) in their study demonstrated that

DWJs failed through the TiA | Ni-alloy interface.

Here, the lateral deformation of the metals diffusion welded was of inelastic-type (plastic deformation); however, the plastic deformation of materials can be correlated with the elastic properties of the respective materials. There are three elastic moduli that derive from the spatial tri-dimensionality of the world. The three elastic moduli represent linear, planar, and volume effects on material. They are A) Young's modulus (E) [resistance to changes in length]; B) shear modulus (G) [resistance to transverse shift]; and C) bulk modulus (K) [resistance to compression or expansion]. Apart from these elastic moduli, there is another property called Poisson's ratio (μ) defined as the ratio of the transverse to the axial strain. These elastic moduli are generally anisotropic in the case of single crystals but, since the engineer usually works with polycrystalline materials in which the individual crystallites are arranged randomly, it can generally be assumed that the mechanical properties of materials are isotropic (Refs. 34–36). Although change in volume is related to the bulk modulus (K) property of the material, it can be related to the other elastic moduli using the following relationships (Equations 2 and 3) (Ref. 36):

$$E=3K(1-2\mu) \quad (2)$$

$$E=2G(1+\mu) \quad (3)$$

Using Equations 2 and 3, it could be perceived that Young's modulus of materials could explain the potential causes for significant differences in the lateral (plastic) deformation of the TiA and SS sides of the DWJs. The elastic (Young's) modulus of Ti-alloy (Ti-6Al-4V) and austenitic stainless steels (304 SS) is ~120 GPa (Ref. 3) and ~198 GPa (Ref. 37), respectively. As Young's modulus of Ti-6Al-4V is much lower as compared to Young's modulus of 304 SS, the TiA side of DWJs underwent an excess amount of lateral deformation as compared to the SS side of the respective DWJs; hence, it could be stated that the lateral deformation of the material is inversely proportional to its elastic modulus (Equation 4).

$$\text{Lateral deformation} \propto \frac{1}{\text{Elastic modulus}} \quad (4)$$

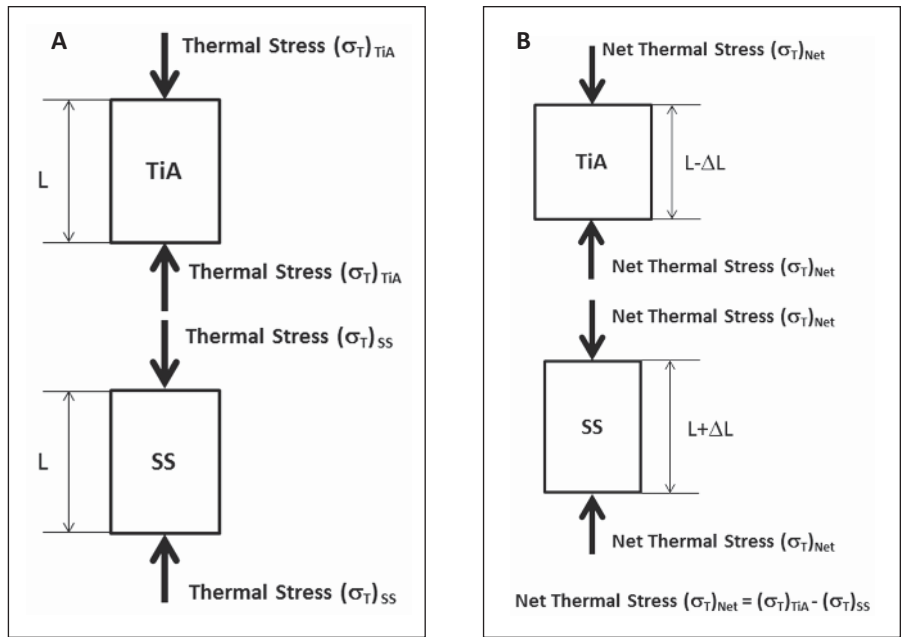


Fig. 11 — Free body diagram of the base materials of DWJs when thermal stresses act at A — 32°C (ambient temperature); B — 750°C (welding temperature).

Mathematically, the slope of the lateral deformation graph (Fig. 5) was in increasing order (Equation 5) with the welding pressure utilized; hence, the lower-range has less slope than the middle-range, and the middle-range has less slope than the higher-range of welding pressure.

$$\text{Welding pressure} \propto \text{lateral deformation of DWJs} \quad (5)$$

And it was also noticed that DWJs fractured at the TiA | Ni interface because the TiA | Ni interface (~750 HV) is much harder than the Ni | SS interface (~330 HV). Consequently, the TiA | Ni interface is more brittle as compared to the Ni | SS interface. In this study, it was also noted that the hardness differences at the TiA | Ni interface (=750 HV–200 HV=550 HV) was higher than that of the hardness difference at the Ni | SS interface (=400 HV–200 HV=200 HV). This observation testified the claim made by Simões et al. (Ref. 38) that DWJs fracture at the interfaces with high hardness differences. The fracture path observations also supported the claim that DWJs fractured along the TiA | Ni interface. This inference was quite consistent with the findings of the reported literature (Refs. 17–19) as well.

Base materials diffusion welded experienced stresses at three successive stages. First, the base materials under-

went deformation (purely elastic in nature) due to the static stresses caused by the dead load (welding pressure from 2 to 10 MPa) (Fig. 10A) application just before the furnace was switched 'ON.' Second, the base materials underwent deformation due to increasing dynamic thermal stresses (Fig. 10B) induced due to the linear thermal expansion of the other base materials because of the continuous increase in the furnace temperature from room temperature to the welding temperature (say, 750°C). Thermal stresses reach the maximum value at the welding temperature (750°C). And third, after reaching the designated welding temperature (say, 750°C) the base materials were held at the temperature for 60 min of the welding interval, i.e., during that time onward, the materials were typically subjected to a slowly continuous deformation at constant load (due to welding pressure applied and the thermal stresses induced, see Fig. 10B) at elevated temperatures. This phenomenon is termed as creep (Refs. 39–41).

Of these three stress fields encountered by the materials diffusion welded, the effect of static stresses caused by the dead load was trivial, while the effect of creep phenomenon on the materials diffusion welded was insignificant due to the low order time scale, whereas, the effect of thermal stresses due to

temperature changes had a huge impact on DWJs. Although the thermal stresses encountered by the material were uniformly increasing from the time the furnace was switched 'ON' till the time it reached the welding temperature (750°C).

Thermal stress (σ_T)_{TiA} on TiA due to thermal expansion of SS because of temperature change (ΔT) is ~1867.31 MPa (see Appendix), whereas the thermal ((stress) σ_T)_{SS} on SS due to thermal expansion of TiA is ~219.70 MPa (see Appendix). To calculate the net thermal stress (σ_T)_{Net} acting on the materials, a free body diagram (Fig. 11) of the materials diffusion welded was constructed. As both thermal stresses acting at the interface are opposite in nature, the net thermal stress ($(\sigma_T)_{Net} = (\sigma_T)_{TiA} - (\sigma_T)_{SS} = 1867.31 \text{ MPa} - 219.70 \text{ MPa}$) acting on the TiA and SS is ~1647.61 MPa ($(\sigma_T)_{Net}$).

Conclusion

This study was performed to know the extent of the influence of welding pressure on the evolution of interfacial microstructure, mechanical properties, and fracture features of solid-state diffusion welded joints of Ti-6Al-4V and 304 stainless steel using 200- μm -thick nickel as an interlayer. DWJs were processed in vacuum at 750°C (welding temperature) for 60 min (welding time) using welding pressure in the range of 2 to 10 MPa in step of 2 MPa. Characterization of the DWJs revealed the following:

1) Interfaces of the DWJs were free from the brittle Fe-Ti-based intermetallics due to the usage of Ni interlayer.

2) Optimal tensile strength of ~560 MPa along with substantial elongation of ~12% was obtained for the DWJs processed at 6-MPa welding pressure considering the minimal lateral deformation of the base metals welded. The tensile strength was more or less flat for the DWJs processed above 6 MPa. Elongation dropped insignificantly for the DWJs processed above 6 MPa.

3) TiA|Ni interface (~750 HV) was much harder than the Ni|SS interface (~330 HV).

4) It was clearly demonstrated that the failure of the DWJs was initiated and propagated specifically at the

TiA|Ni interface primarily due to higher hardness difference at the TiA|Ni interface compared to the Ni|SS interface.

5) The fracture surfaces for lower welding pressure (2 MPa) yielded brittle fracture morphologies; whereas the higher welding pressure (8 MPa) yielded mixed mode fractural features.

6) Apart from the welding pressure applied, an additional stress (thermal stress) of ~1647.61 MPa (compressive in nature) was induced on the materials (TiA and SS) diffusion welded due to linear thermal expansion of the materials at the welding temperature (750°C).

Appendix

Considering the materials to be homogeneous and with a uniform cross section throughout the length, stress (σ_T) in any material due to temperature change (ΔT) and the restriction in the linear thermal expansion of another material is given by the following relationship:

$$(\sigma_T)_1 = (E_T)_2 (\alpha_T)_2 (\Delta T) \text{ (Refs. 42, 43)}$$

where

(σ_T)₁: Thermal stress induced in the material '1' at temperature 'T'

(E_T)₂: Young's modulus of material '2' at temperature 'T'

(α_T)₂: Coefficient of thermal expansion of the material '2' at temperature 'T'

ΔT : Increase in the temperature

T: Welding temperature (750°C)

T₀: Room temperature (32°C)

$$\text{so, } \Delta T = T - T_0 = 750^\circ\text{C} - 32^\circ\text{C} = 718^\circ\text{C}$$

Case 1: Thermal stress (σ_T)_{TiA} on TiA due to thermal expansion of SS because of temperature change (ΔT)

$$(\sigma_T)_{TiA} = (E_T)_{SS} \times (\alpha_T)_{SS} \times (\Delta T)$$

$$(E_T)_{SS} = 133.37 \text{ GPa (Ref. 44)}$$

$$(\alpha_T)_{SS} = 19.5 \times 10^{-6} \text{ (m/m-}^\circ\text{C)} \text{ (Ref. 45)}$$

$$\text{so, } (\sigma_T)_{TiA} = 19.5 \times 10^{-6} \text{ (m/m-}^\circ\text{C)} \times$$

$$133.37 \text{ GPa} \times 718^\circ\text{C}$$

$$\text{so, } (\sigma_T)_{TiA} = 1867.31 \text{ MPa (compressive in nature)}$$

Case 2: Thermal stress (σ_T)_{SS} on SS due to thermal expansion of TiA because of temperature change (ΔT)

$$(\sigma_T)_{SS} = (E_T)_{TA} (\alpha_T)_{TA} (\Delta T)$$

Material properties at higher temperatures are less available in literature, so the authors extrapolated using the available resources at hand.

$$(E_T)_{TA} < 30 \text{ GPa (Ref. 46)}$$

$$(\alpha_T)_{TA} = 10.2 \times 10^{-6} \text{ (m/m-}^\circ\text{C)} \text{ (Ref. 47)}$$

$$\text{so, } (\sigma_T)_{SS} < 10.2 \times 10^{-6} \text{ (m/m-}^\circ\text{C)} \times 30 \text{ GPa} \times 718^\circ\text{C}$$

$$\text{so, } (\sigma_T)_{SS} < 219.70 \text{ MPa (compressive in nature)}$$

In all of the above calculations, thermal stresses induced in the nickel interlayer due to the expansion of both SS and TiA were not considered for the sake of its negligible thickness (~200 μm) with respect to the thickness of SS and TiA (both ~30 mm).

References

- Cobb, H. M. 2012. *Dictionary of Metals*. 70, Materials Park, Ohio, ASM International.
- Banerjee, D., and Williams, J. C. 2013. Perspectives on titanium science and technology. *Acta Materialia* 61: 844–879.
- Polmear, I. J. 2006. *Light Alloys— from Traditional Alloys to Nanocrystals*. 299–365, 339, Oxford: Butterworth-Heinemann.
- Yamada, M. 1996. An overview on the development of titanium alloys for non-aerospace application in Japan. *Materials Science and Engineering* 213A: 8–15.
- McGuire, M. F. 2008. *Stainless Steels for Design Engineers*. 69–90, Materials Park, Ohio, ASM International.
- Rodin, M. E., Semenov, A. N., Senov, M. I., Plyshevskii, M. I., Novozhilov, S. N., and Rassoshkina, N. S. 2013. Investigations of the strength of steel-titanium diffusion welded joints. *Welding International* 27(6): 482–484.
- He, P., Yue, X., and Zhang, J. H. 2008. Hot pressing diffusion bonding of a titanium alloy to a stainless steel with an aluminum alloy interlayer. *Materials Science and Engineering* 486A: 171–176.

8. Ghosh, M., Chatterjee, S., and Mishra, B. 2003. The effect of intermetallics on the strength properties of diffusion bonds formed between Ti-5.5Al-2.4V and 304 stainless steel. *Materials Science and Engineering* 363A: 268–274.
9. <http://www.aerospacemetals.com/>
10. Kahraman, N., Gulenc, B., and Findik, F. 2007. Corrosion and mechanical-microstructural aspects of dissimilar joints of Ti-6Al-4V and Al plates. *International Journal of Impact Engineering* 34: 1423–1432.
11. Sun, Z., Annergren, I., Pan, D., and Mai, T. A. 2003. Effect of laser surface remelting on the corrosion behaviour of commercially pure titanium sheet. *Materials Science and Engineering* 345A: 293–300.
12. Zeer, G. M., Zelenkova, E. G., Koroleva, Yu. P., Mikheev, A. A., and Prokopyev, S. V. 2013. Diffusion bonding through interlayers. *Welding International* 27(8): 638–643.
13. Hinotani, S., and Ohmori, Y. 1988. The microstructure of diffusion-bonded Ti/Ni interface. *Transactions of the Japan Institute of Metals* 29(2): 116–124.
14. Kundu, S., and Chatterjee, S. 2006. Interfacial microstructure and mechanical properties of diffusion-bonded titanium-stainless steel joints using a nickel interlayer. *Materials Science and Engineering* 425A: 107–113.
15. He, P., Zhang, J., Zhou, R., and Li, X. 1999. Diffusion bonding technology of a titanium alloy to a stainless steel web with an Ni interlayer. *Materials Characterization* 43: 287–292.
16. Kazakov, N. F. 1985. *Diffusion Bonding of Materials*. 11–12, Moscow, Mir Publishers.
17. Thirunavukarasu, G., Kundu, S., Mishra, B., and Chatterjee, S. 2014. Effect of bonding temperature on interfacial reaction and mechanical properties of diffusion-bonded joint between Ti-6Al-4V and 304 stainless steel using nickel as an intermediate material. *Metallurgical and Materials Transactions* 45A: 2067–2077.
18. Thirunavukarasu, G., Kundu, S., Mishra, B., and Chatterjee, S. 2014. Effect of bonding time on interfacial reaction and mechanical properties of diffusion-bonded joint between Ti-6Al-4V and 304 stainless steel using nickel as an intermediate material. *Metallurgical and Materials Transactions* 45A: 2078–2090.
19. Sam, S., Kundu, S., and Chatterjee, S. 2012. Diffusion bonding of titanium alloy to micro-duplex stainless steel using a nickel alloy interlayer: Interface microstructure and strength properties. *Materials and Design* 40: 237–244.
20. Kundu, S., Mishra, B., Olson, D. L., and Chatterjee, S. 2013. Interfacial reactions and strength properties of diffusion bonded joints of Ti64 alloy and 17-4PH stainless steel using nickel alloy interlayer. *Materials and Design* 51: 714–722.
21. Kundu, S., Sam, S., and Chatterjee, S. 2013. Interfacial reactions and strength properties in dissimilar titanium alloy/Ni alloy/microduplex stainless steel diffusion bonded joints. *Materials Science and Engineering* 560A: 288–295.
22. John, V. 1992. *Introduction to Engineering Materials*, p. 104, London, Macmillan.
23. Shanmugarajan, B., and Padmanabham, G. 2012. Fusion welding studies using laser on Ti-SS dissimilar combination. *Optics and Lasers in Engineering* 50: 1621–1627.
24. Wang, T., Zhang, B. G., and Feng, J. C. 2014. Influences of different filler metals on electron beam welding of titanium alloy to stainless steel. *Transactions of Nonferrous Metals Society of China* 24: 108–114.
25. Balasubramanian, M. 2015. Development of processing windows for diffusion bonding of Ti-6Al-4V titanium alloy and 304 stainless steel with silver as intermediate layer. *Transactions of Nonferrous Metals Society of China* 25: 2932–2938.
26. Balasubramanian, M. 2016. Characterization of diffusion-bonded titanium alloy and 304 stainless steel with Ag as an interlayer. *The International Journal of Advanced Manufacturing Technology* 82: 153–162.
27. Tomashchuk, I., Sallamand, P., Belyavina, N., and Pilloz, M. 2013. Evolution of microstructures and mechanical properties during dissimilar electron beam welding of titanium alloy to stainless steel via copper interlayer. *Materials Science and Engineering* 585A: 114–122.
28. Norouzi, E., Atapour, M., Shamanian, M., and Allafchian, A. 2016. Effect of bonding temperature on the microstructure and mechanical properties of Ti-6Al-4V to AISI 304 transient liquid phase bonded joint. *Materials and Design* 99: 543–551.
29. Kumar, R., and Balasubramanian, M. 2015. Experimental investigation of Ti-6Al-4V titanium alloy and 304L stainless steel friction welded with copper interlayer. *Defence Technology* 11: 65–75.
30. Fischer, T. 2009. *Materials Science for Engineering Students*. 97, 19–21, 112–115, San Diego, Academic Press.
31. Porter, D. A., Easterling, K. E., and Sherif, M. Y. 2009. *Phase Transformations in Metals and Alloys*. 65, 7–9, 100–104, Boca Raton, CRC.
32. Jr Messler, R. W. 2011. *The Essence of Materials for Engineers*. 307–308, Burlington, Massachusetts: Jones & Bartlett.
33. Dieter, G. E. 1988. *Mechanical Metallurgy*. 231–233, Singapore, McGraw-Hill.
34. Kelly, P. F. 2015. *Properties of Materials*. 7–12, Boca Raton, CRC.
35. White, M. A. 2012. *Physical Properties of Materials*. 383–394, Boca Raton, CRC.
36. Lovell, M. C., Avery, A. J., and Vernon, M. W. 1984. *Physical Properties of Materials*. 87–92, Wokingham, Berkshire, UK, Van Nostrand Reinhold.
37. Brandes, E. A., and Brook, G. B. 1992. *Smithells Metals Reference Book*. 15–3, Oxford, Butterworth-Heinemann.
38. Simões, S., Viana, F., Koçak, M., Ramos, A. S., Vieira, M. T., and Vieira, M. F. 2011. Diffusion bonding of TiAl using reactive Ni/Al nanolayers and Ti and Ni foils. *Materials Chemistry and Physics* 128: 202–207.
39. Gottstein, G. 2007. *Physical Foundations of Materials Science*. 281–282, New Delhi, Springer.
40. Finnie, I., and Heller, W. R. 1959. *Creep of Engineering Materials*. 16, New York, McGraw-Hill.
41. Hetnarski, R. B., and Eslami, M. R. *Thermal Stresses—Advanced Theory and Applications*. 499–510, Springer.
42. Beer, F. P., Jr Johnston, E. R., and DeWolf, J. T. 2006. *Mechanics of Materials*. 74–75, New Delhi, Tata McGraw-Hill.
43. Srinath, L. S., Desayi, P., Murthy, N. S., and Ramu, S. A. 2001. *Strength of Materials*. 60–61, New Delhi, Macmillan India.
44. <http://bssa.org.uk/topics.php?article=139>.
45. <http://asm.matweb.com/search/SpecificMaterial.asp?bassnum=MQ304A>
46. Veiga, C., Davim, J. P., and Loureiro, A. J. R. 2012. Properties and applications of titanium alloys: A brief review. *Reviews on Advanced Materials Science* 32: 133–148.
47. <http://asm.matweb.com/search/SpecificMaterial.asp?bassnum=MTP641>.

Microstructure and Mechanical Property of Aluminum/Copper Dissimilar Friction Welded Joints

Sound aluminum/copper dissimilar joints can be produced with continuous drive friction welding after a 2-h postweld heat treatment at 100°C

BY S. CHEN, H. DONG, P. LI, S. NIU, L. YU, AND H. JI

ABSTRACT

Continuous drive friction welding of commercial pure aluminum to copper bars was conducted. Sound joints were produced after postweld heat treatment (PWHT) at 100°C for 2 h with an ultimate tensile strength of 91 MPa and a bending angle of 90 deg without breaking. All heat-treated tensile samples failed at the aluminum/copper interface with a cleavage fracture feature. The microstructure, composition, and fractograph of the joints were analyzed with an electron probe microanalyzer and a scanning electron microscope. Copper was stirred into the aluminum matrix due to mechanical excavation during welding. After PWHT at 100°C for 2 h, the minimized amount of Cu distributed at the interface, which benefited the mechanical property of the joints. Massive formations of brittle intermetallic compounds (IMCs) at the interface could deteriorate the mechanical property of joints. Fractographs revealed that Al-Cu IMCs initially formed at one-third of the radius of the faying surface due to comprehensive influences of rotation speed and friction pressure.

KEYWORDS

- Continuous Drive Friction Welding • Aluminum/Copper Dissimilar Joints
- Postweld Heat Treatment • Mechanical Property • Intermetallic Compounds

Introduction

Application of copper is quite prominent in electronic and electrical industries due to its excellent conductivity, but it is limited by copper's high density and price. Recently, dissimilar materials welding between aluminum and copper has attracted plenty of attention due to the scarcity of copper and the relatively acceptable conductivity of aluminum. Aluminum/copper welded structures also offer the benefits of cost saving and weight reduction.

Veerkamp (Ref. 1) reported various types of aluminum copper welded structures had been used in electrical applications, especially in high direct-current bus systems. However, several challenges prevent sound aluminum/copper joints, such as oxidation, the

high conductivity of base materials, the great difference in thermal-physical properties between the two materials, and the inevitable formation of brittle intermetallic compounds (IMCs) during welding.

The early investigation on aluminum/copper diffusion system undertaken by Funamizu and Watanabe (Ref. 2) showed the formation of Al-Cu IMCs was controlled by the process of volume diffusion mechanism, and the rate of layer growth obeyed the parabolic law. Peng et al. (Ref. 3) reported that as time and/or temperature of heat treatment increased, Kirkendall voids formed and agglomerated, resulting in a weak layer in the roll-bonded aluminum/copper interface.

Therefore, to avoid the massive generation of Al-Cu IMCs and Kirkendall voids, low heat input welding

methods became the research focus in joining aluminum and copper. Mai and Spowage (Ref. 4) achieved laser welding between oxygen-free copper and 4047 aluminum alloy at lower welding speeds, but they also claimed it was difficult to obtain a sound aluminum/copper joint by fusion welding due to the high reflectivity and high thermal conductivity of the two materials.

A large number of recent papers have discussed friction stir welding of aluminum alloy and copper plates. Xue et al. (Ref. 5) focused on the relationship of welding parameters to the microstructure and mechanical property of aluminum/copper friction stir welded joints. Also studied by Xue et al. (Ref. 6) were the influences of postweld heat treatment (PWHT) on the interfacial microstructure evolution, tensile strength, and fracture behavior of aluminum copper dissimilar friction stir welded joints. Beygi et al. (Ref. 7) performed friction stir welding of aluminum/copper bilayer sheets and observed the anomalous structure of Al-Cu IMCs in backscattered electron (BE) images.

Friction welding (FW) relies on relative motion between the parts being joined to generate friction heat while pressure is applied. Meshram et al. (Ref. 8) documented that FW could produce sound dissimilar joints with acceptable mechanical property. Figure 1 schematically shows the continuous drive friction welding process of aluminum and copper bars applied in this research. This welding process can be briefly distinguished into four main stages: (a) rotating and ap-

S. CHEN, H. DONG (donghg@dlut.edu.cn), P. LI, S. NIU, and L. YU are with the School of Materials Science and Engineering, Dalian University of Technology, Dalian, China. DONG is also with the State of Key Laboratory of Advanced Welding and Joining, Harbin Institute of Technology, Harbin, China. LI is also with the State Key Laboratory of Solidification Processing, Northwestern Polytechnical University, Xi'an, China. H. JI is with Shanghai Aerospace Equipment Manufacturer, Shanghai, China.

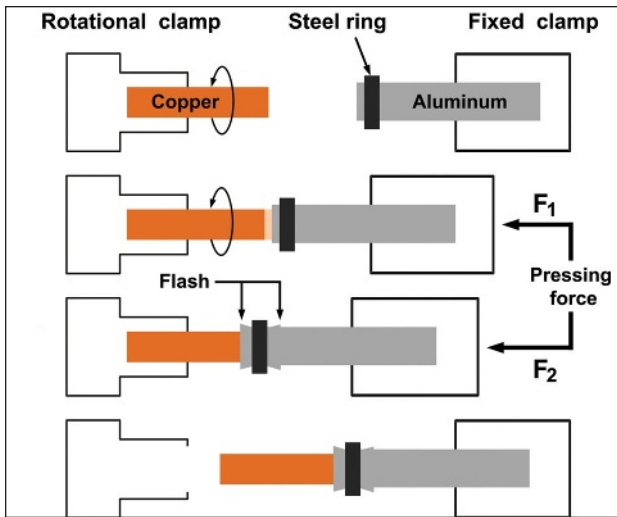


Fig. 1 — Schematic illustration of the continuous drive friction welding process.

proaching, (b) frictional heating, (c) forging, and (d) retreating.

During welding, friction heat is generated by the comprehensive effect of rotational motion and friction load (F_1), and then forging is achieved by forging load (F_2). Considering the large difference in hardness between aluminum (HB 18) and copper (HB 65) in this research, to avoid severe deformation on the aluminum bar, a 15-mm-length steel ring was set on the aluminum bar with a 10-mm distance from the faying surface before welding. These steel rings were made from plain carbon steel with inner and external diameters of 16 mm and 25 mm, respectively.

Braunović and Aleksandrov (Ref. 9) systematically studied the influences of Al-Cu IMCs on the electric and mechanical property of aluminum copper dissimilar friction welded joints, and documented that Al-Cu IMCs at the interface could seriously impair the mechanical property when the total width of IMCs phases at the interface exceed $2\ \mu\text{m}$. The coupled effect of the main parameters of the aluminum/copper dissimilar FW process on the mechanical property of joints was statistically studied by Yilbas et al. (Ref. 10).

Lee et al. (Ref. 11) employed various annealing conditions to research the electric and mechanical property of aluminum/copper dissimilar friction welded joints, and experimentally determined the growth kinetic of Al-Cu IMCs along the aluminum/copper interface. The influences of the initial geometry of

prestrain aluminum alloy and copper bars on FW were investigated by Manjubhargavi et al. (Ref. 12). The large residual stress leaving in the joint after the FW process deteriorated the bending property, which is significant for the aluminum/copper joints used in the electric power industry.

Dong et al. (Ref. 13) reported PWHT could enhance comprehensive properties of friction welded joints between TC4 titanium alloys and 40Cr steel bars. Therefore, considering the residual stress leaving in the joint, PWHT was also performed in this research.

In addition, although some papers have reported the effect of PWHT on the mechanical property of aluminum/copper joints, there are few reports on low-temperature heat treatments (less than 300°C) and

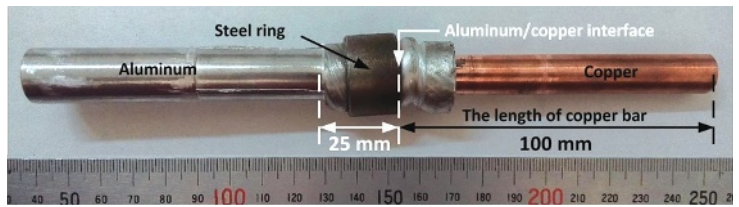


Fig. 2 — The appearance of the as-welded sample.

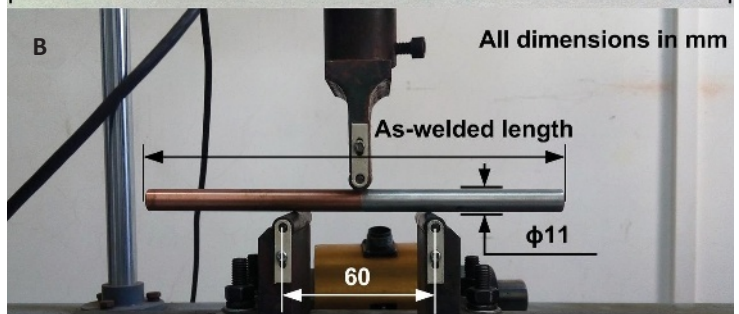
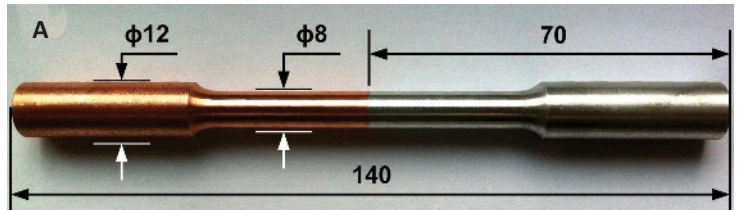


Fig. 3 — Dimensions: A — Tensile sample; B — three-point bending test sample.

short dwelling times (1–2 h) for aluminum/copper friction welded joints.

This paper will focus on the effect of PWHT with low temperature and short dwelling time on the mechanical property and microstructure of aluminum/copper friction welded joints.

Experimental Procedure

Continuous drive friction welding of commercially pure aluminum bars to copper bars was conducted using a HSMZ-20 friction welding machine produced by Harbin Welding Institute, China. The nominal composition of the base materials is listed in Table 1. The ultimate tensile strength (UTS)

Table 1 — Nominal Composition of Base Materials

Base Materials		Composition (wt-%)				
Aluminum	—	—	Fe	Si	Ti	Al
	—	—	0.2	0.17	0.13	Bal.
Copper	S	Bi	Sb	As	Fe	Cu
	0.005	0.001	0.002	0.002	0.005	Bal.

forced air electrical furnace.

Tensile and bending tests were carried out to evaluate the effect of PWHT on the mechanical property of the resultant joints. The dimensions of the tensile test sample is shown in Fig. 3A. According to China National Standards GB/T 232-2010, selected samples with as-welded length and a diameter of 11 mm (Fig. 3B) were employed for the three-point bending test over a 60-mm span with a crosshead speed of 0.5 mm/s. Both tensile and bending tests were performed using the DNS-100 universal test machine at ambient temperature. All mechanical results of the tensile and bending tests were obtained by averaging the results of three individual samples.

Metallographic samples prepared from the as-welded and PWHT conditions were subjected to mechanical grinding and final polishing with a solution of 0.5- μ m silica suspension, and chemically etched with Keller's reagent (4 mL HF, 6 mL HCl, 10 mL HNO₃, and 180 mL H₂O). The microstructural features were obtained using a Leica MEF4A optical microscope.

Microstructural morphology and composition analysis of joints were carried out by electron probe micro-analyzer (EPMA) (Shimadzu, Japan) complemented with a wavelength dispersive spectrometer (WDS). The fractographs and composition detection were presented by EPMA and JSM-5600LV scanning electron microscope (SEM) (Zeiss, Germany) with energy dispersive spectrometer (EDS) under an accelerating voltage of 15 kV.

Results

Mechanical Property and Microstructure

Braunović and Aleksandrov (Ref. 9) and Xue et al. (Ref. 6) reported PWHT had remarkable influences on the evolution of Al-Cu IMCs, leading to a variation in the mechanical property of aluminum/copper joints. The results of tensile and bending tests of aluminum copper dissimilar friction welded joints are listed in Table 3. As shown, the UTS and bending angle of joints initially increased with the help of PWHT, and reached an optimal mechanical property of 91 MPa in UTS

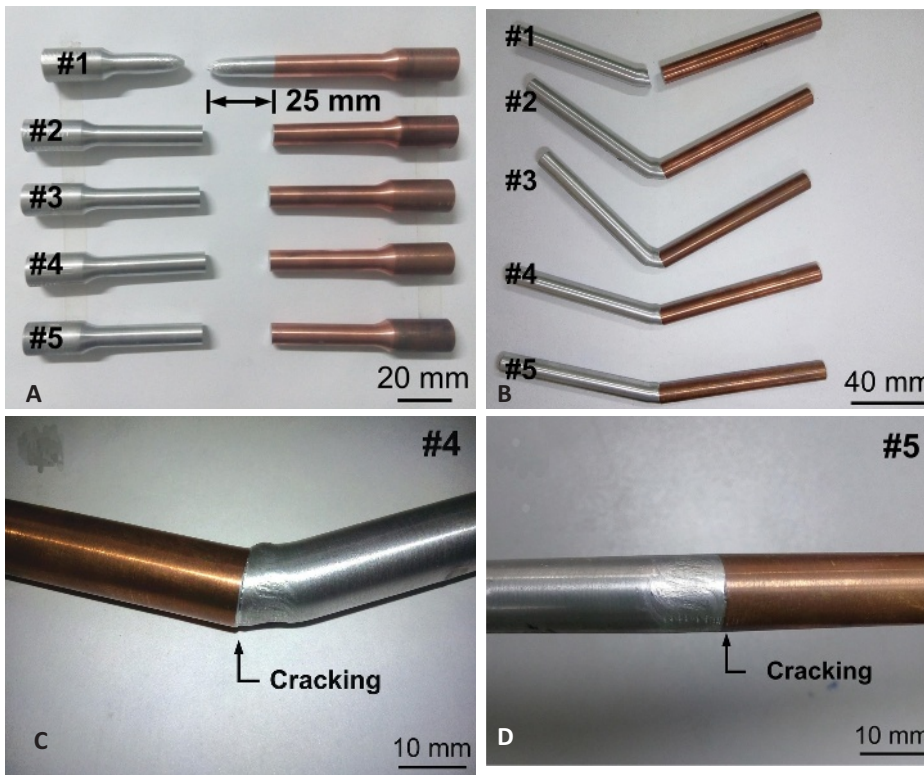


Fig. 4 — Fractured samples: A — Tensile test; B — bending test and the details on the bottom of the bending samples; C — sample 4; D — sample 5.

and elongation of copper bars were 295 MPa and 3%, and those of aluminum bars were 90 MPa and 80%, respectively.

The copper bars were machined to 100 mm in length and 12 mm in diameter. The dimensions of the aluminum bars were 120 mm in length and 16 mm in diameter. Both the aluminum and copper bars had 60 deg chamfers with 1-mm thickness at the faying surfaces on two ends after processing. Before welding, the faying surfaces of the aluminum and copper bars were polished by SiC paper up to grit 1000 for removal of oxide film, and then cleaned by acetone.

After trial welding, the optimized welding parameters were determined. The friction load (F_1) and forging load

(F_2) displayed in Fig. 1 were set at 75 and 100 MPa, respectively, the burn-off length remained around 22 mm, the forging time was 5 s, and the total time of the welding process was 12 s. The as-welded sample is shown in Fig. 2.

As mentioned, the copper bar could be considered inconsumable during welding due to the higher hardness of copper than that of aluminum. The aluminum/copper interface location was approximately determined in Fig. 2, based on the original length of the copper bar. After welding, the samples labeled from 2 to 5 were heat treated under four conditions, as listed in Table 2. The samples were subjected to heat treatments for a given time and then cooled to room temperature in a

Table 2 — PWHT Parameters for Aluminum/Copper Friction Welded Samples

Sample	Temperature (°C)	Dwelling Time (h)
1	—	—
2	100	1
3	100	2
4	200	2
5	300	2

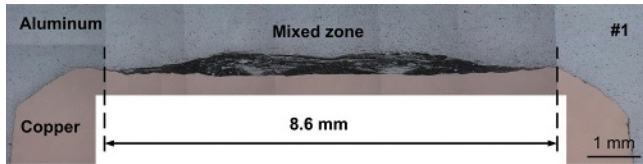


Fig. 5 — Metallograph of sample 1 at the aluminum/copper interface.

and 90 deg in bending angle under PWHT at 100°C for 2 h, as shown in the results for sample 3.

Then, UTS deteriorated from 91 to 51 MPa with the increasing temperature of PWHT. Most tensile samples failed at the aluminum/copper interface, as shown in Fig. 4A, except sample 1, which necked and fractured on the aluminum side. This indicated that the aluminum/copper interface is the weakest part of the heat-treated joint. The fracture analysis will be presented later.

Figure 4B presents fractured samples after the bending test. Sample 1 fractured entirely at the interface, leaving some extent of deformation on the aluminum side. As mentioned previously, the satisfactory bending angle was obtained in sample 3, which could reach 90 deg without breaking. Afterward, the bending angle dropped sharply, just like the variation tendency of UTS. Samples 2, 4, and 5 failed during the bending tests because cracks formed on the bottom of the bending samples, as presented in Fig. 4C, D.

Because of the large difference in hardness, flash formed during the FW process only from aluminum, whereas copper didn't participate in flash formation. This phenomenon was also reported by Manjubhargavi et al. (Ref. 12).

The metallograph of sample 1 is displayed in Fig. 5. It is obvious that severe mechanical stir action and mechanical excavation occurred, leaving a concave interface on the copper side, where perhaps there was copper that detached from the base material. Because of the difference in corrosion property between base materials and Al-Cu IMCs, there is an obvious black-mixed zone consisting of aluminum, copper, and Al-Cu IMCs.

It is worth noting the diameter of the tensile sample at the interface is 8 mm, which is less than the mixed zone diameter. According to the frac-

ture position shown in the mechanical test results, this mixed zone may play a predominant role in the mechanical property of aluminum/copper dissimilar friction welded joints.

To understand the effect of PWHT on the evolution of the microstructure at the interface of the aluminum/copper joints, the composition analysis of all samples was performed as shown in Fig. 6. The BE images clearly show copper was detached from the base material and stirred into the aluminum matrix. The composition distributions at the interface varied with the PWHT condition.

There is no big difference between samples 1 and 2 in the distribution of Cu on the aluminum side, except for a relatively large decrease or absence in sample 3. The agglomeration of Cu occurred both in samples 4 and 5, whereas it was more serious in sample 5. The distribution of Cu in the aluminum matrix is consistent with the fluctuation of UTS, which implies the distribution of Cu influences the mechanical property of friction welded joints.

Beygi et al. (Ref. 7) reported many lamellar structure phases formed in aluminum/copper dissimilar friction stir welded joints. This phenomenon is also

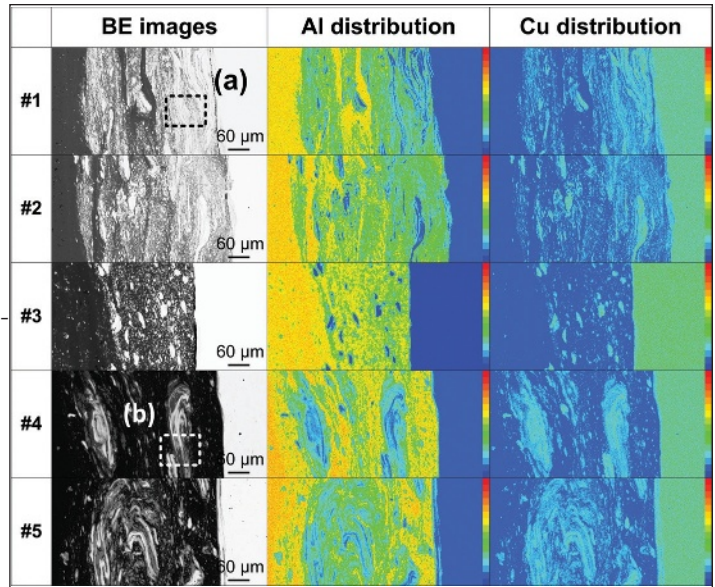


Fig. 6 — Composition analysis of all samples at the interface center.

observed in Fig. 7A from the magnified view marked in the dotted rectangle in Fig. 6. Composition analysis results listed in Table 4 reveal that the lamellar structure phases may consist of copper and Al₂Cu phases. There were various phases in the magnified view of sample 4, as shown in Fig. 7B.

According to the nature of the BE image and the results of composition analysis, as the color deepened from white to black, the Al content in the phases increased, which implied the existence of various Al-Cu IMCs due to the PWHT. The same phenomenon was also observed in the microstructure of sample 5 with a higher PWHT temperature than sample 4.

Fracture Morphology

In this research, the fracture surfaces from samples 2 to 5 on the copper side revealed a pale grey aluminum layer, which Manjubhargavi et al. (Ref. 12) attributed to interatomic diffusion during the aluminum/copper FW process. Frac-

Table 3 — Results of Tensile and Bending Tests

Sample	UTS (MPa)	Fracture Position	Bending Angle (deg)
1	68	Aluminum side	40
2	76	Interface	66
3	91	Interface	>90
4	74	Interface	35
5	51	Interface	22

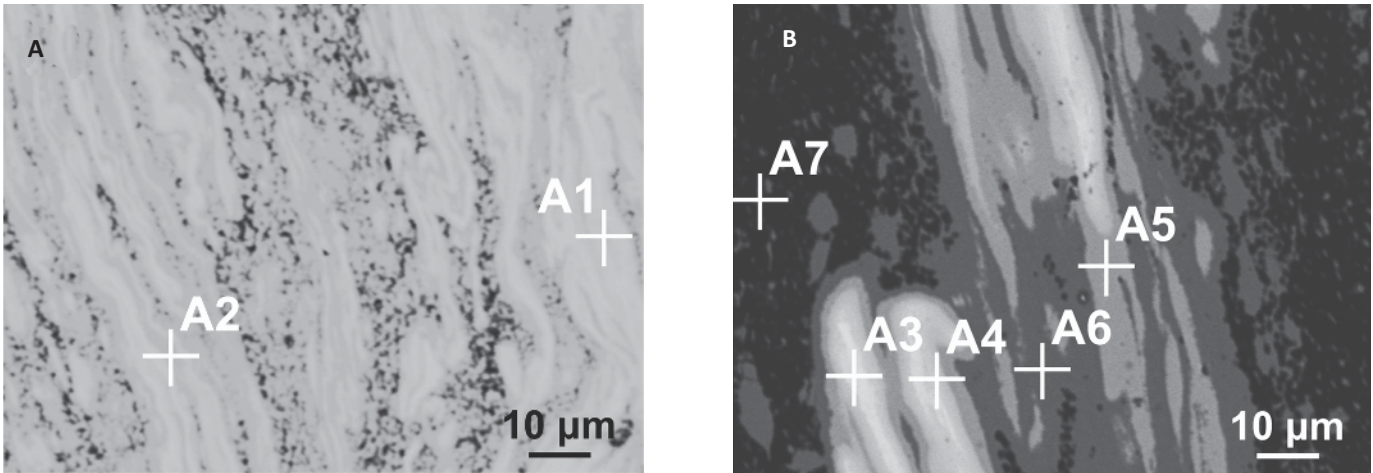


Fig. 7 — Magnified views: A — Sample 1; B — sample 4 marked in Fig. 6.

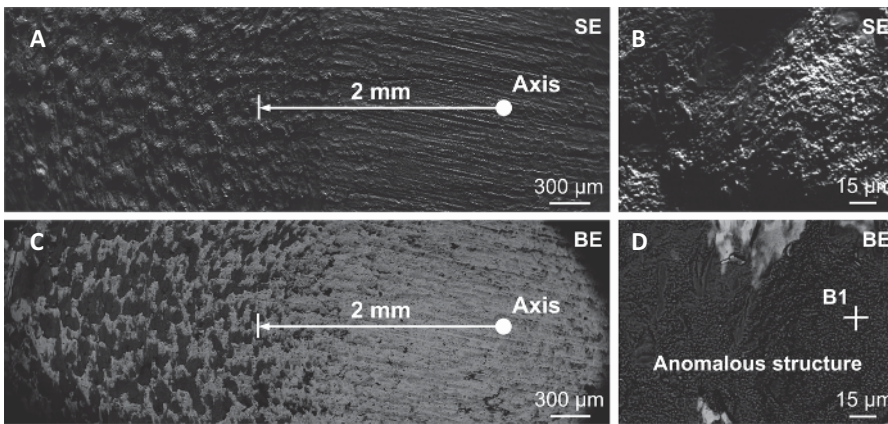


Fig. 8 — A, B — SE images; C, D — BE images of fracture of tensile sample 2 on the copper side.

topographs of sample 2 are presented in Fig. 8. Observable in the secondary electron (SE) images are the existence of small hemispherical “embossments” at a concentric annulus area beyond 2 mm radius, which showed the anomalous structure phases in the BE image. These phases were also reported by Beygi et al. (Ref. 7).

Composition analysis at point B1

listed in Table 5 suggests anomalous structure phases seem to be mainly Al_2Cu . According to the distribution of anomalous structure phases, these phases formed due to the synthetic effect of friction heat and pressure. Not only were anomalous structure phases found in the fracture surface of tensile sample 2, but these phases were also observed on bending sample 1.

The morphology of the anomalous structure phases evolved with PWHT conditions. Figure 9A is the BE image of sample 3 on the fracture surface of the copper side. It shows that some unchanged anomalous structure phases remain, but others transformed into strip structure phases. Additionally, many cracks generated at the strip structure phases and propagated through the strip direction.

The same phenomenon was also found in sample 4, as shown in Fig. 9B, but the size of the strip structure phases diminished with the disappearance of the anomalous structure phases. However, the BE image of sample 5 was totally changed compared with that of former samples. In Fig. 9C, white phases are distributed on the fracture surface and surrounded by dark phases. According to the composition analysis results in Table 5, these dark phases (B2) and white phases (B3) seem to be mainly Al_2Cu and Al_2Cu_3 , respectively.

According to the fractographs of tensile samples under different PWHT conditions, it can be determined that PWHT is responsible for the formation and growth of IMCs at the interface, resulting in influences on the mechanical property of joints.

SEM images revealed more details about the tensile fracture behavior of heat-treated joints. Shallow cleavage step patterns were clearly observed in the fracture surfaces of samples 3 and 5 on the copper side, as shown in Figs. 10A and 10C, respectively. The same patterns also existed on the fracture surfaces of samples 2 and 4. In the fur-

Table 4 — Major Composition of Different Positions Marked in Fig. 7

Position	Composition (at.-%)				Possible Phase
	Al	Cu	O	Al/Cu	
A1	16.60	80.71	2.69	0.2	Copper
A2	63.38	31.65	4.97	2.0	Al_2Cu
A3	12.28	82.25	5.47	0.1	Copper
A4	29.46	58.64	11.90	0.5	Al_4Cu_9/Al_2Cu_3
A5	49.34	42.20	8.46	1.2	AlCu
A6	61.99	32.49	5.51	1.9	Al_2Cu
A7	92.42	6.36	1.22	14.5	Aluminum

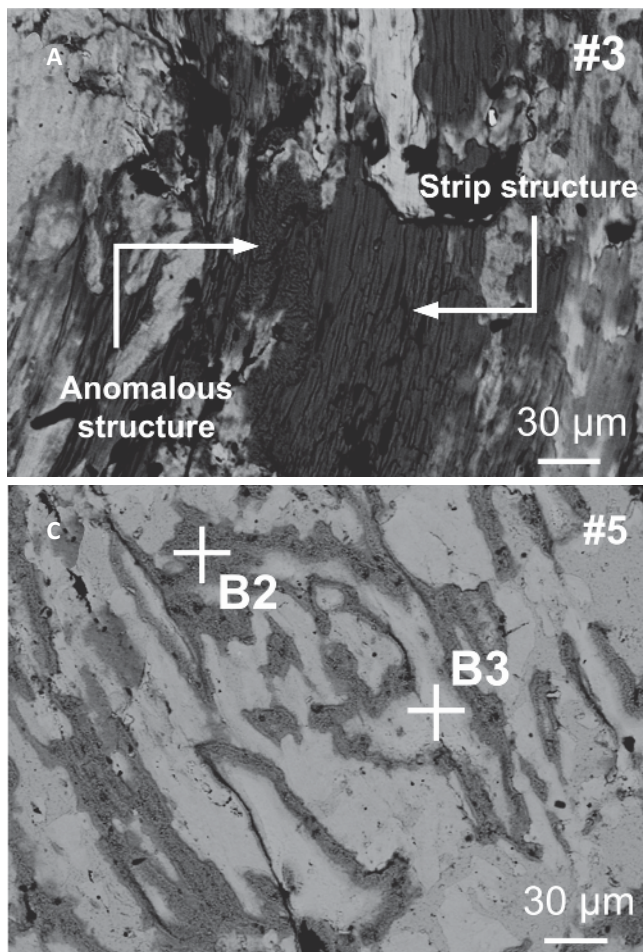


Fig. 9 — BE images on the fracture surface of tensile: A — Sample 3; B — sample 4; C — sample 5 on the copper side.

ther magnified views of Figs. 10B and 10D, the intergranular fracture feature on sample 3 turned to the transgranular one on sample 5 by PWHT, which is consistent with what Xue et al. (Ref. 6) reported.

According to composition analysis results, equiaxed grains on the fracture surface of sample 3 seemed to be mainly Al_2Cu , but Al_2Cu_3 was detected on sample 5, which is consistent with former analysis with EPMA.

Discussion

As mentioned, this research focused on the effect of PWHT on the microstructural evolution and mechanical property of aluminum/copper joints. The sound aluminum/copper joints were obtained in sample 3, and had an optimal mechanical property of 91 MPa in UTS and 90 deg in bending angle without breaking. Heat-treated samples fractured at the aluminum/copper interface in the tensile test, and mainly cracked at the bottom of samples during the bending test.

However, sample 1 necked and fractured on the aluminum side around 25 mm away from the interface. As Fig. 2 shows, the root of flash on the aluminum side is approximately located at the fracture position of sample 1 in Fig. 4A. The results are mainly caused by residual stress leaving in deformed aluminum. After friction welding, residual stress caused by severe deformation remained on the aluminum side, which weakened the mechanical property of the joints.

Residual stress leaving in the joint also resulted in the total fracture of sample 1, rather than a crack at the bottom during the bending test. During PWHT, the residual stress in the joint was gradually released, and the mechanical property was improved. Meanwhile, Al-Cu IMCs formed and grew at the interface. Therefore, the

weakest position of the joints shifted from the aluminum side to the aluminum/copper interface.

Composition analysis in Fig. 6 revealed the minimized amount of Cu distributed on the aluminum side under 100°C PWHT for 2 h. The sound aluminum/copper joints were also obtained under this PWHT condition. As the temperature of PWHT increased, Cu agglomerated on the aluminum side in samples 4 and 5, which was consistent with the sharp drops in the mechanical property of the aluminum/copper joints.

According to the study by Lee et al. (Ref. 11), aluminum/copper friction welded joints with excellent tensile strength reaching 87 MPa were obtained under PWHT at 375 K (100°C) for 129.6 ks (36 h), and fracture occurred at the heat-affected zone on the aluminum alloy side. With the increasing temperature of PWHT, the tensile strength tended to decrease, and the fracture location changed from the heat-affected zone to the aluminum/copper interface, which

Table 5 — Major Composition of Different Positions Marked from Figs. 8 to 10

Position	Composition (at.-%)				Possible Phase
	Al	Cu	O	Al/Cu	
B1	64.48	31.50	4.02	2.0	Al_2Cu
B2	55.49	32.55	11.95	1.7	Al_2Cu
B3	35.71	58.36	5.92	0.6	Al_2Cu_3
C1	63.12	34.33	2.55	1.8	Al_2Cu
C2	40.15	56.15	3.10	0.7	Al_2Cu_3

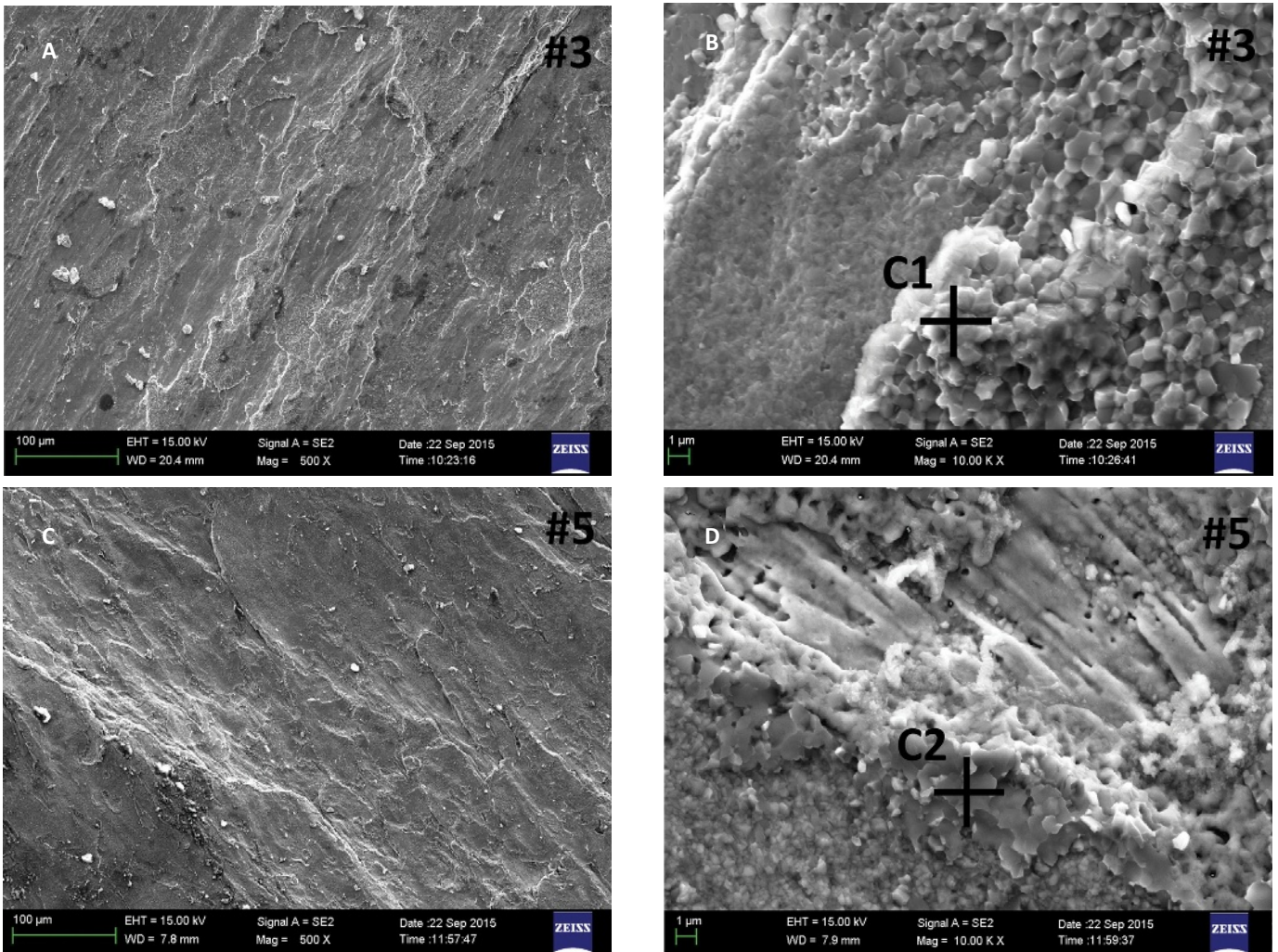


Fig. 10 — Fractographs of tensile: A, B — Sample 3 ; C D — sample 5 on the copper sides.

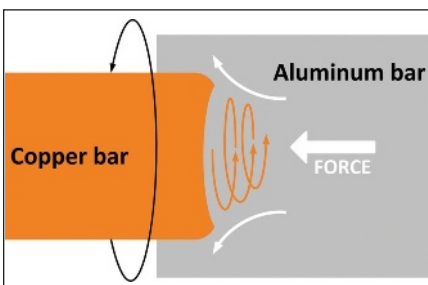


Fig. 11 — Schematic illustration of stirring action at the aluminum/copper interface.

had the same tendency as the results obtained in this research.

Xue et al. (Refs. 5, 14) reported copper particles friction stirred into the aluminum matrix would react with aluminum, resulting in the formation of IMCs. Severe mechanical stir action and mechanical excavation can be observed in Figs. 5 and 6, resulting in the detach-

ment of copper from the base material. According to the aluminum copper concave interface and lamellar structure phases in Fig. 7A, it is assumed copper was stirred into the aluminum side spirally and pressed to the aluminum/copper interface, as schematically shown in Fig. 11. Composition analysis shows lamellar structure phases consist of copper and Al_2Cu phases, which may be attributed to short-circuit diffusion through the defects caused by the severe mechanical stir action.

The evolution of Al-Cu IMCs at the interface is related to the reaction temperature, which was mainly decided by PWHT conditions in this research. As Fig. 7 shows, the lamellar structure phases observed in sample 1 transformed into the combinational structure phases, consisting of various kinds of IMCs in sample 4 due to PWHT.

Anomalous structure phases were observed at a concentric annulus area

beyond 2 mm in radius on the fracture surface of sample 2. It can be explained by the nature of the FW process. At the beginning of welding, the faying surfaces of metal bars are in the elastic contact stage. The variation of the temperature field along the radius was inhomogeneous, because the relative rotation speed was zero at the center but increased to the maximum at the edge, and the friction pressure unevenly distributed on the contacted faying surfaces between the aluminum and copper bars.

Under the comprehensive influences of rotation speed and friction pressure, generally, the heating starts at one-third or half of the radius of the faying surfaces from the center, and leads to an annular heated zone, which is also supported by Li et al. (Ref. 15). In our research, since the radius of the copper bar was 6 mm, it is reasonable that the Al-Cu IMCs formed at a concentric an-

nulus area beyond radius 2 mm. The composition analysis indicated these anomalous structure phases seem to be mainly Al₂Cu.

Additionally, it was found that the morphology and composition of IMCs changed on the fracture surface, and cracks formed and propagated along IMCs. All of these revealed that the mechanical property of aluminum/copper dissimilar friction welded joints was controlled by the formation and growth of Al-Cu IMCs in this research. Furthermore, the cleavage fracture feature was observed in all heat-treated samples, and in further magnified views, the intergranular fracture mode turned to transgranular fracture mode due to PWHT.

Conclusions

In this paper, the effect of PWHT on the mechanical property, microstructure, and fracture feature of friction welded joints between commercially pure aluminum and copper bars was investigated. The main conclusions are drawn as follows:

- 1) Sound joints were produced under PWHT at 100°C for 2 h with UTS of 91 MPa and a bending angle reaching 90 deg without breaking. The mechanical property was impaired by PWHT with higher temperatures. Heat-treated samples failed at the interface during the tensile test, but the as-welded sample fractured on the aluminum side.
- 2) Copper was stirred into the aluminum matrix due to mechanical excavation during welding. After PWHT at 100°C for 2 h, the minimized amount of Cu distributed on the aluminum side, which enhanced the mechanical property of aluminum/copper joints. Various Al-Cu IMCs formed and overgrew under PWHT at 200° or 300°C for 2 h.
- 3) Fractographs showed Al-Cu IMCs initially formed at one-third of the radius of the faying surface from the center due to the comprehensive

influences of rotation speed and friction pressure. Additionally, IMCs could generate and propagate cracks. Moreover, all heat-treated samples presented the cleavage fracture feature, and in further magnified views, the intergranular fracture mode turned to transgranular fracture mode under the effect of PWHT.

Acknowledgments

This work was financially supported by the National Natural Science Foundation of China (Grant No. 51374048 and 50904012); the Fundamental Research Funds for the Central Universities (No. DUT13ZD209 and DUT16RC(3)009); Collaborative Innovation Center of Major Machine Manufacturing in Liaoning; State Key Laboratory of Advanced Welding & Joining, Harbin Institute of Technology (AWJ-M14-06); and State Key Laboratory of Solidification Processing in NWPU (SKLSP201614).

References

1. Veerkamp, W. 1995. Copper-to-aluminum transitions in high direct-current bus systems. *Petroleum and Chemical Industry Conference*. Industry Applications Society, pp. 187–195. doi: 10.1109/PCI-CON.1995.523953.
2. Funamizu, Y., and Watanabe, K. 1970. Interdiffusion in the Al-Cu system. Autumn Meeting of the Japan Institute of Metal, Hiroshima, Japan, pp. 147–152.
3. Peng, X., Wuhler, R., Heness, G., and Yeung, W. 1999. On the interface development and fracture behaviour of roll bonded copper/aluminium metal laminates. *J. Mater. Sci.* 34(9): 2029–2038.
4. Mai, T., and Spowage, A. 2004. Characterisation of dissimilar joints in laser welding of steel-kovar, copper-steel and copper-aluminium. *Mater. Sci. Eng. A* 374: 224–233.
5. Xue, P., Ni, D., Wang, D., Xiao, B., and Ma, Z. 2011. Effect of friction stir welding parameters on the microstructure and mechanical properties of the dissimilar Al-Cu joints. *Mater. Sci. Eng. A* 528: 4683–4689.
6. Xue, P., Xiao, B., and Ma, Z. 2015. Effect of interfacial microstructure evolution on mechanical properties and fracture behavior of friction stir-welded Al-Cu joints. *Metall. Mater. Trans. A* 46(7): 3091–3103.
7. Beygi, R., Kazeminezhad, M., Kokabi, A., and Loureiro, A. 2015. Friction stir welding of Al-Cu bilayer sheet by tapered threaded pin: Microstructure, material flow, and fracture behavior. *Metall. Mater. Trans. A* 46(6): 2544–2553.
8. Meshram, S., Mohandas, T., and Reddy, G. 2007. Friction welding of dissimilar pure metals. *Journal of Materials Processing Technology* 184: 330–337.
9. Braunović, M., and Aleksandrov, N. 1994. Intermetallic compounds at aluminum-to-copper electrical interfaces: Effect of temperature and electric current. *IEEE Transactions on Components, Packaging, and Manufacturing Technology — Part A* 17(1): 78–85.
10. Yilbas, B., Sahin, A., Kahraman, N., and Al-Garni, A. 1995. Friction welding of St-A1 and Al-Cu materials. *Journal of Materials Processing Technology* 49: 431–443.
11. Lee, W., Bang, K., and Jung, S. 2005. Effects of intermetallic compound on the electrical and mechanical properties of friction welded Cu/Al bimetallic joints during annealing. *Journal of Alloys and Compounds* 390(1): 212–219.
12. Manjubhargavi, V., Chakravarthy, P., Venugopal, P., and Achar, D. Influence of rubbing profile on friction welding of pre-strained aluminum to copper. *Second International Conference on Emerging Trends in Engineering and Technology*, ICETET-092009, pp. 510–514.
13. Dong, H., Yu, L., Deng, D., Zhou, W., and Dong, C. 2015. Effect of post-weld heat treatment on properties of friction welded joint between TC4 titanium alloy and 40Cr steel rods. *Journal of Materials Science & Technology* 31(9): 962–968.
14. Xue, P., Xiao, B., Ni, D., and Ma, Z. 2010. Enhanced mechanical properties of friction stir welded dissimilar Al-Cu joint by intermetallic compounds. *Mater. Sci. Eng. A* 527: 5723–5727.
15. Li, P., Li, J., Li, X., Xiong, J., Zhang, F., and Li, L. 2015. A study of the mechanisms involved in initial friction process of continuous drive friction welding. *Journal of Adhesion Science and Technology* 29(12): 1246–1257.

Weld Formation Characteristics in Resistance Spot Welding of Ultra-Thin Steel

High welding current and short welding time were found to produce the best combination of strength and weld size

BY Y. Y. ZHAO, Y. S. ZHANG, AND PEI-CHUNG WANG

ABSTRACT

Recent trends toward economically fabricating lightweight vehicles while ensuring structural performance makes thin (e.g., < 0.5 mm) steels increasingly attractive in the automotive industry. In the present study, the formation of the weld during resistance spot welding (RSW) of a 0.35-mm-thick 600 MPa grade dual-phase steel was investigated. The results indicated the weld initiated early and grew to reach a maximum size of 2.8 mm within a welding time of 40 ms, and then its size remained virtually unchanged, and gradually exhibited a unique “double-layer” feature. Furthermore, the mechanism for the formation of weld layering was modeled from the perspective of temperature evolution. Modeling results indicated the temperature weld zone increased initially but then surprisingly decreased for the remaining welding process, and eventually resulted in a “double-layer” weld. It was found that the strength of the weld increased with the weld size and was improved little with the occurrence of the weld layering. Therefore, the use of high welding current and short welding time is preferable to join ultra-thin steel.

KEYWORDS

- Resistance Spot Welding (RSW) • Ultra-Thin Steel • Weld Formation
- Temperature History

Introduction

Facing the increasing pressure of fuel crisis, vehicle lightweighting is one of the most effective remedies to improve fuel efficiency and cut emissions in the automotive industry. Reduction in weight is usually achieved by using lightweight materials (e.g., aluminum) or by optimization of structural design throughout the vehicle structures. For now, most of the vehicle outer panels are still made of mild steel with the thickness in the range of 0.65 ~ 0.8 mm (Ref. 1). Analyses indicated that if these pan-

els can be substituted by advanced high-strength steel sheets whose thicknesses are below 0.6 or 0.5 mm, significant weight reduction could be achieved (Ref. 1). Moreover, the application of ultra-thin steels might have some advantages over the use of aluminum in terms of manufacturing cost (Refs. 1–3).

Resistance spot welding (RSW) has been the predominant joining method for vehicle assembly due to its robustness and low cost (Refs. 4, 5). A literature survey indicated that although extensive studies have been reported for RSW of steel thicker than 0.65 mm, there was limited information

about RSW of ultra-thin high-strength steels (< 0.5 mm) for automotive applications. A few of the early articles have reported some analytical results to investigate the effect of steel thickness on heat transfer in resistance spot welding. Gould (Ref. 6) has studied the weld development of three gauges of an AISI 1008 steel (nominally 0.5, 1, and 1.5 mm) and concluded that steel gauge strongly affected the ratio of heat flow into the electrodes and surrounding sheet. Decreasing steel gauge led to an increasing importance of heat loss through the electrode.

Eagar (Ref. 7) reported that the decrease in steel thickness led to lower resistance of the substrates, and thus the contact resistance at the faying interfaces accounted for a larger proportion of the total joule heat generation. As the sheet metal became thinner, the temperature gradients in the sheet became steeper and a greater portion of the total heat was lost into the electrodes, which may increase the electrode tip temperature and cause a significant reduction in electrode life. It was also reported that the cooling rate in the RSW process showed a strong gauge effect (Refs. 8, 9). The cooling rate was significantly reduced as the workpiece thickness became thick, ranging from over 100,000°C/s for gauges less than 0.5 mm to roughly 2000°C/s at a 2.0-mm gauge. Moreover, the combination of the variations in heat generation and dissipa-

Y. Y. ZHAO and Y. S. ZHANG (zhangyansong@sytu.edu.cn) are with Shanghai Key Laboratory of Digital Manufacture for Thin-walled Structures, Shanghai Jiao Tong University, Shanghai, China. PEI-CHUNG WANG is with the Manufacturing Systems Research Lab, General Motors Research & Development Center, Warren, Mich.

tion due to the variation of work-piece thickness would eventually lead to changes in weld nugget shape (Refs. 10, 11). For thin sheet, the majority of weld nugget growth occurred rapidly after initial melting, with weld nugget shape being generally elliptical. The weld nugget of the thick sheet showed a more rectangular or square shape. Although these qualitative analyses provided insightful information regarding the effect of steel gauge on heat transfer and weld characteristics in resistance welding, quantitative and experimental results related to the weld growth and microstructural evolution in resistance spot welding of ultra-thin steels are still lacking.

Most of the published studies so far dealing with joining very thin metal sheets (thinner than 0.2–0.5 mm) focused primarily on fabrication of electronic and medical devices (Refs. 12–18). The workpieces used in these studies were mostly similar or dissimilar combinations of nonferrous metals. Moreover, this kind of RSW is usually termed small scale RSW (SSRSW) compared to the large scale RSW (LSRSW) used for vehicle assembly. Compared with LSRSW, the welding parameters and energy input used in SSRSW are not in the same order of magnitude (Ref. 19). Due to the differences in welding equipment and materials, the published results on SSRSW provided limited guidance for RSW of ultra-thin high-strength steel intended for automotive applications.

The present study was undertaken to understand the weld growth characteristics during LSRSW of ultra-thin steel sheets. A series of experiments were conducted to study the weld initiation and growth behavior. Microstructures and weld formation mechanism were analyzed and the correlation between the joint strength and weld size was investigated. Due to the difficulty of measuring the temperature at the faying interfaces during resistance welding, finite element model coupled with thermal-electric-structural analysis was adopted to estimate the temperature history and explain the resultant weld formation process. Finally, the best practice for LSRSW of ultra-thin steel is discussed.

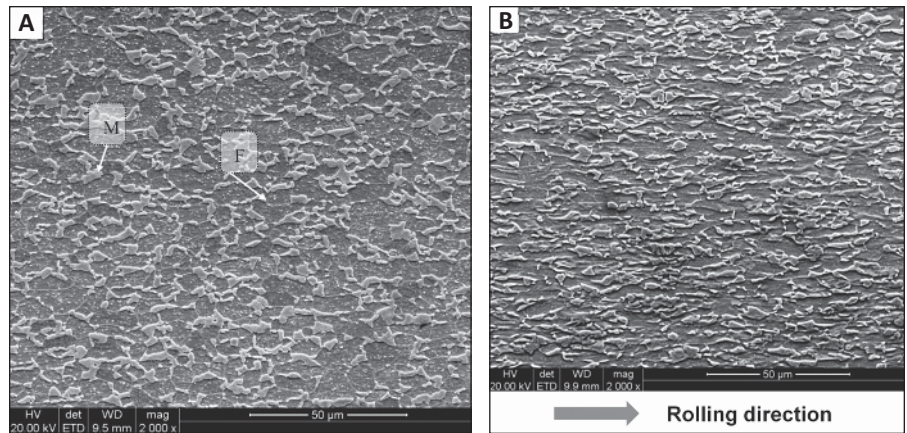


Fig. 1 — Microstructures. A — As-received 0.8-mm-thick DP600 steel; B — cold-rolled 0.35-mm-thick DP600 steel.

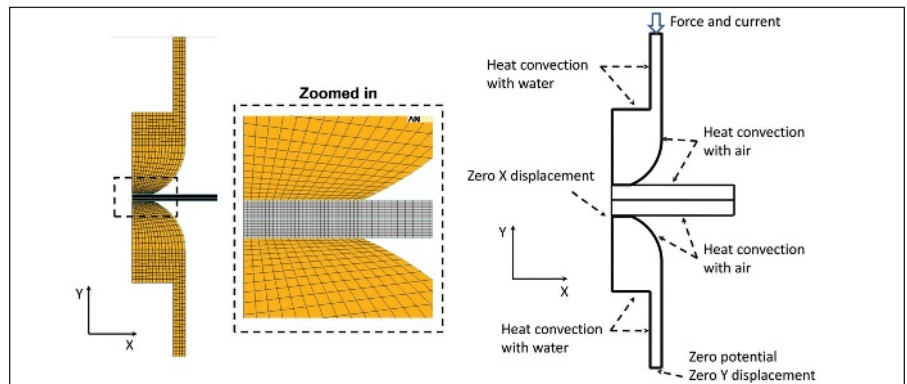


Fig. 2 — Geometrical model and boundary condition for modeling of the resistance welding process.

Table 1 — Chemical Composition in wt-% and Mechanical Properties of DP600 Steel

Steel	Chemical Composition in wt-%							Mechanical Properties		
	C	Si	Mn	P	S	Al	Nb	Yield Strength	Tensile Strength	Elongation
DP600	0.1	0.2	0.8	0.01	0.002	0.04	0.015	350 MPa	600 MPa	16%

Experimental Procedures

Materials

Bare 0.35-mm-thick dual-phase steel (DP600) was used in this study. Since 0.35-mm-thick DP600 steel is not readily available from the steel suppliers, the materials employed in this study were prepared by ourselves. The material we purchased is a 0.8-mm-thick DP600 steel of the Docol® series from SSAB (Ref. 20). Per manufacturers' data sheet, chemical compositions and typical mechanical properties of the as-received 0.8-mm-thick steel are listed in Table 1. These as-received sheets were machined into 30-mm wide strips to fit the width

of the roller and cold-rolled to 0.35 mm thick. Figure 1A and B show the microstructures of the as-received and cold-rolled steels, respectively. Referring to Fig. 1, ferrite and martensite were present in the cold-rolled DP600 steel (Ref. 21). The grains were elongated along the rolling direction and the microhardness of the cold-rolled DP600 increased from 250 to 330 HV after rolling.

Sample Fabrication

Resistance spot welding of 0.35-mm-thick DP600 steel was performed using a medium-frequency direct cur-

fixed at the values given in Table 2, and these included a squeezing time of 200 ms (before the current was applied) and a holding time of 100 ms after the welding current was shut off. Three replicas were performed at each welding condition.

Dynamic Resistance Measurement

The variation of dynamic resistance was measured to facilitate the understanding of the characteristics of heat generation during the welding process. Test results were collected by the welding monitor (MM-370A) from MIYACHI® (Ref. 22). Three replicates were prepared for the measurement of dynamic resistance. A detailed description of the experimental setup and procedure are in Refs. 23 and 24.

Cross-Section Examinations

Cross-section examinations of the welds were performed using a standard metallographic procedure up to the stage of grinding with 1200 silicon carbide polishing papers and further polishing using colloidal silica polishing suspension. The polished welds were subjected to hardness and metallographic examinations. The Vicker hardness was measured by a DHT HV-1000 hardness tester at intervals of 0.25 mm under an applied load of 294 g and a dwelling time of 10 s. Metallographic examinations were carried out to observe the microstructural evolutions and possible weld discrepancies. Specimens for metallographic examinations were prepared using standard metallography procedure and then etched with a 4% Picral reagent for 30 s and rinsed by ethanol. All surfaces were analyzed using standard optical and stereo microscopes. To obtain high-resolution images, scanning electron microscopy (FEI® Sirion Field Emission) was also employed (Ref. 25).

Modeling

Geometric Model

Finite element modeling coupled with electrical-thermal-mechanical

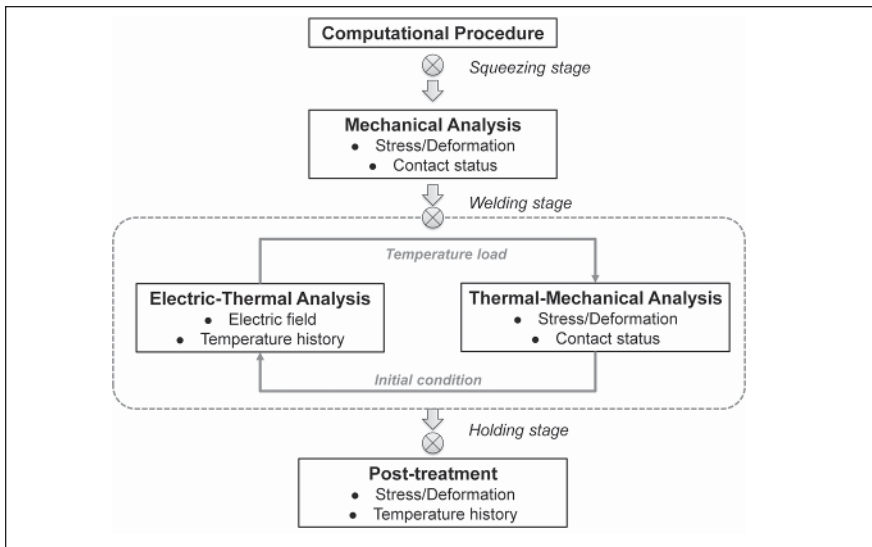


Fig. 3 — Computational procedure for finite element modeling of the resistance welding process.

Table 2 — Welding Parameters

Parameters	Electrode Force (kN)	Welding Current (kA)	Squeeze Time (ms)	Weld Time (ms)	Hold Time (ms)	Cooling Water Flow Rate (L/min)
Value	1.8	5.3	200	160	100	3

Table 3 — Welding Current vs. Peak Temperature/Time-to-Peak

Welding Current (kA)	Time-to-Peak Temperature (ms)	Peak Temperature (°C)
3.5	126.4	1530.2
3.9	97.6	1656.9
4.2	80.6	1749.6
4.6	68.7	1841.7
4.9	59.8	1930.2
5.3	52.3	2017.0
5.7	47.8	2100.7
6.0	45.4	2181.2
6.4	41.0	2273.2
6.7	39.4	2346.7

rent (MFDC) welding machine with a servo actuator. The joints were made using the coupons approximately 100 mm long and 30 mm wide with an overlap distance of 40 mm. Electrodes with a 5.0-mm-diameter flat tip end made of copper-chromium alloy of Resistance Welder Manufacturers Association (RWMA) class II were used, the composition of which is Cu-0.2Zr-0.5Cr-0.01Al (wt-%). Unless otherwise specified, all resistance welding testing was performed using the parameters listed in Table 2, which had been de-

termined based on a series of preliminary tests.

Weld Initiation and Growth

The purpose of these experiments was to understand the weld initiation and growth process. Resistance spot welding of 0.35-mm-thick DP600 steel was performed with a range of welding time (20–160 ms) at an increment of 20 ms. Other than the welding time, all other welding parameters were

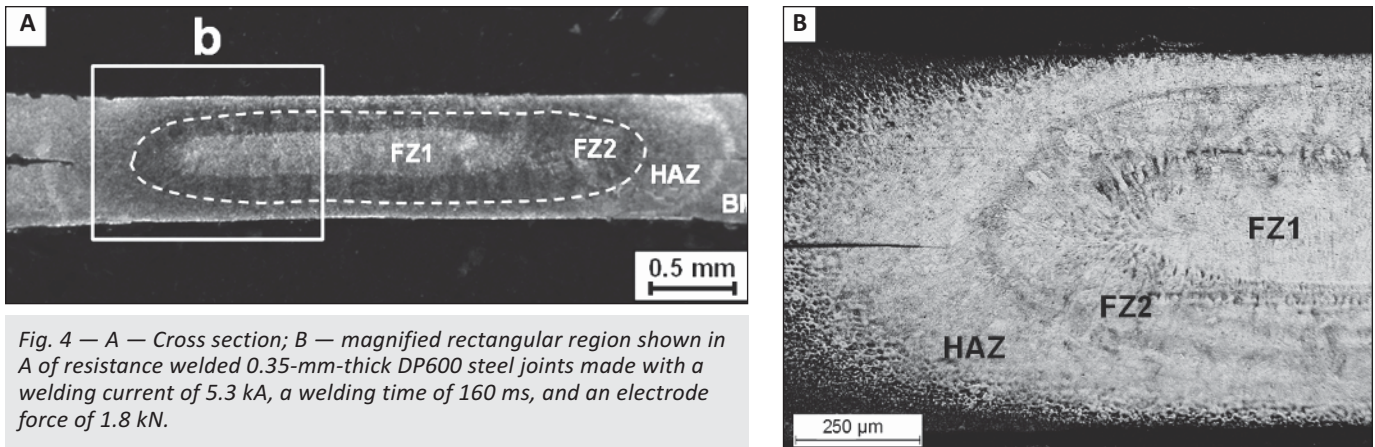


Fig. 4 — A — Cross section; B — magnified rectangular region shown in A of resistance welded 0.35-mm-thick DP600 steel joints made with a welding current of 5.3 kA, a welding time of 160 ms, and an electrode force of 1.8 kN.

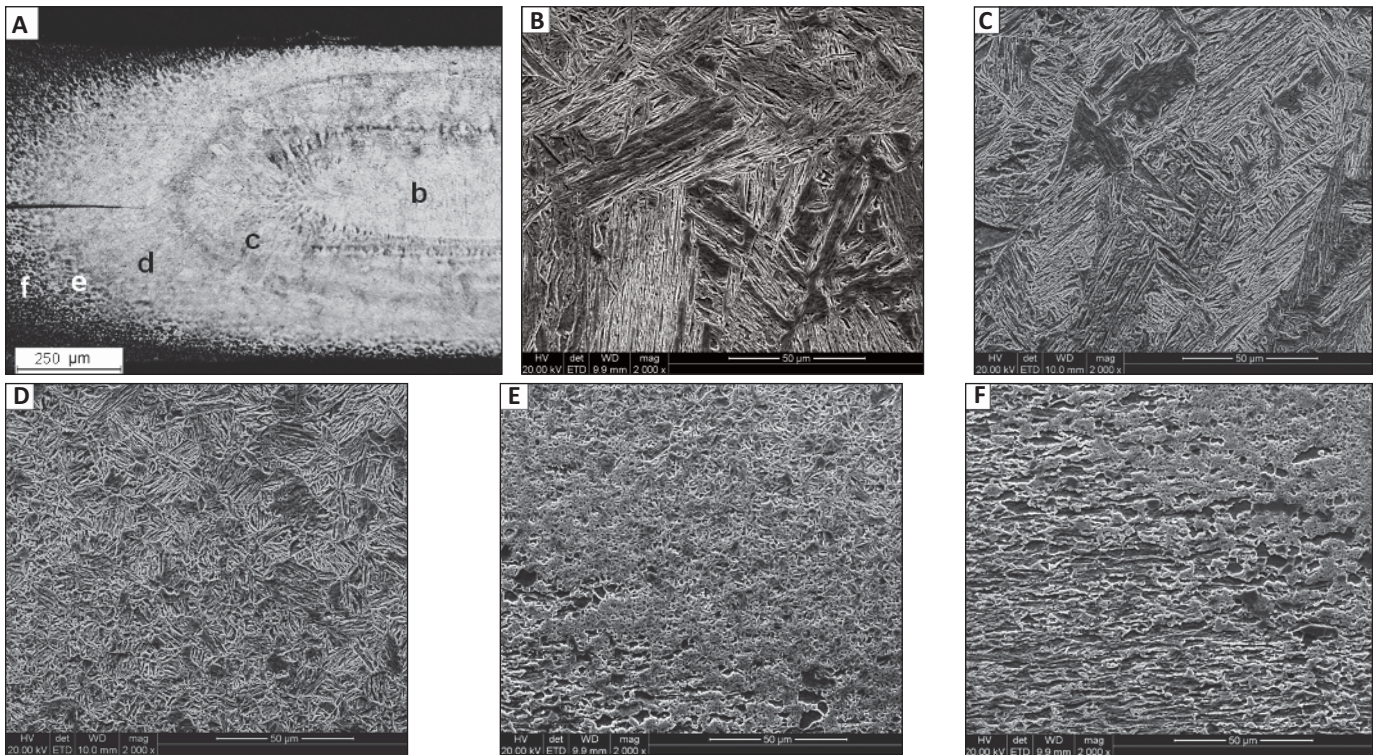


Fig. 5 — Microstructural evolutions from the weld center to the base metal. A — An overall view of the etched sample; B — center of the FZ1; C — FZ3; D — center of HAZ; E — HAZ close to base metal; F — HAZ boundary.

analysis was conducted using commercial software ANSYS 15.0. The physical configuration of the resistance spot welding process can be simplified to a two-dimensional axisymmetric model. Figure 2A shows the element grid used in the present analysis. As shown, four-node axisymmetric elements (i.e., PLANE67) were used to model the electrode and steel sheets. Special contact elements were inserted between the electrode/sheet and sheet/sheet interfaces to model contact state at those regions. The model was composed of 2608 nodes and 2664 elements, wherein 360 of

them were contact elements. Refined meshes shown in the enlarged area of Fig. 2A were used to capture the region where the temperature gradient was steep. Element types used for electrical-thermal and thermal-mechanical analysis were PLANE67 and PLANE42, respectively.

Boundary Conditions

Two types of boundary conditions, i.e., thermal-electrical and thermal-mechanical conditions shown in Fig. 2B, were applied to the finite element model as follows:

The thermal-electrical boundary conditions are

Table 4 — Recommended Welding Time for Various Steel Gauges

Steel Gauge (mm)	0.2	0.3	0.4	0.5	0.6	0.7
Critical Welding Time (ms)	40	60	80	100	120	160

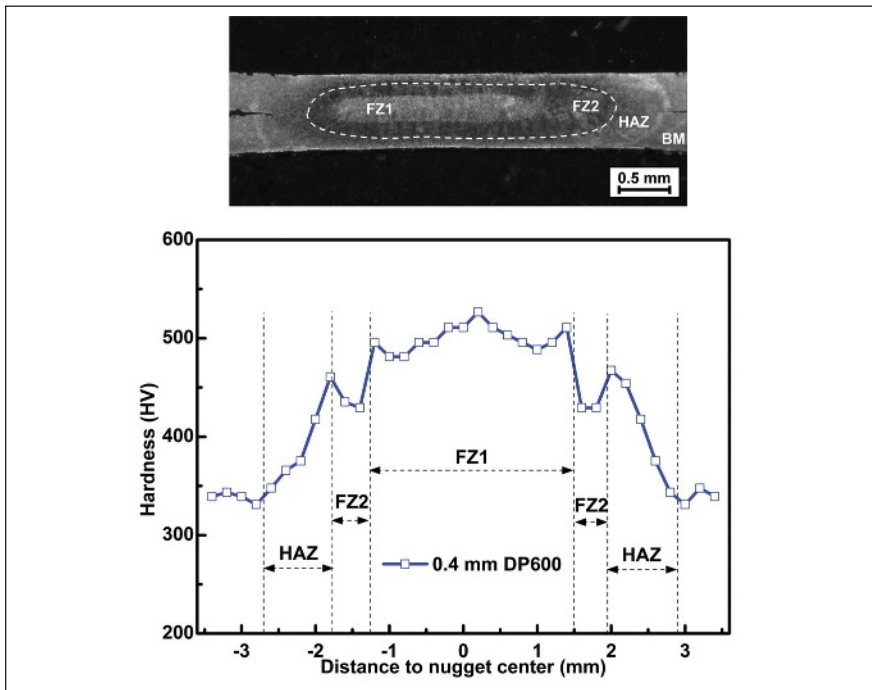


Fig. 6 — A typical microhardness profile of the resistance spot welded 0.35-mm-thick DP600 steel made with a welding current of 5.3 kA, an electrode force of 1.8 kN, and a weld time of 160 ms.

1) The electrical potential at the bottom end of the lower electrode was assumed zero, and the welding current was applied uniformly to the top of the upper electrode.

2) The convective heat transfer to the surrounding air was considered by using a convective heat transfer coefficient of $19.4 \text{ Wm}^{-2}\text{K}^{-1}$.

3) Both the ambient air and initial water temperatures were assumed to be 21°C .

Thermal-mechanical boundary conditions are

1) Electrode force was applied evenly to each nodal point at the top end of the upper electrode.

2) The displacement of the surface of the lower electrode was set to zero.

3) The centerline of the model was constrained to extend only along the Y-axis, without displacement along the X-axis.

Material Properties

In order to model the RSW process properly, all of the relevant mechanical (i.e., modulus, Poisson ratio, and stress-strain relationship), physical (i.e., density, thermal conductivity, expansion coefficient, and specific heat),

and electrical (i.e., resistivity) properties for the steel sheets and copper electrodes are needed. Since mechanical, electrical, and physical properties under elevated temperature are not readily available, many of these values were estimated from literature and assumed homogeneous and isotropic. Details on the determination of material properties are given in Refs. 26 and 27.

Contact Resistance Model

Despite the temperature-dependent material properties, the contact resistances at the faying interfaces are also crucial for the accuracy of the finite model. The contact resistance model employed in this study was a micro-electrical contact model proposed by Li (Ref. 28) derived from Kohlrausch's theory (Ref. 29). A relationship was developed between the voltage drop across a metallic contact interface and its resistance. According to the model, the voltage drop across the contact interface can be estimated by the following equation:

$$V^2 = 4L(T_s^2 - T_0^2) \quad (1)$$

where V is the voltage drop across the contact interfaces, T_s and T_0 are the contact super temperature and the bulk temperature at the interfaces, respectively, and L is the Lorentz constant of iron (about $2.0 \times 10^{-8} (\text{V}/^\circ\text{C})^2$). In the present computations, T_s at the workpiece/workpiece interface was specified to be the solidus of steel (1500°C), and at the electrode/workpiece interface to be the melting point of the electrodes (1084°C).

From Equation 1, the voltage drop across the interface at any bulk temperature (T_0) below T_s can be obtained. Based on this temperature-dependent voltage drop, the temperature-dependent contact resistance of the interface can be calculated by dividing by the welding current. Furthermore, the contact resistance value can be converted to an equivalent electrical resistivity using the geometrical information of the contact elements at the interfaces. Once the temperature of the contact elements exceeded its melting point, the contact resistance disappeared and the contact elements were disabled in this model. This contact resistance model has been reported in Refs. 19 and 30; good agreements were reported between the calculated and experimental measurements in weld growth and dynamic resistance.

Computational Procedure

The computational procedure is shown in Fig. 3. Referring to Fig. 3, at the squeezing stage, only mechanical analysis was conducted to calculate the contact status and stress distributions. At the welding stage, electric-thermal-mechanical coupled analysis is needed. However, due to the difficulty of direct coupling of the electric-thermal-mechanical field, the coupled analysis in this study was conducted in two steps. The rise in temperature obtained from the electric-thermal analysis was then applied as thermal loading for the thermal-mechanical analysis, while the contact status of the thermal-mechanical was used as the initial conditions for electric-thermal analysis. The time step of iteration for the coupling was 5 ms. And the temperature of the contact elements was checked every 5 ms as well. Once it exceeded the melting point, the corresponding contact element was disabled.

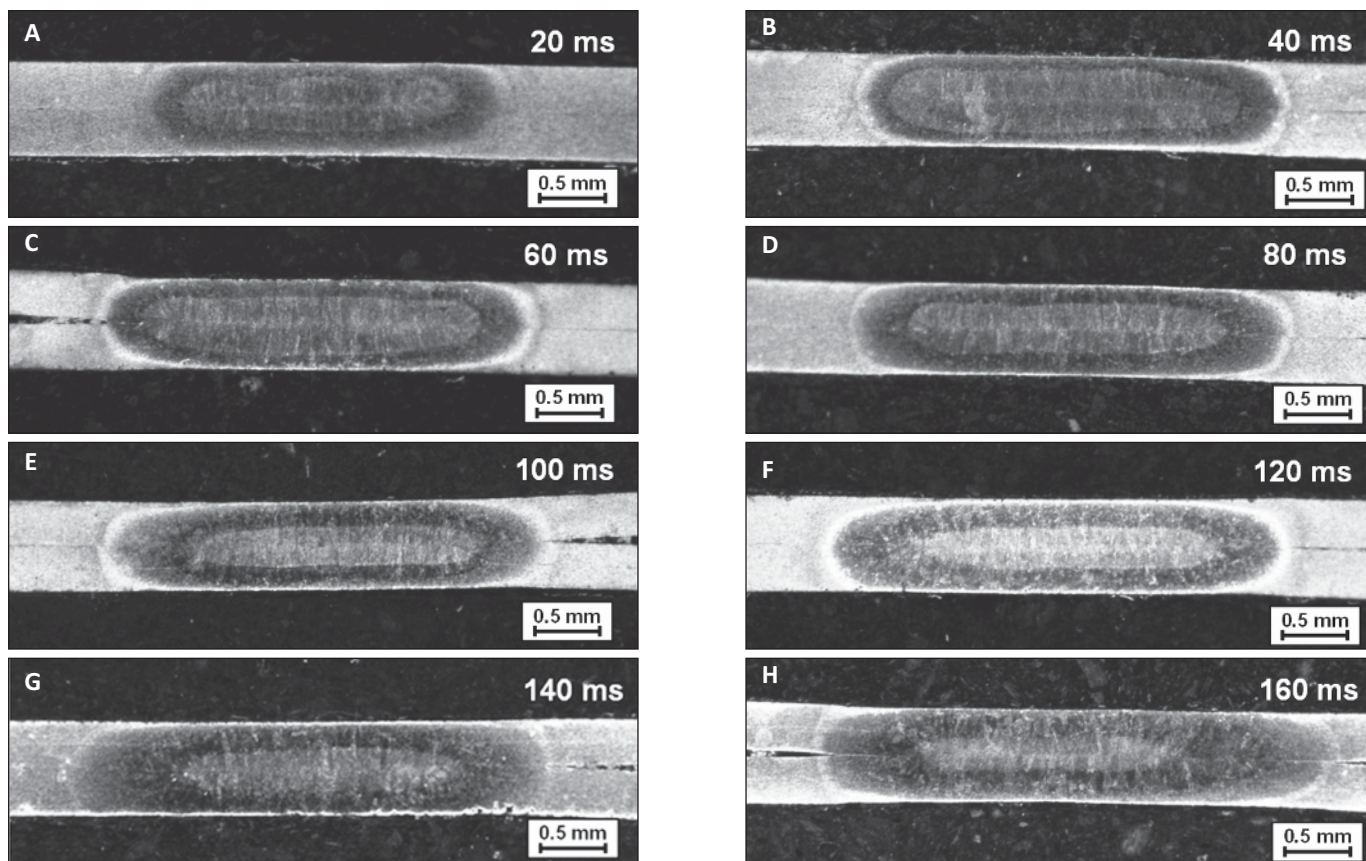


Fig. 7 — Effect of welding time on the weld initiation and growth of resistance spot welded 0.35-mm-thick DP600 steel: A — 20 ms; B — 40 ms; C — 60 ms; D — 80 ms; E — 100 ms; F — 120 ms; G — 140 ms; H — 160 ms.

Results

Microstructural Evolution

To understand the weld formation characteristics in resistance spot welding of 0.35-mm-thick DP600 steel, extensive welding tests were performed. In setting up the welding machine to produce a series of uniform welds, initial values of suitable electrode force and welding time were established. The welding controller was programmed in an attempt to maintain these values to produce consistent welds.

Figure 4 presents the typical cross section of the welds made from lap joint welded 0.35-mm-thick DP600 steel with a welding current of 5.3 kA and a welding time of 160 ms. Referring to Fig. 4A, the base metal (BM), heat-affected zone (HAZ), and fusion zone (FZ) of the weld were clearly identified. Examinations of the results shown in Fig. 4A revealed there was a comparatively darker region between the bright fusion zone and HAZ. High-

er magnification of the whole fusion zone is shown in Fig. 4B. Referring to Fig. 4B, a unique “double-layer” fusion zone was observed. The inner and outer weld zones are hereinafter referred to as FZ1 and FZ2, respectively. In the remaining part of this study, experiments were carried out to investigate the weld formation and microstructures of the “double-layer” fusion zone.

Referring to Fig. 1B, the base metal, DP600 steel, was primarily composed of ferrite and martensite (Ref. 21). The microstructure in the base metal was composed of evenly distributed martensite within the ferrite phase, which was elongated along the rolling direction. Figure 5B and C present the microstructures at location B (i.e., FZ1) and location C (i.e., FZ2) shown in Fig. 5A, respectively. As shown, both FZ1 and FZ2 zones consisted virtually of martensite. However, the martensite lath in the FZ2 was slightly finer than that of the FZ1. Referring to Fig. 5D to F, the volume fraction of martensite in the HAZ is higher than that in the base metal. Since the peak temperature during

welding in the HAZ ranged from just below the liquidus to martensite tempering temperatures, Fig. 5D to F showed the transitions of the HAZ from the coarsened grain region to the fine grain region and intercritical region (Ref. 31).

Figure 6 shows a typical hardness profile of the resistance welded 0.35-mm-thick DP600 steel. As shown, the results exhibited a significant hardness increase in the FZ1 compared to the base metal. Due to the high content of alloying elements in the steel and high cooling rate, the hardness of the FZ1, at a value of approximately 500 HV, was about 1.5 times more than that of the base metal (BM). The higher hardness in the FZ1 was apparently attributed to the fully martensite microstructure of the FZ1. The hardness of the FZ2 is about 430 HV, about 15% lower than that of the FZ1. The hardness of the HAZ from the FZ to the BM gradually decreased from 460 HV to a comparable hardness of the BM, which can be attributed to the decreasing volume fraction of martensite in the HAZ from the FZ side to the BM side.

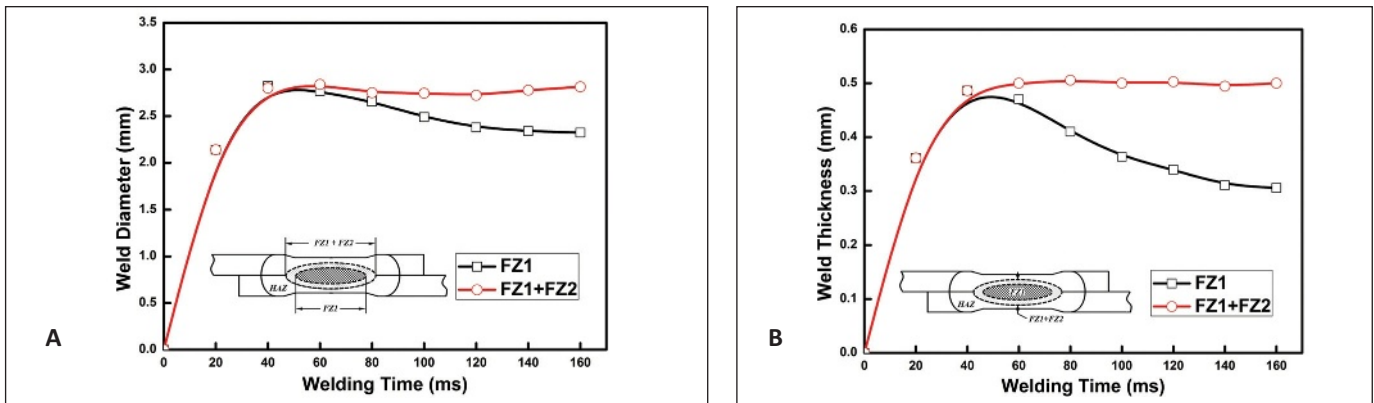


Fig. 8 — Effect of welding time on the A weld diameter and B weld thickness of resistance welded 0.35-mm-thick DP600 steel.

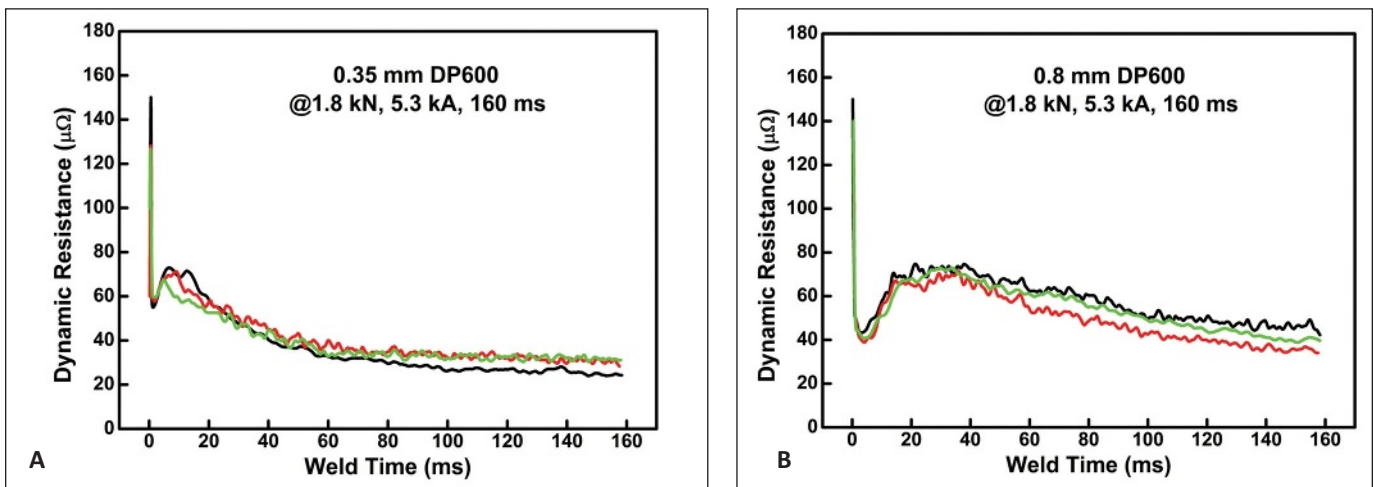


Fig. 9 — Dynamic resistance vs. time during resistance welding. A — 0.35-mm-thick steel; B — 0.8-mm-thick steel.

Weld Growth

In order to understand the “double-layer” phenomena, the welding time was increased from 0 to 160 ms at the increment of 20 ms, and the cross sections of the welds were examined. Figures 7 and 8 show the effect of welding time on the weld growth at various welding times.

Referring to Fig. 7, the fusion zone had two distinctive stages, namely the expanding and layering stages. In the expanding stage (i.e., 0–40 ms), the fusion zone grew with welding time. A rapid growth in weld size was observed for the first 20 ms, and after which the weld grew more gradually. At a welding time of 40 ms, the fusion zone reached a diameter of about 2.8 mm and a thickness of 0.48 mm. The rapid growth in weld size, to some extent, was similar to RSW of aluminum. Rashid et al. (Ref. 32) reported that the formation of a complete weld was observed during the

first cycle in RSW of aluminum AA5182.

As the welding time exceeded 40 ms, the outer layer, FZ2, gradually emerged, which was accompanied with the diminishing of an inner fusion zone, FZ1. The size of the FZ1 decreased to about 2.3 mm in diameter and 0.3 mm in thickness at a welding time of 160 ms. Furthermore, the diameter and thickness of the weld (i.e., sum of FZ1 and FZ2) almost remained unchanged after a welding time of 40 ms. Referring to Fig. 8, the extent of the weld layering was more pronounced in the thickness direction than in the radial direction. This phenomenon likely was attributed to the fact that the fraction of heat dissipated through the electrodes dominated the heat dissipation in welding of thin steel sheets (Refs. 6, 7).

Dynamic Resistance

To understand the mechanism of the formation of a “double-layer” weld in re-

sistance welds, heat generation during the welding process was considered. In the resistance spot welding process, the primary heat source is Joule heating (i.e., resistance heating when the welding current passes through the stack-up of workpieces between the electrodes). The amount of Joule heat generation per unit time is proportional to the square of the current and resistance. Since the welding current was constant, Joule heat generation per unit time was primarily determined by the contact resistance and resistivity of steel. Thus, the dynamic resistance of resistance spot welding 0.35-mm-thick dual-phase steel was measured, and the results are shown in Fig. 9A. For the purpose of comparison, the dynamic resistances of 0.8-mm-thick steel were also acquired, and the results are presented in Fig. 9B.

Referring to Fig. 9, the dynamic resistances in resistance welding both 0.35- and 0.8-mm-thick steels experienced a “decrease-increase-decrease”

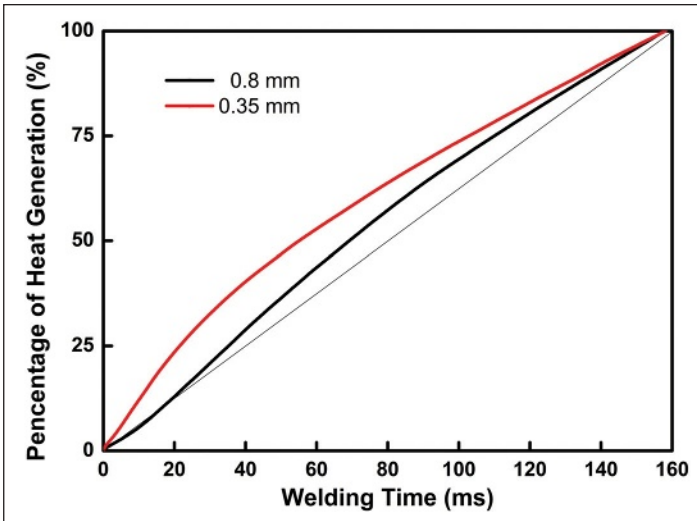


Fig. 10 — Effect of sheet thickness on heat generation in resistance welding steels.

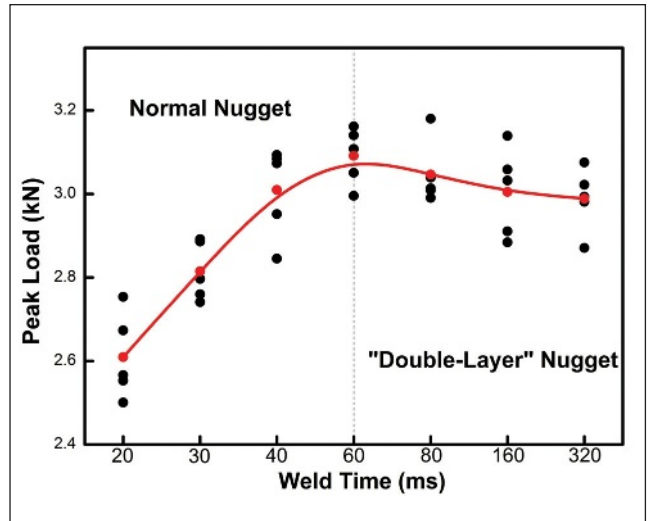


Fig. 11 — Effect of welding time on the strength of resistance welded 0.35-mm-thick DP600 steel.

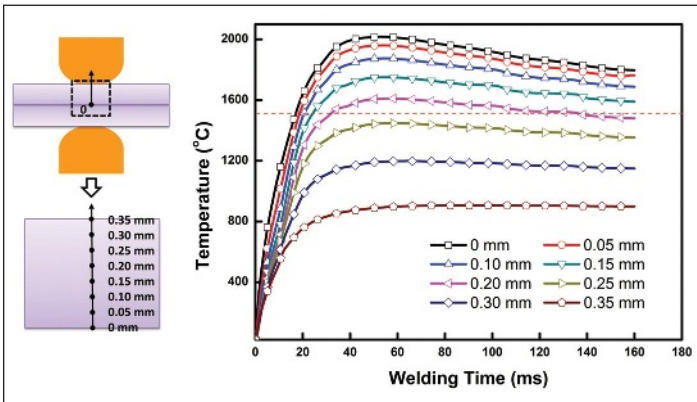


Fig. 12 — Calculated temperature histories in resistance welding of 0.35-mm-thick DP600 steel [results are presented for different levels of penetration in the workpiece, ranging from 0 mm (faying interface) to 0.35 mm (electrode surface)].

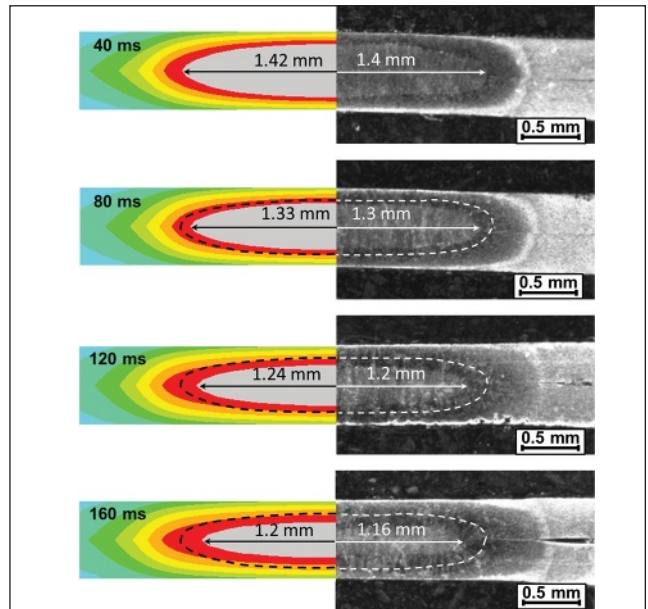


Fig. 13 — Comparison of modeling and experimental results in resistance welding 0.35-mm-thick DP600 steel.

pattern with increasing the welding time. As can be seen in Fig. 9A and B, the dynamic resistance dropped dramatically and reached a valley at the welding times of about 2 and 4 ms for resistance welding of 0.35- and 0.8-mm-thick steels, respectively. This sharp drop in resistance was related to the breaking down of the surface asperities caused by Joule heating (Ref. 27). While the dynamic resistances for both steels gradually increased to a peak, the time span of the increasing stage differed widely between them. The times to reach the resistance peak were about 10 and 40 ms for 0.35- and 0.8-mm-thick steels, respectively. This difference can be explained as follows:

The dynamic resistance in resistance welding of steel consisted of two

aspects, namely bulk resistance of the workpieces and contact resistance at the faying interfaces. The increase in dynamic resistance resulted primarily from the increase in bulk resistance of steel as a result of the increase in temperature. Because the increase in bulk resistance is quite limited for 0.35-mm-thick steel, the time span for the increasing stage of dynamic resistance was significantly less than that of 0.8-mm-thick steel. After the peak, the size of the molten region increased progressively, which also enlarged the cross-sectional area available for current flow and led to further decrease in dynamic resistance (Ref. 33).

To understand the effect of sheet thickness on the heat generation, the dynamic resistance over the welding time was integrated and the results are shown in Fig. 10. Referring to Fig. 10, about 23.3% of the total Joule heat was generated within the initial welding time of 20 ms, and 50% within the initial 55 ms in resistance welding 0.35-mm-thick steel, while only 12.7% at a welding time of 20 ms and 50% at a welding time of 70 ms for 0.8-mm-thick steel. It can be inferred that the heat generation strongly concentrated at the initial stage of the resistance welding

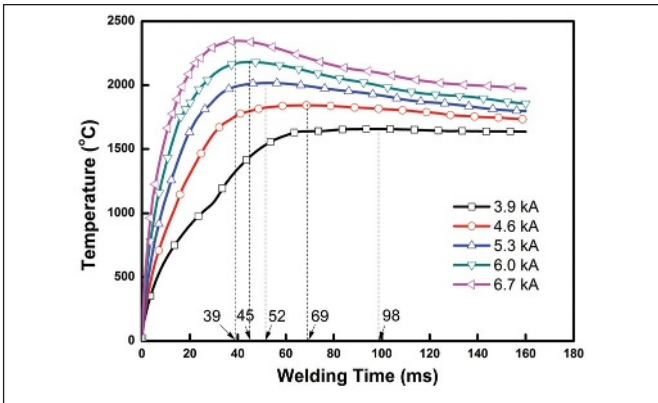


Fig. 14 — Calculated effect of welding current on the temperature histories in resistance welding 0.35-mm-thick DP600 steel.

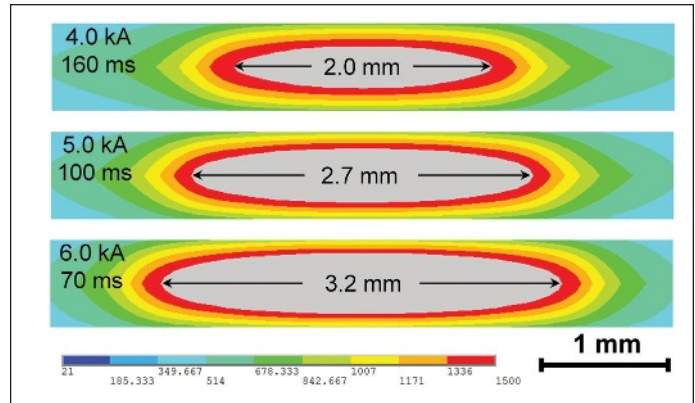


Fig. 15 — Calculated effect of welding variables on the weld sizes in resistance welding 0.35-mm-thick DP600 steel.

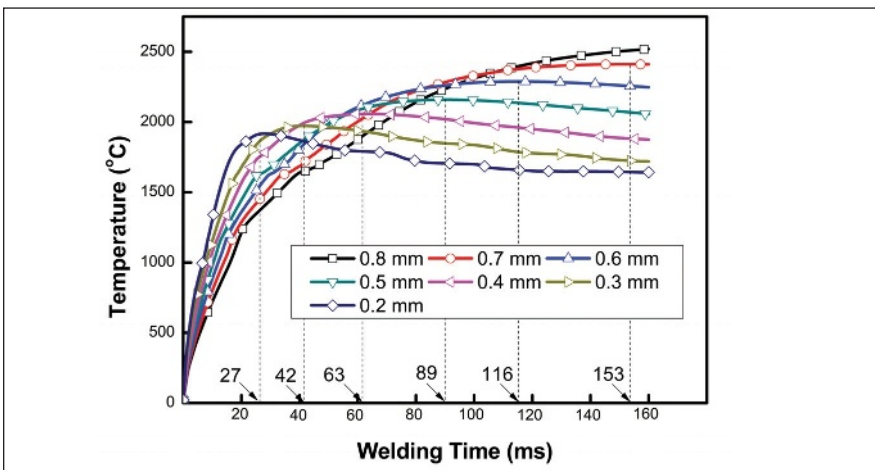


Fig. 16 — Calculated effect of sheet thickness on the temperature histories in resistance spot welding steel.

process of ultra-thin steels. This observation in dynamic resistance and heat generation were in line with the testing results of the weld formation. A high resistance in the beginning resulted in significant heat generation, and these results explained the rapid weld growth during the initial welding stage. Low resistance in the latter half of the welding process also agreed with the stable fusion size observed in Fig. 7.

Effect of Weld Layering

From the aforementioned results, the weld layering occurred in resistance welding of 0.35-mm-thick steel. Naturally, it is necessary to examine how the weld layering would affect the joint strength. Welds with various degrees of layering were fabricated. Figure 11 shows the effect of welding time on the strength of the welded 0.35-mm-thick steel. Referring to Fig. 11, the joint

strength increased from about 2.5 to 3.1 kN as the welding time increased from 20 to 40 ms, which can be attributed to the increase in weld size with prolonging the welding time. The joint strength changed little when the welding time was prolonged from 60 to 320 ms. Examination of the test results revealed all joints failed in button pull-out mode. Based on these results, it can be concluded that the joint strength was proportional to the weld size (i.e., sum of the FZ1 and FZ2). Once the weld layering occurred (i.e., at a welding time of ~ 60 ms), the weld size grew little, and consequently it had little benefit on the joint strength, and indeed even slightly impaired the joint strength.

Discussions

Temperature History

To further clarify the formation

mechanism of “double-layer” weld, transient temperature histories for the locations from the faying interfaces to the electrode face were estimated, and the results are shown in Fig. 12. As shown, the temperatures rose first and then fell, which was quite different from the monotonic increase in temperature in resistance welding of thick steel (e.g., > 1 mm) (Refs. 27 and 34). Referring to Fig. 12, calculated temperature at the faying interfaces achieved the melting point of steel at a welding time of 15 ms and reached the peak (~ 2017°C) at a welding time of about 52 ms. After that, the temperature at the faying interfaces decreased. The temperature histories for the locations from the faying interfaces to the electrode-workpiece interface all exhibited “first-rise-then-fall” pattern. Furthermore, the temperature decrease in the latter stage of the welding process was more pronounced at the faying interfaces than at the electrode-workpiece interface.

This “first-rise-then-fall” temperature history was likely the cause of the “double-layer” weld shown in Fig. 7. Referring to Fig. 12, the temperature at the location of 0.2 mm above the faying interfaces achieved the solidus (i.e., 1500°C) at a welding time of about 32 ms and increased to 1610°C at a welding time of 56 ms, and then dropped below the solidus at about 120 ms. These results suggested the workpieces became molten at a welding time of 32 ms, and started to solidify at 120 ms. However, the temperatures for the locations between the faying interfaces and 0.15 mm above the faying interfaces were still higher than the solidus at a welding time of 160 ms, and thus the workpiece

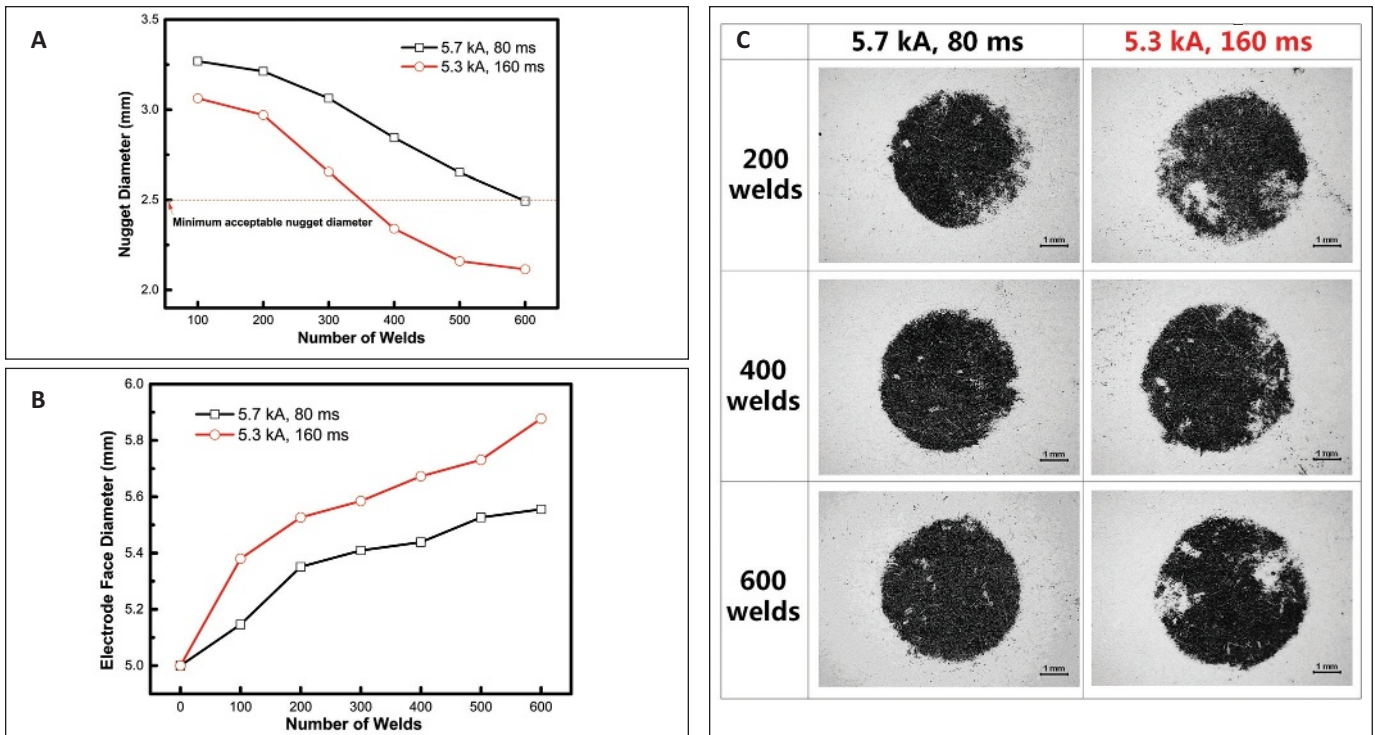


Fig. 17 — A — Weld diameter; B — electrode face diameter; C — electrode imprints as a function of number of welds during the electrode wear testing.

Table 5 — Welding Parameters for Electrode Wear Test

No. of Parameter	Electrode Force (kN)	Welding Current (kA)	Squeeze Time (ms)	Weld Time (ms)	Hold Time (ms)	Cooling Water Flow Rate (L/min)
Parameter I		5.7		80		
Parameter II	1.8	5.3	200	160	100	3

at those locations solidified after the welding current was shut off. Based on these results, two kinds of solidification processes occurred; the portion of the molten metal started to solidify after the welding current was turned off (Mode 1) and formed an inner layer, FZ1, while the outer layer of the molten zone had already solidified progressively during the welding process (Mode 2) and resulted in an outer layer (i.e., FZ2). Therefore, the boundary of the outer region of the double layer (FZ2) was defined by the boundary of the melting area at the moment when the temperature at the faying interface achieved the peak (i.e., 52 ms), while the boundary of the inner layer (FZ1) was defined by the boundary of the melting area when the welding current was about to shut off. Since the temperature at the outer layer was lower than the inner one, the nucleation rate at the outer layer would have been higher than the inner layer, and

thus led to finer microstructure, referring to Fig. 3. Furthermore, the cooling rates in RSW was well above the critical cooling rates for martensite formation for DP steel (i.e., 120°C/s) (Ref. 8), and thus both FZ1 and FZ2 were composed fully of martensite. The results shown indicated that the calculated temperature history provided a good explanation for the experimental observations.

Comparison of Modeling and Experimental Results

The finite element model was used to analyze the temperature evolution during resistance welding. Figure 13 shows the comparison of calculated and measured weld sizes. As shown, once the calculated temperature exceeded the melting point (i.e., 1500°C) of steel, it was colored in gray. The grey area thus indicated the area of FZ1, melting region at different welding time. The

black dash line indicated the calculated boundary of the FZ2, which was determined by the melting region at 52 ms, while the white dash line showed the boundary of FZ2 in the cross sections. Referring to Fig. 13, the weld had a diameter of 2.8 mm and a depth of 0.48 mm after only a welding time of 40 ms, and nugget layering was not observed. However, as the welding time was prolonged, the weld nugget layering gradually developed where the diameter and depth of the inner layer of nugget (FZ1) gradually decreased, especially the depth. For example, the diameter and depth of the FZ1 decreased to 2.4 and 0.32 mm, respectively, after a welding time of 160 ms. These results inferred that the melting zone experienced an “expand-shrink” evolution during the resistance welding of 0.35-mm-thick steel, which was in line with the measured results shown in Fig. 7 that the FZ1 grew fast within the initial welding

time of 40 ms, and then gradually diminished as the welding time continued. In addition, the calculated size and shape of both FZ1 and FZ2 showed good agreement with the cross sections.

Effect of Welding Current

From the aforementioned results, it was found that the weld layering was strongly related to the temperature history during the welding process. Since the Joule heat generation is proportional to the welding current, the effect of welding current on the variations of the weld layering was also studied from the perspective of temperature history. Figure 14 presents the effect of welding current on the calculated temperature histories in resistance spot welding of 0.35-mm-thick DP600 steel. Table 3 lists the correlations between the welding current and peak temperature and time-to-reach the peak temperature. Referring to Fig. 14 and Table 3, although the application of high welding current resulted in an increase in maximum temperature, it hardly changed the “first-rise-then-fall” temperature history. Moreover, the time to reach the peak temperature occurred earlier under high welding current, and a more prominent “first-rise-then-fall” temperature phenomenon was observed.

Another interesting observation was seen, referring to Fig. 15. In RSW thick steel (> 0.8 mm), a desired weld size can be achieved by using either high welding currents with short welding times or low welding currents with long welding times under thermal equivalent principles (Refs. 6, 7). However, it was not the case for steel with a thickness of 0.35 mm. For example, although the Joule heat of these three sets of welding parameters (4.0 kA, 160 ms; 5.0 kA, 100 ms; and 6.0 kA, 70 ms under an electrode force of 1.8 kN) were similar, the resultant calculated weld sizes were quite different, referring to Fig. 15. The calculated weld sizes were 2.0, 2.7, and 3.2 mm under the welding parameters of 4.0 kA, 160 ms; 5.0 kA, 100 ms; and 6.0 kA, 70 ms, respectively. These results can be explained by the dynamic resistance results shown in Fig. 7. As shown, the dynamic resistance virtually kept decreasing in resistance welding of 0.35-mm-thick DP600 steel, and

consequently most of the Joule heat was generated at the initial stage of the welding process. Therefore, it can be concluded that high welding current and short welding time are preferable for RSW of 0.35-mm-thick steel.

Recommended Welding Practice

The aforementioned results demonstrated that the weld size increased rapidly at the initial stage of the welding process and reached its maximum at a critical welding time. After that, the weld size remained virtually unchanged. Then, the weld gradually grew to form a two-layer structure as the welding continued. Furthermore, testing results showed that the joint strength increased with the weld size, and weld layering provided little benefit from the joint strength perspective. Therefore, the use of high welding current and short welding time is recommended to join ultra-thin steel.

Figure 16 presents the effect of sheet gauge on the temperature at the weld center for RSW of steels. Referring to Fig. 16, while the temperature was always rising within the welding time of 160 ms for 0.8-mm-thick steel, the temperatures all rose first and then fell for steel gauges varying from 0.7 ~ 0.2 mm. As the steel gauge decreased, the time to reach the peak temperature occurred earlier and the phenomenon of temperature decrease became more pronounced. Thus, the weld layering happened earlier with a decrease in steel gauge. The recommended welding time can be identified by the round numbers of the turning point in the temperature histories, referring to Table 4. As shown, the recommended welding time decreased significantly with the decrease in steel gauge. These results inferred that high welding current and short welding time were preferred for RSW of thin steels.

To further validate this observation, electrode wear tests at a welding rate of 30 welds per minute were conducted. Two sets of welding parameters shown in Table 5 were selected. Carbon imprints of electrode and peel specimens at every 100-weld interval were conducted to monitor the electrode wear and weld diameter, respectively. The weld diameter was estimated by measuring the diameter of pull-

out buttons during the peel tests. Figure 17A and B presents the variations of weld diameter and electrode face diameter vs. the number of welds, respectively. Referring to Fig. 17A, the weld diameters obtained using parameter I (i.e., a welding current of 5.7 kA and a weld time of 80 ms) were larger than those with the use of welding parameter II (i.e., a welding time of 5.3 kA and a weld time of 160 ms). While the weld diameters made with parameter II fell below the minimum acceptable size (i.e., 2.5 mm) after 400 welds, the weld diameters obtained with the use of welding parameter I were still greater than 2.5 mm after 600 welds. Moreover, the rate of electrode degradation with welding parameter I was comparatively lower than that with welding parameter II, referring to Fig. 17B. The difference in electrode degradation was further observed from carbon imprints shown in Fig. 17C. Referring to Fig. 17C, severe cavitation at the electrode surface (i.e., white areas) was observed using parameter II after 600 welds, while the electrode imprints of the electrode using parameter I remained relatively sound conditions. These results confirmed that high welding current and short welding time were more preferable for RSW thin steels (< 0.5 mm).

Conclusions

In this study, experiments and numerical modeling conducted on resistance welding of 0.35-mm-thick DP600 steel concluded the following:

1) The weld initiated early and grew to reach a maximum diameter of 2.8 mm within a welding time of 40 ms. Afterward, the weld gradually formed an inner layer and an outer layer with the overall size virtually unchanged. The extent of the weld layering became pronounced with prolonging the welding time.

2) The formation of the weld layering was primarily attributed to the unique temperature history developed for welding ultra-thin (i.e., 0.35 mm) steel. The temperature in the middle of the weld zone initially increased rapidly and reached a maximum value at a welding time of about 52 ms, and then fell in the remaining of the welding process. As the temperature dropped, the molten zone solidified

gradually from the edge to the internal molten zone, and consequently the weld layering was emerged.

3) The joint strength increased with the weld size and was improved little with the occurrence of the weld layering. Therefore, it is preferable to use high welding current and short welding time for resistance welding ultra-thin steel.

Acknowledgments

This research was supported by the General Motors Collaborative Research Laboratory at Shanghai Jiao Tong University and National Natural Science Foundation of China (Project 51675338). The authors also sincerely thank Prof. Hyun Chung from Korea Advanced Institute of Science and Technology (KAIST) for his kind help during the preparation of this manuscript, and the Brain Korea 21 (BK21) fellowship from the Ministry of Education of Korea.

References

- Singh, H., and Coates, G. 2014. Advanced high-strength steel lightweighting: minimum thickness study and AHSS application guidelines. *Great Designs in Steel*, American Iron and Steel Institute.
- Zhao, Y. Y., Zhang, Y. S., Lai, X. M., and Wang, P.-C. 2013. Resistance spot welding of thin automotive steel. *ASME Journal of Manufacturing Science and Engineering* 135(2): 021012.1-10.
- Zhao, Y. Y., Zhang, Y. S., Lai, X. M., and Wang, P.-C. 2014. Effect of inserted strips on electrode degradation in resistance spot welding. *Welding Journal* 93(11): 411-s to 420-s.
- Agashe, S., and Zhang, H. 2003. Selection of schedules based on heat balance in resistance spot welding. *Welding Journal* 82(7): 179-s to 183-s.
- Sun, X., Stephens, E. V., Davies, R. W., Khaleel, M. A., and Spinella, D. J. 2004. Effects of fusion zone size on failure modes and static strength of aluminum resistance spot welds. *Welding Journal* 83(11): 308-s to 318-s.
- Gould, J. E. 1987. An examination of nugget development during spot welding using both experimental and analytical techniques. *Welding Journal* 66(1): 1-s to 11-s.
- Euiwhan, K., and Eagar, T. W. 1988. Parametric study of heat flow during resistance spot welding. Modeling and control of casting and welding Processes IV. *Proceedings of the Fourth International Conference on Modeling of Casting and Welding Processes*.
- Gould, J. E., Khurana, S. P., and Li, T. 2006. Predictions of microstructures when welding automotive advanced high-strength steels. *Welding Journal* 85(5): 111-s to 116-s.
- Ho, J. E., Wei, P. S., and Wu, T. H. 2012. Workpiece property effect on resistance spot welding. *IEEE Transactions on Components, Packaging and Manufacturing Technology* 2(6): 925-934.
- Williams, N. T., and Parker, J. D. 2004. Review of resistance spot welding of steel sheets: Part 1 modelling and control of weld nugget formation. *International Materials Reviews* 49(2): 45-75.
- Williams, N. T., and Jones, T. B. 1984. Resistance spot welding of low carbon and high strength low-alloy (HSLA) steels, Report no. EUR 8693, Commission of European Communities, Technical Steel Research Programme, Brussels, Belgium.
- Zhou, Y., Gorman, P., Tan, W., and Ely, K. J. 2000. Weldability of thin sheet metals during small-scale resistance spot welding using an alternating-current power supply. *Journal of Electronic Materials* 29(9): 1090-1099.
- Ely, K. J., and Zhou, Y. 2001. Microresistance spot welding of Kovar, steel, and nickel. *Science and Technology of Welding and Joining* 6(2): 63-72.
- Zhou, Y., Dong, S. J., and Ely, K. J. 2001. Weldability of thin sheet metals by small-scale resistance spot welding using high-frequency inverter and capacitor-discharge power supplies. *Journal of Electronic Materials* 30(8): 1012-1020.
- Tan, W., Zhou, Y., and Kerr, H. W. 2002. Effects of Au plating on small-scale resistance spot welding of thin-sheet nickel. *Metallurgical and Materials Transactions A*, 33(8): 2667-2676.
- Tan, W., Zhou, Y., Kerr, H. W., and Lawson, S. 2004. A study of dynamic resistance during small scale resistance spot welding of thin Ni sheets. *Journal of Physics D: Applied Physics* 37(14): 1998-2008.
- Fukumoto, S., Fujiwara, K., Toji, S., and Yamamoto, A. 2008. Small-scale resistance spot welding of austenitic stainless steels. *Materials Science and Engineering: A*, 492(1): 243-249.
- Fujiwara, K., Fukumoto, S., Yokoyama, Y., Nishijima, M., and Yamamoto, A. 2008. Weldability of Zr 50 Cu 30 Al 10 Ni 10 bulk glassy alloy by small-scale resistance spot welding. *Materials Science and Engineering: A* 498(1): 302-307.
- Chang, B. H., Li, M. V., and Zhou, Y. 2001. Comparative study of small scale and 'large scale' resistance spot welding. *Science and Technology of Welding and Joining* 6(5): 1-8.
- ssab.com
- Marya, M., and Gayden, X. Q. 2005. Development of requirements for resistance spot welding dual-phase (DP600) steels Part 1 — The causes of interfacial fracture. *Welding Journal* 84(11): 172-s to 182-s.
- www.amadamiyachi.com
- Zhang, Y. S., Sun, H. T., Wang, P. C., and Chen, G. L. 2014. Improvement of process robustness in weld bonding of galvanized DP780 steel. *Welding Journal* 93(12): 472-s to 481-s.
- Shen, J., Zhang, Y. S., Lai, X. M., and Wang, P. C. 2012. Adhesive placement in weld-bonding of multiple stacks of steel sheets. *Welding Journal* 91(2): 59-s to 66-s.
- www.fei.com
- Shen, J., Zhang, Y. S., Lai, X. M., and Wang, P. C. 2010. Modeling of resistance spot welding of multiple stacks of steel sheets. *Materials & Design* 32(2): 550-560.
- Wan, X. D., Wang, Y. X., and Zhang, P. 2014. Modeling the effect of welding current on resistance spot welding of DP600 steel. *Journal of Materials Processing Technology* 214(11): 2723-2729.
- Li, M. V., Dong, P., and Kimchi, M. 1997. A contact resistance model for resistance spot welding process: theory and implementation. *ICAWT 97: High Productivity Joining Processes*, San Francisco, Calif.
- Kohlrausch, F. 1900. Ueber das Problem eines elektrisch erwärmten leiters. *Annalen der Physik* 306(2): 312-325.
- Chang, B. H., and Zhou, Y. 2003. Numerical study on the effect of electrode force in small-scale resistance spot welding. *Journal of Materials Processing Technology* 139(1-3): 635-641.
- Khan, M. I., Kuntz, M. L., Su, P., Gerlich, A., North, T., and Zhou, Y. 2007. Resistance and friction stir spot welding of DP600: a comparative study. *Science and Technology of Welding and Joining* 12(2): 175-182.
- Rashid, M., Medley, J. B., and Zhou, Y. 2011. Nugget formation and growth during resistance spot welding of aluminum alloy 5182. *Canadian Metallurgical Quarterly* 50(1): 61-71.
- Dickinson, D. W., Franklin, J. E., and Stanya, A. 1980. Characterization of spot welding behavior by dynamic electrical parameter monitoring. *Welding Journal* 59(6): 170-s to 176-s.
- Eisazadeh, H., Hamed, M., and Halvae, A. 2010. New parametric study of nugget size in resistance spot welding process using finite element method. *Materials and Design* 31(1): 149-157.

Arcos Delivers Solutions to Stainless Steel Alloy Welding Challenges.



Arcos Industries, LLC offers over 100 stainless steel electrode products to handle the countless array of demanding welding applications that challenge you daily. Our reputation for exceptional quality and outstanding service ensures that you can depend on Arcos to provide you with the finest in bare wire, covered and tubular stainless steel alloy welding electrodes.

Discover for yourself how Arcos **stainless steel alloy electrodes** can help you solve your critical welding problems. Call us today at **800-233-8460** or visit our website at **www.arcos.us**.



For Info, go to aws.org/ad-index

Safer Workers. Lower Cost.

Weld Fume Extraction Equipment by The Welding Experts®



There's no arguing that healthier workers are more productive. Now with weld fume extraction equipment from Lincoln Electric, you can increase employee safety at a lower cost – up to 30% lower costs.

Lincoln Electric is committed to the lowest total cost of ownership for weld fume control equipment. Easy to use, reliable systems – assembled here in the USA*.

Find out how Lincoln Electric can lower cost and improve worker safety. Visit us at www.lincolnelectric.com/weld-fume-control



*U.S.A. made of U.S. and foreign content
AR16-66 ©2016 Lincoln Global, Inc. All Rights Reserved.



For Info, go to aws.org/ad-index